



Universiteit
Leiden
The Netherlands

Synthesis and characterization of squaramide-based supramolecular polymers

Lauria, F.

Citation

Lauria, F. (2022, November 1). *Synthesis and characterization of squaramide-based supramolecular polymers*. Retrieved from <https://hdl.handle.net/1887/3485180>

Version: Publisher's Version

License: [Licence agreement concerning inclusion of doctoral thesis in the Institutional Repository of the University of Leiden](#)

Downloaded from: <https://hdl.handle.net/1887/3485180>

Note: To cite this publication please use the final published version (if applicable).

Synthesis and characterization of squaramide-based supramolecular polymers

Proefschrift

ter verkrijging van
de graad van doctor aan de Universiteit Leiden,
op gezag van rector magnificus prof.dr.ir. H. Bijl,
volgens besluit van het college voor promoties
te verdedigen op dinsdag 1 november 2022
klokke 16:15 uur

door

Francesca Lauria
geboren te Napels, Italy
in 1990

Promotiecommissie

Promotor: Prof. dr. A. Kros

Copromotor: Dr. R. E. Kieltyka

Overige commissieleden:

Prof. dr. H. Overkleeft

Dr. G. F. Schneider

Dr. L. Albertazzi (Institute for Bioengineering of Catalonia, Barcelona, Spain)

Prof. dr. I. Voets (Eindhoven University of Technology)

Prof. dr. S. Bonnet

Doctoral Thesis, Leiden University, 2022

Cover Design: Image from Shutterstock.com

Printed by Ridderprint BV

To my parents, my sisters Ilaria and Teresa and my friends,
without your support this would not have been possible

TABLE OF CONTENTS

Chapter 1	7
Introduction	
Chapter 2	43
Supramolecular copolymerization of oxo- and thiosquaramide monomers	
Chapter 3	83
Tripodal acids as building blocks for the Ugi multicomponent reactions	
Chapter 4	145
Understanding the self-assembly of tripodal squaramide-based monomers through structural substitution	
Chapter 5	179
Visible light crosslinking of squaramide-based supramolecular polymers through tyrosine cross-linking	
Chapter 6	209
Summary and perspectives	
Samenvatting	215
Curriculum Vitae	219
List of publications	221

Introduction

1.1 Supramolecular biomaterials

Biomaterials are a class of materials that are in contact with biological systems.¹ The growing demand for smart materials that are designed to interact with the biological environment to improve the patient's condition and experience in injury and disease is rapidly increasing.² Although this is a field that has been classically associated with covalent polymers, that are largely irreversible in character, there is a second class of polymers that have been applied more recently in this area and are based on dynamic or non-covalent interactions, such as electrostatic, hydrogen-bonding, π - π , and hydrophobic effects; these are supramolecular polymers.³⁻⁶ This class of dynamic or supramolecular materials are extremely attractive in areas such as tissue engineering, regenerative medicine and drug delivery due to their modular, stimuli-responsive, tunable, and biomimetic character.⁷⁻¹²

Supramolecular polymers can be further subdivided into two main classes based on their mode of assembly. In the first class the monomers stack together through non-covalent interactions into fibrillar aggregates, whereas in the second one macromers with molecular recognition units interact to form networked structures. This thesis will focus on the former and explores the use of hydrogen bonding interactions in combination with hydrophobicity to drive monomer assembly in water.

1.1.2 Supramolecular polymerization mechanisms of stacked monomers

Supramolecular monomers can self-assemble into polymer structures through one of three mechanisms: ring-chain, isodesmic or cooperative (**Fig 1.1**).¹³⁻¹⁵ In this section, I will only focus on stacked aggregates that self-assemble through isodesmic and cooperative mechanisms.

The isodesmic mechanism involves the successive addition of monomers with the same binding constant to a growing polymer chain.¹⁶ The addition of each monomer results in an equivalent decrease in free energy with monomer affinity being independent of the length of the polymer. The polymers formed according to this mechanism are polydisperse and there is a lack of critical concentration and temperature.

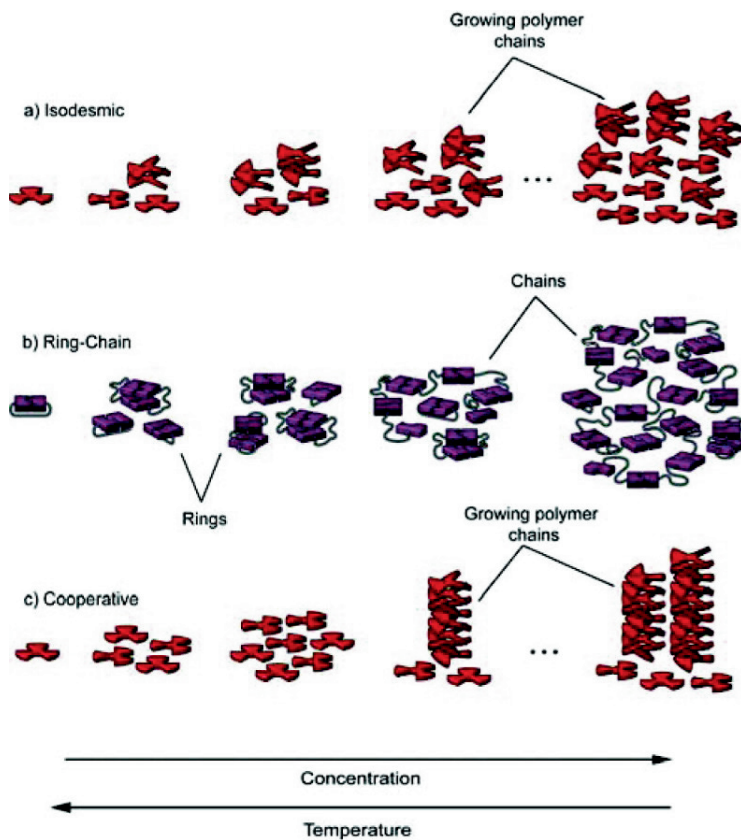


Figure 1.1 Mechanism of supramolecular polymerization: isodesmic (a), ring-chain (b), and cooperative (c). Figure adapted from reference 13

In the cooperative mechanism, supramolecular polymerization occurs in two steps, one involving formation of the nucleus of length s , that is often an unfavourable process and then an energetically favourable second step where elongation of the polymer occurs. Each of these steps are represented by their own binding constant; K_n for the nucleus formation and K_e for the elongation step. Additionally, the result of such polymerizations are nanostructures with a high degree of internal order. The degree of cooperativity of such polymerizations can be determined from the ratio of $\sigma = K_n/K_e$, when $\sigma < 1$ the polymerization is cooperative whereas polymerization with $\sigma > 1$ are anticooperative.

To determine the mechanism and to gain insight into the thermodynamic properties of the polymerization, several experiments can be performed and

then fit with the various models that rely on input parameters involving: i) concentration ii) temperature or iii) solvent-based changes.^{13, 15} Changes in polymerization are followed by spectroscopic methods such as circular dichroism (CD), ultraviolet (UV), nuclear magnetic resonance (NMR) or infrared (IR) spectroscopy.^{15, 17} From these experiments, the fraction of polymerized material, (ϕ) as a function of the changing parameter, monomer concentration, temperature, or good solvent, can be determined yielding insight into the polymerization mechanism.

Whereas the sigmoidal curves are obtained for isodesmic polymerizations, sharper and asymmetric curves are obtained for cooperative polymerizations. For cooperative growth, the thermodynamic models consider the formation of an initial nucleus with an unfavorable binding constant, followed by an elongation step with a very high binding constant.¹⁷ For example, the mean-field chemical equilibrium model developed by Goldstein and Stryer¹⁸ describes the two stages of a cooperative polymerization process ($\sigma=K_n/K_e < 1$) by their equilibrium constants, K_n and K_e . The equilibrium constant of elongation can be defined as $K_e = \exp(-\Delta G_0'/RT)$ where ΔG_0 is the Gibbs energy gain for each successive monomer, R is the gas constant and T is temperature. Meijer and coworkers¹⁹ expanded this model to consider the effect of a 'good' solvent on the supramolecular polymerization process and where a linear relationship between the Gibbs free energy and solvent volume fraction is observed:

$$\Delta G_0' = \Delta G_0 + m \cdot f$$

where f is volume fraction of the good solvent and ΔG^0 is the Gibbs free energy gain upon monomer addition in the pure solvent.

In this study, both simulations and predicted models demonstrate the presence of a critical solvent composition for a cooperative polymerization ($\sigma < 1$) and the lack of it for an isodesmic polymerization ($\sigma = 1$). Additionally, the obtained values for ΔG^0 and σ agreed with temperature-dependent analysis enabling extrapolation of the thermodynamic parameters such as the nucleation enthalpy, elongation enthalpy (ΔH_{nucl} , ΔH_{el}) and the entropy (ΔS) that can be used to calculate the two binding constants and the cooperativity factor.^{20, 21}

Electronic, structural and hydrophobic effects are known to be involved in cooperative growth of supramolecular polymers, often in combination with one another. C_3 -symmetric monomers based on 1,3,5-benzenetricarboxamides have been demonstrated to self-assemble through a cooperative mechanism. The molecular origin of cooperativity in this system arises due to the three amide units that engage in hydrogen bonding and π - π stacking of the aromatic rings.^{22, 23} In the case of OPV (oligo(p-phenylenevinylene)), the formation of supramolecular polymers in chloroform was achieved through π - π interactions of the aromatic core and the hydrogen bonding of the attached ureidotriazines driven by the structure.²⁴ Conversely in aqueous solution, cooperativity is driven by the hydrophobic effect. Fernandez and coworkers explored this effect investigating the self-assembly of oligophenyleneethynylenes (OPE)-based bolaamphiphiles functionalized with poly(2-ethyl-2-oxazoline) (PEtOx) moieties of different lengths.²⁵ While the more water soluble derivatives self-assembled in spherical aggregates by an isodesmic mechanism, the formation of 2D anisotropic platelets according to cooperative mechanism were determined by the self-assembly of the molecules with shorter PEtOx chains.

Although most mechanistic investigations are performed in organic solvents, the growing interest in the self-assembly in supramolecular biomaterials that are self-assembled in water calls for more investigation into understanding their aggregation processes. In the next section, the effect of the monomer designs on their self-assembly behavior and application is discussed.

1.1.3 Characterization of supramolecular polymers

Spectroscopic methods can assist in revealing the supramolecular polymerization mechanism of the monomers in their response to a particular stimulus (e.g. heat, solvent), but they can also provide the much needed insight into arrangement of the monomers and non-covalent interactions between them. For monomers containing a chromophore, UV-Vis spectroscopy can be used to pinpoint their arrangement (e.g. stacking face-to-face or slipped) in the polymers by comparing blue and/or red-shifting and increase or decreased intensity of the monomer bands relative to the absorbance spectrum of the polymer.¹⁵ Wurthner and coworkers investigated the intramolecular aggregation of a series of bis(merocyanine) dyes by UV-Vis spectroscopy revealing a marked hypsochromic shift as a consequence of the π - π -stacking disposition of the dyes on aggregation.²⁶ Circular dichroism can be used to understand the influence of chiral substituents in directing supramolecular polymer (e.g. sergeants and soldiers²⁷) assembly by examining increases in signal intensity. Infrared spectroscopy can be used to understand if hydrogen-bonding interactions are present between the monomers following changes in absorbance of the N-H and C=O stretch regions. Bouteiller and coworkers exploited the infrared spectroscopy to investigate the cooperativity in the self-assembly of bis-urea based supramolecular polymers²⁸ Nuclear magnetic resonance experiments can confirm such interactions in the solution²⁹ and solid state³⁰ depending on solvent, but also monomer stacking looking at aromatic ring protons in response to changes in concentration or solvent composition.³¹ Often such experiments are used collectively to understand how monomers interact through non-covalent interactions at the molecular level.

To further characterize supramolecular polymer morphology at the nano- and microscales, imaging techniques such as scanning (SEM) and transmission electron (TEM), atomic force (AFM) and stochastic optical reconstruction microscopy (STORM) can be used. SEM and conventional TEM require the use of electrons either being reflected or removed, or transmitted through the sample, respectively to image dried supramolecular polymer samples. AFM involves scanning of the supramolecular polymer surface by a sharp tip connected to a cantilever interfaced with a laser light that is reflected onto a photodiode yielding an image that reveals the morphology of the aggregates. These imaging techniques have been used within the field to analyze the

morphology of concentrated³² and dilute solutions³³ of supramolecular polymers from a range of solvents, however use of dried samples and staining artifacts (e.g. through use of heavy metals) can play a role in the observed structures.¹⁵ Alternatively, this issue can be mitigated in water using the cryo-EM technique, where the rapid cooling (vitrification) of the sample is executed to enable its visualization.³⁴ More recently, STORM has been used to understand the structure and dynamics of supramolecular polymers in water. The technique relies on the use of fluorescently labelled supramolecular monomers that are switched on and off in multiple cycles and their localization enables the reconstruction of a high resolution image with sub-diffraction resolution on the nanometer scale.^{35, 36} As an example, Albertazzi and coworkers use this technique to study the self-assembled peptide nanostructure³⁷ unmasking the dynamic nature of supramolecular polymers.

Light scattering techniques are also routinely used to probe the morphology and internal order of supramolecular polymers. Small angle X-ray or neutron scattering (SAXS/SANS) are frequently performed on solution phase samples. This technique measures the scattering cross section of a sample subtracting the scattering of the solvent.³⁸ With the mathematical equations, information on the size, shape, and internal diameters of self-assembled objects are obtained.³⁹ Previously, we determined the cross sectional mass (M_L) of the squaramide-based tripodal and bolaamphiphile assemblies by SAXS.^{40, 41} Specifically, the transition from bolaamphiphile to tripodal monomer geometry resulted in a reduction M_L and thus, the number of monomers in the cross-section from approximately 10-30 molecules to a single monomer, a reduced lateral aggregation and an increased fiber length. Often labeling and the staining of the supramolecular polymers can be circumvented due to sufficient contrast. Additionally, through static light scattering (SLS) information regarding morphology and the critical aggregation concentration (c_{ac}) of the monomers to form polymers can be determined.⁴² For certain monomers above a critical concentration gel phase materials can be formed through entanglement or physical interactions between supramolecular polymers.⁴³ Oscillatory rheology can be used to characterize the bulk mechanical properties of hydrogel materials, such as stiffness, viscoelasticity or strain stiffening.^{44, 45} These properties are highly relevant to understand for their applications in the biomedical field, such as in 3D cell culture.⁴⁶ The group of Dankers and coworkers designed Upy-based hydrogels where changing the

ratio between molecules with a bivalent (B) and monovalent (M) presentation modulating the viscoelastic properties for its application as a cell scaffold.⁴⁷

1.2 Supramolecular monomers

In aqueous media, the self-assembly process of amphiphilic monomers is driven mainly by the hydrophobic effect, in combination with other forces such as hydrogen bonding and π - π interactions. Commonly applied monomer geometries are tripodal, C_3 -symmetric and linear. These are described in the following paragraphs.

1.2.1 Bolaamphiphile monomers

Bolaamphiphiles are a class of amphiphilic molecules characterized by two hydrophilic head groups connected by a hydrophobic spacer that can self-assemble into several stable nanostructures such as micelles, fibers, tubes, cylindrical aggregates.⁴⁸ In the literature, a wide variety of bolaamphiphile scaffolds based on molecular building blocks such as peptides, carbohydrates and lipids can be found.⁴⁹ Although a major application focus is based on pharmaceutical formulations, there is a growing interest for their abilities to self-assemble in stable nanostructures. The properties and structures of these assemblies are tuned by length of the central hydrophobic core or the type of hydrophilic head groups.

In biomedical field since many drugs suffer of very low solubility in water, bolaamphiphile architectures are considered promising candidates for drug delivery applications. For example, Sharma and coworkers reported the self-assembly of a series of symmetric bolaamphiphiles with distinct hydrophilic domains (polyethylene glycol (PEG) or dendritic polyglycerol (dPG)) and examined their potential as nanocarriers (**Fig. 1.2a**).⁵⁰ Moreover, Jianxi and coworkers explored the use of a bolaamphiphile scaffold consisting of peptides to prepare collagen mimetic materials.⁵¹ A family of peptides consisting of the triple helical collagen sequence ((GPO)_m or (PPG)_m) with aspartic acid groups at its periphery was synthesized forming nanospheres in a broad pH range.

In contrast to conventional bolaamphiphiles, asymmetric bolaamphiphiles are characterized by two hydrophilic head groups of different size. They can contain a functional moiety with a cell-targeting⁵² or pH-sensitive function that can be used for specific gene and drug delivery applications.⁵²⁻⁵⁴ For example, Cui and coworkers designed a reverse asymmetric bolaamphiphile (RAB) tagged with an metalloproteinases (MMP-2) cleavable peptide to engineer enzyme-responsive supramolecular hydrogels.⁵⁵ The structure was characterized by two different peripheral hydrophobic units that were MMP-2 sensitive (**Fig. 1.2b**). Since most supramolecular filaments lack accessibility to enzymes, this work demonstrates successful fiber degradation by MMP-2 with additional anticancer drug release.⁵⁵

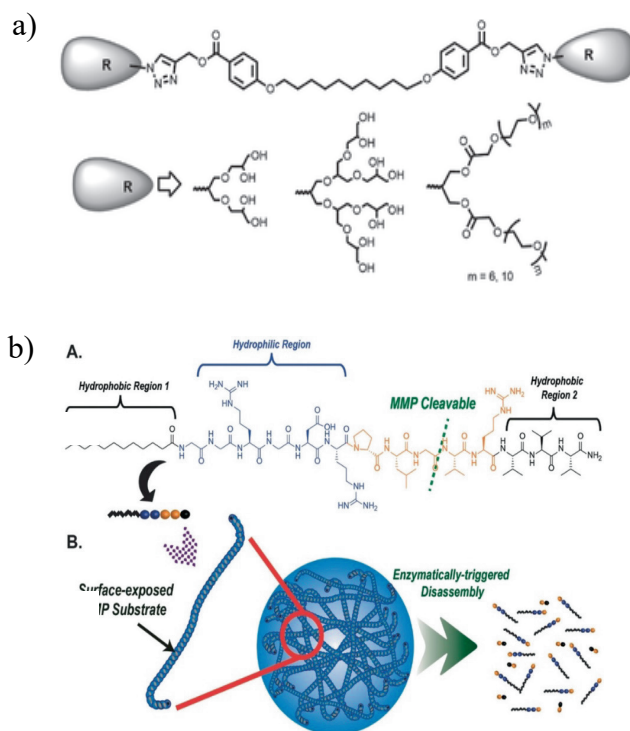


Figure 1.2 a) Pegylated (PEG) and dendronized (dPGs) symmetrical bolaamphiphiles for drug delivery applications. b) Molecular design of asymmetric reverse bolaamphiphile (RAB). The monomers self-assemble in water forming hydrogels and are degraded in presence of MMP-2 (metalloproteinases). Figure adapted from reference 28 (a), 29 (b).

1.2.2 C_3 -symmetric and tripodal monomers

Monomers bearing C_3 –symmetric cores are one of the most often used and exploited geometries in the formation of self-assembled supramolecular polymer materials. The main reasons for their use are the easy and established synthetic protocols that enable the modification of C_3 -symmetric synthons, the formation of helical supramolecular aggregates and cooperativity in comparison to their C_2 -symmetric counterparts.^{56,57} More specifically, their rigidity compared to their non-helical counterparts, results in their entanglements forming gel phase materials in a range of solvents. When in water, the hydrophobic environment shields the hydrogen-bonding units from the surrounding solvent.⁵⁸ Concentration also plays an important role, with its increase resulting in gel phase materials.

An often-used core is 1,3,5-benzenetricarboxamide (BTA) whose self-assembly is predominantly driven by π - π stacking of the aromatic core and the formation of the intramolecular hydrogen bonds between the amide units. Initially, the investigation of the BTAs self-assembly, and their supramolecular polymerization, was performed in organic solvents.^{22,23} More recently, the self-assembly of pegylated BTAs in aqueous solution has opened up numerous potential biomedical applications. Besides fundamental studies on supramolecular polymerization,⁵⁹⁻⁶¹ BTA-based assemblies were used for intracellular drug delivery (**Fig. 1.3a**).⁶² Moreover Webber and coworkers explored the effect of pH on the self-assembly of isopeptide-modified BTAs.⁶³ Connecting the BTA core to glutamic acids by benzoic acid linkers, the effect a pH stimulus on the morphology of supramolecular polymers was examined (**Fig. 1.3b**). Rapid acidification with HCl resulted in the formation of highly branched entanglements, whereas the slow acidification with D-glucono-delta-lactone (GdL) enabled a more thermodynamic self-assembly process with the formation of a less interconnected structure.

van Esch and coworkers explored the effect of catalysis on the reaction coupled self-assembly of cyclohexane-based low molecular hydrogelators (**Fig. 1.3c**). Hydrazone bond formation between a cyclohexane trishydrazide building block and three aldehydes was executed in presence and in absence of a catalyst (acid and base) to obtain in situ fiber self-assembly and gelation and their mechanical properties were assessed. Scanning electronic microscopy confirmed the formation of a dense homogeneous network in the

catalyzed systems, while a less dense and more open network was formed in the absence thereof.⁶⁴

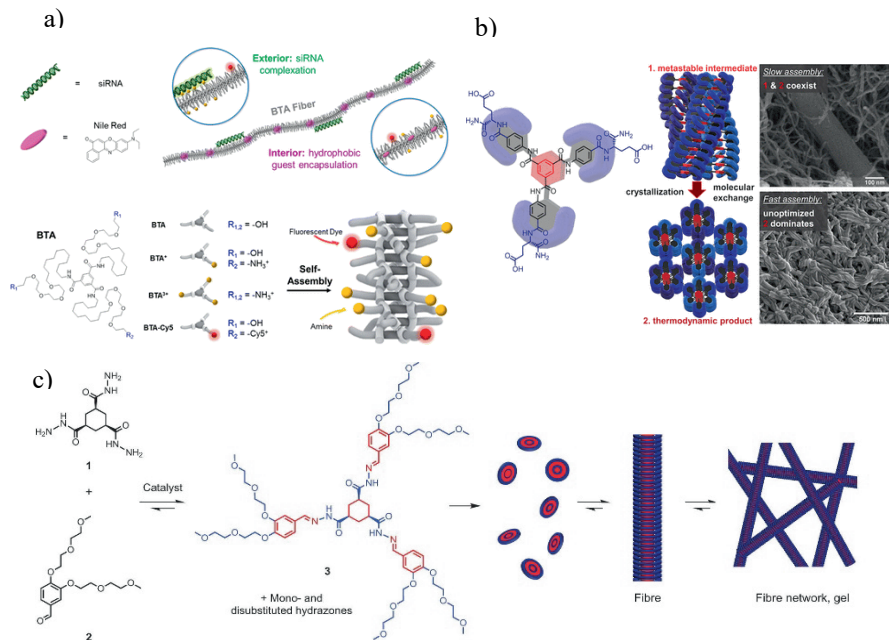


Figure 1.3 a) BTA supramolecular polymers for applications in intracellular delivery. The system was prepared through co-assembly of nonfunctional, positively charged, and fluorescently-labeled BTA monomers; b) Self-assembly of BTA-(bE)₃ monomer in water varying the rates of pH stimulus; c) Reaction-coupled self-assembly between cyclohexane trishydrazide building block (1) and three molecules of aldehydes (2). The formation of hydrazone bond gives the formation of fibers. Figures adapted from references 40 (a), 41 (b) and 42 (c).

Next, the effect of crosslinking by DNA and PEG on the properties of a cyclohexyl trishydrazide core-based hydrogel was investigated.⁶⁵ The addition of 1 mol% of DNA-crosslinkers showed a 4.5-fold increase of the stiffness of the native hydrogel while at higher percentage (2 and 3 mol%) a decrease in stiffness was reported. Oscillatory rheology and their structures imaged by cryoTEM and CSLM revealed the presence of spherical aggregates or a collapsed network at higher concentrations of crosslinkers. In contrast, the presence of 1 mol% PEG crosslinkers resulted in the formation of weaker hydrogel in comparison to the native material. These findings reveal that the physical properties of the polymer and the concentration of crosslinkers are

critical in the hydrogelation process and on the final mechanical properties of the materials.⁶⁵

1.2.3 Peptide-based monomers

A monomer class that has gained the attention of chemists for the development of supramolecular biomaterials is based on peptides. Their ability to be biodegradable, biocompatible and to adopt a range of nanostructures makes them attractive for numerous applications in the biomedical domain.⁶⁶⁻⁶⁸

Peptide-based self-assembly is dictated by a combination of several non-covalent interactions such as hydrogen bonds, π - π , van der Waals, hydrophobic and electrostatic interactions. Functional groups such as amides, amines and carboxylic acids in the peptides facilitate hydrogen bond interactions which facilitate the formation of higher order peptide structures.⁶⁹ Moreover, the π - π stacking contribution of aromatic side groups is relevant not only in water, but also in organic solvents such as toluene where this effect plays an important role.

Peptide-based scaffolds have been actively employed as mimics of the natural extracellular matrix.^{70, 71} The main classes of peptide-based hydrogels are: short oligopeptides, peptides with secondary structure and peptide amphiphiles. Individual amino acids or dipeptides protected with Fmoc (fluorenylmethyloxycarbonyl) group are already able to self-assemble in well-defined structures.⁷² The self-assembly is determined by the combination of π - π interactions from the Fmoc group and hydrogen bonds from the amides.⁷²⁻⁷⁴ Tyrosine dipeptides also belong to this class and self-assemble into nanofibers.⁷⁵

In the second class, the formation of specific secondary structures such as beta-sheet, alpha-helix, and beta-hairpin gives rise to self-assembled nanofibers that can form a 3D network in water.⁷² Alternating hydrophobic and hydrophilic residues in combination with electrostatic interactions can facilitate this process.⁷⁶ This family of peptides has been employed for cell culture, namely cell adhesion and osteogenic differentiation.^{77, 78}

Peptide amphiphiles are the third class, and are characterized by a charged, beta-sheet and bioactive domain peptide sequence coupled to an aliphatic or aromatic spacer (**Fig 1.4**). In the last decade it was extensively studied not

only how to modulate their self-assembly behaviour changing the aliphatic spacer, the aminoacids, the solvent, the co-assembly with other molecules, but also their potential in tissue engineering.^{79, 80}

The co-assembly of two or more peptides is gaining a particular attention to tune the mechanical properties of peptide-based supramolecular systems.⁸¹⁻⁸³ According to the type of monomers that are combined and the type of interactions between them (aromatic, electrostatic, enantiomeric and enzymatic), either cooperative, disruptive co-assembly and self-sorting can take place.⁸⁴ In cooperative co-assembly, the final properties of the materials are generally improved in comparison to the single component systems. When the two components interfere with one another in the self-assembly process, weaker mechanical properties of the materials are observed and is called disruptive co-assembly. When the components self-assemble independently of one another, this phenomenon is called self-sorting.

Adler-Abramovich and coworkers explored the cooperative co-assembly of the gels formed by Fmoc-FF (Fmoc-diphenylalanine) and Fmoc-pentafluorophenylalanine. The mixing of these two components in a 1:1 molar ratio gave rise to a hybrid hydrogel having a stiffness with an order of magnitude greater than the single component systems.^{81, 85}

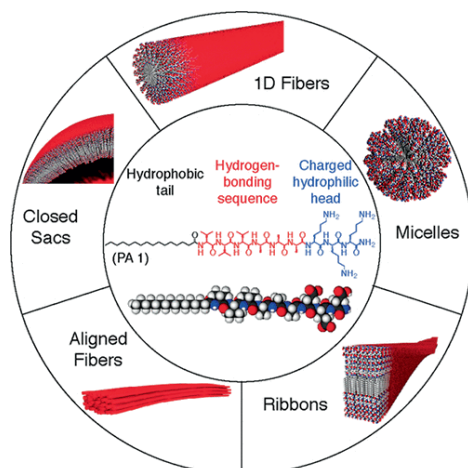


Figure 1.4 Chemical structure of the peptide amphiphile (PA) (center): charged, hydrogen-bonding sequences are coupled to an aliphatic spacer. Possible supramolecular nanostructures are presented surrounding the PA. Figure adapted from reference 57.

1.2.4 Hydrogen bonding interactions

Although an isolated hydrogen bond is typically too weak to control self-assembly, the combination of several hydrogen bonds results in a selective, directional non-covalent interaction to control self-assembly in solution.⁸⁶ Consequently, triple hydrogen bonding arrays have been investigated extensively for the formation of stable aggregates.⁸⁷⁻⁹⁰

Despite a linear correlation between the free energy and the number of hydrogen bonds in a monomer,⁹¹ the type of hydrogen bond, secondary interactions, and the solvent also need to be considered for their effect on strength of such systems. Moreover, the acidity of hydrogen bond acceptor and basicity of the hydrogen bond donor play a key role on the interaction.⁹² Generally, the more basic the hydrogen bond acceptor (A) is and the more acidic the hydrogen bond donor (D) is, the stronger will be their interaction.⁹³

Another important factor to consider are the secondary interactions between adjacent hydrogen bond donor and acceptor groups; this feature has an effect on the association constants of the monomers and on the stability of their interactions.⁹⁴ The order of donors and acceptors DDAA, results in an association constant ($K_a = 10^5 \text{ L mol}^{-1}$) that is three orders of magnitude greater than when the order is DADA ($K_a = 10^2 \text{ L mol}^{-1}$). This difference in association constants can significantly impact the stability of the formed self-assembled polymers (**Fig 1.5a**).

The solvent further plays a critical role in affecting the stability of the self-assembly monomers formed. Although in organic solvent the formation of well-defined architectures can be controlled by the combination of several non-covalent interactions,⁵⁸ in water hydrogen bonds are often weakened because the solvent molecules compete with the monomers. Therefore, hydrogen bonds have been combined with the hydrophobic effect in monomer design to drive monomer assembly into well-defined structures.^{95, 96} In BTA assembly, the hydrogen-bonded amides of adjacent aromatic cores are shielded by an aliphatic or aromatic spacer to drive self-assembly in water.⁹⁷ A similar same design strategy has been applied to drive the self-assembly of bisurea derivatives in water. Boué and coworkers have demonstrated the importance of hydrophobic spacer for the formation of hydrogen bonds between the ureas units.⁹⁸

More recently, the effect of the aromatic character on hydrogen bonding in supramolecular systems has been examined. The effect of aromaticity on multiarray hydrogen bonding scaffolds was examined by the Wu group.⁹⁹ They showed through DFT calculations that heterocycles that participate in $4n+2$ π -delocalization show increased hydrogen bonding strength than those that do not (**Fig 1.5b**). The limitation of SEI (secondary electrostatic interaction) model introduced by Zimmermann, based on the hydrogen bond donor/acceptor pattern was demonstrated through BLW (block-localized wavefunction) calculations showing a linear correlation between the aromatic gain and association constant of multiarray hydrogen bond scaffolds further highlighting its importance.⁹⁹ Moreover, in the Kieltyka group, the contribution of aromaticity to squaramides in their self-assembly in aqueous media was uncovered.⁴⁰ Hydrogen-bonded squaramide monomers showed an increase in the aromatic character of the synthons pointing out the interplay of these two variables on supramolecular polymerization of such monomers.

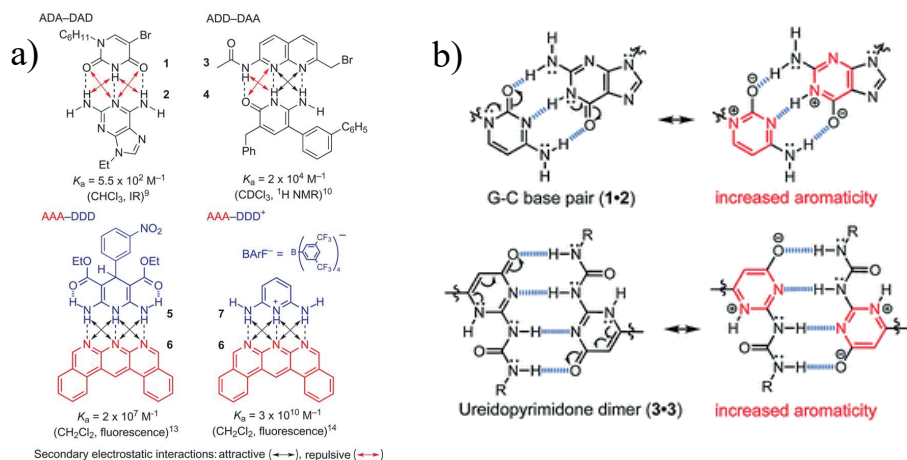


Figure 1.5 a) Examples of triple hydrogen-bond arrays and their association constants in various solvents. b) Aromaticity-modulated hydrogen bonding (AMHB) in the guanine-cytosine (G-C) base pair, 1·2, and ureidopyrimidone (UPy) dimer, 3·3. Figures adapted from references 72 and 77.

1.3 Squaramides

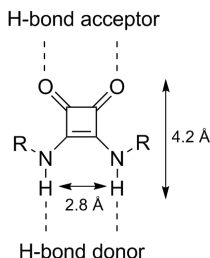


Figure 1.6 Chemical structure of squaramide moiety

Squaramides consist of a cyclobutenedione ring with two NH hydrogen bond donors opposite two CO hydrogen bond acceptors.¹⁰⁰ They can be easily synthesized from combining the desired amine with their commercially available squarate esters. Moreover, Liu *et al.* reported that their squarate ester precursors can be synthesized in high yield (77-97%) starting from squaric acid in the presence of a specific alcohol.¹⁰¹ Because of their high synthetic accessibility, squaramides have been applied in areas such as catalysis, medicinal chemistry, bioconjugation, anion recognition and also in the field of supramolecular materials.^{102, 103}

In organocatalysis, squaramides have been applied using the hydrogen bond formation between the catalyst and the substrate to drive chemical transformation. The increased donor character of squaramide in comparison to thioureas results in the formation of stronger hydrogen bonds with various substrates.¹⁰⁴

Moreover, Bae and Song explored the addition of beta-carbonyl compounds to nitroolefins ‘on water’ using a cinchona squaramide as a catalyst.¹⁰⁵ The success of the reaction ‘on water’ compared to the reaction in DCM was due to the hydrophobic hydration effect of the catalyst. Notably, the isolated products showed very high stereoselectivity (90-93%) and yields (86-99%) at low catalyst loading (0.01 mol%).

Another area where the squaramide moiety has been used is in the bioconjugation chemistry. Recently diethyl squarate (DES) has been used as a novel chemical crosslinker for gelatin-based hydrogels. In particular Cipolla and coworkers examined the ability of 5% gelatin – DES as 3D cell culture scaffolds for chondrocyte growth.¹⁰⁶

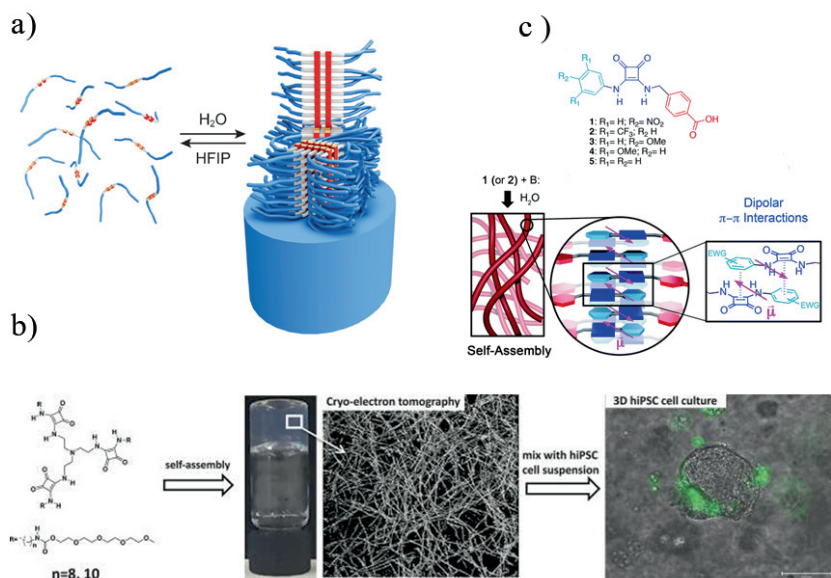
Additionally, squaramides have been applied as drug precursors in the field of medicinal chemistry because of their isosterism with ureas.¹⁰² Kitov and coworkers, for example, demonstrated the ability of di- and trisaccharides conjugated with squaramides to inhibit verotoxins produced by *E. coli* that cause gastrointestinal and urinary disorders.¹⁰⁷ Moreover, the chemoselectivity of squaric esters for the amino acid groups in the peptides were exploited in the synthesis of potential antitumor vaccines based on glycopeptides.¹⁰⁸

One of the peculiar properties of squaramide moiety is its partial aromatic character (Hückel's rule $(4n + 2) \pi$ electrons, $n = 0$, as a consequence of the delocalization of the nitrogen lone pair attached to the squaramide inside the cyclobutenedione ring.¹⁰⁹ In contrast to other H-bonding motifs such as urea,¹¹⁰⁻¹¹² thiourea or pyrimidones, the aromatic character of squaramide is enhanced in a synergistic manner with the formation of stronger and directional hydrogen bonding.¹⁰⁹ This remarkable property renders squaramide an attractive and minimalistic module for the design of supramolecular materials.¹⁰⁰ Kieltyka group for the first time demonstrated that the squaramide synthon can be used to drive the self-assembly of a squaramide-based bolaamphiphile into nanostructured fibers in water. More specifically, the combination of spectroscopic and computational studies (NICS, HOMA, ASE) confirmed how the synergy between the increased aromaticity of squaramide and stronger hydrogen bonds is determining in the self-assembly process of these polymers (**Fig.1.6a**).⁴⁰ In a follow up work, Kieltyka group reported a family of squaramide-based bolaamphiphiles where the length of the PEG chains and the aliphatic chains were independently modulated.¹¹³ It was shown that at least 8 carbons between undecaethylene glycol chains and the squaramides were critical to enable monomer self-assembly into fibrillar aggregates. In contrast, maintaining the length of the hydrophobic core and changing the length of the oligoethylene glycol chains resulted in a morphological transition from fibrillar to spherical aggregates opening the door to their exploration in the field of nanomedicine.¹¹³

Hydrogel materials could not be formed from the bolaamphiphilic monomers, therefore in a follow up work, squaramides were introduced into a tripodal monomer geometry to achieve such materials.⁴¹ Specifically, self-assembly of these tripods resulted in a decreased number of monomers within nanofiber cross-section, increased fiber length and hydrogelation. Moreover, the effect

of the hydrophobic spacer and introduction of a urea moiety in the place of the squaramide were examined, with spacer lengths of C8 and C10 providing hydrogel materials whereas the use of urea did not yield the same result. These hydrogels were also examined for their capacity to easily seed and release human induced pluripotent stem cell (hiPSCs) aggregates using the supramolecular nature of the material. High cell viability and retention of the pluripotent character of the hiPSCs were observed (**Fig.1.6b**).

Intermolecular hydrogen bonding between squaramides is not always involved in the self-assembly process. Soberats and coworkers demonstrated the self-assembly of squaramide-based monomers by the combination of hydrophobic effect and π - π dipolar interaction to form hydrogel materials.¹¹⁴ A small library of aryl-squaramide amphiphiles hydrogelators were prepared with a benzoic acid moiety making the molecule easily ionizable.¹¹⁴ The aromatic ring had different substituents, but only the electron-deficient ones can give rise to self-assembly. The absence of hydrogen bonding was confirmed by FT-IR and NMR measurements due to the lack of an N-H signal at 3160 cm^{-1} . In NMR spectra, the aromatic protons were shielded and no N-H signal was present in water (**Fig. 1.6c**).¹¹⁴



1.4 Thiosquaramides

Thiosquaramides are prepared from oxosquaramides by a thionation reaction that involves the exchange of oxygen for sulfur on the cyclobutenedione ring. The thiosquaramide was synthesized for the first time in 1966 when N,N'-dicyclohexylsquaramide was thionated using diphosphorus pentasulfide in dichloromethane. More recent synthetic methods involve the use of pyridine complex (pentathiodiphosphorus(V) acid-P,P'-bis(pyridinium betaine))).¹¹⁵

From supramolecular point of view, thiosquaramides form less directional hydrogen bonds in comparison to oxosquaramides due to the more polarizable nature of thiocarbonyl groups. According to Cambridge structural database (CSD), C=S \cdots H interactions show an angle of almost 90° from the lone-pair

plane, in contrast with the $C=O\cdots H$ interactions where small deviations from the lone pairs plan were observed ($0-20^\circ$).¹¹⁶

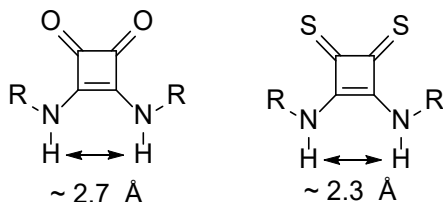


Figure 1.7 Chemical structure of squaramide and thiosquaramide

Several works have shown oxosquaramides to be excellent catalysts in enantioselective reactions because of their ability to form very strong hydrogen bonds.¹¹⁷ However, oxosquaramides are characterized by low solubility in non-polar solvents due to the self-aggregation.¹¹⁷ This issue is solved by substitution of carbonyl by the thiocarbonyl group resulting in its increased solubility in apolar solvents opening the door for its use in organocatalysis.¹¹⁷

Pedrosa and coworkers reported the synthesis of chiral, bifunctional thiosquaramide catalysts that were applied in nitro-Michael addition of 3,3-disubstituted oxindole to beta-aryl substituted nitroalkenes.¹¹⁸ In comparison to thiourea and oxosquaramide catalysts, high reaction yields (82%) and enantioselectivity (94:6) using a catalyst loading of 5 mol% was demonstrated. The enantioselectivity of thiosquaramide was also demonstrated by Kupai and coworkers in an asymmetric Michael reaction between 2,4-pentanedione and trans-nitrostyrene, and a Diels-Alder reaction between siloxydiene and benzylideneacetone.¹¹⁹ Although oxo and thio derivative cinchona catalysts provided the same yield (90 %) in both reactions, the thiosquaramide showed improved enantioselectivity over the oxo (99% ee compared to 93% ee).

Earlier publications demonstrated the ability of oxosquaramide to act as an ion transporter as an alternative to ureas and thioureas.¹²⁰ More recent works show that thioureas have an improved capacity to transport ions in comparison to ureas because of the increased acidic character of NH and greater lipophilicity of sulfur atom.¹²¹ Bussacaert showed that thiosquaramide-based transporters demonstrate a pH-dependent ion transport behavior.¹²¹ The ion transporter was synthesized by a thionation reaction using the pyridine complex

(pentathiodiphosphorus(V) acid-P,P'-bis(pyridinium betaine). While anion transport is favored in acidic conditions ($\text{pH} < 7$), at high pH ($\text{pH} > 7$) deprotonation of thiosquaramide occurs promoting anion release.

Although thiosquaramides have been examined for use in organocatalysis and anion transport, they have not been explored for the self-assembly of supramolecular polymers.

1.5 Multicomponent reaction

Most of the synthetic pathways for the preparation of supramolecular monomers are characterized by several synthetic steps. In the case of peptide-based materials with various functionalities, the synthesis of peptides on solid phase is low yielding and costly on a large scale. Thus, it is necessary to find a methodology that improves the synthetic efficiency of such monomers.

Multicomponent reactions (MR) involve the reaction of 3 or 4 components under mild conditions with high yield and selectivity in one pot with high atom efficiency. This strategy is in contrast to a multistep synthetic approach, where the product of each reaction step is the reagent for the next reaction. In a multicomponent reaction, all the synthetic steps are condensed in one reaction. This approach avoids the challenges related to the purification and, isolation of the formed chemical compounds, which are typical of other synthetic strategies.¹²² Commonly used reagents in these reactions are amines, carboxylic acids, isonitriles, aldehyde or ketones. The most widely used multicomponent reactions are the Ugi, Passerini and Biginelli reactions that have been known for more than 100 years.¹²³ With these methodologies it is possible to make large libraries of compounds with minimal synthetic effort. Multicomponent reactions are considered to be an important approach to design and discover biologically active scaffolds.¹²⁴ Moreover, the structural complexity on MCR compound can be increased by post-modification with bifunctional or multifunctional scaffolds. When this approach is used, MCR compounds can then be involved in another MCR.¹²⁵

One of the main applications of MCRs is related to the synthesis of stapling peptides and their macrocyclization. This compounds class can be applied as antimicrobials, anticancer agents and enzyme inhibitors¹²⁶ and are usually

synthesized by click chemistry or lactamization. By an MCR approach, it is possible to obtain compounds with high structure diversity.¹²⁷

An important class of multicomponent reactions involves the reactive isocyanide group that is often found in peptide chemistry. The first isocyanide-based MCR, discovered in 1921 was the Passerini reaction that has been extensively used for the synthesis of cyclic peptides.¹²⁸ This reaction is performed in presence of isocyanide, aldehyde and carboxylic acid, resulting in the formation of an ester bond. Another important reaction that belongs to this class is the Ugi reaction that will be discussed in the following section.

1.5.1 Ugi reaction

The Ugi reaction is an isocyanide based-multicomponent reaction that involves the use of an amine, carboxylic acid, isocyanide, and aldehyde or ketone. The formation of the final compound that has a peptide-like structure is due to the reactivity of isocyanide that reacts with both electrophiles or nucleophiles to form alpha-adducts. The mechanism starts with the condensation of the aldehyde or ketone with an amine, forming an imine that is protonated by a carboxylic acid. Imine formation is then followed by nucleophilic attack of the isocyanide and addition of the carboxylic acid to give rise to the formation of a nitrilium intermediate. In a final step, an irreversible Mumm rearrangement takes place resulting in the alpha-amide product (**Fig. 1.8a**).¹²⁹

The high yield, selectivity and mild reactions conditions render the Ugi reaction a useful synthetic strategy for a wide variety of applications. This reaction has been applied in post polymerization reactions that are difficult to perform by conventional strategies due to the steric hindrance of the polymeric chains.¹³⁰ Moreover, polymers formed by the Ugi reaction have also been reported and exploited in the synthesis of α,ω -diene monomers by Meier et coworkers¹³¹ and acrylate monomers.¹³²

The generation of peptide-like structures, or peptidomimetics, by the Ugi reaction is gaining attention. Classical solid-phase peptide synthesis is often low yielding and can be costly depending on the peptide sequence. The Ugi reaction provides an alternative to this approach in the synthesis of polypeptoids and hybrid copolymers such as peptide-peptoids for applications in biomedicine.¹³³⁻¹³⁶

In supramolecular chemistry, the Ugi reaction was exploited in the synthesis of peptoid-based low molecular hydrogelators. Mild conditions were used and very high yields were obtained for a small family of low molecular gelators, and their capacity to gelate in aqueous solutions such as water/DMSO and in water/EtOH mixtures (20 % of organic solvent) was examined.¹³⁷ The Ugi reaction has found several application in the covalent functionalization of supramolecular materials (**Fig.1.8b**).¹³⁸ Mironov and coworkers exploited the Ugi reaction to crosslink microgels of cellulose. With this synthetic method particles with a diameter in a range of 170-230 nm were obtained and used as stabilizers for oil/water emulsions.¹³⁹

These preliminary results have opened new possibilities in the design of new supramolecular biomaterials where their synthesis is challenged by low yields and efficiency.¹³⁷

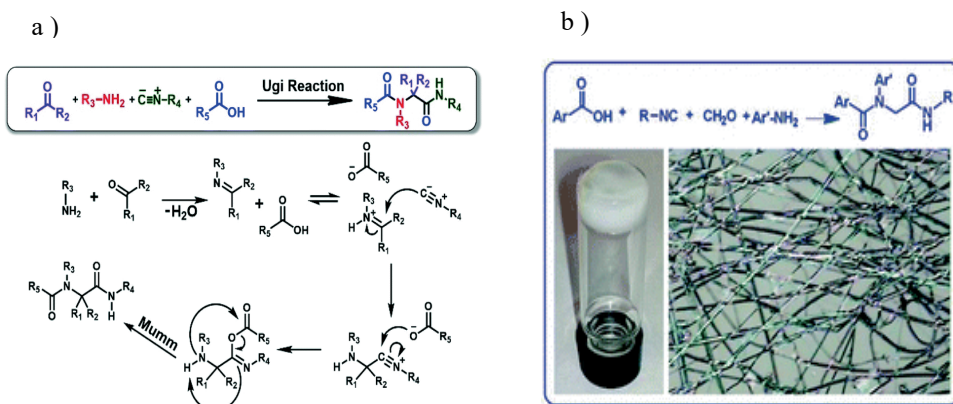


Figure 1.8 (a) Mechanism of Ugi reaction; (b) A small family of supramolecular hydrogelators synthesized by Ugi reaction. Figure adapted from reference 109 (a) and 117 (b).

1.6 Aim and outline

The field of squaramide-based supramolecular polymers has been growing steadily over the past few years. The remarkable ability of squaramide moiety to form directional hydrogen bonds that can synergistically benefit from an increase in their aromatic character, can be exploited in the design of supramolecular biomaterials. In water, the self-assembly of stable nanostructures is largely driven by the hydrophobic effect in combination with hydrogen bonding determining the final properties of the nanostructures. The formation of a particular nanostructure depends on several variables such as the chemical structure of the building block, if any other building blocks are used and the environmental conditions. Moreover, as the synthesis of the building blocks can be challenging and costly, and thus novel strategies to synthesize tripodal squaramide supramolecular polymers such as using multicomponent strategies will be examined.

In **Chapter 2**, the substitution of O \rightarrow S in squaramide monomers for supramolecular polymerization results in the formation of rod-like nanostructures with a decreased persistence length. This morphological difference results from the less directional hydrogen bonds afforded by the thiocarbonyl group, resulting in a distinct self-assembly mode. From computational and UV-vis studies the oxosquaramide can self-assemble in a head-to-tail manner, while thiosquaramide prefers a stacked configuration. In this chapter, we investigated the supramolecular polymerization mechanism of oxosquaramide and thiosquaramide-based bolaamphiphiles using a concentration-based experiment. Moreover, the effect of the mixing of both monomers and their potential for co-assembly or self-sorting in aqueous solution is examined.

In **Chapter 3**, a new approach for the synthesis of tripodal squaramide-based supramolecular polymers by multicomponent reaction will be disclosed. The Ugi reaction will be examined for the synthesis of tripodal scaffolds using nitrilotriacetic and squaric acid as the acidic component of the reaction. In this

chapter, the optimal reaction conditions such as reagent concentration, temperature and substitution of the components will be examined.

In **Chapter 4**, the synthesis of a small family of tripodal squaramide-based supramolecular polymers is described and their self-assembly in water was investigated. The monomers have varied hydrophobic and hydrophilic ratios that affect their final self-assembly properties. Spectroscopic techniques (UV-vis, fluorescence), AFM and mechanical properties were used to understand the effect of the various monomer designs on these aggregates over various length scales.

In **Chapter 5**, the synthesis of dityrosine outfitted monomers with and without carbamate linkages and investigation of their self-assembly and visible light mediated crosslinking in the presence of photoinitiator is described. In the previous chapter, we found that even removal of one squaramide moiety from the core and further modulating the hydrophilic-hydrophobic balance can result in gels. Hence, we opted for removal of one squaramide arm because of the solubility of the tyrosine and bridged its attachment to the squaramide core with a tetraethylene glycol chain. The self-assembly was investigated by spectroscopic techniques (UV-vis, fluorescence) and by AFM in presence and absence of two different photoinitiators (FMN or $\text{Ru}(\text{bpy})_3^{2+}$ /SPS).

References:

1. Behera, A., Classification of Biomaterials used in Medicine. *Int. J. Adv. Appl. Sci.* **2012**, *1*, 125-129.
2. Ren, H.; Wu, L.; Tan, L.; Bao, Y.; Ma, Y.; Jin, Y.; Zou, Q., Self-assembly of amino acids toward functional biomaterials. *Beilstein J. Nanotechnol.* **2021**, *12*, 1140-1150.
3. Han, W.; Xiang, W.; Li, Q.; Zhang, H.; Yang, Y.; Shi, J.; Ji, Y.; Wang, S.; Ji, X.; Khashab, N. M.; Sessler, J. L., Water compatible supramolecular polymers: recent progress. *Chem. Soc. Rev.* **2021**, *50*, 10025-10043.
4. Rehm, T.; Schmuck, C., How to achieve self-assembly in polar solvents based on specific interactions? Some general guidelines. *Chem. Comm.* **2008**, 801-813.
5. Yang, L.; Tan, X.; Wang, Z.; Zhang, X., Supramolecular Polymers: Historical Development, Preparation, Characterization, and Functions. *Chem. Rev.* **2015**, *115*, 7196-7239.
6. de Greef, T. F. A.; Meijer, E. W., Supramolecular polymers. *Nature* **2008**, *453*, 171-173.
7. Webber, M. J.; Appel, E. A.; Meijer, E. W.; Langer, R., Supramolecular biomaterials. *Nat. Mater.* **2016**, *15*, 13-26.
8. Webber, M. J., Engineering responsive supramolecular biomaterials: Toward smart therapeutics. *Bioeng. Transl. Med.* **2016**, *1*, 252-266.
9. Stephanopoulos, N.; Ortony, J. H.; Stupp, S. I., Self-assembly for the synthesis of functional biomaterials. *Acta Mater.* **2013**, *61*, 912-930.
10. Goor, O.; Hendrikse, S. I. S.; Dankers, P. Y. W.; Meijer, E. W., From supramolecular polymers to multi-component biomaterials. *Chem. Soc. Rev.* **2017**, *46*, 6621-6637.
11. Rosales, A. M.; Anseth, K. S., The design of reversible hydrogels to capture extracellular matrix dynamics. *Nat. Rev. Mater.* **2016**, *1*, 15012.
12. Webber, M. J.; Langer, R., Drug delivery by supramolecular design. *Chem. Soc. Rev.* **2017**, *46*, 6600-6620.
13. De Greef, T. F. A.; Smulders, M. M. J.; Wolffs, M.; Schenning, A. P. H. J.; Sijbesma, R. P.; Meijer, E. W., Supramolecular Polymerization. *Chem. Rev.* **2009**, *109*, 5687-5754.
14. Vill, R.; Gülcher, J.; Khalatur, P.; Wintergerst, P.; Stoll, A.; Mourran, A.; Ziener, U., Supramolecular polymerization: challenges and advantages of various methods in assessing the aggregation mechanism. *Nanoscale* **2019**, *11*, 663-674.
15. Hartlieb, M.; Mansfield, E. D. H.; Perrier, S., A guide to supramolecular polymerizations. *Polym. Chem.* **2020**, *11*, 1083-1110.

16. Aida, T.; Meijer, E. W.; Stupp, S. I., Functional Supramolecular Polymers. *Science* **2012**, *335*, 813-817
17. Rest, C.; Kandanelli, R.; Fernandez, G., Strategies to create hierarchical self-assembled structures via cooperative non-covalent interactions. *Chem. Soc. Rev.* **2015**, *44*, 2543-2572.
18. Goldstein, R. F.; Stryer, L., Cooperative polymerization reactions. Analytical approximations, numerical examples, and experimental strategy. *Biophys. J.* **1986**, *50*, 583-599.
19. Korevaar, P. A.; Schaefer, C.; de Greef, T. F. A.; Meijer, E. W., Controlling Chemical Self-Assembly by Solvent-Dependent Dynamics. *J. Am. Chem. Soc.* **2012**, *134*, 13482-13491.
20. ten Eikelder, H. M. M.; Markvoort, A. J.; de Greef, T. F. A.; Hilbers, P. A. J., An Equilibrium Model for Chiral Amplification in Supramolecular Polymers. *J. Phys. Chem.* **2012**, *116*, 5291-5301.
21. Markvoort, A. J.; ten Eikelder, H. M. M.; Hilbers, P. A. J.; de Greef, T. F. A.; Meijer, E. W., Theoretical models of nonlinear effects in two-component cooperative supramolecular copolymerizations. *Nat. Comm.* **2011**, *2*, 509, 1-9
22. Cantekin, S.; de Greef, T. F. A.; Palmans, A. R. A., Benzene-1,3,5-tricarboxamide: a versatile ordering moiety for supramolecular chemistry. *Chem. Soc. Rev.* **2012**, *41*, 6125-6137.
23. van Gorp, J. J.; Vekemans, J. A. J. M.; Meijer, E. W., C3-Symmetrical Supramolecular Architectures: Fibers and Organic Gels from Discotic Trisamides and Trisureas. *J. Am. Chem. Soc.* **2002**, *124*, 14759-14769.
24. Jonkheijm, P.; van der Schoot, P.; Schenning, A. P. H. J.; Meijer, E. W., Probing the Solvent-Assisted Nucleation Pathway in Chemical Self-Assembly. *Science* **2006**, *313*, 80-83.
25. Rudolph, T.; Kumar Allampally, N.; Fernández, G.; Schacher, F. H., Controlling Aqueous Self-Assembly Mechanisms by Hydrophobic Interactions. *Eur. Chem. J.* **2014**, *20*, 13871-13875.
26. Kirchner, E.; Bialas, D.; Wehner, M.; Schmidt, D.; Würthner, F., Bis(merocyanine) Homo-Folda-Dimers: Evaluation of Electronic and Spectral Changes in Well-Defined Dye Aggregate Geometries. *Eur. Chem. J.* **2019**, *25*, 11285-11293.
27. Smulders, M. M. J.; Schenning, A. P. H. J.; Meijer, E. W., Insight into the Mechanisms of Cooperative Self-Assembly: The “Sergeants-and-Soldiers” Principle of Chiral and Achiral C3-Symmetrical Discotic Triamides. *J. Am. Chem. Soc.* **2008**, *130*, 606-611.
28. Simic, V.; Bouteiller, L.; Jalabert, M., Highly Cooperative Formation of Bis-Urea Based Supramolecular Polymers. *J. Am. Chem. Soc.* **2003**, *125*, 13148-13154.

29. Shao, C.; Grüne, M.; Stolte, M.; Würthner, F., Perylene Bisimide Dimer Aggregates: Fundamental Insights into Self-Assembly by NMR and UV/Vis Spectroscopy. *Eur. Chem. J.* **2012**, *18*, 13665-13677.
30. Rest, C.; Philips, D. S.; Dünnebacke, T.; Sutar, P.; Sampedro, A.; Droste, J.; Stepanenko, V.; Hansen, M. R.; Albuquerque, R. Q.; Fernández, G., Tuning Aqueous Supramolecular Polymerization by an Acid-Responsive Conformational Switch. *Eur. Chem. J.* **2020**, *26*, 10005-10013.
31. Chen, Z.; Stepanenko, V.; Dehm, V.; Prins, P.; Siebbeles, L. D. A.; Seibt, J.; Marquetand, P.; Engel, V.; Würthner, F., Photoluminescence and Conductivity of Self-Assembled π - π Stacks of Perylene Bisimide Dyes. *Eur. Chem. J.* **2007**, *13*, 436-449.
32. Wang, F.; Zheng, B.; Zhu, K.; Zhou, Q.; Zhai, C.; Li, S.; Li, N.; Huang, F., Formation of linear main-chain polypseudorotaxanes with supramolecular polymer backbones via two self-sorting host-guest recognition motifs. *Chem. Comm.* **2009**, 4375-4377.
33. Leenders, C. M. A.; Albertazzi, L.; Mes, T.; Koenigs, M. M. E.; Palmans, A. R. A.; Meijer, E. W., Supramolecular polymerization in water harnessing both hydrophobic effects and hydrogen bond formation. *Chem. Comm.* **2013**, *49*, 1963-1965.
34. Murata, K.; Wolf, M., Cryo-electron microscopy for structural analysis of dynamic biological macromolecules. *Biochim. Biophys. Acta Gen. Subj.* **2018**, *1862*, 324-334.
35. Cox, H.; Georgiades, P.; Xu, H.; Waigh, T. A.; Lu, J. R., Self-Assembly of Mesoscopic Peptide Surfactant Fibrils Investigated by STORM Super-Resolution Fluorescence Microscopy. *Biomacromolecules* **2017**, *18*, 3481-3491.
36. da Silva, R. M. P.; van der Zwaag, D.; Albertazzi, L.; Lee, S. S.; Meijer, E. W.; Stupp, S. I., Super-resolution microscopy reveals structural diversity in molecular exchange among peptide amphiphile nanofibres. *Nat. Comm.* **2016**, *7*, 11561, 1-10.
37. Pujals, S.; Tao, K.; Terradellas, A.; Gazit, E.; Albertazzi, L., Studying structure and dynamics of self-assembled peptide nanostructures using fluorescence and super resolution microscopy. *Chem. Comm.* **2017**, *53*, 7294-7297.
38. Kikhney, A. G.; Svergun, D. I., A practical guide to small angle X-ray scattering (SAXS) of flexible and intrinsically disordered proteins. *FEBS Lett.* **2015**, *589*, 2570-2577.
39. Liu, J.; Schotman, M. J. G.; Hendrix, M. M. R. M.; Lou, X.; Marín San Román, P. P.; Voets, I. K.; Sijbesma, R. P., Effects of structural variation on the self-assembly of bis-urea based bolaamphiphiles. *J. Polym. Sci.* **2021**, *59*, 1162-1170.

40. Saez Talens, V.; Englebienne, P.; Trinh, T. T.; Noteborn, W. E.; Voets, I. K.; Kieltyka, R. E., Aromatic Gain in a Supramolecular Polymer. *Angew. Chem. Int. Ed.* **2015**, *54*, 10502-10506.
41. Tong, C.; Liu, T.; Saez Talens, V.; Noteborn, W. E. M.; Sharp, T. H.; Hendrix, M.; Voets, I. K.; Mummery, C. L.; Orlova, V. V.; Kieltyka, R. E., Squaramide-Based Supramolecular Materials for Three-Dimensional Cell Culture of Human Induced Pluripotent Stem Cells and Their Derivatives. *Biomacromolecules* **2018**, *19*, 1091-1099.
42. Wishard, A.; Gibb, B. C., Dynamic light scattering – an all-purpose guide for the supramolecular chemist. *Supramol. Chem.* **2019**, *31*, 608-615.
43. Mondal, S.; Das, S.; Nandi, A. K., A review on recent advances in polymer and peptide hydrogels. *Soft Matter* **2020**, *16*, 1404-1454.
44. Jaspers, M.; Dennison, M.; Mabesoone, M. F. J.; MacKintosh, F. C.; Rowan, A. E.; Kouwer, P. H. J., Ultra-responsive soft matter from strain-stiffening hydrogels. *Nat. Comm.* **2014**, *5*, 5808,1-8
45. Carberry, B. J.; Rao, V. V.; Anseth, K. S., Phototunable Viscoelasticity in Hydrogels Through Thioester Exchange. *Ann. Biom. Eng.* **2020**, *48*, 2053-2063.
46. Geckil, H.; Xu, F.; Zhang, X.; Moon, S.; Demirci, U., Engineering hydrogels as extracellular matrix mimics. *Nanomedicine* **2010**, *5*, 469-484.
47. Diba, M.; Spaans, S.; Hendrikse, S. I. S.; Bastings, M. M. C.; Schotman, M. J. G.; van Sprang, J. F.; Wu, D. J.; Hoeben, F. J. M.; Janssen, H. M.; Dankers, P. Y. W., Engineering the Dynamics of Cell Adhesion Cues in Supramolecular Hydrogels for Facile Control over Cell Encapsulation and Behavior. *Adv. Mater.* **2021**, *33*, 2008111, 1-16
48. Nuraje, N.; Bai, H.; Su, K., Bolaamphiphilic molecules: Assembly and applications. *Progr. Polym. Sci.* **2013**, *38*, 302-343.
49. Fariya, M.; Jain, A.; Dhawan, V.; Shah, S.; Nagarsenker, M. S., Bolaamphiphiles: a pharmaceutical review. *Adv. Pharm. Bull.* **2014**, *4*, 483-491.
50. Rashmi; Singh, A. K.; Achazi, K.; Schade, B.; Böttcher, C.; Haag, R.; Sharma, S. K., Synthesis of non-ionic bolaamphiphiles and study of their self-assembly and transport behaviour for drug delivery applications. *RSC Adv.* **2018**, *8*, 31777-31782.
51. Yao, L.; He, M.; Li, D.; Liu, H.; Wu, J.; Xiao, J., Self-assembling bolaamphiphile-like collagen mimetic peptides. *New J. Chem.* **2018**, *42*, 7439-7444.
52. Huang, Z.; Zhao, D.-M.; Deng, X.; Zhang, J.; Zhang, Y.-M.; Yu, X.-Q., Functionalized Asymmetric Bola-Type Amphiphiles for Efficient Gene and Drug Delivery. *Nanomaterials* **2018**, *8*, 115, 1-18

53. Grinberg, S.; Kipnis, N.; Linder, C.; Kolot, V.; Heldman, E., Asymmetric bolaamphiphiles from vernonia oil designed for drug delivery. *Eur. J. Lipid Sci. Technol.* **2010**, *112*, 137-151.
54. Jain, N.; Arntz, Y.; Goldschmidt, V.; Duportail, G.; Mély, Y.; Klymchenko, A. S., New Unsymmetrical Bolaamphiphiles: Synthesis, Assembly with DNA, and Application for Gene Delivery. *Bioconjugate Chem.* **2010**, *21*, 2110-2118.
55. Chakroun, R. W.; Sneider, A.; Anderson, C. F.; Wang, F.; Wu, P.-H.; Wirtz, D.; Cui, H., Supramolecular Design of Unsymmetric Reverse Bolaamphiphiles for Cell-Sensitive Hydrogel Degradation and Drug Release. *Angew. Chem. Intern. Ed.* **2020**, *59*, 4434-4442.
56. Wang, F.; Gillissen, M. A. J.; Stals, P. J. M.; Palmans, A. R. A.; Meijer, E. W., Hydrogen Bonding Directed Supramolecular Polymerisation of Oligo(Phenylene-Ethynylene)s: Cooperative Mechanism, Core Symmetry Effect and Chiral Amplification. *Eur. Chem. J.* **2012**, *18*, 11761-11770.
57. Dorca, Y.; Matern, J.; Fernández, G.; Sánchez, L., C₃-Symmetrical π -Scaffolds: Useful Building Blocks to Construct Helical Supramolecular Polymers. *Isr. J. Chem.* **2019**, *59*, 869-880.
58. Hirschberg, J. H. K. K.; Brunsveld, L.; Ramzi, A.; Vekemans, J. A. J. M.; Sijbesma, R. P.; Meijer, E. W., Helical self-assembled polymers from cooperative stacking of hydrogen-bonded pairs. *Nature* **2000**, *407*, 167-170.
59. Leenders, C. M. A.; Baker, M. B.; Pijpers, I. A. B.; Lafleur, R. P. M.; Albertazzi, L.; Palmans, A. R. A.; Meijer, E. W., Supramolecular polymerisation in water; elucidating the role of hydrophobic and hydrogen-bond interactions. *Soft Matter* **2016**, *12*, 2887-2893.
60. Baker, M. B.; Gosens, R. P. J.; Albertazzi, L.; Matsumoto, N. M.; Palmans, A. R. A.; Meijer, E. W., Exposing Differences in Monomer Exchange Rates of Multicomponent Supramolecular Polymers in Water. *ChemBioChem* **2016**, *17*, 207-213.
61. Leenders, C. M. A.; Mes, T.; Baker, M. B.; Koenigs, M. M. E.; Besenius, P.; Palmans, A. R. A.; Meijer, E. W., From supramolecular polymers to hydrogel materials. *Mater. Horiz.* **2014**, *1*, 116-120.
62. Bakker, M. H.; Lee, C. C.; Meijer, E. W.; Dankers, P. Y. W.; Albertazzi, L., Multicomponent Supramolecular Polymers as a Modular Platform for Intracellular Delivery. *ACS Nano* **2016**, *10*, 1845-1852.
63. VandenBerg, M. A.; Sahoo, J. K.; Zou, L.; McCarthy, W.; Webber, M. J., Divergent Self-Assembly Pathways to Hierarchically Organized Networks of Isopeptide-Modified Discotics under Kinetic Control. *ACS Nano* **2020**.
64. Boekhoven, J.; Poolman, J. M.; Maity, C.; Li, F.; van der Mee, L.; Minkenberg, C. B.; Mendes, E.; van EschJan, H.; Eelkema, R., Catalytic control over supramolecular gel formation. *Nat. Chem.* **2013**, *5*, 433-437.

65. Noteborn, W. E.; Zwagerman, D. N.; Talens, V. S.; Maity, C.; van der Mee, L.; Poolman, J. M.; Mytnyk, S.; van Esch, J. H.; Kros, A.; Eelkema, R.; Kieltyka, R. E., Crosslinker-Induced Effects on the Gelation Pathway of a Low Molecular Weight Hydrogel. *Adv. Mater.* **2017**, *29*, 1603769
66. Sato, K.; Hendricks, M. P.; Palmer, L. C.; Stupp, S. I., Peptide supramolecular materials for therapeutics. *Chem. Soc. Rev.* **2018**, *47*, 7539-7551.
67. Sharma, P.; Pal, V. K.; Roy, S., An overview of latest advances in exploring bioactive peptide hydrogels for neural tissue engineering. *Biom. Sci.* **2021**, *9*, 3911-3938.
68. Mukherjee, N.; Adak, A.; Ghosh, S., Recent trends in the development of peptide and protein-based hydrogel therapeutics for the healing of CNS injury. *Soft Matter* **2020**, *16*, 10046-10064.
69. Wang, J.; Liu, K.; Xing, R.; Yan, X., Peptide self-assembly: thermodynamics and kinetics. *Chem. Soc. Rev.* **2016**, *45*, 5589-5604.
70. Levin, A.; Hakala, T. A.; Schnaider, L.; Bernardes, G. J. L.; Gazit, E.; Knowles, T. P. J., Biomimetic peptide self-assembly for functional materials. *Nat. Rev. Chem.* **2020**, *4*, 615-634.
71. Acar, H.; Srivastava, S.; Chung, E. J.; Schnorenberg, M. R.; Barrett, J. C.; LaBelle, J. L.; Tirrell, M., Self-assembling peptide-based building blocks in medical applications. *Adv. Drug Deliv. Rev.* **2017**, *110-111*, 65-79.
72. Li, J.; Xing, R.; Bai, S.; Yan, X., Recent advances of self-assembling peptide-based hydrogels for biomedical applications. *Soft Matter* **2019**, *15*, 1704-1715.
73. Fichman, G.; Gazit, E., Self-assembly of short peptides to form hydrogels: design of building blocks, physical properties and technological applications. *Acta Biomater.* **2014**, *10*, 1671-1682.
74. Tomasini, C.; Castellucci, N., Peptides and peptidomimetics that behave as low molecular weight gelators. *Chem Soc Rev* **2013**, *42*, 156-72.
75. Lee, J.; Ju, M.; Cho, O. H.; Kim, Y.; Nam, K. T., Tyrosine-Rich Peptides as a Platform for Assembly and Material Synthesis. *Adv. Sci.* **2018**, *6*, 1801255-1801255.
76. Rivas, M.; del Valle, L. J.; Alemán, C.; Puiggali, J., Peptide Self-Assembly into Hydrogels for Biomedical Applications Related to Hydroxyapatite. *Gels* **2019**, *5*, 14, 1-29
77. Zhang, F.; Shi, G.-S.; Ren, L.-F.; Hu, F.-Q.; Li, S.-L.; Xie, Z.-J., Designer self-assembling peptide scaffold stimulates pre-osteoblast attachment, spreading and proliferation. *J. Mater. Sci.: Mater. Med.* **2009**, *20*, 1475-1481.
78. Horii, A.; Wang, X.; Gelain, F.; Zhang, S., Biological Designer Self-Assembling Peptide Nanofiber Scaffolds Significantly Enhance Osteoblast

- Proliferation, Differentiation and 3-D Migration. *PLoS One* **2007**, *2*, e190, 1-9
79. Cui, H.; Webber, M. J.; Stupp, S. I., Self-assembly of peptide amphiphiles: from molecules to nanostructures to biomaterials. *Biopolymers* **2010**, *94*, 1-18.
 80. Hendricks, M. P.; Sato, K.; Palmer, L. C.; Stupp, S. I., Supramolecular Assembly of Peptide Amphiphiles. *Acc. Chem. Res.* **2017**, *50*, 2440-2448.
 81. Sheehan, F.; Sementa, D.; Jain, A.; Kumar, M.; Tayarani-Najjaran, M.; Kroiss, D.; Ulijn, R. V., Peptide-Based Supramolecular Systems Chemistry. *Chem. Rev.* **2021**, *121*, 13869-13914.
 82. Raymond, D. M.; Nilsson, B. L., Multicomponent peptide assemblies. *Chem. Soc. Rev.* **2018**, *47*, 3659-3720.
 83. Okesola, B. O.; Mata, A., Multicomponent self-assembly as a tool to harness new properties from peptides and proteins in material design. *Chem. Soc. Rev.* **2018**, *47*, 3721-3736.
 84. Makam, P.; Gazit, E., Minimalistic peptide supramolecular co-assembly: expanding the conformational space for nanotechnology. *Chem. Soc. Rev.* **2018**, *47*, 3406-3420.
 85. Halperin-Sternfeld, M.; Ghosh, M.; Sevostianov, R.; Grigoriants, I.; Adler-Abramovich, L., Molecular co-assembly as a strategy for synergistic improvement of the mechanical properties of hydrogels. *Chem. Comm.* **2017**, *53*, 9586-9589.
 86. Wilson, A. J., Non-covalent polymer assembly using arrays of hydrogen-bonds. *Soft Matter* **2007**, *3*, 409-425.
 87. Murray, T. J.; Zimmerman, S. C., New triply hydrogen bonded complexes with highly variable stabilities. *J. Am. Chem. Soc.* **1992**, *114*, 4010-4011.
 88. Fenlon, E. E.; Murray, T. J.; Baloga, M. H.; Zimmerman, S. C., Convenient synthesis of 2-amino-1,8-naphthyridines, building blocks for host-guest and self-assembling systems. *J. Org. Chem.* **1993**, *58*, 6625-6628.
 89. Murray, T. J.; Zimmerman, S. C.; Kolotuchin, S. V., Synthesis of heterocyclic compounds containing three contiguous hydrogen bonding sites in all possible arrangements. *Tetrahedron* **1995**, *51*, 635-648.
 90. Yang, S. K.; Zimmerman, S. C., Hydrogen Bonding Modules for Use in Supramolecular Polymers. *Isr. J. Chem.* **2013**, *53*, 511-520.
 91. Schneider, H.-J.; Juneja, R. K.; Simova, S., Solvent and Structural Effects on Hydrogen Bonds in Some Amides and Barbiturates. An Additive Scheme for the Stability of Corresponding Host-Guest Complexes. *Chem. Ber.* **1989**, *122*, 1211-1213.
 92. Kyogoku, Y.; Lord, R. C.; Rich, A., The effect of substituent on the hydrogen bonding of adenine and uracil derivatives *PNAS* **1967**, *57*, 250-257.

93. Beijer, F. H.; Sijbesma, R. P.; Vekemans, J. A. J. M.; Meijer, E. W.; Kooijman, H.; Spek, A. L., Hydrogen-Bonded Complexes of Diaminopyridines and Diaminotriazines: Opposite Effect of Acylation on Complex Stabilities. *J. Org. Chem.* **1996**, *61*, 6371-6380.
94. Pranata, J.; Wierschke, S. G.; Jorgensen, W. L., OPLS potential functions for nucleotide bases. Relative association constants of hydrogen-bonded base pairs in chloroform. *J. Am. Chem. Soc.* **1991**, *113*, 2810-2819.
95. Krieg, E.; Bastings, M. M.; Besenius, P.; Rybtchinski, B., Supramolecular Polymers in Aqueous Media. *Chem. Rev.* **2016**, *116*, 2414-2477.
96. Gruschwitz, F. V.; Klein, T.; Catrouillet, S.; Brendel, J. C., Supramolecular polymer bottlebrushes. *Chem. Comm.* **2020**, *56*, 5079-5110.
97. Leenders, C. M.; Albertazzi, L.; Mes, T.; Koenigs, M. M.; Palmans, A. R.; Meijer, E. W., Supramolecular polymerization in water harnessing both hydrophobic effects and hydrogen bond formation. *Chem. Commun.* **2013**, *49*, 1963-1965.
98. Obert, E.; Bellot, M.; Bouteiller, L.; Andrioletti, F.; Lehen-Ferrenbach, C.; Boué, F., Both Water- and Organo-Soluble Supramolecular Polymer Stabilized by Hydrogen-Bonding and Hydrophobic Interactions. *J. Am. Chem. Soc.* **2007**, *129*, 15601-15605.
99. Wu, C.-H.; Zhang, Y.; van Rickley, K.; Wu, J. I., Aromaticity gain increases the inherent association strengths of multipoint hydrogen-bonded arrays. *Chem. Comm.* **2018**, *54*, 3512-3515.
100. Marchetti, L. A.; Kumawat, L. K.; Mao, N.; Stephens, J. C.; Elmes, R. B. P., The Versatility of Squaramides: From Supramolecular Chemistry to Chemical Biology. *Chem.* **2019**, *5*, 1398-1485.
101. Liu, H.; Tomooka, C. S.; Moore, H. W., An Efficient General Synthesis of Squarate Esters. *Synth. Comm.* **1997**, *27*, 2177-2180.
102. Wurm, F. R.; Klok, H. A., Be squared: expanding the horizon of squaric acid-mediated conjugations. *Chem. Soc. Rev.* **2013**, *42*, 8220-8236.
103. Storer, R. I.; Aciro, C.; Jones, L. H., Squaramides: physical properties, synthesis and applications. *Chem. Soc. Rev.* **2011**, *40*, 2330-2346.
104. Zhao, B.-L.; Li, J.-H.; Du, D.-M., Squaramide-Catalyzed Asymmetric Reactions. *Chem. Rec.* **2017**, *17*, 994-1018.
105. Bae, H. Y.; Song, C. E., Unprecedented Hydrophobic Amplification in Noncovalent Organocatalysis “on Water”: Hydrophobic Chiral Squaramide Catalyzed Michael Addition of Malonates to Nitroalkenes. *ACS Catal.* **2015**, *5*, 3613-3619.
106. Stucchi, S.; Colombo, D.; Guizzardi, R.; D'Aloia, A.; Collini, M.; Bouzin, M.; Costa, B.; Ceriani, M.; Natalello, A.; Pallavicini, P.; Cipolla, L., Squarate Cross-Linked Gelatin Hydrogels as Three-Dimensional Scaffolds for Biomedical Applications. *Langmuir* **2021**, *37*, 14050-14058.

107. Kitov, P. I.; Bundle, D. R., Synthesis and structure–activity relationships of di- and trisaccharide inhibitors for Shiga-like toxin Type 1. *J. Chem. Soc., Perkin Trans. I* **2001**, 838-853.
108. Kaiser, A.; Gaidzik, N.; Westerlind, U.; Kowalczyk, D.; Hobel, A.; Schmitt, E.; Kunz, H., A Synthetic Vaccine Consisting of a Tumor-Associated Sialyl-TN-MUC1 Tandem-Repeat Glycopeptide and Tetanus Toxoid: Induction of a Strong and Highly Selective Immune Response. *Angew. Chem. Int. Ed.* **2009**, *48*, 7551-7555.
109. Prohens, R.; Portell, A.; Font-Bardia, M.; Bauzá, A.; Frontera, A., Experimental and Theoretical Study of Aromaticity Effects in the Solid State Architecture on Squaric Acid Derivatives. *Cryst. Growth Des.* **2014**, *14*, 2578-2587.
110. Fukushima, K.; Liu, S.; Wu, H.; Engler, A. C.; Coady, D. J.; Maune, H.; Pitera, J.; Nelson, A.; Wiradharma, N.; Venkataraman, S.; Huang, Y.; Fan, W.; Ying, J. Y.; Yang, Y. Y.; Hedrick, J. L., Supramolecular high-aspect ratio assemblies with strong antifungal activity. *Nat. Comm.* **2013**, *4*, 2861, 1-9
111. Fukushima, K.; Tan, J. P. K.; Korevaar, P. A.; Yang, Y. Y.; Pitera, J.; Nelson, A.; Maune, H.; Coady, D. J.; Frommer, J. E.; Engler, A. C.; Huang, Y.; Xu, K.; Ji, Z.; Qiao, Y.; Fan, W.; Li, L.; Wiradharma, N.; Meijer, E. W.; Hedrick, J. L., Broad-Spectrum Antimicrobial Supramolecular Assemblies with Distinctive Size and Shape. *ACS Nano* **2012**, *6*, 9191-9199.
112. Kim, S. H.; Nederberg, F.; Jakobs, R.; Tan, J. P. K.; Fukushima, K.; Nelson, A.; Meijer, E. W.; Yang, Y. Y.; Hedrick, J. L., A Supramolecularly Assisted Transformation of Block-Copolymer Micelles into Nanotubes. *Angew. Chem. Int. Ed.* **2009**, *48*, 4508-4512.
113. Saez Talens, V.; Makurat, D. M. M.; Liu, T.; Dai, W.; Guibert, C.; Noteborn, W. E. M.; Voets, I. K.; Kieltyka, R. E., Shape modulation of squaramide-based supramolecular polymer nanoparticles. *Polym. Chem.* **2019**, *10*, 3146-3153.
114. Bujosa, S.; Castellanos, E.; Frontera, A.; Rotger, C.; Costa, A.; Soberats, B., Self-assembly of amphiphilic aryl-squaramides in water driven by dipolar π – π interactions. *Org. Biomol. Chem.* **2020**, *18*, 888-894.
115. Kupai, J.; Kisszékelyi, P.; Nagy, S., Synthesis and Application of Thiosquaramides and Their Derivatives: A Review. *Period. Polytechn. Chem. Eng.* **2018**, *62*, 467-475
116. Allen, F. H.; Bird, C. M.; Rowland, R. S.; Raithby, P. R., Resonance-Induced Hydrogen Bonding at Sulfur Acceptors in R1R2C=S and R1CS2-Systems. *Acta Crystallogr. Sec. B* **1997**, *53*, 680-695.
117. Rombola, M.; Sumaria, C. S.; Montgomery, T. D.; Rawal, V. H., Development of Chiral, Bifunctional Thiosquaramides: Enantioselective Michael Additions of Barbituric Acids to Nitroalkenes. *J. Am. Chem. Soc.* **2017**, *139*, 5297-5300.

118. Rodríguez-Ferrer, P.; Naharro, D.; Maestro, A.; Andrés, J. M.; Pedrosa, R., Chiral Bifunctional Thiosquaramides as Organocatalysts in the Synthesis of Enantioenriched 3,3-Disubstituted Oxindoles. *Eur. J. Org. Chem.* **2019**, 2019, 6539-6549.
119. Nagy, S.; Dargó, G.; Kisszékelyi, P.; Fehér, Z.; Simon, A.; Barabás, J.; Höltzl, T.; Mátravölgyi, B.; Kárpáti, L.; Drahos, L.; Huszthy, P.; Kupai, J., New enantiopure binaphthyl-cinchona thiosquaramides: synthesis and application for enantioselective organocatalysis. *New J. Chem.* **2019**, 43, 5948-5959.
120. Busschaert, N.; Kirby, I. L.; Young, S.; Coles, S. J.; Horton, P. N.; Light, M. E.; Gale, P. A., Squaramides as Potent Transmembrane Anion Transporters. *Angew. Chem. Int. Ed.* **2012**, 51, 4426-4430.
121. Busschaert, N.; Elmes, R. B.; Czech, D. D.; Wu, X.; Kirby, I. L.; Peck, E. M.; Hendzel, K. D.; Shaw, S. K.; Chan, B.; Smith, B. D.; Jolliffe, K. A.; Gale, P. A., Thiosquaramides: pH switchable anion transporters. *Chem. Sci.* **2014**, 5, 3617-3626.
122. Cioc, R. C.; Ruijter, E.; Orru, R. V. A., Multicomponent reactions: advanced tools for sustainable organic synthesis. *Green Chem.* **2014**, 16, 2958-2975.
123. Biggs-Houck, J. E.; Younai, A.; Shaw, J. T., Recent advances in multicomponent reactions for diversity-oriented synthesis. *Curr. Opin. Chem. Biol.* **2010**, 14, 371-382.
124. Domling, A.; Wang, W.; Wang, K., Chemistry and biology of multicomponent reactions. *Chem. Rev.* **2012**, 112, 3083-30135.
125. Zhi, S.; Ma, X.; Zhang, W., Consecutive multicomponent reactions for the synthesis of complex molecules. *Org. Biomol. Chem.* **2019**, 17, 7632-7650.
126. Driggers, E. M.; Hale, S. P.; Lee, J.; Terrett, N. K., The exploration of macrocycles for drug discovery — an underexploited structural class. *Nat. Rev. Drug Disc.* **2008**, 7, 608-624.
127. Reguera, L.; Rivera, D. G., Multicomponent Reaction Toolbox for Peptide Macrocyclization and Stapling. *Chem. Rev.* **2019**, 119, 9836-9860.
128. Morejón, M. C.; Laub, A.; Kaluđerović, G. N.; Puentes, A. R.; Hmedat, A. N.; Otero-González, A. J.; Rivera, D. G.; Wessjohann, L. A., A multicomponent macrocyclization strategy to natural product-like cyclic lipopeptides: synthesis and anticancer evaluation of surfactin and mycosubtilin analogues. *Org. Biomol. Chem.* **2017**, 15, 3628-3637.
129. Váradi, A.; Palmer, T. C.; Notis Dardashti, R.; Majumdar, S., Isocyanide-Based Multicomponent Reactions for the Synthesis of Heterocycles. *Molecules* **2016**, 21, 19, 1-22

130. Yang, B.; Zhao, Y.; Wei, Y.; Fu, C.; Tao, L., The Ugi reaction in polymer chemistry: syntheses, applications and perspectives. *Poly. Chem.* **2015**, *6*, 8233-8239.
131. Kreye, O.; Türlüç, O.; Sehlinger, A.; Rackwitz, J.; Meier, M. A. R., Structurally Diverse Polyamides Obtained from Monomers Derived via the Ugi Multicomponent Reaction. *Eur. J. Chem.* **2012**, *18*, 5767-5776.
132. Sehlinger, A.; Ochsenreither, K.; Bartnick, N.; Meier, M. A. R., Potentially biocompatible polyacrylamides derived by the Ugi four-component reaction. *Eur. Polym. J.* **2015**, *65*, 313-324.
133. Hartweg, M.; Edwards-Gayle, C. J. C.; Radvar, E.; Collis, D.; Reza, M.; Kaupp, M.; Steinkoenig, J.; Ruokolainen, J.; Rambo, R.; Barner-Kowollik, C.; Hamley, I. W.; Azevedo, H. S.; Becer, C. R., Ugi multicomponent reaction to prepare peptide-peptoid hybrid structures with diverse chemical functionalities. *Polym. Chem.* **2018**, *9*, 482-489.
134. Lau, K. H. A., Peptoids for biomaterials science. *Biomater. Sci.* **2014**, *2*, 627-633.
135. Kirshenbaum, K.; Zuckermann, R. N., Peptoids in Wonderland. *Biopolymers* **2019**, *110*, 1-2
136. Al Samad, A.; De Winter, J.; Gerbaux, P.; Jerome, C.; Debuigne, A., Unique alternating peptide-peptoid copolymers from dipeptides via a Ugi reaction in water. *Chem. Commun.* **2017**, *53*, 12240-12243.
137. Mangunuru, H. P. R.; Yang, H.; Wang, G., Synthesis of peptoid based small molecular gelators by a multiple component reaction. *Chem. Comm.* **2013**, *49*, 4489-4491.
138. Afshari, R.; Shaabani, A., Materials Functionalization with Multicomponent Reactions: State of the Art. *ACS Comb. Sci.* **2018**, *20*, 499-528.
139. Shulepov, I. D.; Kozhikhova, K. V.; Panfilova, Y. S.; Ivantsova, M. N.; Mironov, M. A., One-pot synthesis of cross-linked sub-micron microgels from pure cellulose via the Ugi reaction and their application as emulsifiers. *Cellulose* **2016**, *23*, 2549-2559.

CHAPTER 2

Supramolecular copolymerization of oxo- and thiosquaramide monomers

2.1 Abstract

In polymer chemistry, the formation of well-defined polymer microstructures can be modulated by the copolymerization of two or more monomers through covalent bond formation. This concept applied to the field of supramolecular polymers is still in its infancy with only several examples providing insight into the features of the monomers necessary for their co-assembly and methods to enable their characterization. Non-covalent interactions such as π - π interactions and hydrogen bonding have been used to drive the formation of supramolecular copolymers, with amides being largely used to provide directional interactions in the assemblies. In this chapter, the potential of an underrepresented hydrogen bonding unit, squaramide, to be used for supramolecular copolymerization will be examined. We previously showed that oxosquaramides self-assemble in a head-to-tail fashion whereas thiosquaramides stack upon one another. The potential for their copolymerization through the use of distinct hydrogen bond-acceptor moieties, namely oxo- and thio-derivatives will be explored. In particular, I will first examine the self-assembly properties of the individual monomers into supramolecular polymers and determine conditions for their copolymerization. Spectroscopic and imaging techniques at the nanoscale show progressive fiber shortening and a decreased fiber persistence length providing a handle to tune the supramolecular polymerization behavior of oxosquaramides. To further elucidate the copolymerization behavior of oxo- and thiosquaramide monomers, a fluorescent Cyanine 3 (Cy3) dye-labelled oxo-squaramide and Cyanine 5 (Cy5) dye-labelled thiosquaramide monomers were synthesized. The fluorescence and UV-vis measurements show fluorescence resonance energy transfer (FRET) from oxo-squaramide-Cy3 to thio-squaramide-Cy5 suggestive of the supramolecular copolymerization in a block structure.

2.2 Introduction

The structural complexity of biological systems over several length scales remains an inspiration for the design of functional polymer materials.¹ The sequence-controlled polymerization of biological macromolecules, such as nucleic acids and proteins, leads to a well-defined arrangement of biomolecular building blocks with hierarchical structure and function.² Conversely, in the last several decades the field of covalent polymers has used copolymerization to tune their properties to obtain specific properties and function.^{3, 4} Two or more monomers can be combined within the same polymer using living,⁵ controlled radical,⁶ and ring opening metathesis polymerization⁷ using techniques to gain control over their length, structure and composition. When coupled with monomers of different reactivities^{2, 8} copolymers with alternating, periodic, and blocky structures can be prepared providing a range of structural diversity and vast differences in the physical properties of the resultant materials.

The concept of supramolecular copolymerization⁹⁻¹⁶ is a more recent addition to the supramolecular polymer field consistent with the growing knowledge of monomer assembly and their polymerization mechanisms. Similar to covalent polymers, the aim is to be able to achieve the properties that cannot be accessed through single component systems. However, the structural design of the monomers complexity of the copolymer formation and mechanistic features still faces several challenges.^{17, 18} Nevertheless, supramolecular copolymers that rely on electrostatic, hydrogen bonding,¹⁹ transition metal,^{20, 21} or π - π interactions for their formation have been reported.²² For example, copolymers based on distinct hydrogen bond acceptor groups, oxygen or sulfur, were demonstrated for 1,3,5-benzenetricarboxamides (BTA).²³ Although thio-BTA forms less directional hydrogen bonds, the two monomers can self-assemble independently into one-dimensional long fibers following a cooperative mechanism. When the monomers are co-assembled, random copolymers were observed. Moreover, George and coworkers demonstrated the potential for sequence controlled supramolecular polymerization using two component systems showing pathway complexity.²⁴ In this study the kinetic and thermodynamic pathways in the self-assembly of core-substituted naphthalene diimide monomers (NDI) were exploited to control the formation of various random, block copolymers and self-sorted supramolecular polymers. Despite recent examples that provide analysis and insight into supramolecular monomers that enable copolymerization, there still remains much to understand regarding the

existing repertoire of self-assemblies motifs in this area and the potential to control the microstructural features of the polymers especially in aqueous medium remains untapped.

When hydrogen bonds are employed in the molecular designs of supramolecular monomers,²⁵⁻²⁸ amides and ureas²⁹ are attractive because of their ditopic nature. We recently demonstrated the utility of the squaramide unit to provide directional hydrogen bonding in a ditopic manner to drive the formation of supramolecular polymers in water through their self-assembly in a head-to-tail fashion.³⁰ When we thionate the monomer, replacing the oxygens with sulfur atoms, the monomer self-assembly mode is altered to a stacking mode.³¹ Because of capacity of the squaramide to engage in hydrogen bonding and stacking interactions, we became interested to understand if the individual self-assembly modes of the oxo- and thiosquaramide monomers could be affected in the presence of each other, or if co-assembly occurs. Thus, in this chapter, the protocols to facilitate and evaluate the supramolecular polymerization of the individual oxo- and thiosquaramide monomers, and their copolymerization at various molar ratios is studied.

2.3 Results and discussion

The design of the oxosquaramide (**1**) and thiosquaramide monomers (**2**) involves two ditopic hydrogen-bonding squaramide units within the hydrophobic alkyl chains, surrounded by two oligo(ethylene glycol) methyl ether chains for their self-assembly in water (**Figure 2.1**). **1** was synthesized as previously described by Talens *et al.*³⁰ and **2** was obtained by the thionation reaction of **1** in presence of an excess of P₄S₁₀·pyridine complex (23 eq) in a yield of 30%. Exclusive thionation of squaramide moieties was obtained at room temperature as previously reported for Lawesson's agent in the preparation of *N*-(benzoyloxy)thioamide.³²

In order to track the mixing of the two monomers at the molecular level, a fluorescently-labelled thiosquaramide monomer **12** was synthesized that is asymmetrically outfitted with a sulfo-Cyanine dye (sulfo-Cy5), in addition to a previously reported oxosquaramide monomer **11** (sulfo-Cy3).³³ The two fluorescently-labelled monomers were synthesized following a similar synthetic procedure (**Scheme 1**). Specifically, **12** was obtained firstly by thionation of compound **9**, before being conjugated to sulfo-Cy5 dye (**Scheme 1**). The synthesis of asymmetric fluorescently-labelled molecules was performed starting with O-(2-azidoethyl)undecaethylene glycol that was

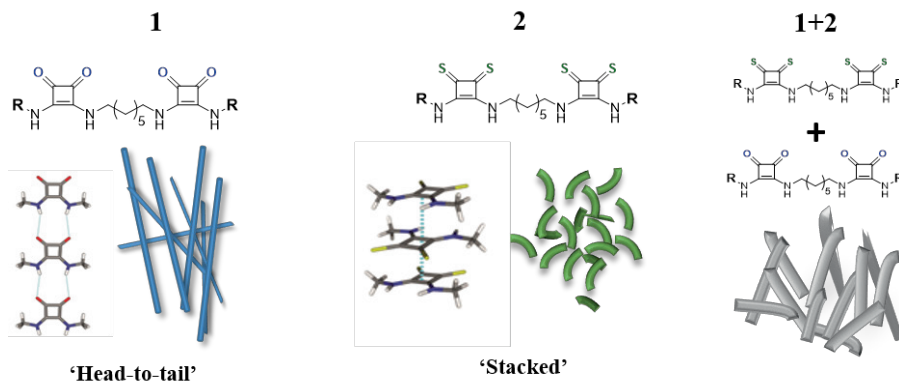
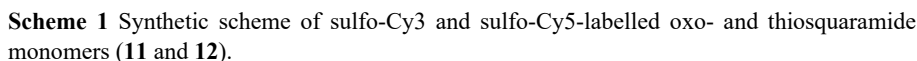


Figure 2.1 Oxosquaramide (**1**) and thiosquaramide (**2**) monomers, supramolecular polymers and copolymers. Oxosquaramide bolaamphiphiles (**1**) self-assemble into rigid nanofibers (*left*), whereas thiosquaramides (**2**) self-assemble into shorter nanorods (*center*) because of their different self-assembly mode. The self-assembly of the two monomers (**1+2**, *right*) results in the formation of copolymers with the characteristics of both individual polymers.

converted to amine by catalytic hydrogenation using Et_3SiH on Pd/C . After Boc-protection of the amine, the hydroxyl group of undecaethylene glycol was activated with CDI and subsequently, coupled with N-Cbz-1,10-decanediamine to obtain **7**. The deprotection of the Cbz group and coupling with squaric ester resulted in squaramide amphiphile **8**. The asymmetric oxosquaramide **9** was synthesized through conjugation of **8** with another squaramide-based amphiphile functionalized with a mono-Boc protected heptanediamine **5**. To obtain the fluorescently-labelled oxosquaramide **11**, **9** was coupled with sulfo-Cyanine 3 N-hydroxysuccinimidyl ester. The Cy5-labelled thiosquaramide **12** was prepared after the thionation of **9** by coupling sulfo-Cyanine 5 N-hydroxysuccinimidyl ester. Both compounds were purified by high performance liquid phase chromatography on reverse phase C18 columns and characterized.



Prior to the co-assembly of the oxo- and thiosquaramide monomers, insight into the self-assembly of the individual monomers at the molecular level and their polymerization mechanisms was carried out. The UV-vis spectra of **1** in water displays two bands at 329 and 255 nm that correspond to π - π^* of hydrogen bond donor N-H and n- π^* transition of C=O hydrogen bond acceptor, respectively, in their aggregated state (**Figure 2.2a**). According to Kasha's theory,³⁴ these blue and red shifted transitions (H- and J- bands) of oxosquaramide are due to the in-line and parallel orientation of transition dipole moments within the squaramide moieties upon self-assembly in a head-to-tail hydrogen bonding orientation as determined from time-dependent density functional theory calculations (TD-DFT) calculations.

Self-assembly of **2** in water resulted in opposite trends as observed in the UV-vis spectroscopy (**Figure 2.2b**). More specifically, the thionation of the squaramide moieties results in the formation of two bands at 272 and 363 nm. According to Kasha's theory, the blue-shifted transition in the UV-vis profile is in line with the formation of H-type aggregates as consequence of the parallel orientation of the transition dipole moments. To further evaluate the thionation of thiosquaramide on the self-assembly in water, critical aggregation concentration (CAC) was determined by SLS. The CAC of **2** was determined by preparing various solutions in the concentration range of 100 μ M and 10 nM and was calculated from the inflection point of the scattering intensity as a function of concentration range. The CAC was comparable to the value previously determined for **1** (8×10^{-5} M, **Figure S2.4**), despite its distinct self-assembly mode.³⁰

To investigate the polymerization mechanisms of **1** and **2**, conditions that would enable depolymerization of the polymers was necessary to determine. Thermal denaturation and titration with a 'good' solvent were examined to induce their self-assembly. Thermal denaturation of **1** was first attempted by recording individual UV-vis spectra from 20 to 65 °C (SI **Figure S2.1**). Despite the disappearance of red shifted band (329 nm) at higher temperatures, the blue shifted band (255 nm) was maintained and only a slight increase in the monomer band (310 nm) was observed. As previously reported,³⁰ depolymerization of **1** was achieved by the addition of very strong hydrogen bond disrupting solvent ('good' solvent) hexafluoroisopropanol (HFIP) to a supramolecular polymer in 'poor' solvent (i.e. water). Depolymerization through the titration with HFIP (hexafluoroisopropanol) results in the gradual loss of the blue (255 nm) and red shifted transition (329 nm) and an increase

of the monomer band at 310 nm (**Figure 2.2a**). To confirm depolymerization of the monomers, NMR spectroscopy and static light scattering (SLS) were performed. NMR spectra of the aggregated (in D₂O) and depolymerized states (in HFIP-d₂) were analyzed. While the NMR spectrum of **1** in D₂O (**Figure S2.6**) suggests aggregation of the monomers that is still present up to 65 °C, in HFIP-d₂ (**Figure S2.5**) a well resolved spectrum is observed and is indicative of the depolymerized state. These results were further supported by SLS measurements, where the scattered light intensities of the aggregated and depolymerized states were analyzed in water and HFIP, respectively. High counts rates for **1** in water were observed in comparison to that of HFIP suggesting the presence of self-assembled aggregates in water and monomer species in HFIP (**Table S1**).

To further examine the solvent-induced depolymerization of **2**, UV-vis spectra in different organic solvents were recorded (**Figure S2.2**). In contrast to **1**, all UV-vis profiles of **2** displayed an increase in the bands at 350 and 380 nm, except for THF (**Figure S2.2**). The UV-vis spectra of **2** in THF showed two bands at 235 and 325 nm that are blue-shifted in comparison to the transitions observed in the presence of water. In order to support the observed UV-vis transitions, atomic force microscopy was performed on drop-casted samples of **2** in water, THF and HFIP. Aggregation was observed in water and HFIP, but not in THF (**Figure S2.2**). Further confirmation of the disassembly of the polymers was evaluated by ¹H NMR spectroscopy. The NMR spectrum of **2** in THF-d₈, is well resolved suggesting of complete depolymerization (**Figure S2.7**). Conversely, the ¹H NMR in D₂O displays a broad signal at 3.5 ppm that is still present up to 65 °C and indicates that **2** retains its self-assembled state (**Figure S2.8**). The depolymerization of **2** in THF was further supported by SLS, where the scattered light intensities of the aggregated and depolymerized states were analyzed in water and THF, respectively. Compared to their respective solvent controls, no scattering species were detected in THF while in water high scattered light intensities are recorded. Hence, these results suggest a lack of aggregation in THF.

Once the conditions for depolymerization were established, UV-vis titrations were performed for **1** and **2**, using co-solvents HFIP and THF as denaturants, respectively, to gain insight into the differences in the thermodynamic parameters associated with their aggregation. In the case of molecule **1** (c = 30 μM), 10 % of HFIP (v/v) was required to achieve depolymerization using disappearance of the band at 329 nm. The same approach was performed for

molecule **2** ($c = 30 \mu\text{M}$) (363 nm) and THF that was added until (10 % (v/v)) until no further changes in the absorption were observed.

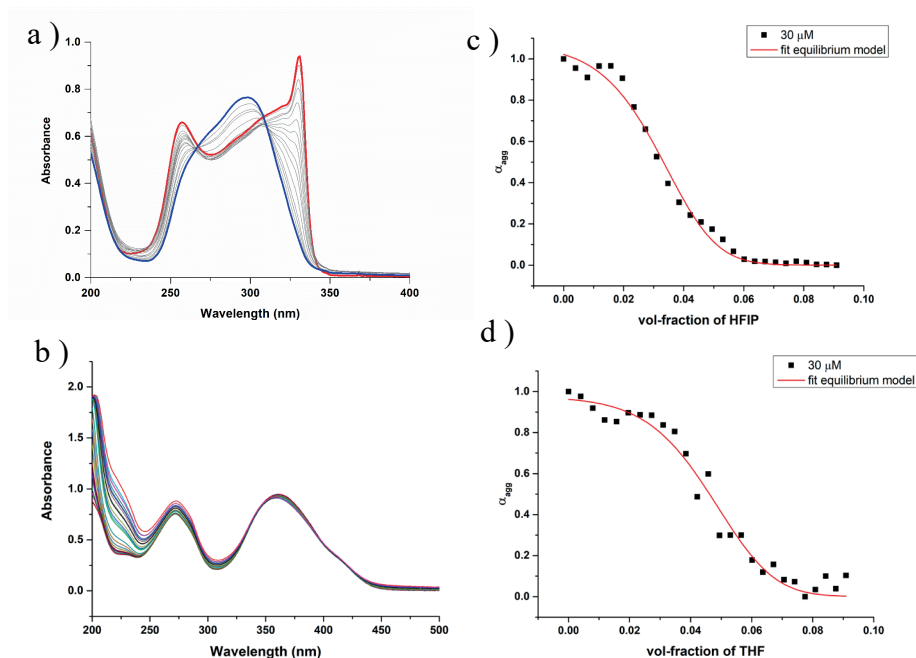


Figure 2.2 UV-vis titrations with the addition of a co-solvent to the squaramide monomer in water: (a) **1** ($c=30 \mu\text{M}$) with HFIP; (b) **2** ($30 \mu\text{M}$) with THF; Plot of α_{agg} as function of volume fraction of co-solvent for (c) **1** at 329 nm; (d) **2** at 363 nm.

The aggregated fraction of supramolecular polymers **1** and **2** were determined using the absorbances at 329 and 363 nm, respectively, (**Figure 2.2 c-d**) and plotted as a function of solvent volume fraction. The depolymerized state of **1** and **2** was observed at different volume fractions of good solvent: while **1** depolymerizes at 6 vol % of HFIP, **2** required more THF (8 vol%) indicative of a more stable polymer. To determine the thermodynamic parameters for the supramolecular polymerization of the monomers (ΔG , m and σ , **Table S1**), the curves were fit with the solvent denaturation model by Korevaar *et al.*^{35, 36} From the fitted data, the cooperativity parameters, σ , of monomers **1** and **2** were less than 1, indicating that the monomers polymerize according to a cooperative mechanism. Moreover, although monomer **2** self-assembles in a stacked mode, the cooperativity parameter ($\sigma = 0.06$) was found to be less than that obtained for **1** ($\sigma = 0.78$). Additionally, comparable ΔG values were

obtained with both monomers **1** (-34 kJ/mol) and **2** (-35 kJ/mol), indicating a similar stability, despite their distinct self-assembly modes.

Conversely, in our previous publication, both of the monomers were titrated with the same solvent (CH₃CN) and the depolymerized state of **1** and **2** was reached with 24.5 vol % and 33.3 vol% of CH₃CN respectively.³¹ Moreover, some differences were observed also in the thermodynamic parameters of polymerization mechanism. Specifically, cooperativity parameter (σ) of **1** (0.013) is an order magnitude smaller compared to **2** (0.610).³¹ However, both of these values are within the calculated error.

2.3.1 Oxo- and thiosquaramide supramolecular copolymers

To better understand if the distinct self-assembly modes of the squaramide unit can support the formation of supramolecular copolymers, studies that examine the extent of their copolymerization were pursued. Using the information gained by dissolving the monomers in various organic solvents and evaluating their dissolution in the earlier section, a protocol for the mixing of both supramolecular monomers was developed. In this protocol, **1** was dissolved in HFIP and **2** in THF, and the organic solvent was removed by a stream of N₂. After the rehydration with water, the monomers were mixed in the appropriate molar ratio as shown in **Figure 2.4a**.

The extent of monomer mixing at the molecular level was first examined by UV-vis and fluorescence spectroscopy. Because of the distinct UV-vis profiles of **1** and **2** that are due to their head-to-tail and stacked self-assembly configurations, respectively, insight into the microstructure of the copolymers can be obtained if they co-assemble. At an equimolar ratio of **1** and **2**, UV-vis profiles shows that there is overlap of the individual spectra of the monomers indicating the retention of their transitions in self-assembled state (**Figure 2.4b**). Moreover, at molar ratios (2:1 and 1:2) (**Figure 2.4c**), the UV-vis absorption spectra of the single monomers are still retained with the bands of the monomer in excess showing an increased intensity in comparison to the other monomer (**Figure 2.4c**).

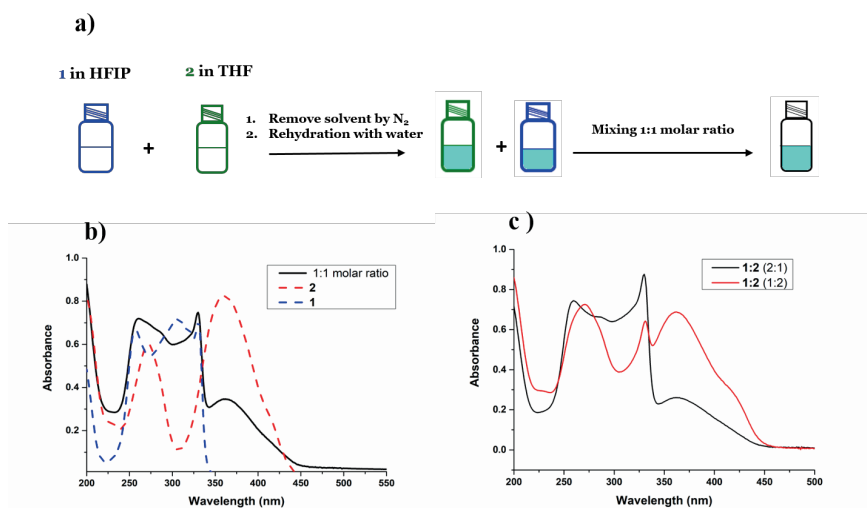


Figure 2.4 (a) Pictorial representation of the co-assembly protocol of **1** and **2** (b) UV-vis absorption spectra of the individual molecules, **1**, **2** and copolymers a 1:1 molar ratio ($C_{\text{tot}} = 30 \mu\text{M}$ each) (c) UV-vis absorption spectra of monomers **1** and **2** mixed in a 1:2 and 2:1 molar ratio to form supramolecular copolymers ($C_{\text{tot}} = 30 \mu\text{M}$, 1:1 molar ratio)

To further understand if monomers **1** and **2** undergo co-assembly or self-sorting under the developed mixing conditions, zeta potential and fluorescence resonance energy transfer (FRET) experiments were performed. Monomers **1** and **2** were conjugated to sulfo-Cy3 and sulfo-Cy5 dyes, respectively, as described above to execute FRET studies for gaining insight into the extent of their mixing. Zeta potential measurements were then used to confirm that the sulfo-Cy dye-labelled monomers can co-assemble with the native monomers. When **1** was mixed with 2 mol% of **11**, a more negative ζ potential value ($-4.9 \pm 5.2 \text{ mV}$) was obtained in comparison to the native monomer ($7.32 \pm 5.5 \text{ mV}$). The same trend was observed in the case of **2** mixed with 2 mol% of **12** ($-8.57 \pm 4.53 \text{ mV}$), compared to the native monomer ($-0.321 \pm 5.65 \text{ mV}$). These slight decrease in zeta potential suggests results co-assembly of the dye-labelled monomers with their non-labelled variants.

Once co-assembly of the dye-labelled monomers was confirmed, a FRET study was carried out on the various copolymer solutions. Copolymerization of the monomers can be followed by excitation of the sulfo-Cy3 donor at 550 nm that undergoes its energy transfer to a sulfo-Cy5 acceptor resulting in a measurable fluorescence signal at 670 nm. The individual monomers **1** and **2** were co-assembled with their respective fluorescent monomers **11** and **12** in

HFIP and THF, respectively, to ensure that a molecularly dissolved state is obtained. Subsequently, after the removal of the solvent under N₂ gas, the solution were rehydrated with water and immediately mixed in an equimolar ratio (total dye concentration: 2 mol%). (**Figure 2.5a**) As shown in the **Figure 2.5c**, the FRET experiment resulted an emission band at 670 nm confirming the co-assembly event when excited at 550 nm.

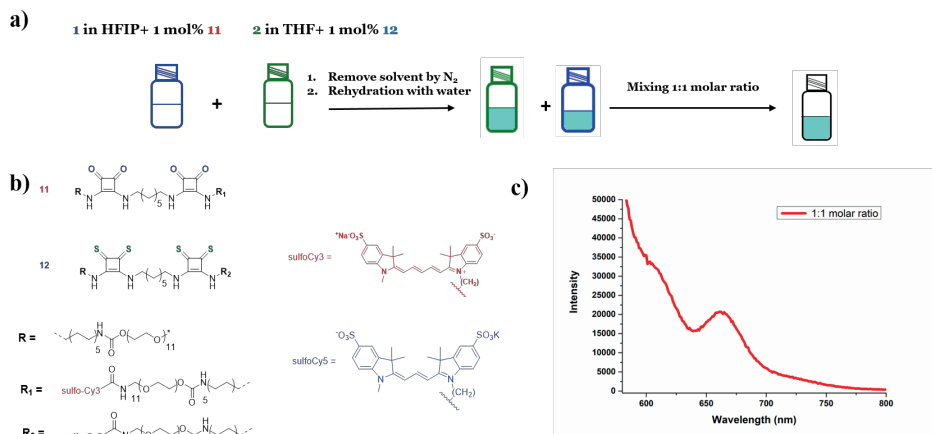


Figure 2.5 (a) Co-assembly protocol of **1** and **2** for FRET experiments (b) Chemical structures of squaramide monomer sulfo-Cy dye-conjugates (**11**) and (**12**) (c) Fluorescence emission spectrum of a solution containing an equimolar ratio of **1** and **2** with 2 mol% of **11** and **12** (2 mol% total dye concentration). Excitation wavelength 550 nm (sulfo-Cy3), Emission range 570-800 nm (sulfo-Cy5).

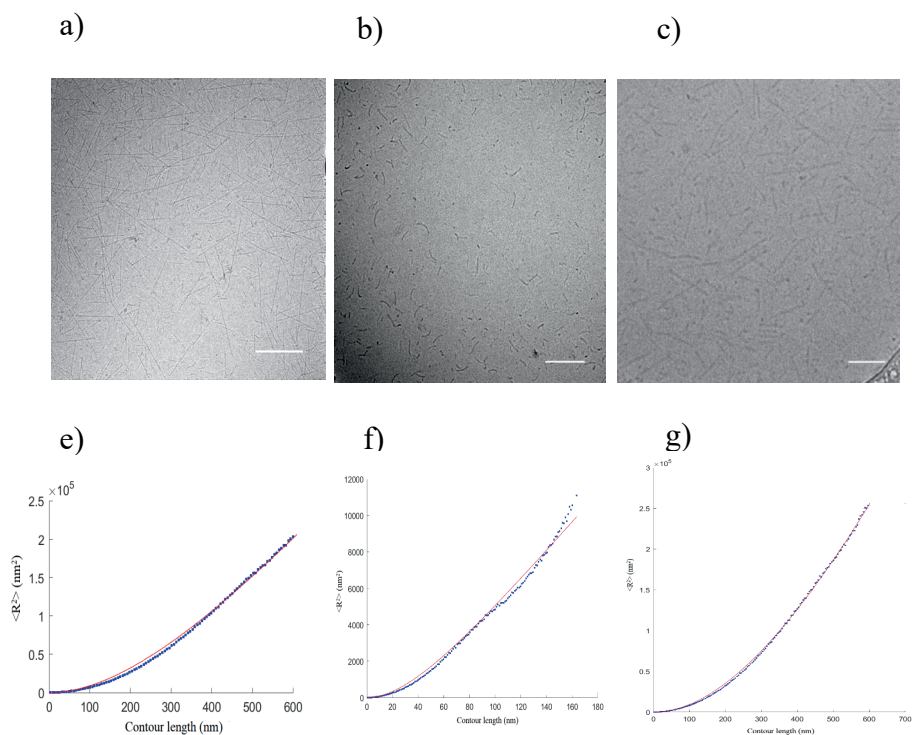


Figure 2.6 CryoTEM micrographs of squaramide-based supramolecular (co)polymers: (a) **1** ($c=580 \mu\text{M}$), scale bar: 100 nm; (b) **2** ($c=580 \mu\text{M}$), scale bar: 100 nm; (c) **1** and **2** in an equimolar ratio ($c=580 \mu\text{M}$), scale bar: 100 nm. End-to-end distance plots (R^2) as function of contour length for **1** (e), **2** (f) and copolymerization of **1** and **2** in an equimolar ratio (g) as obtained from the Easyworm software.

The copolymerization of **1** and **2** were demonstrated on the molecular level through various spectroscopies, but we sought to understand the consequence of their mixing on the aggregates at the nanoscale. Consequently, we performed cryo-EM measurements on the individual monomers (**1**) and (**2**) and their copolymers. While monomers of **1** self-assemble into high-aspect-ratio fibers, monomers of **2** self-assemble into more flexible nanorod-like structures that are approximately 5-times shorter in length. When both monomers are copolymerized, cryoEM micrographs show the formation of nanofibers with a shorter length compared to **1**, but longer than **2**. Image analysis using the Easyworm software³⁷ was performed to quantify various fiber properties. The mean square of the end-to-end distance $\langle R^2 \rangle$ is measured as a function of contour length of the fibers (ℓ) (Figures 2.6d, e and f) and the persistence length of the fibers (P_l) was calculated using the worm-

like chain model (WLC). While **1** and **2** display a P_l value of 581 ± 76 nm and 47 ± 4 nm respectively, the mixing of **1** and **2** results in a decrease in fiber length relative to **1** of 282 ± 16 nm. Moreover, using P_l , bending rigidity of the nanofibers (κ) was determined. Monomers **1** and **2** display a bending rigidity of $(2.4 \pm 0.3) \times 10^{-27} \text{ N}\cdot\text{m}^2$ and $(1.9 \pm 0.2) \times 10^{-28} \text{ N}\cdot\text{m}^2$ respectively, and their equimolar mixture results in a value of $(1.16 \pm 0.07) \times 10^{-27} \text{ N}\cdot\text{m}^2$. These preliminary results demonstrate that the mixing of monomers **1** and **2** prior to their self-assembly results in structural changes to the properties of the formed supramolecular polymers with respect to their length and bending rigidity. Modulation of the oxosquaramide assemblies is likely due to the stacking tendency of the thiosquaramide synthon and its less directional hydrogen bonding character. To further understand the copolymer microstructure, superresolution microscopy experiments would need to be performed using the dye-labelled monomers. A similar approach was recently taken by George and coworkers using structured illumination (SIM) to visualize the supramolecular copolymer microstructure of naphthalene diimide derivatives (NDI).²⁴ Furthermore, to better understand the potential for microstructural control over the polymers, ratios beyond (1:2 and 2:1) should be considered.

2.4 Conclusions

In this chapter, the capacity of two monomers with distinct self-assembly modes to form copolymers was examined. A molecularly dissolved state was achieved for both monomers in different solvents prior to their mixing; HFIP is a good solvent for **1**, while THF is a good solvent for **2**. Solvent denaturation studies using the determined good solvents showed that a cooperative process is followed for their respective self-assemblies. On co-assembly, UV-vis spectra of an equimolar ratio of **1** and **2** reflected the profiles of the individual monomers, based on the retention of their bands. FRET experiments in the presence of sulfo-Cyanine labelled monomers of **1** and **2** are suggestive of co-assembly due to the presence of an emission band at 670 nm. Investigation of the supramolecular copolymer morphology by cryoTEM that showed shorter fibers with a decreased persistence length compared to **1**. In conclusion, since oxo- and thiosquaramide maintain their independent assemblies when mixed, this approach may be pursued to control the copolymerization of squaramide-based monomers in water. Moreover, to further understand the formed copolymer microstructure through self-assembly, superresolution microscopy experiments using the dye-labelled monomers would need to be performed.

References

1. Leibfarth, F. A.; Mattson, K. M.; Fors, B. P.; Collins, H. A.; Hawker, C. J., External regulation of controlled polymerizations. *Angew. Chem. Int. Ed. Engl* **2013**, *52*, 199-210.
2. Lutz, J. F.; Ouchi, M.; Liu, D. R.; Sawamoto, M., Sequence-controlled polymers. *Science* **2013**, *341*, 1238149, 1-8.
3. Lutz, J.-F.; Lehn, J.-M.; Meijer, E. W.; Matyjaszewski, K., From precision polymers to complex materials and systems. *Nat. Reviews Mater.* **2016**, *1*, 1-14.
4. Feng, H.; Lu, X.; Wang, W.; Kang, N. G.; Mays, J. W., Block copolymers: synthesis, self-assembly, and applications. *Polymers (Basel)* **2017**, *9*, 494, 1-31.
5. Szwarc, M., 'Living' polymers. *Nature* **1956**, *178*, 1168-1169.
6. Ouchi, M.; Terashima, T.; Sawamoto, M., Transition metal-catalyzed living radical polymerization: toward perfection in catalysis and precision polymer synthesis. *Chem. Rev.* **2009**, *109*, 4963-5050.
7. Bielawski, C. W.; Grubbs, R. H., Living ring-opening metathesis polymerization. *Progr. Polym. Sci.* **2007**, *32*, 1-29.
8. Satoh, K.; Ishizuka, K.; Hamada, T.; Handa, M.; Abe, T.; Ozawa, S.; Miyajima, M.; Kamigaito, M., Construction of sequence-regulated vinyl copolymers via iterative single vinyl monomer additions and subsequent metal-catalyzed step-growth radical polymerization. *Macromolecules* **2019**, *52*, 3327-3341.
9. Thota, B. N. S.; Lou, X.; Boicchio, D.; Paffen, T. F. E.; Lafleur, R. P. M.; van Dongen, J. L. J.; Ehrmann, S.; Haag, R.; Pavan, G. M.; Palmans, A. R. A.; Meijer, E. W., Supramolecular copolymerization as a strategy to control the stability of self-assembled nanofibers. *Angew. Chem. Int. Ed. Engl.* **2018**, *57*, 6843-6847.
10. Ahlers, P.; Fischer, K.; Spitzer, D.; Besenius, P., Dynamic light scattering investigation of the kinetics and fidelity of supramolecular copolymerizations in water. *Macromolecules* **2017**, *50*, 7712-7720.
11. Albertazzi, L.; van der Veken, N.; Baker, M. B.; Palmans, A. R.; Meijer, E. W., Supramolecular copolymers with stimuli-responsive sequence control. *Chem. Commun. (Camb)* **2015**, *51*, 16166-16168.
12. Engel, S.; Spitzer, D.; Rodrigues, L. L.; Fritz, E. C.; Strassburger, D.; Schonhoff, M.; Ravoo, B. J.; Besenius, P., Kinetic control in the temperature-dependent sequential growth of surface-confined supramolecular copolymers. *Faraday Discuss.* **2017**, *204*, 53-67.

13. Hendrikse, S. I. S.; Su, L.; Hogervorst, T. P.; Lafleur, R. P. M.; Lou, X.; van der Marel, G. A.; Codee, J. D. C.; Meijer, E. W., Elucidating the ordering in self-assembled glycocalyx mimicking supramolecular copolymers in Water. *J. Am. Chem. Soc.* **2019**, *141*, 13877-13886.
14. van Buel, R.; Spitzer, D.; Berac, C. M.; van der Schoot, P.; Besenius, P.; Jabbari-Farouji, S., Supramolecular copolymers predominated by alternating order: theory and application. *J. Chem. Phys.* **2019**, *151*, 014902, 1-17.
15. Ten Eikelder, H. M. M.; Adelizzi, B.; Palmans, A. R. A.; Markvoort, A. J., Equilibrium model for supramolecular copolymerizations. *J. Phys. Chem. B* **2019**, *123*, 6627-6642.
16. Das, A.; Vantomme, G.; Markvoort, A. J.; Ten Eikelder, H. M. M.; Garcia-Iglesias, M.; Palmans, A. R. A.; Meijer, E. W., Supramolecular copolymers: structure and composition revealed by theoretical modeling. *J. Am. Chem. Soc.* **2017**, *139*, 7036-7044.
17. Hirst, A. R.; Smith, D. K., Two-component gel-phase materials--highly tunable self-assembling systems. *Chemistry* **2005**, *11*, 5496-5508.
18. Makam, P.; Gazit, E., Minimalistic peptide supramolecular co-assembly: expanding the conformational space for nanotechnology. *Chem. Soc. Rev.* **2018**, *47*, 3406-3420.
19. Felder, T.; de Greef, T. F.; Nieuwenhuizen, M. M.; Sijbesma, R. P., Alternation and tunable composition in hydrogen bonded supramolecular copolymers. *Chem. Commun. (Camb)* **2014**, *50*, 2455-2457.
20. Frisch, H.; Nie, Y.; Raunser, S.; Besenius, P., pH-regulated selectivity in supramolecular polymerizations: switching between Co- and homopolymers. *Chemistry* **2015**, *21*, 3304-3309.
21. Frisch, H.; Unsleber, J. P.; Ludeker, D.; Peterlechner, M.; Brunklaus, G.; Waller, M.; Besenius, P., pH-Switchable ampholytic supramolecular copolymers. *Angew. Chem. Int. Ed. Engl.* **2013**, *52*, 10097-10101.
22. Gorl, D.; Zhang, X.; Stepanenko, V.; Wurthner, F., Supramolecular block copolymers by kinetically controlled co-self-assembly of planar and core-twisted perylene bisimides. *Nat. Commun.* **2015**, *6*, 7009, 1-8.
23. de Windt, L. N. J.; Kulkarni, C.; Ten Eikelder, H. M. M.; Markvoort, A. J.; Meijer, E. W.; Palmans, A. R. A., Detailed approach to investigate thermodynamically controlled supramolecular copolymerizations. *Macromolecules* **2019**, *52*, 7430-7438.
24. Sarkar, A.; Sasmal, R.; Empereur-Mot, C.; Bochicchio, D.; Kompella, S. V. K.; Sharma, K.; Dhiman, S.; Sundaram, B.; Agasti, S. S.; Pavan, G. M.; George, S. J., Self-Sorted, random, and block supramolecular copolymers via

sequence controlled, multicomponent self-Assembly. *J. Am. Chem. Soc.* **2020**, *142*, 7606-7617.

25. Pinault, T.; Andrioletti, B.; Bouteiller, L., Chain stopper engineering for hydrogen bonded supramolecular polymers. *Beilstein J. Org. Chem.* **2010**, *6*, 869-875.

26. Folmer, B. J. B.; Sijbesma, R. P.; Versteegen, R. M.; van der Rijt, J. A. J.; Meijer, E. W., Supramolecular polymer materials: chain extension of telechelic polymers using a reactive hydrogen-bonding synthon. *Adv. Mater.* **2000**, *12*, 874-878.

27. Mes, T.; Smulders, M. M. J.; Palmans, A. R. A.; Meijer, E. W., Hydrogen-bond engineering in supramolecular polymers: polarity influence on the self-assembly of benzene-1,3,5-tricarboxamides. *Macromolecules* **2010**, *43*, 1981-1991.

28. Yan, X.; Li, S.; Pollock, J. B.; Cook, T. R.; Chen, J.; Zhang, Y.; Ji, X.; Yu, Y.; Huang, F.; Stang, P. J., Supramolecular polymers with tunable topologies via hierarchical coordination-driven self-assembly and hydrogen bonding interfaces. *PNAS* **2013**, *110*, 15585-15590.

29. Isare, B.; Pensec, S.; Raynal, M.; Bouteiller, L., Bisurea-based supramolecular polymers: From structure to properties. *Comptes Rendus Chimie* **2016**, *19*, 148-156.

30. Saez Talens, V.; Englebienne, P.; Trinh, T. T.; Noteborn, W. E.; Voets, I. K.; Kieltyka, R. E., Aromatic gain in a supramolecular polymer. *Angew. Chem. Int. Ed. Engl.* **2015**, *54*, 10502-10506.

31. Saez Talens, V.; Davis, J.; Wu, C.-H.; Wen, Z.; Lauria, F.; Gupta, K. B. S. S.; Rudge, R.; Boraghi, M.; Hagemeijer, A.; Trinh, T. T.; Englebienne, P.; Voets, I. K.; Wu, J. I.; Kieltyka, R. E., Thiosquaramide-based supramolecular polymers: aromaticity gain in a switched mode of self-assembly. *J. Am. Chem. Soc.* **2020**, *142*, 19907-19916.

32. Wang, L.; Phanstiel, Synthesis of N-(hydroxy)amide- and N-(Hydroxy)thioamide-containing peptides. *J. Org. Chem.* **2000**, *65*, 1442-1447.

33. Saez Talens, V.; Arias-Alpizar, G.; Makurat, D. M. M.; Davis, J.; Bussmann, J.; Kros, A.; Kieltyka, R. E., Stab2-Mediated clearance of supramolecular polymer nanoparticles in zebrafish embryos. *Biomacromolecules* **2020**, *21*, 1060-1068.

34. Kasha, M.; Rawls, H. R.; Ashraf El-Bayoumi, M., The exciton model in molecular spectroscopy. *Pure Appl. Chem.* **1965**, *11*, 371-392.

35. Korevaar, P. A.; Schaefer, C.; de Greef, T. F. A.; Meijer, E. W., Controlling chemical self-assembly by solvent-dependent dynamics. *J. Am. Chem. Soc.* **2012**, *134*, 13482-13491.

36. Goldstein, R. F.; Stryer, L., Cooperative polymerization reactions. Analytical approximations, numerical examples, and experimental strategy. *Biophys. J.* **1986**, *50*, 583-599.
37. Lamour, G.; Kirkegaard, J. B.; Li, H.; Knowles, T. P. J.; Gsponer, J., Easyworm: an open-source software tool to determine the mechanical properties of worm-like chains. *Source Code Biol. Med.* **2014**, *9*, 16, 1-6

SUPPORTING INFORMATION

2.6 Materials and methods

2.6.1 Materials

All reagents and chemicals were purchased from Sigma Aldrich and Acros Organics and used without further purification. Deuterated chloroform was obtained from Euriso-top and Milli-Q water was employed for all experiments. For the hydrogenation reaction, acetonitrile was dried with molecular sieves (3 Å, 20 % w/v), whereas for the thionation reaction anhydrous acetonitrile purchased from Sigma Aldrich was employed.

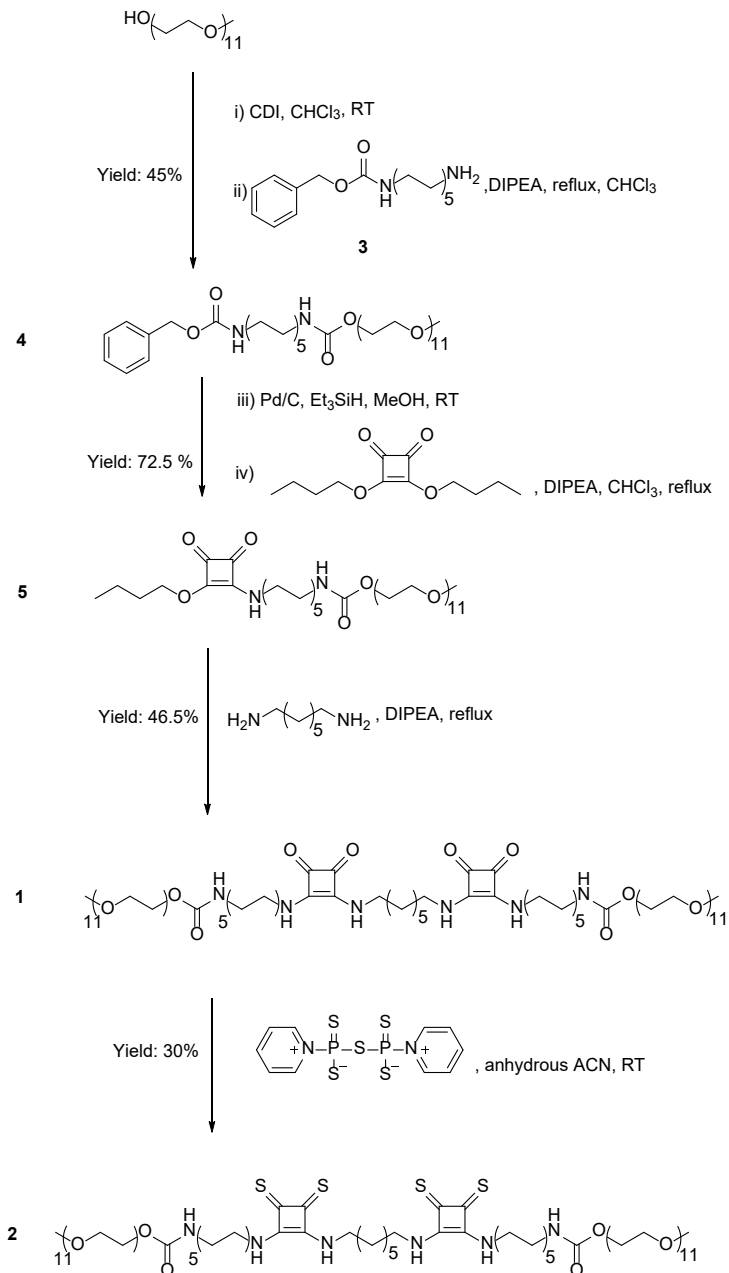
S2.6.2 Instrumentation

Compounds were either purified by silica gel column chromatography or on X1 flash chromatography system equipped with a C18 column from Grace Reveleris using a gradient of H₂O/CH₃CN. ¹H-NMR and ¹³C spectra were obtained on a Bruker (300 MHz) or Bruker DMX-400 (400 MHz). LC-MS analysis was performed on a Finnigan Surveyor HPLC system equipped with a Gemini C18 50 x 4.60 mm column (UV detection at 254 and 214 nm) coupled to a Finnigan LCQ Advantage Max mass spectrometer with ESI. Thiosquaramide-containing molecules were detected using wavelengths of 384 and 228 nm. For the mobile phase, a gradient of 10-90% of CH₃CN/H₂O with 0.1% trifluoroacetic acid over 13.5 minutes was used. MALDI-TOF-MS spectra were obtained on a Bruker Microflex LRF mass spectrometer in reflection positive mode using α -cyano-4-hydroxycinnamic acid with a laser power of 30%. UV-vis measurements were performed on a Cary 300 UV-vis spectrophotometer using a quartz cuvette of 1 cm path length. DLS measurements were carried out using a Malvern Zetasizer Nano ZS ZEN3500 equipped with a laser of 633 nm and a scattering angle of 173°. Atomic force microscopy (AFM) images were recorded in tapping mode on a Veeco-Bruker Multimode AFM with a Nanoscope IIIa controller at room temperature. The AFM tips used were Oltespa Opus probes with a reflex aluminium coating, with a nominal spring constant of 2 N/m, a nominal resonance frequency of 70 kHz and a tip radius of 7 nm. The images were processed using Nanoscope software. Fluorescence experiments were recorded on an Infinite M1000 Pro Tecan plate reader with a black background 96-well plate.

Cryo-TEM images were collected using a Tecnai F12 (FEI Company, The Netherlands) equipped with a field emission gun operating at 120 keV using a Gatan UltraScan charge-couple device (CCD) camera (Gatan company, Germany) with a defocus between -6 and $-9\text{ }\mu\text{m}$.

2.6.3 Synthetic schemes

Synthesis of squaramide-based bolaamphiphiles



Synthesis of 3

1,10-diaminodecane (10 g, 58.03 mmol) was dissolved in DCM (100 mL) and cooled down to 0 °C. Benzyl chloroformate (1.65 mL, 11.6 mmol) in DCM (200 mL) was added dropwise to a solution of 1,10-diaminodecane over a period of 2 h at room temperature prior to being stirred overnight at room temperature (RT). Subsequently, 1 M HCl (10 mL) was added to the reaction mixture and a white precipitate was formed. The solvent was removed by rotary evaporation and the white precipitate was washed several times with ethyl acetate.

Yield: 2.5 g, 69.5 % ^1H NMR (300 MHz, CDCl_3): δ (ppm) = 7.90 (br s, 3H), 7.41-7.25 (m, 5H), 5.02 (s, 2H), 3.02-2.95 (m, 2H), 2.79-2.72 (m, 2H), 1.57-1.50 (m, 2H), 1.42-1.26 (m, 14H). ^{13}C NMR (75 MHz, CDCl_3): δ (ppm) = 156.03, 137.29, 128.29, 127.68, 127.64, 65.01, 40.13, 38.73, 29.35, 28.82, 28.72, 28.64, 28.46, 26.92, 26.18, 25.76.

Synthesis of 4

Undecaethylene glycol methyl ether (0.591 g, 1.11 mmol) was first activated with CDI (0.222 g, 1.37 mmol) for 1 h at RT (LCMS: $t = 4.14$ min, m/z : 611.27 $[\text{M}+\text{H}]^+$). Subsequently, diisopropylethylamine (DIPEA) (0.4 mL, 2.22 mmol) and **2** (0.460 g, 1.48 mmol) were added to the reaction mixture and refluxed overnight. When the reaction was complete (LCMS: $t = 6.7$ min, m/z : 670.5 $[\text{M}+\text{H}]^+$), the compound was purified by flash chromatography on a C18 silica column using a gradient of $\text{H}_2\text{O}/\text{CH}_3\text{CN}$ 20-90% over 40 min. The solvent was removed *in vacuo* and the compound was lyophilized and isolated as white solid.

Yield: 0.336 g, 45%, ^1H NMR (300 MHz, CDCl_3): δ (ppm) = 7.36 – 7.23 (m, 5H), 5.06 (s, 2H), 4.22 – 4.13 (m, 2H), 3.62 (s, 47H), 3.56 – 3.45 (m, 3H), 3.35 (s, 4H), 3.13 (t, 5H), 1.47 – 1.39 (m, 4H), 1.25 (s, 13H). ^{13}C NMR (75 MHz, CDCl_3): δ (ppm) = 156.39, 136.73, 128.42, 127.96, 77.62, 77.19, 76.77, 71.88, 70.52, 70.45, 69.62, 66.40, 63.71, 58.93, 53.49, 41.03, 40.96, 29.88, 29.34, 29.14, 26.64. LCMS: $t = 6.7$ min, (m/z): 670.5 $[\text{M}+\text{H}]^+$.

Synthesis of 5

4 (0.483 g, 0.55 mmol) was dissolved in dry MeOH (5 mL) and Pd/C (0.029 g, 0.275 mmol) was added. The round bottom flask was put under argon atmosphere and Et₃SiH (3.5 mL, 40 mmol) was added dropwise and the reaction mixture was stirred overnight at RT. Subsequently, the catalyst was removed by filtration over celite and the solvent was removed under a stream of N₂ gas overnight. The compound was redissolved in CHCl₃ (20 mL) and 3,4-dibutoxy-3-cyclobutene-1,2-dione (0.096 mL, 0.45 mmol) and DIPEA (0.195 mL, 1.12 mmol) were added and stirred together overnight at RT. The product was purified by flash chromatography on a C18 silica column using a gradient of H₂O/CH₃CN 20-90 % over 40 min. The compound was obtained as white solid.

Yield: 0.346 g, 72.5%, ¹H NMR (300 MHz, CDCl₃) δ (ppm) = 6.74 (s, 1H), 4.71 (q, 2H), 4.20 (m, 2H), 3.71 – 3.49 (m, 44H), 3.36 (s, 3H), 3.13 (m, 2H), 1.76 (m, 2H), 1.60 (m, 2H), 1.33 – 1.23 (m, 12H), 0.96 (t, 3H). ¹³C NMR (75 MHz, CDCl₃): δ (ppm) = 159.46, 77.51, 77.08, 76.66, 73.35, 71.90, 70.54, 69.65, 63.80, 58.72, 44.84, 40.98, 32.00, 29.89, 29.30, 29.12, 29.03, 26.63, 26.28, 18.62, 13.46. LCMS: t_r = 6.5 min, (m/z): 867.83 [M+H]⁺, MALDI: (m/z): 889.456 [M+Na]⁺.

Synthesis of 1

5 (0.240 g, 0.277 mmol) was dissolved in CHCl₃ (15 mL) and 1,7-diaminoheptane (0.012 g, 0.129 mmol) and DIPEA (0.063 mL, 0.360 mmol) were added to the reaction mixture and refluxed overnight. The compound was purified by flash chromatography on a C18 silica column using a gradient of H₂O/CH₃CN 20-90 % over 40 min. The solvent was removed in *vacuo* and the compound was lyophilized and obtained as a white solid.

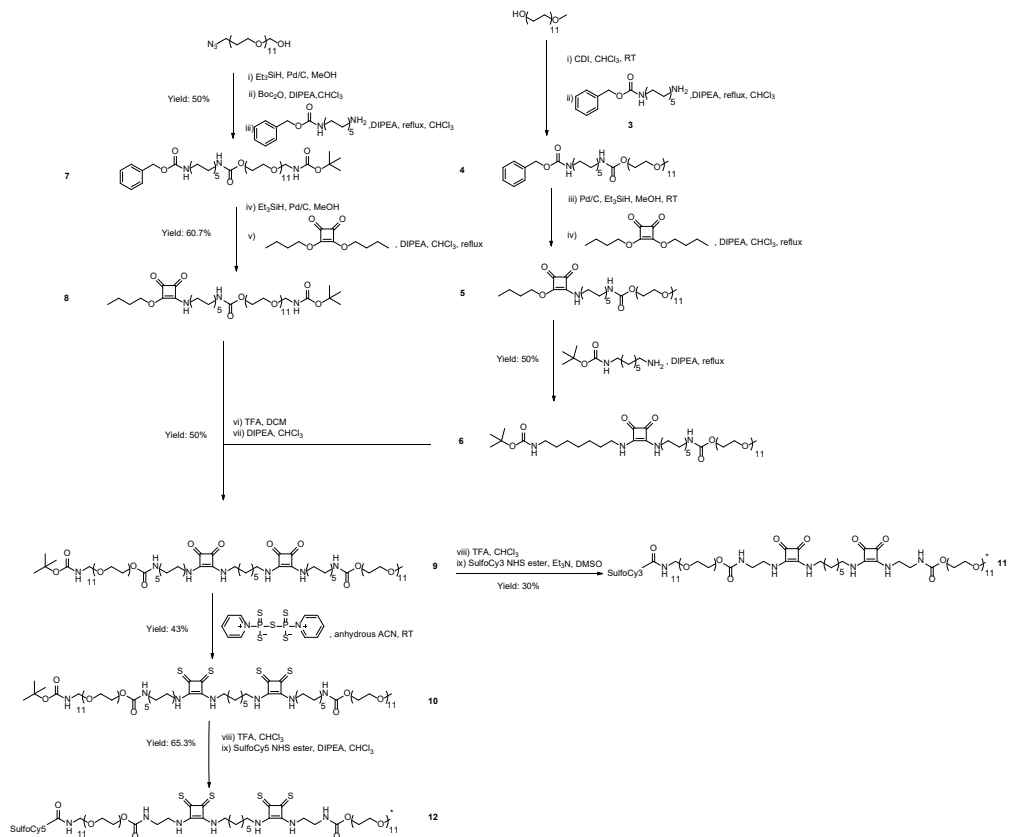
Yield: 0.103 g, 46.5%. ¹H NMR (300 MHz, CDCl₃): δ (ppm) = 7.84 (s, 1H), 7.60 (s, 1H), 5.04 (s, 1H), 4.22 (t, 2H), 3.77 – 3.51 (m, 46H), 3.40 (s, 3H), 3.14 (d, 2H), 1.64 (d, 4H), 1.55 – 1.18 (m, 18H). ¹³C NMR (75 MHz, CDCl₃): δ (ppm) = 169.13, 167.20, 158.79, 156.68, 77.44, 77.01, 76.59, 71.91, 70.58, 70.51, 70.48, 69.73, 63.80, 59.03, 44.77, 41.08, 31.09, 29.93, 29.41, 29.20, 26.72, 26.39. LCMS: t_r = 6.48 min, (m/z): 1716.30 [M+H]⁺, MALDI: (m/z): 1736.553 [M+Na]⁺.

Synthesis of 2

1 (0.061 g, 0.035 mmol) was dissolved in anhydrous acetonitrile (5mL) and pentathiodiphosphorus(V) acid-P,P'-bis(pyridinium betaine (0.311g, 0.805 mmol) was added. The reaction mixture was stirred overnight at RT. After the filtration, the compound was isolated by flash chromatography on a C18 silica column using a gradient of H₂O/CH₃CN 30-90 % over 30 min. The compound was obtained as a yellow solid.

Yield: 0.018 g, 30% ¹H NMR (500 MHz, CDCl₃) δ (ppm) = 8.85 (s, 1H), 8.60 (s, 1H), 5.02 (s, 1H), 4.23-4.21 (m, 4H), 4.16-4.12 (m, 5H), 3.67-3.54 (m, 84H), 3.39 (s, 6H), 3.17-3.13 (m, 4H), 1.76-1.68 (m, 7H), 1.52 – 1.24 (m, 34H). ¹³C NMR (125 MHz, CDCl₃): δ (ppm) = 204.02, 203.57, 170.96, 170.88, 156.58, 77.37, 77.12, 76.86, 71.89, 70.58, 70.43, 70.38, 70.26, 69.89, 63.74, 59.12, 44.20, 43.46, 41.16, 40.50, 31.04, 29.98, 29.47, 29.42, 29.31, 29.17, 26.80, 26.43, 25.51. LCMS: t_r = 7.43 min, (m/z): 1780.28 [M+H]⁺.

Synthesis of sulfo-Cy3 and sulfo-Cy5 dye-conjugated squaramide-based bolaamphiphiles



Synthesis of 6

5 (0.178g, 0.205 mmol) was dissolved in CHCl_3 (10 mL) with 1-boc-1,7-diaminoheptane (0.071g, 0.308 mmol) and DIPEA (0.107 mL, 0.615 mmol) and the mixture was refluxed overnight. The compound was isolated by flash chromatography on a C18 silica column using a gradient of $\text{H}_2\text{O}/\text{CH}_3\text{CN}$ 20-90 % over 30 min and was obtained as a yellowish solid.

Yield: 0.104 g, 50%. ^1H NMR (400 MHz, CDCl_3): δ (ppm) = 7.29 (s, 1H), 5.05 (s, 1H), 4.71 (s, 1H), 4.19-4.15 (m, 2H), 3.63-3.50 (m, 46H), 3.18 – 2.98 (m, 3H), 1.83 – 1.70 (m, 1H), 1.64 – 1.53 (m, 3H), 1.45 (s, 9H), 1.32 – 1.20 (m, 15H). ^{13}C NMR (100 MHz, CDCl_3): δ (ppm) = 182.43, 168.05, 156.62, 77.39, 77.08, 76.76, 73.39, 71.94, 70.57, 69.66, 63.85, 59.02, 44.90, 44.59, 44.53, 41.03, 32.03, 31.17, 30.90, 30.63, 29.91, 29.36, 29.16, 29.05, 28.73, 28.47, 26.65, 26.43, 26.31, 18.65. LCMS: t_r = 6.67min. (m/z): MALDI: (m/z): 923.587 $[\text{M}+\text{H}-\text{Boc}]^+$, 1045.377, $[\text{M}+\text{Na}]^+$.

Synthesis of 7

O-(2-Azidoethyl)undecaethylene glycol (0.642 g, 1.12 mmol) was dissolved in anhydrous MeOH (10 mL) and Pd/C (0.059 g, 0.56 mmol) was added under N_2 atmosphere. Et_3SiH (3.57 mL, 22.4 mmol) was added dropwise to the reaction and stirred overnight. Subsequently, the compound was filtered over celite to remove the catalyst and the solvent was removed using a gentle stream of N_2 gas. Subsequently, the residue was redissolved in CHCl_3 (10 mL) in presence of DIPEA (0.585 mL, 3.36 mmol) and Boc_2O (0.404 g, 1.85 mmol) at room temperature. After 2 h hours, the product was confirmed by LCMS (t_r = 4.76 min, m/z: 545.78 $[\text{M}+\text{H}-\text{Boc}]^+$) and the solvent was removed from the oily residue prior to its activation with CDI (0.205 g, 1.23 mmol) at RT. After that the formation of the product was confirmed by LC-MS (t_r = 4.55 min, 639.17 m/z, $[\text{M}+\text{H}-\text{Boc}]^+$), the mixture was dissolved in CHCl_3 (10 mL) and the DIPEA (0.390 mL, 2.24 mmol) and N-Cbz-1,10-decanediamine (0.457g, 1.49 mmol) were added and refluxed overnight. The final compound was purified by flash chromatography on a C18 silica column using a gradient of $\text{H}_2\text{O}/\text{CH}_3\text{CN}$ 20-90 % over 35 min and lyophilized. The final compound was obtained as a yellowish solid.

Yield: 50 % 0.483 g, ^1H NMR (400 MHz, CDCl_3): δ (ppm) = 7.31 – 7.16 (m, 5H), 4.99 (s, 2H), 4.11 (t, 2H), 3.56-3.42 (m, 66H), 3.54 (s, 11H), 3.23 – 3.18

(m, 2H), 3.11-3.01 (m, 4H), 1.42-1.35 (m, 17H), 1.22 – 1.15 (m, 13H). ^{13}C NMR (100 MHz, CDCl_3): δ (ppm) = 150.98, 77.53, 77.11, 76.69, 70.51, 70.24, 70.19, 69.64, 66.49, 63.73, 40.99, 29.90, 29.37, 29.17, 28.41, 26.67 LCMS: $t=7.87$ min, (m/z): 878.16 $[\text{M}+\text{H}]^+$.

Synthesis of 8

7 (0.410 g, 0.552 mmol) was dissolved in anhydrous MeOH (10 mL) and Pd/C was added under an N_2 atmosphere. Et_3SiH (1.76 mL, 11.04 mmol) was added dropwise and the reaction was stirred overnight. When the reaction was complete (LCMS: $t = 3.65$ min, m/z: 546.13 $[\text{M}+\text{H}]^+$) the compound was filtered over celite and the solvent was removed under a gentle stream of N_2 gas. The reaction mixture was dissolved in CHCl_3 (5 mL) and DIPEA (0.192 mL, 1.1 mmol,) and squaric ester (0.095 mL, 0.442 mmol) were added. The reaction mixture was stirred overnight at RT and the product was purified by flash chromatography on a C18 silica column using a gradient of $\text{H}_2\text{O}/\text{CH}_3\text{CN}$ 10-90 % over 40 min. The product was isolated as a yellowish solid.

Yield: 60.7 % 0.334 g, ^1H NMR (400 MHz, CDCl_3): δ (ppm) = 5.18 (s, 1H), 5.05 (s, 1H), 4.75-4.73 (t, 2H), 4.21-4.20 (t, 2H), 3.76-3.61 (m, 42H), 3.56-3.53 (m, 2H), 3.42-3.37 (m, 2H), 3.31 (s, 2H), 3.16-3.13 (m, 2H), 1.80-1.77 (m, 2H), 1.63-1.58 (m, 4H), 1.49-1.45 (m, 15H), 1.31-1.28 (m, 12H), 1.00 – 0.86 (t, 3H) ^{13}C NMR (100 MHz, CDCl_3): δ (ppm) = 189.32, 184.23, 182.79, 177.23, 172.52, 156.43, 156.00, 79.01, 77.56, 77.24, 76.92, 74.25, 73.23, 70.50, 70.18, 70.13, 69.60, 63.73, 44.80, 40.95, 40.31, 31.98, 31.72, 30.60, 29.87, 29.32, 29.13, 29.03, 28.39, 26.63, 26.31, 18.61, 18.46, 13.59. LCMS: $t=7.43$ min, (m/z): 895.44 $[\text{M}+\text{H}-\text{Boc}]^+$, MALDI: (m/z): 896 m/z $[\text{M}+\text{H}-\text{Boc}]^+$.

Synthesis of 9

6 (0.028 g, 0.030 mmol) was deprotected using trifluoroacetic acid (TFA) (2 mL) stirring for 20 min at RT. After the removal of the acid using a gentle stream of N_2 gas, the compound was redissolved in CHCl_3 (10 mL), and **8** (0.024 mmol, 0.027 g) and DIPEA (2 eq, 0.060 mmol, 0.012 mL) were added. The mixture was refluxed overnight. The product was purified by flash

chromatography on a C18 silica column using a gradient of H₂O/CH₃CN 10-90% over 35 min and was obtained as a yellowish solid.

Yield: 0.0028 g, 50 %, ¹H NMR (400 MHz, CDCl₃): δ (ppm) = 7.92 (s, 1H), 7.66 (s, 1H), 4.22 (t, 4H), 3.68 (d, 89H), 3.61 – 3.53 (m, 4H), 3.34 (s, 3H), 3.16 (m, 6H), 1.65 (m, 7H), 1.49 – 1.25 (m, 49H). ¹³C NMR (100 MHz, CDCl₃): δ (ppm) = 182.69, 181.76, 168.98, 167.34, 156.54, 77.38, 77.07, 76.75, 71.91, 70.57, 70.52, 70.26, 69.70, 63.78, 59.02, 44.73, 43.35, 41.08, 40.39, 31.19, 29.96, 29.47, 29.27, 29.24, 28.45, 26.75, 26.45, 24.97. LCMS: t=6.81 min, m/z: 1745.16 [M+H-Boc]⁺, MALDI: (m/z): 1865.32 [M+Na]⁺.

Synthesis of 10

9 (0.028 g, 0.015 mmol) was dissolved in anhydrous CH₃CN (3 mL) and pentathiodiphosphorus (V) acid-P,P'-bis(pyridinium betaine) (0.133 g, 0.35 mmol) was added to the reaction mixture and stirred at RT overnight. Subsequently, the crude was filtered and purified by HPLC using a gradient of 30-90 % H₂O/ CH₃CN over 30 min. The acetonitrile was removed by rotary evaporation and the compound was lyophilized and isolated as a sticky yellow solid. Yield: 8 mg 30 % LCMS: t=8.00 min, m/z: 1809.83 [M+H-Boc]⁺.

Synthesis of 11

9 (4.52 mg, 0.0023 mmol) was dissolved in TFA (1 mL) to remove the boc-protecting group and it was stirred for 10 min at RT. When the reaction was complete (LCMS: t= 5.77 min, m/z: 1745.27 [M+H]⁺), the solvent was removed by a gentle stream of N₂ gas. The compound was redissolved in DMSO (1.5 mL) and Et₃N (200 μL) were added. Sulfo-Cy3 ester in DMSO (0.284 mL, 0.0028 mmol) was added and the reaction mixture was stirred overnight at RT. When the reaction was complete (LCMS: t=5.86 min, m/z: 2345.8 [M+H]⁺), the solvent was removed by a stream of N₂ gas overnight. The compound was dialyzed for 2 days to remove the excess of dye, and purified by HPLC using a gradient of H₂O/CH₃CN 10-90 % over 30 min. The final compound was obtained as a sticky pink solid and was stored in the dark. Yield: 2.28 mg, 43 %, LCMS: t=5.86 min, m/z: 2345.8 [M+H]⁺.

Synthesis of **12**

10 (4.52 mg, 0.0023 mmol) was dissolved in TFA (1 mL) and stirred for 10 min at RT. When the reaction was complete (LC-MS: $t=8.00$ min, m/z : 1809.83 $[M+H]^+$), the solvent was removed by a gentle stream of N_2 . The compound was redissolved in $CHCl_3$ (1 mL) and DIPEA (250 μ L) was added. Subsequently, sulfo-Cy5 ester in DMSO (0.284 mL, 0.0028 mmol) was added and the reaction was stirred at RT for 3 h. When the reaction was complete (LCMS: $t=6.86$ min, m/z : 2435.20 $[M+H]^+$), the solvent was removed overnight by a stream of N_2 gas. The compound was dialyzed for 2 days to remove the excess of dye and HPLC purified using a gradient of H_2O/CH_3CN 10-90 % over 30 min. The final compound was obtained as a sticky blue solid and was stored in the dark. Yield: 3.77 mg, 65.3 % LCMS: $t=6.86$ min, m/z : 2435.20 $[M+H]^+$.

2.6.4 Characterization

Sample preparation

Supramolecular polymers

Monomers **1** and **2** were weighed independently and dissolved in milliQ water to obtain a 1 mM concentration of each monomer. Aliquots from the stock solutions were taken to prepare solutions at the desired concentration for solution phase measurements in water. All samples were equilibrated at RT overnight before measurement.

Supramolecular copolymers

To prepare supramolecular copolymers, stock solutions of **1** and **2** were first prepared independently. Monomer **1** was dissolved in HFIP (1 mM) and **2** in THF (1 mM) before removing the solvents using a gentle stream of N_2 gas. Subsequently, milliQ water was added to both compounds to obtain a final concentration of 1 mM for each stock. The solutions were then mixed in an equimolar ratio and diluted to the desired concentrations for measurement and equilibrated at RT overnight. A similar approach was used to prepare samples at different molar ratios.

UV-vis spectroscopy

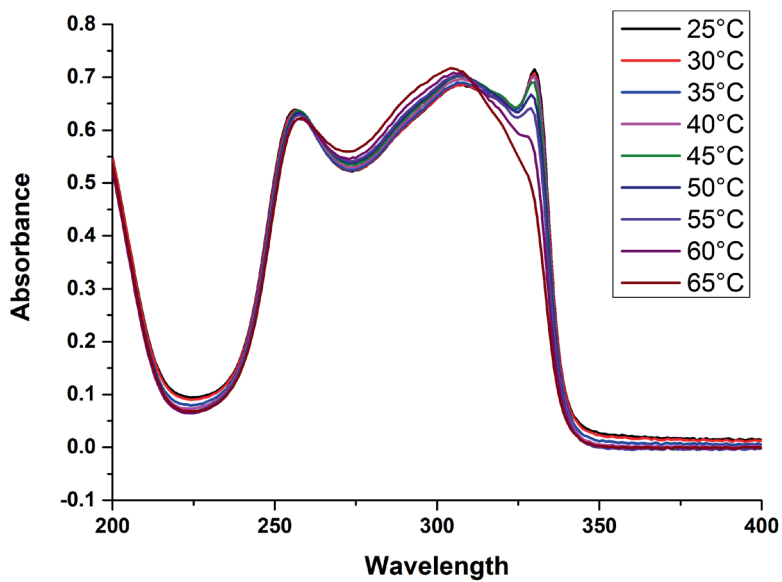
UV-vis spectra of **1** and **2** and their copolymers were acquired on solutions (30 μM) prepared according to the sample preparation protocol described above. UV-vis spectra were recorded from 200-500 nm. Quartz cuvettes with a path length of 1 cm were used for measurements involving temperature or organic solvents (HFIP, DMSO or THF).

UV-vis titration

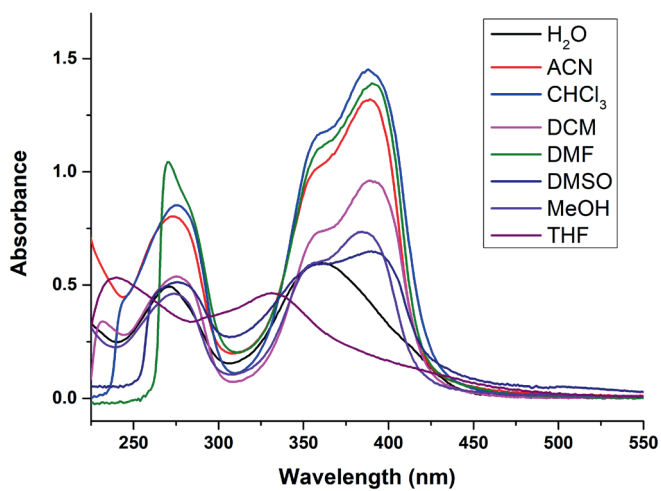
Supramolecular polymers of **1** and **2** (30 μM) were prepared using the preparation protocol described above. Monomer **1** (600 μL) was titrated with HFIP and **2** (600 μL) was titrated with THF (final volume: 652 μL) and a UV-vis spectra was recorded after the addition of each aliquot (2 μL) of organic solvent. The titration was stopped when a plateau in the absorbance was reached for each monomer. The degree of aggregation (α_{agg}) was plotted against the volume fraction of HFIP or THF in water and the experimental data were fitted with the equilibrium model described by Meijer³⁵ and co-workers and the thermodynamic parameters (ΔG° , σ , and m) were obtained in Maple software.

Table S1. Thermodynamic parameters for supramolecular polymerizations of **1** and **2**

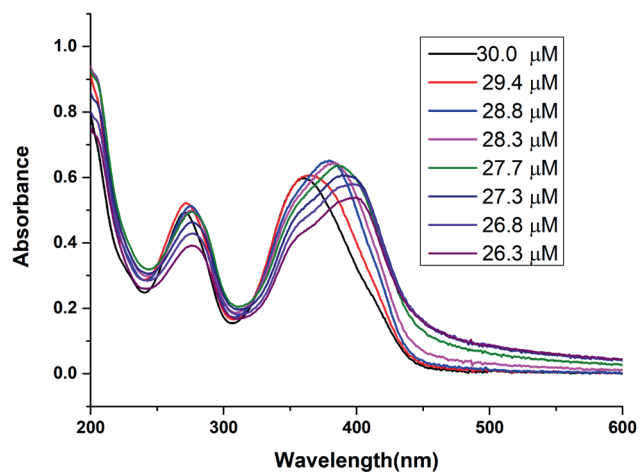
	ΔG° (kJ/mol)	m (kJ/mol)	σ
1	-34	270	0.78
2	-35	200	0.06



S2.1 Temperature-dependent UV-vis spectra of **1** ($c=30\ \mu\text{M}$).



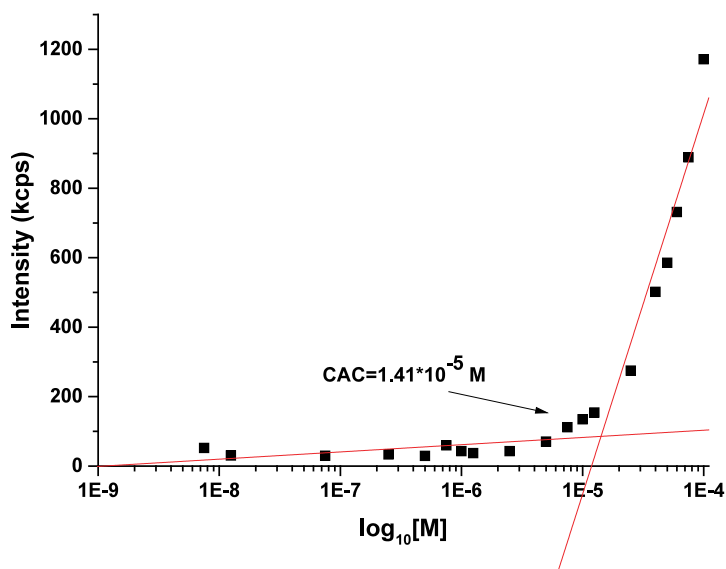
S2.2 UV-vis spectra of **2** ($c=30\ \mu\text{M}$) in various organic solvents.



S2.3 UV-vis titration of **2** ($c=30\ \mu\text{M}$) with HFIP.

Critical aggregation concentration (CAC) determination

A stock solution of **2** (1 mM) was prepared and diluted after overnight equilibration. Concentrations between 100 μM and 2 nM were prepared and then equilibrated for at least 3h. Each scattering measurement was carried out using a disposable DLS cuvette and performed in triplicate. The data was plotted using the scattering intensity as a function of $\log [C]$. The critical aggregation concentration was then determined from the intersection of the two lines drawn through the points collected for the scattering intensities collected at the various concentrations.



S2.4 Critical aggregation concentration determination of **2** using static light scattering.

Table S1: Static light scattering data of **1** and **2** in water, THF and HFIP (6 mM)

	Water (kcps)	THF (kcps)	HFIP (kcps)
solvent	-	1177.1	1506.9
2 (6 mM)	5077.7	1560.7	14871.5
1 (6 mM)	3831.6		3563.5

ζ-potential measurements

Solutions of **1** or **2** (1 mM) co-assembled with **11** or **12** (2 mol%) were prepared according to the protocol described above and equilibrated overnight. The samples were transferred to a ζ-potential dip cell prior the measurements.

Cryo-transmission electron microscopy (cryoTEM)

Two stock solutions were prepared by dissolving **1** in HFIP (3 mM) and **2** (3 mM) in THF. The organic solvents were removed by an N₂ stream and **1** was rehydrated with water and added to **2** to result in a 1:1 molar ratio and a final concentration of 580 μM. The sample was prepared applying 3 μL of the supramolecular (co)polymer solutions (5.8 mM) on to a freshly glow-discharged 300 mesh copper grid with a lacey-carbon support film (Electron Microscopy Sciences).

Calculation of persistence length (PI) and bending rigidity (κ)

Cryo TEM images were converted in JPEG format and were analyzed by the Easyworm software. The fiber contour length was obtained by the copolymerization of oxo- and thiosquaramide. According to worm-like chain model (WLC), the persistence length was calculated from the mean end-to-end distance $\langle R^2 \rangle_{2D}$ of **1**, **2** and the copolymers obtained by the copolymerization of **1** and **2** exploiting the following equation:

$$\langle R^2 \rangle_{2D} = 4P_l l \left[1 - \frac{2P_l}{l} \left(1 - e^{-\frac{l}{2P_l}} \right) \right]$$

Subsequently, the bending rigidity (κ) of the supramolecular polymer fibers was determined using this equation:

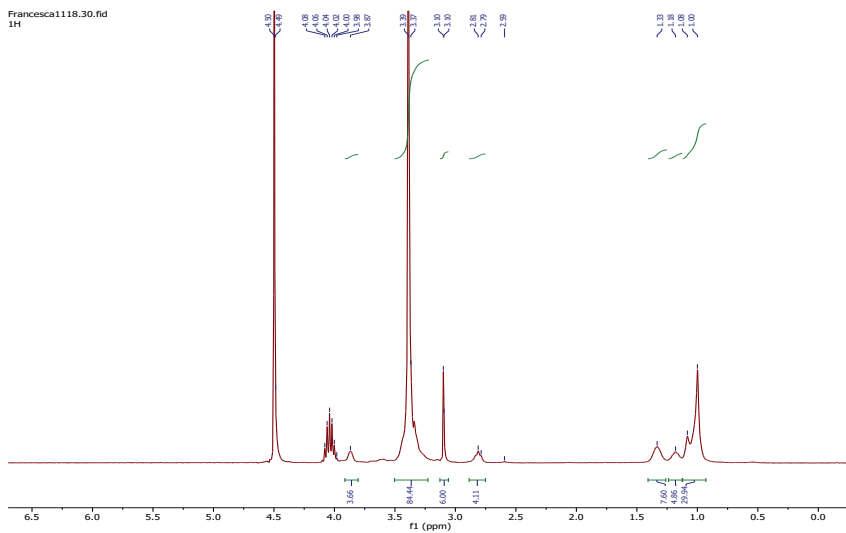
$$\kappa = K_b \cdot T \cdot P_l$$

where K_b is the Boltzmann constant, and T is the temperature expressed in K.

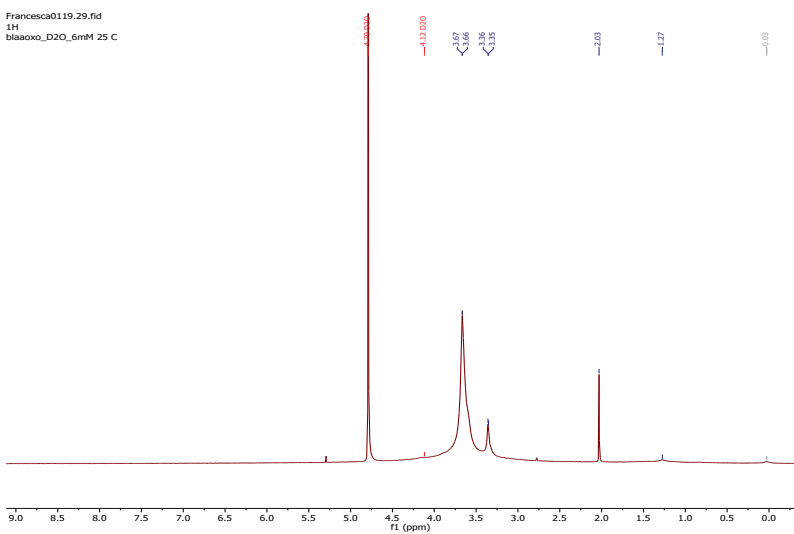
Forster resonance energy transfer (FRET) experiments

A solution of **1** (1 mM) in HFIP with 1 or 2 mol% of **12** was prepared and the solvent was removed by N_2 gas. Similarly, a solution of **2** (1 mM) in THF with 1 or 2 mol% of **11** was prepared and the solvent was removed. Water was added to both vials to obtain a final concentration of 1 mM for each stock and then mixed in an equimolar ratio. Aliquots from the mixed solutions were taken to prepare solutions at a 60 μ M concentration and left to stand overnight. Fluorescence spectra were recorded using an Infinite M1000 Pro Tecan plate reader, using an excitation wavelength of 550 nm and measuring fluorescence emission from 570 to 800 nm.

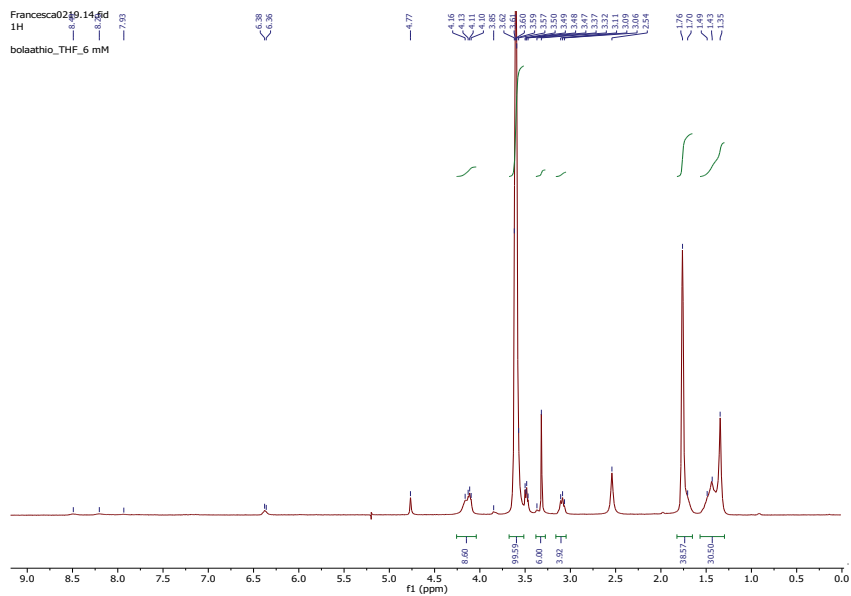
^1H NMR spectra



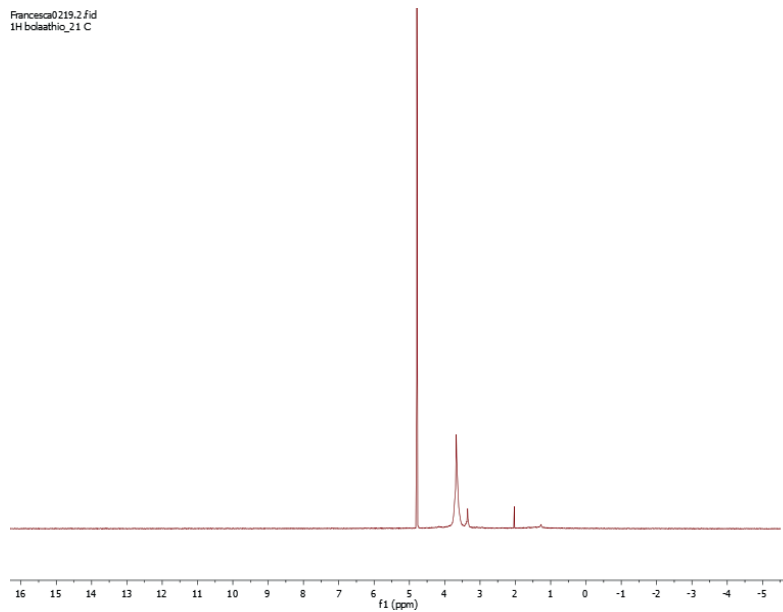
S2.5 ^1H NMR spectra of **1** (6 mM) in HFIP- d_2



S2.6 ^1H NMR spectrum of **1** in D_2O (6 mM)



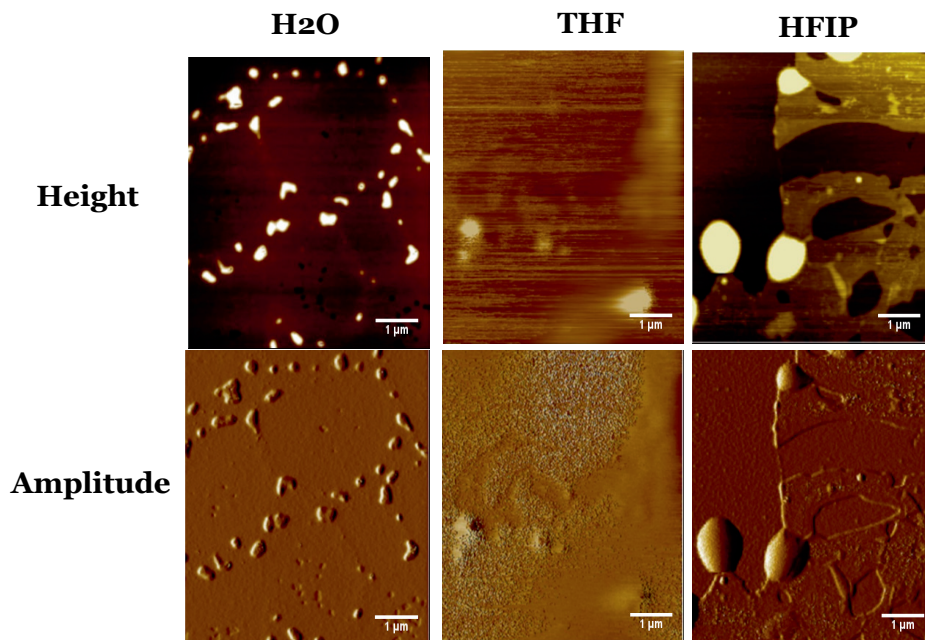
S2.7 ^1H NMR spectra of **2** in THF (6 mM)



S2.8 ^1H NMR spectra of **2** in D_2O (6 mM).

Atomic force microscopy (AFM)

Solutions of **2** (30 μM) were independently prepared in H_2O , THF and HFIP and equilibrated overnight. An aliquot (25 μL) from each of these solutions was pipetted on a cleaved mica surface and dried overnight at RT before the measurements. The obtained AFM images were analyzed using the Nanoscope software.



S2.9 AFM micrographs (height and amplitude) of **2** in water, THF and HFIP (15 μM), scale bar: 1 μm).

CHAPTER 3

Tripodal acids as building blocks for the Ugi multicomponent reactions

3.1 Abstract

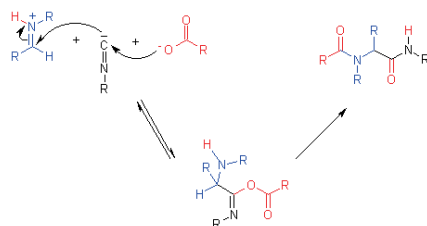
Trigonal molecules have found broad application as scaffolds in the fields of supramolecular, coordination and catalysis chemistry. However, their synthesis often requires multistep reactions to obtain the designed monomer. To expedite the synthesis of trigonal molecules, multicomponent reactions provide a viable approach to obtain functional molecules with high structural diversity and yield in a single step. The Ugi reaction is a multicomponent reaction involving an isocyanide, amine, carboxylic acid and aldehyde or ketone that generates an α -acetamido carboxamide or peptide-like bond that can analogously be seen in numerous supramolecular structures. In this chapter, the use of different acidic tripodal cores based on nitrilotriacetic or squaric acids are examined in the multicomponent Ugi reaction to prepare trigonal scaffolds. Modulation of the amine and isocyanide components and their respective concentrations and the reaction temperature were probed for their efficiency to obtain the trisubstituted product. Reaction of nitrilotriacetic acid with ammonium carbonate resulted in a mixture of mono-, di- and trisubstituted compounds emphasizing the need for a stable imine to be formed to yield the desired trisubstituted compound. In contrast, the use of a tripodal squaric acid with a primary amine, defined reagents concentration, increased temperature and longer reaction times resulted in the preferential formation of the trisubstituted product over mono- and disubstituted compounds.

3.2 Introduction

Trigonal conjugates, including -symmetric, tripodal and triskelion systems, play an important role in biological processes¹ found in Nature. In endocytosis, clathrin that regulates cellular uptake of membrane proteins and neurotransmitters through the formation of coated vesicles, is a triskelion protein with three heavy chains and three light chains.² Trigonal scaffolds have been also exploited in synthetic molecules for several applications in homogeneous catalysis,³ coordination and supramolecular chemistry.^{4, 5} Tripodal ligands have a higher chelating effect towards ions and tunable selectivity that can be modulated according to the bulkiness of the arms in comparison to receptors that are bi- or monopodal.⁶ Additionally, when C₃-symmetric scaffolds are used as cores for supramolecular monomers, they show enhanced ability to self-assemble into supramolecular polymers when put against their C₂-symmetric counterparts.^{7, 8} More specifically, a widely exploited core is based on benzene-1,3,5-tricarboxamide (BTA) that benefits from hydrogen bonding and π - π interactions to form supramolecular polymers with helical character when chiral substituents are used.^{8, 9} This core has provided tremendous insight into the monomer features required for polymerization and its control in a range of media.⁹ However, in order to achieve monomer with specific function, C₃-symmetric and tripodal building blocks usually require several reaction steps to obtain a designed monomer,⁹ thus efficient synthetic approaches are necessary to expedite their preparation for a broad range of applications.

Multicomponent reactions are a class of reactions used to construct functional molecular scaffolds in a high yielding (70-90%), selective and rapid manner, often being performed in one pot.^{10, 11} Compounds with high structural diversity can be obtained in a minimum number of synthetic steps, and have been used to generate libraries for assessing structure activity relationships (SARs) of therapeutics in the drug discovery pipeline.¹² One important multicomponent reaction is the four component Ugi reaction that involves the use of an isocyanide, aldehyde/ketone, carboxylic acid, and amine to generate α -acetamido carboxamides.^{11, 13, 14} In the Ugi mechanism, condensation of the amine with the aldehyde first occurs. This step is critical for the formation of the final product and to increase the yield of the reaction. Subsequently, proton transfer from the carboxylic acid to imine occurs, followed by its reaction with the terminal carbon of the isocyanide yielding the nitrilium ion. The carboxylate then participates in a second nucleophilic addition on the nitrilium ion forming an imidate derivative prior to an irreversible Mumm

rearrangement that drives the reaction and determines the structure of the final Ugi products. Because of the commercial availability of hundreds of amines, aldehydes, and carboxylic acids, a large number of Ugi-end products are synthetically feasible opening the door for use in numerous applications.¹⁵



General Scheme Ugi reaction

Several factors have been identified to steer the outcome of the Ugi reaction such as the type of solvent, chosen amine and carboxylic acid, the overall reactant concentrations and temperature. Notably, the solvent plays a critical role in the Ugi reaction; polar and protic solvents such as MeOH or TFE are often used because of their capacity to stabilize the polar intermediates of the reaction. The choice of amine and carboxylic acid component can also play an important role in the formation and stabilization of the imine. If the chosen amine is not nucleophilic enough, a low Ugi product yield is obtained. Moreover, the presence of a strong acid in the reaction mixture is also critical to increase the electrophilic character of the imine through its protonation for the formation of the subsequent intermediates and to ensure a high yield.¹⁶ Additionally, the reactivity of carbonyl group is critical as aromatic and aliphatic aldehydes react more readily in the Ugi reaction than aliphatic and aromatic ketones.¹⁷ Importantly, these factors have often been explored in the context of monofunctional adducts, however execution of two or more Ugi reaction on the same acid have been examined to a lesser extent.¹⁸⁻²² In a recent work, Dehghan and co-workers successfully introduced trimesic acid as the acid component of Ugi reaction for the synthesis of novel C₃-symmetric peptide-based molecules.²³ Additionally, squaric acids have been reported for their use in the Ugi reaction to yield bifunctional squaramide adducts for use in medicinal chemistry.²² Because of the broad utility of tripodal cores in supramolecular chemistry,²⁴ we became interested to examine the feasibility of using the Ugi reaction to generate tripodal scaffolds based on peptide-like amide and squaramide bonds starting from nitrilotriacetic and squaric acid.

In our research group, we are particularly interested in the use of squaramides in supramolecular systems. Squaramides are ditopic supramolecular synthons that form strong hydrogen bonds by synergizing with a gain in aromatic character of the cyclobutenedione ring on self-assembly.^{25, 26} They have been exploited in the organocatalysis^{27, 28} and anion receptor field.²⁹⁻³³ Previously, we investigated the self-assembly of squaramide-based bolaamphiphiles into supramolecular polymers through hydrogen bonding and hydrophobic interactions in water.³⁴ In a follow up work, we studied the ability of a small family of tripodal squaramide-based monomers to gelate water and to encapsulate stem cells in 3D for their culture.³⁵ We herein examine the use of nitrilotriacetic or trisquaric acids in combination with various Ugi components to establish the optimal conditions for this multicomponent reaction to prepare a range of tripodal scaffolds for supramolecular assembly.

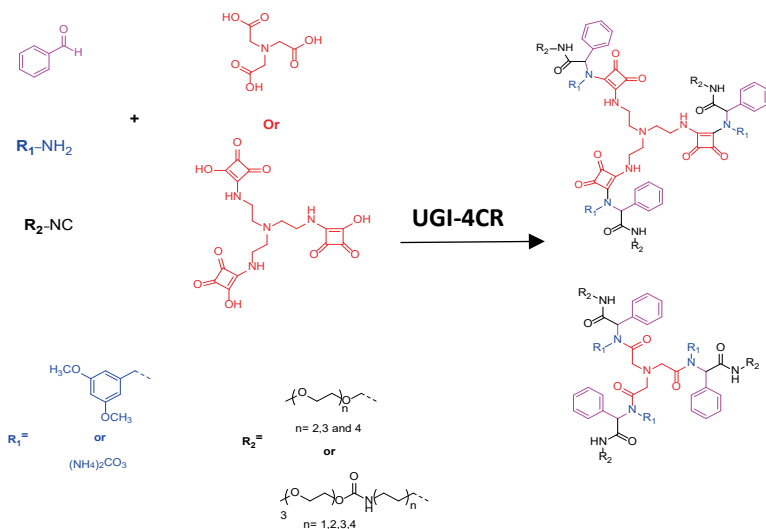


Figure 3.1 General synthetic route to synthesize tripodal compounds by the multicomponent Ugi reaction involving benzaldehyde, ammonium carbonate or 2,4-dimethoxybenzylamine as the amine component, nitrilotriacetic acid or trisquaric acid as the acid component and oligo(ethylene glycol) chains containing isocyanide. 4CR = four component reaction.

3.3 Results and discussion

Because various reaction parameters can influence the outcome of Ugi reaction as described above, their contribution on the preparation of tripodal building blocks for applications in supramolecular chemistry will be evaluated. Since the aim is to prepare a tripodal monomer that is primed for self-assembly in water, the designed Ugi monomers were amphiphilic in character with sufficient hydrophilic and hydrophobic domains and hydrogen-bonding or π - π stacking interactions through intermolecular interactions between amide or squaramide in the hydrophobic domain (**Figure 3.1**). The hydrophilic domains consist of oligo(ethylene glycol) chains that either have a directly coupled isocyanide or a variable number of methylene units ($n = 1, 2, 3, 4$). To introduce units that either π -stack or provide hydrogen bonds in addition to the trigonal geometry to the monomer through Ugi reaction, tripodal acids such as nitrilotriacetic ($pK_{a1} = 3.03$, $pK_{a2} = 3.07$, $pK_{a3} = 10.70$) and the more acidic squaric acid ($pK_{a1} = 0.54$, $pK_{a2} = 3.48$) were used. Specifically, the use of a strong acid plays a determining role in the formation of the imine and subsequently, the Ugi reaction product. Additionally, to prepare the Ugi tripodal molecules, aldehyde and amine components are necessary and thus a range of these components was tested. This chapter has been organized according to the two tripodal cores (nitrilotriacetic acid (3.3.1) and squaric acid (3.3.2)) and the capacity to form the trisubstituted reaction products was examined varying the reaction conditions and the components such as aldehyde (3.3.1.1 and 3.3.2), the isocyanide (3.3.3) and the amine (3.3.4).

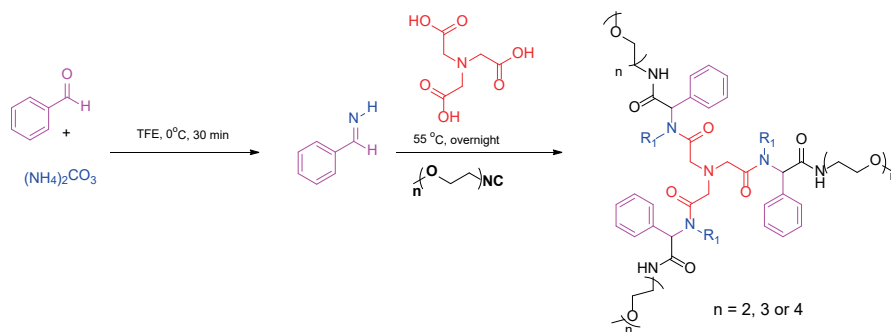
3.3.1 Use of a nitrilotriacetic acid core

In a first step, nitrilotriacetic acid was selected as a tripodal core to provide three peptide-like bonds after the Ugi reaction. The nitrilotriacetic acid core was combined with ammonium carbonate, benzaldehyde and oligo(ethylene glycol) isocyanide (OEG₂, OEG₃, OEG₄) under different reaction conditions to obtain the Ugi product. Ammonium carbonate was used as the source of the amine to avoid an additional deprotection step after the Ugi reaction. The use of ammonium carbonate was previously used by the group of Abbas and coworkers³⁶ in the synthesis of selenocysteine peptides. Oligo(ethylene glycol) isocyanides were prepared starting from oligo(ethylene glycol) (OEG₂, OEG₃, OEG₄) that after reaction with tosyl chloride were converted in phthalimide derivatives in the presence of potassium phthalimide. Subsequently, treatment with hydrazine monohydrate provided the oligo(ethylene glycol) amine derivatives which were quantitatively formylated using ethyl formate. The isocyanides were isolated in high yield (90%) by the reaction of the formylated oligo(ethylene glycol)s with POCl₃.

The Ugi reaction at 55 °C with the above components (entry 1, Table 1) using an isocyanide concentration of 0.2 M resulted in a mixture of di- (d) and tri-substituted (t) products. In order to increase the yield of the trisubstituted product, the equivalents of isocyanide, ammonium carbonate, benzaldehyde and isocyanide were varied. The products and yields of each reaction was determined by LCMS.

3.3.1.1 Modulation of the component ratios and concentration of isocyanide

In this section, the number of equivalents and concentration of isocyanide and the other components on the final product distribution of the Ugi reaction were examined (Table 1, entries 1-7).



Scheme 1

Table 1 Selected entries for the Ugi reaction conditions with nitrilotriacetic acid^a

Entry	R-N≡C (eq)	BA (eq)	(NH ₄) ₂ CO ₃ (eq)	R-N≡C ^b [M]	OEG	Yield*		
						t (%)	d (%)	m (%)
1	10.0	5.0	5.0	0.2	OEG ₃	10	90	NO
2	7.0	5.0	5.0	1.0	OEG ₃	83	17	NO
3	10.0	10.0	10.0	1.0	OEG ₃	72	28	NO
4	10.0	10.0	7.5	1.0	OEG ₃	72	28	NO
5	10.0	5.0	5.0	1.0	OEG ₄	52	48	NO
6	10.0	5.0	5.0	0.2	OEG ₄	48	52	NO
7	10.0	5.0	5.0	1.0	OEG ₂	86	14	NO

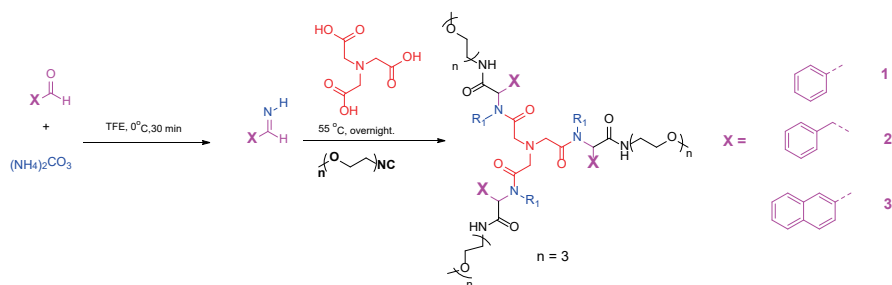
^aReaction conditions: nitrilotriacetic acid (0.05 mmol), isocyanide ((OEG)_nNC), benzaldehyde, ammonium carbonate in TFE at 55 °C, overnight. ^b The reaction conditions were designed considering the concentration of isocyanide in the reaction mixture. The addition of the solvent was modified accordingly to obtain a specific concentration of isocyanide in the reaction mixture. *The yields were determined by LCMS. t = trisubstituted, d = disubstituted, m = monosubstituted, NO = not observed, R-N≡C: isocyanide, BA: benzaldehyde, (NH₄)₂CO₃: ammonium carbonate.

The concentration of the reagents determines the outcome of an Ugi reaction, with higher reagent concentrations resulting in increased yields.¹⁷ While most Ugi reaction conditions are based on a (near-) equimolar distribution of the four components, we opted for an excess of isocyanide (10 eq) because of its known instability in acidic conditions³⁷⁻³⁹ and tendency to polymerize.⁴⁰ The Ugi reaction was performed by first mixing benzaldehyde with ammonium carbonate (5 eq) at 0 °C for 30 min resulting in imine formation, followed by the addition of nitrilotrisquaric acid and OEG_n-NC (n = 2, 3, 4). As shown in Table 1 (entry 1), the nitrilotriacetic acid core in the presence of a 0.2 M concentration of isocyanide OEG₃ (10 eq) yielded predominantly the disubstituted product (90%), compared to the trisubstituted compound (10%). Performing the reaction at 1 M (entry 2) and reducing the number of isocyanide equivalents (7 eq) resulted in a higher yield of the trisubstituted compound (83%). These results confirmed the importance of the isocyanide component concentration on the Ugi reaction with entry 2 displaying the most favorable product distribution. To further optimize the formation of the desired trisubstituted compound, an excess of ammonium carbonate and benzaldehyde at a 1 M isocyanide concentration were used (entries 3, 4) resulting in the trisubstituted compound (72%) as the main product.

To further extend the library of supramolecular monomers with the nitrilotriacetic acid core, the length of the oligo(ethylene glycol) was varied. Using the successful conditions of entry 2, the Ugi reaction was performed with OEG₄-NC using fewer equivalents of ammonium carbonate (5.0 eq, entry 5). A comparable amount of di- and trisubstituted compounds were observed even though being performed at different isocyanide concentrations (0.2 and 1 M) (entries 6-7). On extending these conditions to the OEG₂-NC derivative (entry 7), the most optimal tri- and disubstituted product ratio in this study was obtained (tri-/di-substituted product ratio = 6:1). Moreover, when comparing entries 5 and 7, an effect of the oligo(ethylene glycol) chain length was observed on the reaction yield. This result suggests that the difference in solubility of the OEG isocyanides in the reaction medium have a significant influence on the formation of the trisubstituted product, with the shortest chain length OEG₂ showing the highest yield. In conclusion, the solubility, equivalents and concentration of the reaction components are critical for the success of the tripodal Ugi product.

3.3.1.2 Examination of reaction scope with varying the aldehyde component

The use of various aromatic aldehydes to prepare tripodal compounds were further examined in the Ugi reaction. Benzaldehyde (**1**) was compared against phenylacetaldehyde (**2**) or 2-naphthaldehyde (**3**), because of their increased aliphatic character and number of aromatic rings, respectively, for their ability to effect the efficiency or product distribution in the Ugi reaction. The water soluble oligo(ethylene glycol) isocyanide with three repeats units OEG₃ (10 eq) was used in combination with ammonium carbonate and nitrilotriacetic acid (5 eq) (Table 2, entries 10-15).



Scheme 2

Table 2 Selected entries for the Ugi reaction with nitrilotriacetic acid and different aldehydes^a

<i>Entry</i>	<i>R-N≡C</i> [M] ^b	<i>Aldehyde</i>	<i>Yield*</i>		
			<i>m</i> (%)	<i>d</i> (%)	<i>t</i> (%)
8	1.0	1	NO	23	77
9	0.2	1	NO	70	30
10	1.0	2	100	NO	NO
11	1.0	3	100	NO	NO
12	2.0	2	100	NO	NO
13	2.0	3	100	NO	NO
14	0.1	2	100	NO	NO
15	0.1	3	100	NO	NO

^aReaction conditions: nitrilotriacetic acid (0.05 mmol), isocyanide ((OEG)₃NC), (0.5 mmol), ammonium carbonate (0.25 mmol) and different aldehydes (0.25 mmol) in TFE at 55 °C, overnight. ^bThe reaction conditions were designed considering the concentration of isocyanide in the reaction mixture. The addition of the solvent was modified accordingly to obtain a specific concentration of isocyanide in the reaction mixture. *The yields were determined by LCMS. t = trisubstituted, d = disubstituted, m = monosubstituted, NO= not observed, R-N≡C: isocyanide.

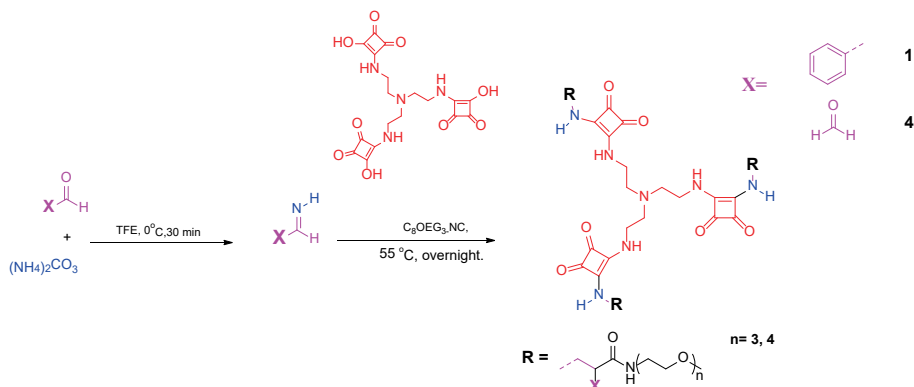
The tripodal compound was predominantly formed (77%) with benzaldehyde at 1 M isocyanide concentration. Conversely, a 0.2 M isocyanide concentration (entry 9) resulted in the disubstituted compound (70%) as the major product, confirming again the importance of concentration in the outcome of Ugi reaction.

Using similar reaction conditions developed for benzaldehyde as described above, its substitution with phenylacetaldehyde or 2-naphthaldehyde were explored (entries 10-15). The exclusive formation of the monosubstituted compound was observed when performing the Ugi reaction at a 1 M isocyanide concentration with **2** or **3** (entry 10 – 11). The same result was obtained when the reaction was carried out at a 2 M isocyanide concentration (entry 12-13). In contrast, Aknin and coworkers previously demonstrated that using a 0.1 M concentration of isocyanide the most optimal yield was obtained for bivalent compounds originating from squaric acid on several parameters including concentration, temperature and various solvents.²² However, the exclusive formation of monosubstituted compound was still observed after executing the Ugi reaction with **2** or **3** using 0.1 M

isocyanide, (entries 14 and 15). One plausible explanation for the exclusive formation of the monosubstituted compound is the increased size of phenylacetaldehyde or 2-naphthaldehyde relative to benzaldehyde. As most Ugi reactions are performed only once on a particular molecular scaffold, sterics may not play an obvious role in their formation. However, sterics has been demonstrated by Rivera *et al.* to influence the Ugi reaction of a third substituent in tripodal peptide-podands.⁴¹ Based on our findings, the size of the aromatic aldehyde is pivotal for the success of Ugi reaction using tripodal acidic cores. Hence, in the subsequent reaction conditions, benzaldehyde was further used as the aldehyde component.

3.3.2 Examination of the Ugi reaction on a tripodal squaric acid core

In the last decade, the squaramide synthon has been explored in the field of supramolecular chemistry for its ability to form very strong hydrogen bonds with a wide range of substrates.²⁴ As demonstrated through DFT calculations and NICS (Nuclear Independent Chemical Shift), this peculiar property is due to the delocalization of π electrons inside the cyclobutenedione ring that confers and increase in aromatic character at the squaramide moieties.^{42, 43} Squaric acid has been used as building block for the Ugi reaction²² and differs from nitrilotriacetic acid not only for the presence of cyclobutenedione moieties that provide distinct non-covalent interactions through their π -surface but also for its stronger acidity. Squaric acid has pKa values similar to sulfuric acid ($\text{pK}_{\text{a}1} = 0.54$, $\text{pK}_{\text{a}2} = 3.48$) is due to the formation of dianionic resonance chemical structures²⁶ as demonstrated by ^{17}O NMR spectroscopy. In the Ugi reaction, the strength of the acid plays an important role in the stabilization of iminium ion resulting in higher yields and faster reaction times.¹⁷ To further examine the potential of an alternative tripodal core for the Ugi reaction and to gain access to new supramolecular scaffolds, a trisquaric acid core was synthesized. The TREN core was reacted with an excess of squaric ester, and successively treated with concentrated HCl solution in dioxane giving rise to the product quantitatively (3.6.2, Scheme S.2, SI).



Scheme 3

Table 3 Selected entries for the Ugi reaction conditions with trisquaric acid and different aldehydes^a

Entry	$R-N\equiv C$ [M] ^b	Aldehyde	Reaction temperature (°C)	OEG	Yield*		
					t (%)	d (%)	m (%)
16	0.02	1	55	OEG ₃	NO	100	NO
17	0.5	1	55	OEG ₃	71	29	NO
18	1.0	1	55	OEG ₃	66	34	NO
19	2.0	1	55	OEG ₃	43	57	NO
20	1.0	4	RT	OEG ₄	NO	NO	NO
21	1.0	1	RT	OEG ₄	44	56	NO
22	1.0	4	55	OEG ₄	NO	NO	NO

^aReaction conditions: trisquaric acid (0.02 mmol), isocyanide ((OEG)₃NC or (OEG)₄NC), (0.2 mmol), ammonium carbonate (0.1 mmol) and benzaldehydes or formaldehyde (0.1 mmol) in TFE at 55 °C or RT, overnight. ^b The reaction conditions were designed considering the concentration of isocyanide in the reaction mixture. The addition of the solvent was modified accordingly to obtain a specific concentration of isocyanide in the reaction mixture. *The yields were determined by LCMS. t = trisubstituted, d = disubstituted, m = monosubstituted, NO= not observed, R-N≡C: isocyanide.

Reaction conditions that favoured the trisubstituted (77%) over the disubstituted (29%) product for nitriloacetic acid (entry 8) were used as a

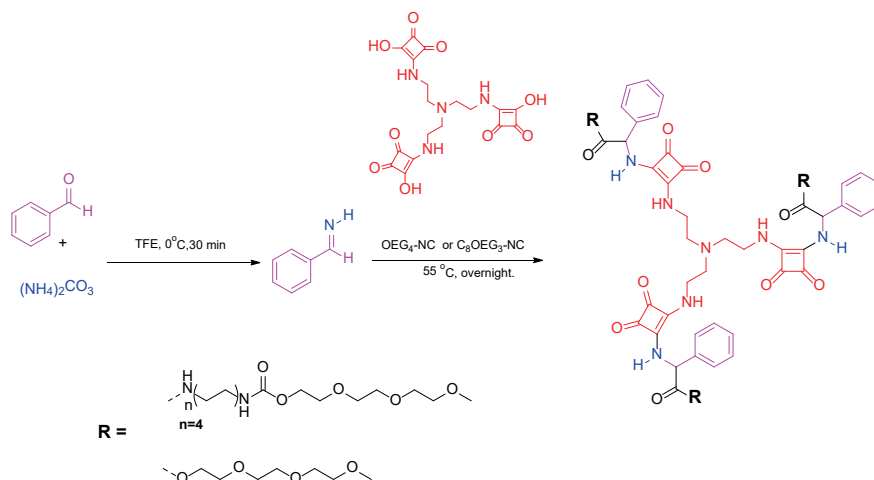
starting point for the reaction with trisquaric acid. Furthermore, the use of different isocyanide concentrations (0.02-2 M), reaction temperature (RT) and type of aldehyde (benzaldehyde or formaldehyde) were explored (Table 3, entries 16-19). In brief, the Ugi reaction with trisquaric acid was carried out mixing ammonium carbonate with benzaldehyde for 30 min at 0 °C (5 eq), followed by the addition of trisquaric acid and OEG₃-NC or OEG₄-NC (10 eq). The trisubstituted product was not observed at an isocyanide concentration of 0.02 M (entry 16), while it is the major product at 0.5 and 1 M (entries 17-18, 71%) and its further increase to 2 M favoured the disubstituted product (57 %).

In an attempt to remove the stereocenters from the tripodal structure, the Ugi reaction was performed with formaldehyde instead of benzaldehyde (entries 20 and 22). Performing the reaction at RT and at 55 °C in the presence of formaldehyde, no products were observed. The failure of the reaction with formaldehyde is likely due to the instability of iminium ion that is generated in the first step of the reaction and prevents the subsequent steps. Previously, to facilitate the coupling to the squaric core, all the Ugi reactions were carried out at 55 °C, but in the entry 21, the effect of the reaction temperature was examined. Specifically, the reaction in the presence of benzaldehyde was performed at RT instead of 55 °C. Comparing the entries 18 and 21, the yield of trisubstituted compound at RT (44%) is significantly lower compared to the reaction at 55 °C (66%). In conclusion, the use of a stronger acid (squaric acid), higher reaction temperature (55 °C), higher isocyanide concentration (1 M) and aromatic aldehyde is critical to promote the trisubstituted Ugi product, thereby minimizing the formation of the mono- and disubstituted species.

3.3.3 Use of an amphiphilic isocyanide component

To further extend the library of Ugi products that can be used as supramolecular scaffolds, an aliphatic-oligo(ethylene glycol) amphiphile isocyanide was prepared. In contrast to the synthesis of (OEG)₃-NC, overnight reaction was required to prepare aliphatic-oligo(ethylene glycol) amphiphiles (C₈(OEG)₃NC, 80-90% yield). In brief their synthesis consisted of the activation of triethylene glycol with 1,1'-carbonyldiimidazole (CDI), followed by its coupling with mono Cbz-protected 1,8-octanediamine. *In situ* hydrogenation with triethylsilane and Pd/C was performed to remove the Cbz protecting group. The primary amine was successively formylated using ethyl formate and the final amphiphile isocyanide was isolated by the reaction with POCl₃. Inspired by the findings of our previous work,³⁵ where the right balance between the hydrophilic and hydrophobic domains in the molecular structure of tripodal squaramide monomers were pivotal for their self-assembly, an aliphatic spacer of 8 carbons was used. Once the isocyanide was obtained, the Ugi reaction was executed starting with the reaction of ammonium carbonate and benzaldehyde at 0 °C to form the imine, followed by squaric acid and C₈(OEG)₃NC.

Starting from previous entries (entries 18-19) where an isocyanide concentration of 0.5 and 1 M and heating of the reaction mixture to 55 °C were necessary to promote the formation of trisubstituted squaramide product, an isocyanide concentration (C₈OEG₃-NC) from 0.1 to 2 M was screened (Table 4, entries 23- 25, 27).



Scheme 4

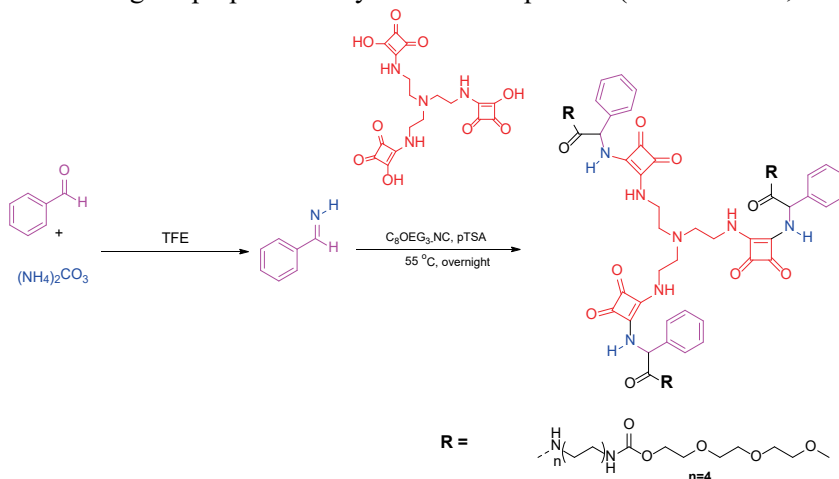
Table 4 Selected entries for the Ugi reaction with trisquaric acid and various isocyanides^a

Entry	Triethyl amine (eq)	$R\text{-N}\equiv\text{C}$ [M] ^b	Solvent	$R\text{-N}\equiv\text{C}$	Reaction temperature ($^\circ\text{C}$)	Yield*		
						<i>t</i> (%)	<i>d</i> (%)	<i>m</i> (%)
23	0.0	1.0	TFE	$\text{C}_8(\text{OEG})_3\text{NC}$	55	22	49	29
24	0.0	0.5	TFE	$\text{C}_8(\text{OEG})_3\text{NC}$	55	32	52	16
25	0.0	0.1	TFE	$\text{C}_8(\text{OEG})_3\text{NC}$	55	45	55	NO
26	0.0	0.5	TFE	$\text{C}_8(\text{OEG})_3\text{NC}$	80	25	51	24
27	0.0	2.0	TFE	$\text{C}_8(\text{OEG})_3\text{NC}$	55	12	27	62
28	5.0	0.5	TFE	$\text{C}_8(\text{OEG})_3\text{NC}$	55	NO	NO	NO
29	5.0	0.5	MeOH	$(\text{OEG})_4\text{NC}$	55	NO	NO	NO
30	5.0	0.5	TFE	$(\text{OEG})_4\text{NC}$	55	NO	NO	NO
31	5.0	0.5	MeOH	$\text{C}_8(\text{OEG})_3\text{NC}$	55	NO	NO	NO

^aReaction conditions: trisquaric acid (0.02 mmol), isocyanide ($\text{C}_8(\text{OEG})_3\text{NC}$ or $(\text{OEG})_4\text{NC}$), (0.2 mmol), ammonium carbonate (0.1 mmol) and benzaldehydes or formaldehyde (0.1 mmol) in TFE or MeOH at 55 or 80°C and in presence of triethylamine (0.1 mmol), overnight. ^b The reaction conditions were designed considering the concentration of isocyanide in the reaction mixture. The addition of the solvent was modified accordingly to obtain a specific concentration of isocyanide in the reaction mixture. *The yields were determined by LCMS. *t* = trisubstituted, *d* = disubstituted, *m* = monosubstituted, NO = not observed, $R\text{-N}\equiv\text{C}$: isocyanide, conc.: concentration.

A significant amount of mono- and disubstituted products were observed in this concentration range of isocyanide. Further increasing the isocyanide concentration (1 and 2 M), resulted in the preferential formation of mono and disubstituted compounds. This concentration screen pointed out that an isocyanide concentration of 0.1 M yields the highest amount of trisubstituted product (45%) (entry 25). Further increasing the reaction temperature to 80 °C (entry 26), decreased the amount of trisubstituted product formed with the mono- and disubstituted products as the predominant species ($m = 24\%$ and $d = 51\%$, respectively). In the synthesis of tripodal peptide-peptoid podands as reported by Rivera⁴¹ and coworkers, triethylamine was used to promote the formation of the iminium ion when starting from amines as their hydrochloride salts. Therefore, triethylamine (5 eq) was added to the Ugi reaction with 0.5 M isocyanide (entries 28-31) using a reaction temperature of 55 °C, but no product was formed. Further changing the solvent (MeOH) and the type of isocyanide ((OEG)₄NC), also did not yield any product formation.

As the formation of the iminium ion in the Ugi reaction determines the success and the yield of reaction, conditions that further can encourage its formation when using amphiphilic isocyanides were probed (entries 32-36, Table 5).



Scheme 5

Table 5 Selected entries for the Ugi reaction with trisquaric acid and different reaction times for the imine formation step^a.

Entry	R-N≡C (eq) ^b	pTSA (eq)	Length of imine formation step (min)	Reaction temperature (°C)	Yield*		
					t (%)	d (%)	m (%)
32	10	0.0	120	0->55	26	54	20
33	10	0.0	120	RT->55	23	36	41
34	5	0.0	30	0->55	11	26	63
35	10	1.0	30	0->55	30	48	22
36	10	3.0	30	0->55	23	43	34

^aReaction conditions: trisquaric acid (0.02 mmol), isocyanide ((OEG)₄NC), (0.2 mmol, 0.5 M), ammonium carbonate (0.1 mmol) and benzaldehyde (0.1 mmol) in TFE at 55 °C and with pTSA for different reaction times in the imine formation step, overnight. ^bThe reaction conditions were designed considering the concentration of isocyanide in the reaction mixture. The addition of the solvent was modified accordingly to obtain a specific concentration of isocyanide in the reaction mixture. *Yields were determined by LCMS. t = trisubstituted, d = disubstituted, m = monosubstituted, NO = not observed, R-N≡C: isocyanide.

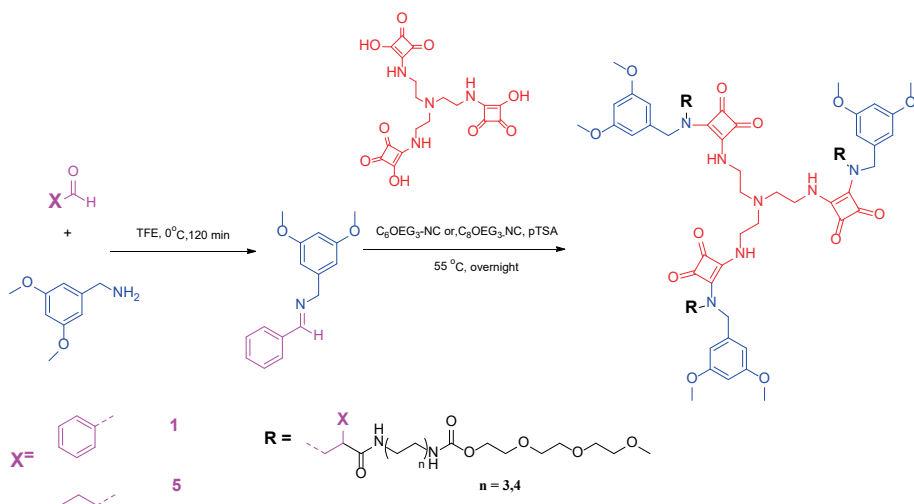
The reaction time used to form the iminium ion prior to the addition of the other components was 30 min at 0 °C. Extension of the reaction time up to 2 h did not further increase the yield of the trisubstituted product (entry 32). When the imine reaction step was carried out at RT (entry 33) based on a previous study by Aknin and coworkers,²² an increased formation of monosubstituted compound was observed alongside the trisubstituted product in comparison to starting at 0°C (entry 32).

To further optimize the yield of the reaction, decreasing the number of equivalents of isocyanide (5 eq) with at a concentration of 0.5 M was examined (entry 34). The importance of an excess of isocyanide on the success of the reaction was highlighted, as an increased yield of the monosubstituted compound (63%) was observed. Subsequently, the effect of adding the Brønsted acid catalyst *p*-toluensulfonic acid (pTSA) after the imine formation was examined to increase the yield of the reaction.^{17,44, 45} The acid plays a pivotal role in the Ugi reaction mechanism because it increases the concentration of the imine ion in the reaction mixture.¹⁷ Hence, pTSA (1 or 3 eq) was used to protonate the acid and to facilitate the formation of a imine ion after the addition of squaric acid (entries 35 and 36). While the use of 1 eq of pTSA slightly increased the yield of the trisubstituted compound (23-30%), the addition of more equivalents (3 eq) increased the amount of mono- and disubstituted compounds. Hence, extending the reaction time to form the iminium ion, increasing the reaction temperature and concentration of the reagents did not result in an increase in yield of the trisubstituted compound. The use of triethylamine was detrimental for the reaction with the lack of product being formed. In contrast, the addition of low amounts of pTSA (1 eq) resulted in the formation of the trisubstituted Ugi compound.

3.3.4 Modulation of the amine components

Earlier the use of ammonium carbonate as the amine component provided a low yield of the trisubstituted Ugi product (entries 23-27). This result is most likely due to the formation of an unstable imine. It was previously reported by Kazmaier and coworkers that when ammonia is used in the Ugi reaction, a side reaction can result to form a semiaminal.⁴⁶ This product can be formed when a second reaction occurs with ammonia instead of the isocyanide on the iminium ion. Thus, to prevent the formation of the semiaminal, 2,4-dimethoxybenzylamine was used.^{47, 48} Additionally, the use of this amine has advantages in the purification step, as it can be easily removed from the product under acidic conditions.⁴⁹⁻⁵¹ To further promote the formation of the trisubstituted product, an excess of the isocyanide (10 eq C₆-OEG-NC) at a 0.5 M concentration was used (entry 37). An excess of disubstituted compound was observed (42%) in comparison to the trisubstituted compound (58%). To further enhance the formation of the trisubstituted compound, pTSA was added. However, using 1 equivalent of pTSA (entry 40), no significant improvement in the yield of trisubstituted compound was observed when compared against reaction in absence of pTSA (entry 39). Moreover, further increasing the equivalents of pTSA was detrimental for product formation (entry 41). Decreasing the amount of isocyanide (from 10 eq to 5 eq) with 1 eq of pTSA, showed a slight improvement in the yield of the trisubstituted product (58%), in contrast to the disubstituted compound (48%).

Finally, to extend the library of the supramolecular monomers, the use of butyraldehyde was further examined. Unfortunately, no reaction was observed under the same conditions (entry 38). This result is likely due to the decreased stability of the imine formed by aliphatic aldehyde as compared to benzaldehyde.



Scheme 6

Table 6 Selected entries for the Ugi reaction with trisquaric acid and primary amine^a

Entry	R-N≡C (eq) ^b	PTSA (eq)	Aldehyde	R-N≡C type	Yield*		
					<i>t</i> (%)	<i>d</i> (%)	<i>m</i> (%)
37	10.0	0.0	1	C ₈ OEG ₃	58	42	NO
38	10.0	0.0	5	C ₈ OEG ₃	NO	NO	NO
39	10.0	0.0	1	C ₆ OEG ₃	42	57	NO
40	10.0	1.0	1	C ₆ OEG ₃	45	55	NO
41	10.0	3.0	1	C ₆ OEG ₃	27	73	NO
42	5.0	1.0	1	C ₆ OEG ₃	58	48	NO

^aReaction conditions: trisquaric acid (0.02 mmol), isocyanide ((C₈OEG)₄NC, 0.5 M), (0.2 mmol), 2,4-dimethoxybenzylamine (0.1 mmol) and benzaldehydes or butyraldehyde (0.1 mmol), with pTSA in TFE at 55 °C overnight. ^bThe reaction conditions were designed considering the concentration of isocyanide in the reaction mixture. The addition of the solvent was modified accordingly to obtain a specific concentration of isocyanide in the reaction mixture. *Yields were determined by LCMS. *t* = trisubstituted, *d* = disubstituted, *m* = monosubstituted, NO = not observed, R-N≡C: isocyanide.

Based on previous improvements of the Ugi reaction yield in the formation of the trisubstituted product (entries 43-49, Table 7), the number of equivalents of isocyanide and the reaction time for the imine formation was investigated (Scheme 7). A decrease in the isocyanide, benzaldehyde and amine components from 5 to 3.5 eq (entry 44) favoured the disubstituted compound (65%). Moreover, the addition of 1 eq of pTSA did not improve the yield of the trisubstituted compound (entry 45). Consequently, the effect of the reaction time to prepare the imine was further investigated. Increasing the reaction time from 30 min to 2 h, was found to slightly favor the formation of trisubstituted compound (31%, entry 46). In entries 47 and 48, an additional decrease in equivalents of the other components did not increase the trisubstituted product. The use of 5 eq of isocyanide, benzaldehyde, and 2,4-dimethoxybenzylamine with 1 eq of pTSA and an increased reaction time for imine formation, showed nearly full conversion to the trisubstituted product (79%) with a considerable reduction in the disubstituted product formed.



Entry	R-N≡C (eq)	Aldehyde & 2,4- dimethoxy benzylamine (eq)	PTSA (eq)	Time imine- formation step (min)	Yield*		
					<i>t</i> (%)	<i>d</i> (%)	<i>m</i> (%)
43	5.0	5.0	0.0	30	47	53	NO
44	3.5	3.5	0.0	30	35	65	NO
45	3.5	3.5	1.0	30	25	75	NO
46	3.5	3.5	0.0	120	31	69	NO
47	3.05	3.05	1.0	30	14	86	NO
48	5.0	3.05	1.0	30	21	79	NO
49	5.0	5.0	1.0	120	79	21	NO

106

Table 8 Selected entries for the Ugi reaction conditions with trisquaric acid and different reaction times

<i>Entry</i>	<i>Reaction time (h)</i>	<i>R-N≡C (0.5 M)^b</i>	<i>Percentage yield[*]</i>		
			<i>t (%)</i>	<i>d (%)</i>	<i>m (%)</i>
50	72	C ₆ OEG ₃ NC	79	21	NO
51	144	C ₈ OEG ₃ NC	82	17	NO

^aReaction conditions: trisquaric acid (0.02 mmol), isocyanide ((0.1 mmol, C₆(OEG)₄NC or C₈OEG₄NC), 2,4-dimethoxybenzylamine (0.1 mmol) and benzaldehydes (0.1 mmol), in presence of pTSA (0.02 mmol), with different reaction times of imine formation, in TFE at 55 °C, for 72 or 144h. ^bThe reaction conditions were designed considering the concentration of isocyanide in the reaction mixture. The addition of the solvent was modified accordingly to obtain a specific concentration of isocyanide in the reaction mixture. ^{*}Yields were determined by LCMS. t = trisubstituted, d = disubstituted, m = monosubstituted, NO = not observed, R-N≡C: isocyanide.

3.4 Self-assembly of tripodal squaramides obtained by the Ugi reaction

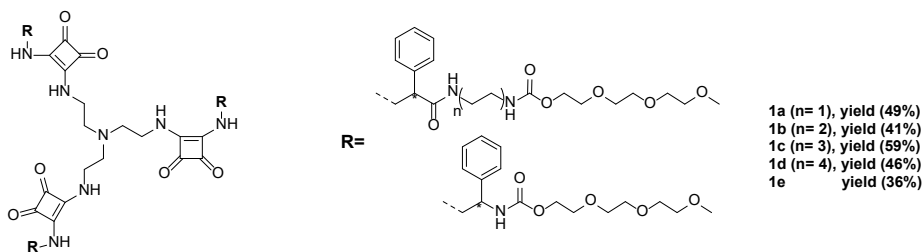


Figure 3.2 Chemical structure of the molecules synthesized by Ugi reaction.

Using the synthetic protocol described in the prior sections, a small family of tripodal compounds was prepared using squaric acid, benzaldehyde, 2,4-dimethoxybenzylamine and an amphiphilic isocyanide with different aliphatic spacer lengths and an oligoethylene glycol chain were synthesized and their capacity for self-assembly was assessed ($n = 1-4$, **Figure 3.2**). The various squaramide supramolecular scaffolds were synthesized and isolated in moderate yields (36-59%). Because the tripodal squaramide scaffolds consist of hydrophilic, hydrophobic and hydrogen-bonding segments, we investigated their potential for aggregate formation in water. To facilitate the self-assembly of the monomers, 2,4-dimethoxybenzyl protecting group was removed under acidic conditions revealing the squaramide. Firstly, a solubility test of the various compounds (**1a - e**) between 1 and 5 mM was executed. Whereas **1c** and **1d** precipitated at concentrations of 1 mM, **1e** and **1a** were soluble up to 5 mM concentration. Compound **1b** was soluble up to a 1 mM concentration. In all cases, no gels were formed even though typical domains encountered in gelator molecules were used. Once the solubility of the compounds was determined, atomic force microscopy (AFM), and UV-vis studies were used to provide more insight into their aggregation behavior (**Figure 3.3**). AFM imaging of compounds **1a** and **1b** at a concentration of 15 μM displayed the formation of spherical aggregates (**Figure S3.1** and **S3.2**). Self-assembly of the squaramide compounds was further probed by UV-vis spectroscopy at the molecular level. We previously demonstrated that the simultaneous red- and blue-shifting of the HOMO-LUMO and HOMO-LUMO+1 bands of the squaramides and their increased intensity is consistent with the head-to-tail

hydrogen bond assembly of the squaramide rings. However, the lack of shifting of these bands in the Ugi compounds **1a** and **1e** suggests an aggregation mode of the squaramides that is distinct from head-to-tail hydrogen bonding. One possible explanation for the observed aggregate morphology and organization of the squaramide synthons is the presence of three stereocenters observed in the Ugi products that preclude their self-assembly in a head-to-tail mode. To control the stereochemistry of Ugi products, the use of a chiral catalyst as demonstrated by Zhang and coworkers should be considered.⁵² Alternatively, ketones such as acetone or diethylketone can be used in the Ugi reaction to remove the stereocenters opening the use of these amphiphilic scaffolds for the formation of supramolecular polymers.

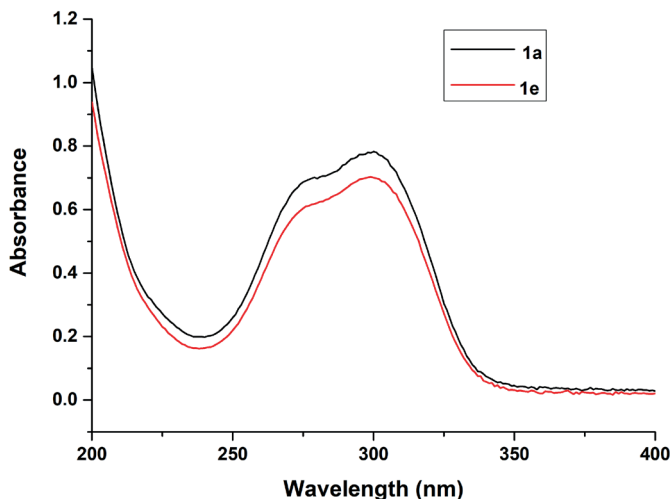


Figure 3.3 UV-vis spectra of **1a** and **1e** ($c=15\ \mu\text{M}$) in water

3.5 Conclusions

In summary, several Ugi reaction conditions were tested to obtain and optimize the synthesis of the tripodal supramolecular scaffolds. These compounds consist of a hydrophilic domain (triethylene glycol) and a variable number of methylene units ($n = 0, 2, 4, 6$) connected to a central squaramide or amide core. More specifically, the effect of varying the aldehyde, amine, isocyanide and acidic components, such as the use of nitrilotriacetic and squaric acid were investigated. Performing the reaction with nitrilotriacetic acid, benzaldehyde, ammonium carbonate, and OEG_{*n*}-NC resulted in a distribution of di- and trisubstituted compounds. The use of 2,4-dimethoxybenzylamine in combination with squaric acid, benzaldehyde and amphiphilic isocyanides allowed the preparation of a small family of tripodal compounds to investigate their self-assembly in water. The use of an aromatic aldehyde causes the formation of diastereomers in the final products. The ability of the synthesized squaramide-based Ugi compounds to self-assemble in water was examined. Compounds **1a** and **1e** showed their aggregation in spheres. This result was supported by UV-vis results of **1a** and **1e** that lack the typical HOMO-LUMO and HOMO-LUMO+1 transitions of squaramide when assembled into a head-to-tail hydrogen bond array. The lack of self-assembly into fibrillar aggregates can be due to the existence of diastereomers in the final products. Although no fibrillar aggregates are observed, the optimized Ugi reaction with trisquaric acid core can be considered as novel strategy for the preparation of tripodal squaramide compounds.

References

1. Long, K.; Liu, Y.; Li, Y.; Wang, W., Self-assembly of trigonal building blocks into nanostructures: molecular design and biomedical applications. *J. Mater. Chem. B* **2020**, *8*, 6739-6752.
2. Royle, S. J., The cellular functions of clathrin. *Cell. Mol. Life Sci.* **2006**, *63*, 1823-1832.
3. Zhu, Z.; Chen, H.; Li, S.; Yang, X.; Bittner, E.; Cai, C., Tripodal amine ligands for accelerating Cu-catalyzed azide-alkyne cycloaddition: efficiency and stability against oxidation and dissociation. *Catal. Sci Techn.* **2017**, *7*, 2474-2485.
4. Gibson, S. E.; Castaldi, M. P., C₃ symmetry: molecular design inspired by nature. *Angew. Chem. Int. Ed. Engl.* **2006**, *45*, 4718-4720.
5. Rao, J.; Lahiri, J.; Isaacs, L.; Weis, R. M.; Whitesides, G. M., A trivalent system from vancomycin·D-Ala-D-Ala with higher affinity than Avidin·Biotin. *Science* **1998**, *280*, 708-711.
6. Kuswandi, B.; Nuriman; Verboom, W.; Reinhoudt, D. N., Tripodal receptors for cation and anion sensors. *Sensors (Basel)* **2006**, *6*, 978-1017.
7. Wang, F.; Gillissen, M. A. J.; Stals, P. J. M.; Palmans, A. R. A.; Meijer, E. W., Hydrogen bonding directed supramolecular polymerisation of Oligo(Phenylene-Ethynylene)s: cooperative mechanism, core symmetry effect and chiral amplification. *Chem. Eur. J.* **2012**, *18*, 11761-11770.
8. Dorca, Y.; Matern, J.; Fernández, G.; Sánchez, L., C₃-symmetrical π -scaffolds: useful building blocks to construct helical supramolecular polymers. *Isr. J. Chem.* **2019**, *59*, 869-880.
9. Cantekin, S.; de Greef, T. F. A.; Palmans, A. R. A., Benzene-1,3,5-tricarboxamide: a versatile ordering moiety for supramolecular chemistry. *Chem. Soc. Rev.* **2012**, *41*, 6125-6137.
10. Dömling, A.; Wang, W.; Wang, K., Chemistry and biology of multicomponent reactions. *Chem. Rev.* **2012**, *112*, 3083-3135.
11. Rocha, R. O.; Rodrigues, M. O.; Neto, B. A. D., review on the Ugi multicomponent reaction mechanism and the use of fluorescent derivatives as functional chromophores. *ACS Omega* **2020**, *5*, 972-979.
12. Domling, A.; Wang, W.; Wang, K., Chemistry and biology of multicomponent reactions. *Chem. Rev.* **2012**, *112*, 3083-135.
13. Domling, A., Recent developments in isocyanide based multicomponent reactions in applied chemistry. *Chem. Rev.* **2006**, *106*, 17-89.

14. Sadjadi, S.; Heravi, M. M.; Nazari, N., Isocyanide-based multicomponent reactions in the synthesis of heterocycles. *RSC Advances* **2016**, *6*, 53203-53272.
15. Simila, S. T. M.; Martin, S. F., Applications of the Ugi reaction with ketones. *Tetrahedron Lett.* **2008**, *49*, 4501-4504.
16. Choudhury, L. H.; Parvin, T., Recent advances in the chemistry of imine-based multicomponent reactions (MCRs). *Tetrahedron* **2011**, *67*, 8213-8228.
17. MarCACcini, S.; Torroba, T., The use of the Ugi four-component condensation. *Nat. Protoc.* **2007**, *2*, 632-639.
18. Shaabani, A.; Ghadari, R.; Sarvary, A.; Rezayan, A. H., Synthesis of Highly Functionalized Bis(4H-chromene) and 4H-Benzo[g]chromene Derivatives via an isocyanide-based pseudo-five-component reaction. *J. Org. Chem.* **2009**, *74*, 4372-4374.
19. Echemendía, R.; Rabêlo, W. F.; López, E. R.; Coro, J.; Suárez, M.; Paixão, M. W.; Rivera, D. G., A bidirectional access to novel thiadiazine hybrid molecules by double multicomponent reactions. *Tetrahedron Lett.* **2018**, *59*, 4050-4053.
20. Balalaie, S.; Bigdeli, M. A.; Sheikhhosseini, E.; Habibi, A.; Moghadam, H. P.; Naderi, M., Efficient synthesis of novel coumarin-3-carboxamides (=2-Oxo-2H-1-benzopyran-3-carboxamides) Containing Lipophilic Spacers. *Helv. Chim.* **2012**, *95*, 528-535.
21. Ghashghaei, O.; Seghetti, F.; Lavilla, R., Selectivity in multiple multicomponent reactions: types and synthetic applications. *Beilstein J. Org. Chem.* **2019**, *15*, 521-534.
22. Akin, K.; Gauriot, M.; Totobenazara, J.; Deguine, N.; Deprez-Poulain, R.; Deprez, B.; Charton, J., Squaric acid is a suitable building-block in 4C-Ugi reaction: access to original bivalent compounds. *Tetrahedron Lett.* **2012**, *53*, 458-461.
23. Dehghan, N.; Nasr-Isfahani, H.; Sarvary, A.; Bakherad, M., Trimesic acid is a suitable building block in triple four-component Ugi reaction: access to unique trivalent compounds. *Monatsh. Chem.* **2020**, *151*, 397-404
24. Marchetti, L. A.; Kumawat, L. K.; Mao, N.; Stephens, J. C.; Elmes, R. B. P., The Versatility of squaramides: from supramolecular chemistry to chemical biology. *Chem.* **2019**, *5*, 1398-1485.
25. Storer, R. I.; Aciro, C.; Jones, L. H., Squaramides: physical properties, synthesis and applications. *Chem. Soc. Rev.* **2011**, *40*, 2330-2346.
26. Wurm, F. R.; Klok, H. A., Be squared: expanding the horizon of squaric acid-mediated conjugations. *Chem. Soc. Rev.* **2013**, *42*, 8220-8236.

27. Zhao, B.-L.; Li, J.-H.; Du, D.-M., Squaramide-catalyzed asymmetric reactions. *Chem. Rec.* **2017**, *17*, 994-1018.
28. Bae, H. Y.; Song, C. E., Unprecedented hydrophobic amplification in noncovalent organocatalysis “on water”: hydrophobic chiral squaramide catalyzed michael addition of malonates to nitroalkenes. *ACS Catalysis* **2015**, *5*, 3613-3619.
29. Cai, X. J.; Li, Z.; Chen, W. H., Tripodal squaramide conjugates as highly effective transmembrane anion transporters. *Bioorg. Med. Chem. Lett.* **2017**, *27*, 1999-2002.
30. Fan, L.; Xu, T.; Feng, J.; Ji, Z.; Li, L.; Shi, X.; Tian, C.; Qin, Y., Tripodal squaramide derivative as a neutral chloride ionophore for whole blood and sweat chloride measurement. *Electroanalysis* **2020**, *32*, 805-811.
31. Jin, C.; Zhang, M.; Wu, L.; Guan, Y.; Pan, Y.; Jiang, J.; Lin, C.; Wang, L., Squaramide-based tripodal receptors for selective recognition of sulfate anion. *Chem. Commun. (Camb)* **2013**, *49*, 2025-2027.
32. Liu, Y.; Qin, Y.; Jiang, D., Squaramide-based tripodal ionophores for potentiometric sulfate-selective sensors with high selectivity. *Analyst* **2015**, *140*, 5317-23.
33. Qin, L.; Hartley, A.; Turner, P.; Elmes, R. B. P.; Jolliffe, K. A., Macrocyclic squaramides: anion receptors with high sulfate binding affinity and selectivity in aqueous media. *Chem. Sci.* **2016**, *7*, 4563-4572.
34. Saez Talens, V.; Englebienne, P.; Trinh, T. T.; Noteborn, W. E.; Voets, I. K.; Kiełtyka, R. E., Aromatic gain in a Supramolecular polymer. *Angew. Chem. Int. Ed. Engl.* **2015**, *54*, 10502-10506.
35. Tong, C.; Liu, T.; Saez Talens, V.; Noteborn, W. E. M.; Sharp, T. H.; Hendrix, M.; Voets, I. K.; Mummery, C. L.; Orlova, V. V.; Kiełtyka, R. E., Squaramide-based supramolecular materials for three-dimensional cell culture of human induced pluripotent stem cells and their derivatives. *Biomacromolecules* **2018**, *19*, 1091-1099.
36. Abbas, M.; Wessjohann, L. A., Direct synthesis of sensitive selenocysteine peptides by the Ugi reaction. *Org. Biomol. Chem.* **2012**, *10*, 9330-9333.
37. Sung, K.; Chen, C.-C., Kinetics and mechanism of acid-catalyzed hydrolysis of cyclohexyl isocyanide and pKa determination of N-cyclohexylnitrilium ion. *Tetrahedron Lett.* **2001**, *42*, 4845-4848.
38. Lim, Y. Y.; Stein, A. R., Acid-catalyzed solvolysis of isonitriles. I. *Can. J. Chem.* **1971**, *49*, 2455-2459.
39. Massarotti, A.; Brunelli, F.; Aprile, S.; Giustiniano, M.; Tron, G. C., Medicinal chemistry of isocyanides. *Chem. Rev.* **2021**, *121*, 10742-10788.

40. Millich, F., Polymerization of isocyanides. *Chem. Rev.* **1972**, *72*, 101-113.
41. Rivera, D. G.; León, F.; Concepción, O.; Morales, F. E.; Wessjohann, L. A., A Multiple Multicomponent approach to chimeric peptide-peptoid Podands. *Chem. Eur. J.* **2013**, *19*, 6417-6428.
42. West, R.; Niu, H.-Y.; Powell, D. L.; Evans, M. V., Symmetrical resonance stabilized anions, 1 CnOn-2. *J. Am. Chem. Soc.* **1960**, *82*, 6204-6205.
43. Quiñonero, D.; Frontera, A.; Ballester, P.; Deyà, P. M., A theoretical study of aromaticity in squaramide and oxocarbons. *Tetrahedron Lett.* **2000**, *41*, 2001-2005.
44. Purohit, P.; Pandey, A. K.; Kumar, B.; Chauhan, P. M. S., Diversity oriented synthesis of β -carboline and indolo-pyrazinone analogues based on an Ugi four component reaction and subsequent cyclisation of the resulting indole intermediate. *RSC Advances* **2016**, *6*, 21165-21186.
45. Dömling, A., Recent developments in isocyanide based multicomponent reactions in applied Chemistry. *Chem. Rev.* **2006**, *106*, 17-89.
46. Kazmaier, U.; Hebach, C., Peptide syntheses via Ugi reactions with ammonia. *Synlett* **2003**, 1591-1594.
47. Kazmaier, U.; Ackermann, S., A straightforward approach towards thiazoles and endothiopeptides via Ugi reaction. *Org. Biomol. Chem.* **2005**, *3*, 3184-3187.
48. Plant, A.; Thompson, P.; Williams, D. M., Application of the Ugi reaction for the one-pot synthesis of uracil Polyoxin C analogues. *J. Org. Chem.* **2009**, *74*, 4870-4873.
49. Mroczkiewicz, M.; Ostaszewski, R., A new and general method for the synthesis of tripeptide aldehydes based on the multi-component Ugi reaction. *Tetrahedron* **2009**, *65*, 4025-4034.
50. Shaw, A. Y.; Xu, Z.; Hulme, C., Ugi/Robinson-Gabriel reactions directed toward the synthesis of 2,4,5-trisubstituted oxazoles. *Tetrahedron Lett.* **2012**, *53*, 1998-2000.
51. Tanino, T.; Al-Dabbagh, B.; Mengin-Lecreux, D.; Bouhss, A.; Oyama, H.; Ichikawa, S.; Matsuda, A., Mechanistic analysis of muraymycin analogues: a guide to the design of MraY inhibitors. *J. Med. Chem.* **2011**, *54*, 8421-8439.
52. Zhang, J.; Yu, P.; Li, S.-Y.; Sun, H.; Xiang, S.-H.; Wang, J.; Houk, K. N.; Tan, B., Asymmetric phosphoric acid-catalyzed four-component Ugi reaction. *Science* **2018**, *361*, 1-9.

SUPPORTING INFORMATION

3.5 Materials and methods

3.5.1 Materials

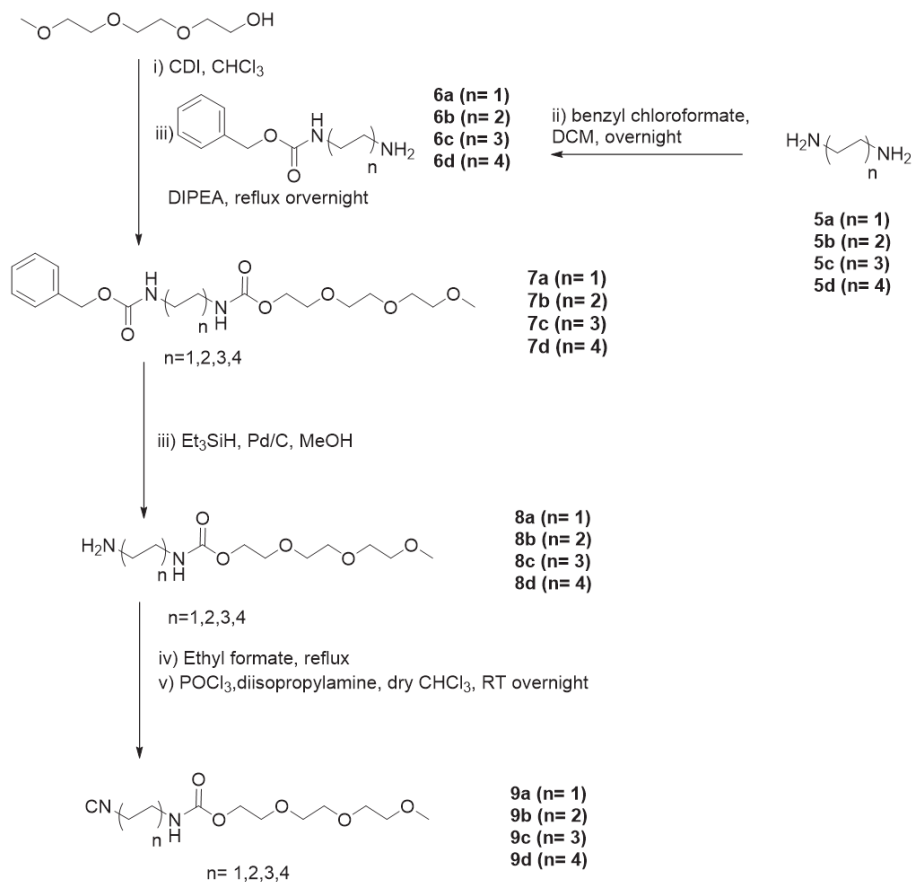
All reagents and chemicals were purchased at Sigma Aldrich and Acros Organic and were used without further purification. Deuterated chloroform was purchased from Euriso-top and Milli-Q water was employed for all the experiments. Acetonitrile for the hydrogenation reaction was dried using molecular sieves 3 Å (20% w/v) and used after 24 h of equilibration.

3.5.2. Instrumentation

The compounds were purified by normal-phase silica chromatography or on X1 flash chromatography system equipped with a C18 column from Grace Reveleris using a gradient of H₂O/CH₃CN. ¹H-NMR and ¹³C-NMR spectra were obtained on a Bruker (300 MHz) or Bruker DMX-400 (400 MHz) spectrometer. LC-MS analysis was performed on a Finnigan Surveyor HPLC system equipped with a Gemini C18 50 x 4.60 mm column (UV detection at 228, 214 nm) coupled to Finnigan LCQ Advantage Max mass spectrometer with ESI. For the mobile phase of LC-MS, a gradient of 10-90% of CH₃CN/H₂O with 0.1% trifluoroacetic acid over 13.5 minutes was used. To report the various Ugi reaction conditions that were screened, the yields of the mono-, di- and trisubstituted products were calculated from the peak areas of the LCMS spectra. The peak areas were divided by the number of substituents attached to the squaric acid cores. To calculate the percentage yield for each compound in the mixture, the individual peak areas of mono-, di- and trisubstituted compounds were divided by the total area and multiplied by 100. Atomic force microscopy (AFM) images were recorded in tapping mode on a Veeco-Bruker Multimode AFM with a Nanoscope IIIa controller at room temperature. The AFM tips used were Oltespa Opus probes with a reflex aluminium coating, with a nominal spring constant of 2 N/m, a nominal resonance frequency of 70 kHz and a tip radius of 7 nm. UV-vis measurements were performed on a Cary 300 UV-VIS spectrophotometer using a quartz cuvette of a 1 cm path length.

3.6 Synthetic Schemes

3.6.1 Scheme S.1 – Synthesis of the amphiphilic isocyanide



Scheme S.1

Synthesis of compound 6

To a solution of alkyldiamine **5a-d** (**5a**: ethane-1,2-diamine (20.00 g, 0.333 mol); **5b**: butane-1,4-diamine (30.00 g, 0.312 mol), **5c**: hexane-1,6-diamine (10.00 g, 0.086 mol); **5d**: octane-1,8-diamine (8.03 g, 55.66 mmol)) in DCM (275 mL), benzyl chloroformate (**a**: 9.50 mL, 0.067 mol, **b**: 8.91 mL, 10.64 g, 0.062 mol, **c**: 2.46 mL, 2.94 g, 0.017 mol, **d**: 1.58 mL, 1.89 g, 0.011 mol) was added dropwise over 2 hours at 0°C and was stirred overnight at room temperature. The solvent was removed by rotary evaporation and the residue was redissolved in EtOAc (250 mL) and washed with water (3 x 200 mL). The combined organic layers were dried with MgSO₄ and after the removal of the solvent, the product was isolated as white solid.

6a: Yield: 11.35 g, 88%. ¹H NMR (300 MHz, CD₃OD): δ (ppm) = 7.38 – 7.28 (m, 5H), 4.90 (s, 2H), 3.27 (s, 2H), 3.20 – 3.04 (m, 2H), 2.65 (t, 1H), 1.52 (q, 2H). ¹³C NMR (75 MHz, CDCl₃): δ (ppm) = 128.06, 127.58, 127.44, 66.05, 48.45, 48.17, 47.89, 47.60, 47.32, 47.04, 46.75, 43.02, 40.93.

6b: Yield: 11.89 g, 86%. ¹H NMR (300 MHz, CD₃OD): δ (ppm) = 7.39 – 7.28 (m, 5H), 5.07 (s, 2H), 3.36 – 3.06 (m, 6H), 2.64 (q, 1H), 1.51 (m, 4H). ¹³C NMR (75 MHz, CDCl₃): δ (ppm) = 166.42, 135.87, 128.03, 127.53, 127.34, 65.90, 48.44, 48.15, 47.87, 47.59, 47.30, 47.02, 46.74, 40.03, 31.81, 26.73

6c: Yield: 4.28 g, 99%. ¹H NMR (300 MHz, CD₃OD): δ (ppm) = 7.35 (d, 5H), 4.88 (s, 2H), 3.19 – 3.07 (m, 2H), 2.63 (m, 2H), 1.60 – 1.29 (m, 8H). ¹³C NMR: (300 MHz, CDCl₃): δ (ppm) = 157.49, 137.12, 128.05, 127.52, 127.35, 65.86, 48.47, 48.18, 47.90, 47.61, 47.33, 47.05, 46.76, 41.09, 41.03, 40.30, 32.34, 32.29, 29.47, 26.48, 26.23, 26.02.

6d: Yield: 6.20 g, 100%. ¹H NMR (300 MHz, CD₃OD): δ (ppm) = 7.40 – 7.26 (m, 5H), 5.07 (s, 2H), 3.11 (m, 3H), 2.88 (m, 1H), 1.64 (m, 2H), 1.50 (m, 2H), 1.35 (q, 8H). ¹³C NMR (75 MHz, CDCl₃): δ (ppm) = 156.67, 136.01, 128.07, 127.56, 127.34, 65.89, 48.20, 47.92, 47.63, 47.35, 47.06, 46.78, 40.33, 39.43, 29.44, 28.68, 27.31, 26.24, 25.97.

Synthesis of 7

Triethylene glycol monomethyl ether (**a**: 2.50 mL, 15.23 mmol; **b**: 2.50 mL, 15.23 mmol; **c**: 4.14 mL, 25.88 mmol; **d**: 2.63 mL, 16.44 mmol) was activated with 1,1'-carbonyldiimidazole (CDI) (**a**: 2.72 g, 16.75 mmol; **b**: 2.72 g, 16.75

mmol; **c**: 4.62 g, 28.47 mmol; **d**: 2.93 g, 18.09 mmol) for 1 h at RT. Subsequently, **6a-d** (**6a**: 4.44 g, 22.84 mmol; **6b**: 5.08 g, 22.84 mol; **6c**: 9.72 g, 38.83 mmol; **6d**: 5.95 g, 21.38 mmol) and DIPEA (**7a**: 5.30 mL, 30.45 mmol; **7b**: 5.30 mL, 30.45 mmol; **7c**: 9.02 mL, 51.77 mmol; **7d**: 5.73 mL, 32.88 mmol) were dissolved in CHCl₃ (70 mL) and were added to the reaction mixture and refluxed overnight. Once the reaction was complete, DCM (100 mL) was added and the reaction mixture was washed with H₂O (3 x 200 mL). The combined aqueous fractions were then back-extracted 3x with DCM (3 x 100 mL). The combined organic fractions were dried with MgSO₄, prior to removal of the solvent in *vacuo*. The crude product was purified by silica column chromatography using a DCM/EtOAc gradient (20-50% DCM: EtOAc). The product was isolated as a white solid.

7a: Yield: 5.59 g, 96%. ¹H NMR (300 MHz, CDCl₃): δ (ppm) = 7.43 – 7.27 (m, 5H), 5.41 (d, 2H), 5.10 (s, 2H), 4.27 – 4.14 (m, 2H), 3.65 (q, 8H), 3.57 – 3.52 (m, 2H), 3.37 (s, 3H), 3.33 – 3.25 (m, 4H). ¹³C NMR (75 MHz, CDCl₃): δ (ppm) = 160.55, 157.14, 140.43, 128.51, 128.13, 77.49, 77.06, 76.64, 71.90, 70.53, 70.48, 69.49, 66.75, 64.05, 58.98, 41.22, 41.05.

7b: Yield: 4.15 g, 66%. ¹H NMR (300 MHz, CDCl₃): δ (ppm) = 7.41 – 7.27 (m, 5H), 5.10 (s, 2H), 4.95 (s, 3.26 – 3.13 (m, 4H), 1.53 (q, 4H). ¹³C NMR (75 MHz, CDCl₃): δ (ppm) = 159.17, 156.47, 137.26, 128.51, 128.09, 77.48, 77.06, 76.63, 71.92, 70.55, 70.51, 69.61, 66.62, 63.87, 59.01, 40.55, 27.20.

7c: Yield 7.20 g, 63%. ¹H NMR (300 MHz, CDCl₃): δ (ppm) = 7.34 (m, 5H), 5.08 (s, 2H), 4.27 – 4.02 (m, 3H), 3.74 – 3.49 (m, 11H), 3.36 (s, 4H), 3.15 – 3.01 (m, 5H), 1.57 – 1.41 (m, 5H), 1.41 – 1.18 (m, 6H). ¹³C NMR (75 MHz, CDCl₃): δ (ppm) = 157.52, 137.13, 128.08, 127.39, 71.57, 70.16, 70.00, 69.21, 65.88, 63.56, 57.73, 48.50, 48.22, 47.94, 47.65, 47.37, 47.09, 46.80, 40.31, 40.25, 29.45, 26.07.

7d: Yield: 5.70 g, 74%. ¹H NMR (300 MHz, CDCl₃): δ (ppm) = 7.43 – 7.28 (m, 5H), 5.10 (s, 2H), 4.89 – 4.72 (m, 2H), 4.22 (t, 2H), 3.66 (d, 8H), 3.61 – 3.54 (m, 2H), 3.39 (s, 3H), 3.26 – 3.09 (m, 4H), 1.47 (q, 4H), 1.30 (s, 8H). ¹³C NMR (75 MHz, CDCl₃): δ (ppm) = 158.48, 156.41, 136.69, 128.05, 77.50, 77.07, 76.65, 71.93, 70.56, 70.54, 70.50, 69.66, 66.53, 63.79, 59.02, 40.96, 29.88, 29.10, 26.60.

Synthesis of **8**

To perform the hydrogenation reaction **7a-d** (**7a**, $n=1$: 5.59 g, 14.53 mmol; **7b**, $n=2$: 3.25 g, 7.876 mmol; **7c**, $n=3$: 1.47 g, 3.35 mmol; **7d**, $n=4$: 1.80 g, 3.84 mmol) was dissolved in dry MeOH (20 mL), and Pd/C (**a**: 558.6 mg, 5.249 mmol; **b**: 324.9 mg, 3.053 mmol; **c**: 178.1 mg, 1.673 mmol; **d**: 204.4 mg, 1.921 mmol) was added. The solution was put under a N₂ atmosphere and triethylsilane (**a**: 34.82 mL, 218.0 mmol; **b**: 18.87 mL, 118.1 mmol; **c**: 26.73, 167.3 mmol; **d**: 61.36 mL, 384.1 mmol) was added dropwise. When the reaction was complete (TLC, 95:5 v/v DCM/MeOH), the solution was filtered through Celite to remove Pd/C. The filtrate was concentrated by rotary evaporation and afterwards, a gentle stream of N₂ gas to give the product **8** as a white sticky solid. In all cases, the reaction was quantitative as determined by LCMS.

8a: ¹H NMR (300 MHz, CDCl₃): δ (ppm) = 5.85 (d, 1H), 4.16 – 4.06 (m, 2H), 3.62 – 3.49 (m, 8H), 3.45 (m, 2H), 3.28 (s, 3H), 3.14 (q, 2H), 2.72 (t, 2H), 2.52 (s, 2H). ¹³C NMR (75 MHz, CDCl₃): δ (ppm) = 156.78, 77.65, 77.22, 76.79, 71.76, 70.38, 70.33, 69.49, 63.68, 58.87, 43.25, 41.39.

8b: ¹H NMR (300 MHz, CDCl₃): δ (ppm) = 5.55 (s, 1H), 4.04 (t, 2H), 3.57 – 3.44 (m, 8H), 3.43 – 3.35 (m, 2H), 3.22 (s, 3H), 3.00 (q, 2H), 2.55 (t, 2H), 2.27 (s, 2H), 1.34 (m, 4H). ¹³C NMR (75 MHz, CDCl₃): δ (ppm) = 156.50, 77.74, 77.31, 76.88, 72.70, 71.73, 71.69, 70.38, 70.35, 70.29, 70.20, 70.08, 69.47, 63.51, 61.03, 61.03, 58.80, 41.43, 40.60, 30.32, 27.15.

8c: ¹H NMR (300 MHz, CDCl₃): δ (ppm) = 4.94 (s, 1H), 4.26 – 4.17 (m, 2H), 3.72 – 3.62 (m, 8H), 3.61 – 3.55 (m, 2H), 3.39 (s, 3H), 3.24 – 3.10 (m, 2H), 2.69 (t, 2H), 1.85 (s, 2H), 1.48 (m, 4H), 1.33 (m, 4H). ¹³C NMR (75 MHz, CDCl₃): δ (ppm) = 156.39, 77.72, 77.29, 76.87, 71.76, 70.40, 70.37, 70.33, 69.51, 63.54, 58.84, 41.77, 40.73, 33.18, 29.77, 26.43, 26.37.

8d: ¹H NMR (300 MHz, CDCl₃): δ (ppm) = 5.13 (d, 1H), 4.16 – 4.09 (m, 2H), 3.65 – 3.52 (m, 8H), 3.50 – 3.44 (m, 2H), 3.30 (s, 3H), 3.10 – 3.01 (m, 2H), 2.60 (m, 2H), 1.38 (q, 4H), 1.21 (s, 10H). ¹³C NMR (75 MHz, CDCl₃): δ (ppm) = 156.41, 77.57, 77.15, 76.72, 71.84, 70.47, 70.44, 69.63, 63.65, 58.94, 41.85, 41.74, 40.93, 38.00, 33.09, 29.84, 29.42, 29.26, 29.14, 29.07, 26.71, 26.65, 26.61.

Synthesis of 9

The formylation reaction was performed by dissolving **8a-d** (**8a**, n=1: 3.64g, 14.54 mmol; **8b**, n=2: 2.18, 2.78 mmol; **8c**, n=3: 1.48g, 4.81 mmol; **8d**, n=4: 1.29g, 3.86 mmol) in ethylformate (20 mL) and refluxing overnight. The reaction was monitored by ^1H NMR and after ethyl formate was removed by rotary evaporation, the compound was used for the next step without further purification. Subsequently, the crude was dissolved in DCM (20 mL) and diisopropylamine (**a**: 3.02 mL, 21.56 mmol; **b**: 3.11 mL, 22.19 mmol; **c**: 2.03 mL, 14.48 mmol; **d**: 2.48 mL, 17.71 mmol) was added at 0 °C. Phosphorus oxychloride (**a**: 0.81 mL, 8.62 mmol; **b**: 0.83 mL, 8.88 mmol; **c**: 0.54 mL, 5.78 mmol; **d**: 0.66 mL, 7.09 mmol) was added dropwise and the reaction mixture was stirred overnight. Sodium carbonate was added to quench the reaction and was stirred for another 30 min before dilution with water. The aqueous layers were extracted with DCM (3 x 40 mL) and dried with Na_2SO_4 . The solvent was removed under vacuum and purified by silica column chromatography using DCM:MeOH (95:5) as the eluent.

9a: Yield: 1.63 g, 87%. ^1H NMR (300 MHz, CDCl_3): δ (ppm) = 6.00 (t, 1H), 4.14 – 3.89 (m, 2H), 3.50 – 3.41 (m, 8H), 3.35 (m, 4H), 3.22 (t, 2H), 3.17 (s, 3H). ^{13}C NMR (75 MHz, CDCl_3): δ (ppm) = 156.47, 71.68, 70.28, 70.25, 70.22, 69.18, 64.00, 58.71, 41.53, 40.01.

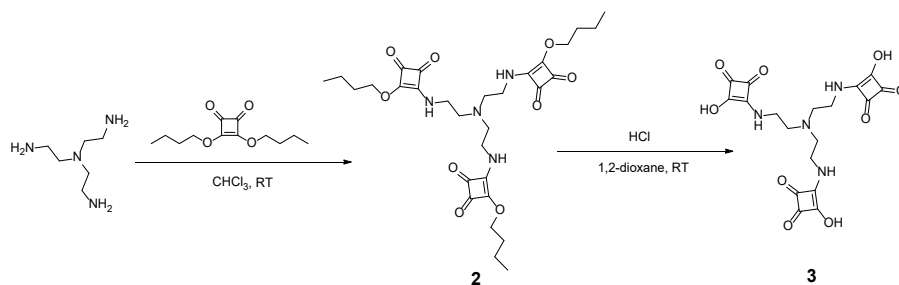
9b: Yield: 2.00 g, 94%. ^1H NMR (300 MHz, CDCl_3): δ (ppm) = 5.36 – 4.96 (m, 1H), 4.25 – 4.01 (m, 2H), 3.56 (d, 10H), 3.46 (m, 2H), 3.29 (d, 3H), 3.08 (d, 2H), 1.44 (dq, 4H). ^{13}C NMR (75 MHz, CDCl_3): δ (ppm) = 156.55, 156.55, 77.82, 77.40, 76.98, 71.75, 70.52, 70.43, 70.37, 70.31, 69.42, 69.39, 65.99, 65.91, 63.70, 63.61, 58.81, 41.15, 41.07, 40.98, 40.40, 39.66, 27.01, 26.74, 26.08.

9c: Yield: 1.26 g, 83%. ^1H NMR (300 MHz, CDCl_3): δ (ppm) = 4.92 (t, 1H), 4.17 (t, 2H), 3.68 – 3.58 (m, 8H), 3.56 – 3.48 (m, 2H), 3.40 – 3.30 (m, 5H), 3.13 (q, 2H), 1.72 – 1.58 (m, 2H), 1.53 – 1.27 (m, 6H). ^{13}C NMR (75 MHz, CDCl_3): δ (ppm) = 156.42, 77.60, 77.17, 76.74, 71.88, 70.51, 70.49, 70.46, 69.58, 63.80, 58.99, 41.52, 41.43, 41.35, 40.73, 29.74, 28.93, 25.97, 25.80.

9d: Yield: 1.82 g, 90%. ^1H NMR (300 MHz, CDCl_3): δ (ppm) = 4.22 (t, 2H), 3.66 (d, 8H), 3.56 (m, 2H), 3.39 (s, 4H), 3.17 (q, 2H), 1.76 – 1.61 (m, 2H), 1.46 (m, 4H), 1.32 (q, 6H). ^{13}C NMR (75 MHz, CDCl_3): δ (ppm) = 156.41,

155.48, 77.56, 77.13, 76.71, 71.89, 70.52, 70.50, 70.47, 69.62, 63.77, 58.99, 41.59, 41.51, 41.43, 40.91, 29.86, 29.00, 28.96, 28.56, 26.54, 26.20

3.6.2 Scheme S.2: Synthesis of trisquaric acid



Scheme S.2

Synthesis of 2

Tris(2-aminoethyl)amine (200 mg 1.37 mmol) was dissolved in CHCl_3 (30 mL). DIPEA (1.2 mL, 6.84 mmol) and 3,4-dibutoxy-3-cyclobutene-1,2-dione (1.18 mL, 5.47 mmol) were added to the mixture and refluxed overnight at 75 °C. The compound was purified by flash chromatography using a gradient of $\text{H}_2\text{O}/\text{CH}_3\text{CN}$ 10-90% over 30 min and the product was isolated as yellow solid.

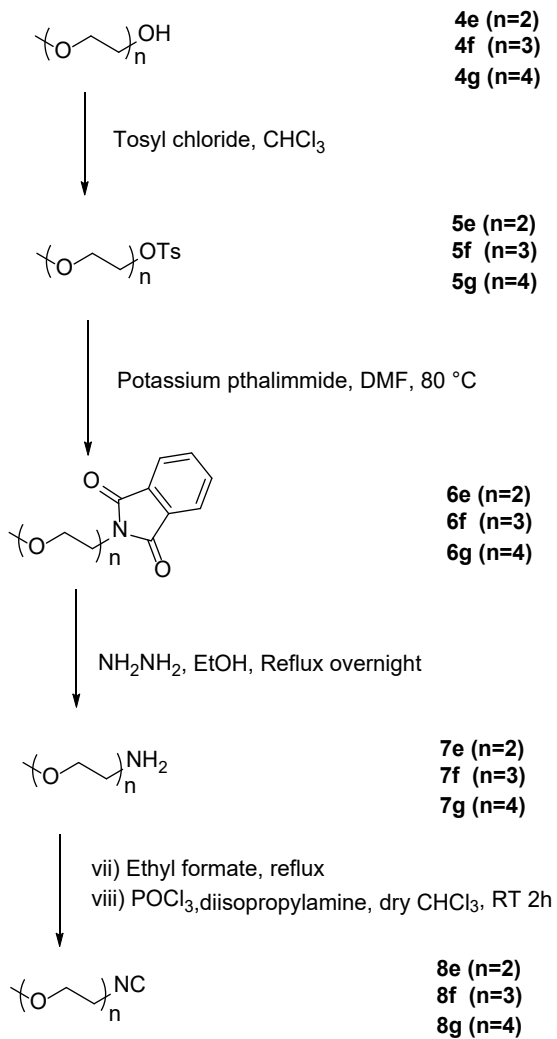
Yield: 1.25 g, 89%. ^1H NMR (300 MHz, CDCl_3): δ (ppm) = 7.97 – 7.50 (m, 3H), 4.68 (t, 6H), 3.67 (d, 7H), 2.74 (s, 6H), 1.77 (p, 6H), 1.41 (m, 7H), 0.97 (t, 9H). ^{13}C NMR (75 MHz, CDCl_3): δ (ppm) = 160.89, 145.78, 130.66, 77.47, 77.04, 76.62, 73.67, 54.83, 42.04, 31.95, 31.95, 18.62, 13.66.

Synthesis of 3

Compound 2 (624.8 mg, 1.04 mmol) was dissolved in 1,2-dioxane (10 mL) and HCl 37 % (2 mL) was added. The mixture was stirred overnight at room temperature and the final compound was isolated by removing the solvent with a gentle stream of N_2 gas. The white solid was washed with DCM and was used without further purification.

Yield: 464.7 mg, 100%. ^1H NMR (300 MHz, $\text{DMSO-}d_6$): δ (ppm) = 8.20 (t, 3H), 3.74 (q, 6H), 3.28 (t, 6H). ^{13}C NMR (75 MHz, CDCl_3): δ (ppm) = 187.29, 185.64, 175.14, 53.55, 43.54, 40.73, 40.45, 40.17, 39.89, 39.61, 39.33, 39.05. HRMS: m/z = 434.11 $[\text{M}+\text{H}]^+$.

3.6.3 Scheme S.3 – Synthesis of oligo(ethylene) glycol isocyanide



Scheme S.3

Synthesis of 5e, 5f, 5g

A solution of **4e-f** (**4e**: diethylene glycol methyl ether (9.75 mL, 83.23 mmol); **4f**: triethylene glycol monomethyl ether (4.87 mL, 30.45 mmol); **4g**: tetraethylene glycol monomethyl ether (4.78 mL, 24.01 mmol)) in THF (**e**: 14 mL; **f**: 7 mL; **g**: 7 mL) was reacted with a solution of NaOH (**e**: 6.09 g, 152.31 mmol; **f**: 2.23 g, 55.72 mmol; **g**: 1.76 g, 40.0 mmol) in distilled water (**e**: 17 mL; **f**: 6 mL; **g**: 6 mL) with stirring for 15 min at 0 °C. Subsequently, a solution of TsCl (**e**: 15.87 g, 30.45 mmol; **f**: 5.81 g, 30.45 mmol; **g**: 4.58 g, 24.01 mmol) in THF (**e**: 26 mL; **f**: 10 mL; **g**: 10 mL) was added dropwise at 0 °C. The reaction mixture was stirred at RT for other 30 min. The volatile materials were removed by rotary evaporation and water (100 mL) was added. An extraction with Et₂O (3 x 100mL) was performed, and afterwards the organic layers were dried with Na₂SO₄. The products were isolated as a pale-yellow oil after rotary evaporation.

5e: Yield: 22.19 g, 97%. ¹H NMR (300 MHz, CDCl₃): δ (ppm) = 7.83 – 7.73 (m, 2H), 7.38 – 7.30 (m, 2H), 4.21 – 4.12 (m, 2H), 3.72 – 3.62 (m, 2H), 3.58 – 3.53 (m, 2H), 3.50 – 3.43 (m, 2H), 3.34 (d, 3H), 2.43 (s, 3H). ¹³C NMR (75 MHz, CDCl₃): δ (ppm) = 144.84, 129.82, 127.96, 77.55, 77.13, 76.70, 71.77, 70.63, 69.25, 68.67, 59.02, 21.63.

5f: Yield: 9.26 g, 96%. ¹H NMR (300 MHz, CDCl₃): δ (ppm) = 7.76 – 7.62 (m, 1H), 7.32 – 7.22 (m, 1H), 4.10 – 4.03 (m, 1H), 3.61 – 3.56 (m, 1H), 3.56 – 3.48 (m, 3H), 3.46 – 3.40 (m, 1H), 3.26 (s, 2H), 2.35 (s, 2H). ¹³C NMR (75 MHz, CDCl₃): δ (ppm) = 144.76, 132.95, 129.79, 127.83, 77.75, 77.33, 76.90, 71.79, 70.57, 70.40, 69.28, 68.52, 58.84, 21.49.

5g: Yield: 7.40 g, 85%. ¹H NMR (300 MHz, CDCl₃): δ (ppm) = 7.85 – 7.76 (m, 2H), 7.41 – 7.31 (m, 2H), 4.24 – 4.10 (m, 2H), 3.71 – 3.67 (m, 2H), 3.63 (d, 6H), 3.59 (s, 4H), 3.57 – 3.52 (m, 2H), 3.38 (s, 3H), 2.45 (s, 3H). ¹³C NMR (75 MHz, CDCl₃): δ (ppm) = 44.80, 142.79, 129.82, 127.98, 77.50, 77.07, 76.65, 71.91, 70.72, 70.58, 70.51, 69.25, 68.66, 59.02, 21.64.

Synthesis of compound 6e, 6f, 6g

Compounds **5e-f** (**5e**, n=2: 22.19 g, 80.88 mmol, **5f**, n=3: 9.26 g, 29.10 mmol; **5g**, n=4: 7.40 g, 20.42 mmol) were dissolved in DMF (**e**: 50 mL; **f**: 40 mL; **g**:

36 mL). phthalimide potassium salt (**e** 22.47 g, 121.31 mmol; **f**: 8.08 g, 43.65 mmol; **g**: 5.67 g, 30.63 mmol) was added to the solution and heated to stirring 80 °C with stirring overnight. After the removal of the solvent by rotary evaporation, water (100 mL) was added to the solid and extracted with DCM (3 x 100 mL). Subsequently, the combined organic layers were dried with NaSO₄ and purified by silica column chromatography (petroleum ether: EtOAc 1/4), and the product was isolated as a white solid.

6e: Yield: 15.32 g, 76%. ¹H NMR (300 MHz, CDCl₃): δ (ppm) = 7.80 (m, 2H), 7.68 (m, 2H), 3.93 – 3.82 (m, 2H), 3.76 – 3.67 (m, 2H), 3.64 – 3.59 (m, 2H), 3.49 – 3.43 (m, 2H), 3.33 – 3.23 (m, 3H). ¹³C NMR (75 MHz, CDCl₃): δ (ppm) = 168.22, 133.89, 132.10, 123.17, 77.56, 77.13, 76.71, 71.85, 69.85, 67.90, 58.95, 37.12.

6f: Yield: 7.38 g, 87%. ¹H NMR (300 MHz, CDCl₃): δ (ppm) = 7.92 – 7.82 (m, 2H), 7.77 – 7.65 (m, 2H), 3.94 – 3.85 (m, 2H), 3.74 (t, 2H), 3.71 – 3.57 (m, 6H), 3.52 – 3.44 (m, 2H), 3.34 (s, 3H). ¹³C NMR (75 MHz, CDCl₃): δ (ppm) = 168.12, 133.84, 132.07, 123.11, 77.62, 77.19, 76.76, 71.81, 70.49, 70.45, 70.07, 67.82, 58.87, 37.22.

6g: Yield: 6.89 g, 100%. ¹H NMR (300 MHz, CDCl₃): δ (ppm) = 7.83 (m, 2H), 7.76 – 7.68 (m, 2H), 3.89 (t, 2H), 3.73 (t, 2H), 3.66 – 3.57 (m, 10H), 3.52 (m, 2H), 3.36 (d, 3H). ¹³C NMR (75 MHz, CDCl₃): δ (ppm) = 171.64, 133.92, 132.32, 123.23, 77.46, 77.04, 76.61, 71.92, 70.60, 70.56, 70.49, 70.08, 67.91, 59.02, 37.26.

Synthesis of **7e**, **7f** and **7g**

Compound **6e-g** (**6e**, n=2: 9.33 g, 25.17 mmol; **6f**, n=3: 5.74g, 19.56 mmol; **6g**, n=4: 3.34 g, 9.89 mmol) was dissolved in ethanol (100 mL) and hydrazine monohydrate (**e**: 10.40 mL, 214.05 mmol; **f**: 5.44 mL, 111.91 mmol; **g**: 2.75 mL, 56.63 mmol) was added. The mixture was refluxed overnight and a white solid precipitate was formed. the solvent was removed by rotary evaporation, the solid was dissolved in DCM (200 mL) and washed with 1M NaOH (3x 200 mL). Subsequently, the product was extracted from the aqueous layer with DCM (3 x 100 mL), dried with NaSO₄ and concentrated by rotary evaporation. The product was used for the next step without further purification.

7e: Yield: 1.95 g, 44%. ^1H NMR (300 MHz, CDCl_3): δ (ppm) = 3.56 – 3.50 (m, 2H), 3.49 – 3.41 (m, 4H), 3.30 (d, 3H), 2.80 (t, 2H), 2.28 (s, 2H). ^{13}C NMR (75 MHz, CDCl_3): δ (ppm) = 77.60, 77.17, 76.74, 73.02, 71.81, 70.14, 58.95, 41.45.

7f: Yield: 2.82 g, 88%. ^1H NMR (300 MHz, CDCl_3): δ (ppm) = 3.62 (m, 6H), 3.56 – 3.47 (m, 4H), 3.35 (s, 3H), 2.90 – 2.70 (m, 4H). ^{13}C NMR (75 MHz, CDCl_3): δ (ppm) = 77.53, 77.11, 76.68, 72.86, 71.88, 70.53, 70.48, 70.22, 58.99, 41.46.

7g: Yield: 1.51 g, 74%. ^1H NMR (300 MHz, CDCl_3): δ (ppm) = 7.83 (m, 2H), 7.76 – 7.68 (m, 2H), 3.89 (t, 2H), 3.73 (t, 2H), 3.66 – 3.57 (m, 10H), 3.52 (m, 2H), 3.36 (d, 3H). ^{13}C NMR (75 MHz, CDCl_3): δ (ppm) = 168.16, 133.90, 131.98, 123.12, 77.70, 77.27, 76.84, 72.63, 72.44, 70.49, 70.37, 70.27, 70.17, 69.95, 69.78, 67.80, 61.46, 61.22, 37.14.

Synthesis of 8e, 8f and 8g

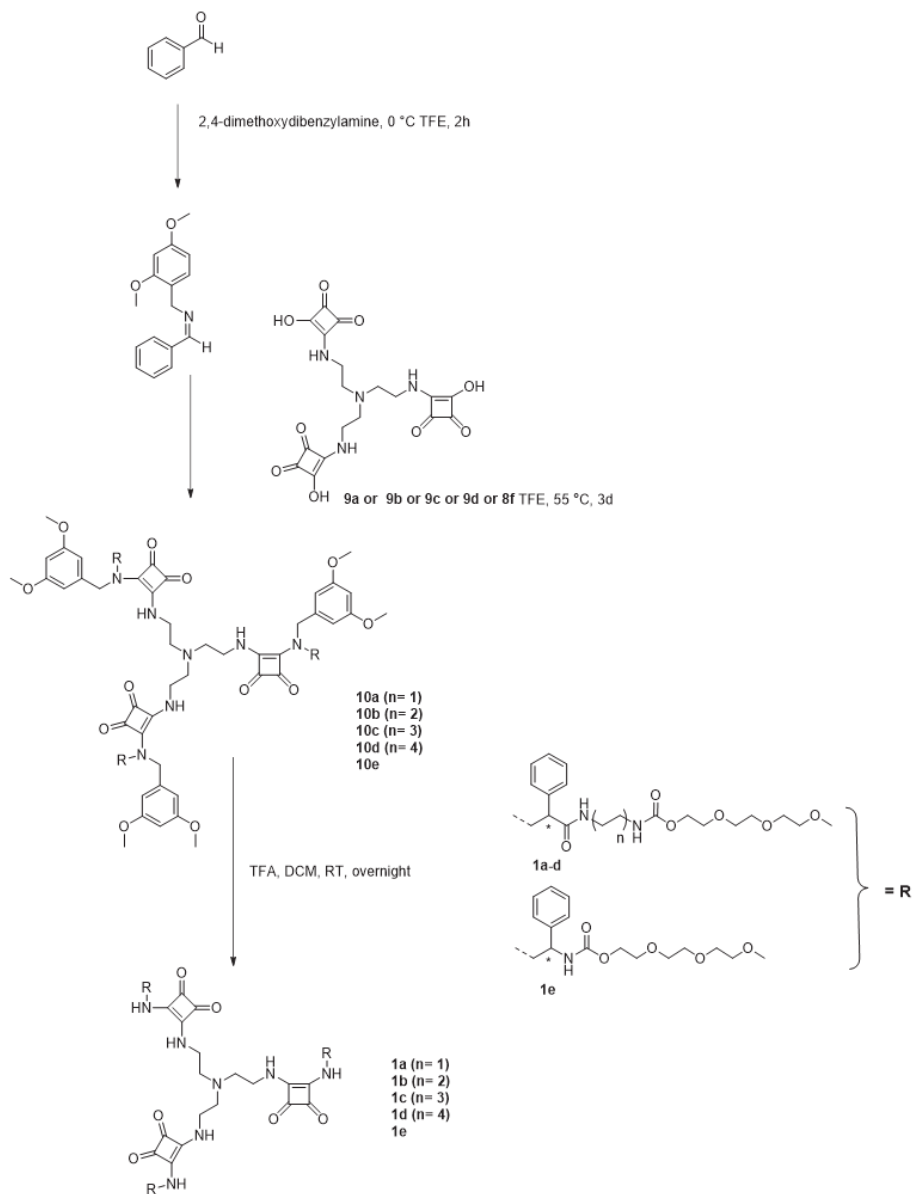
Compounds **7e-g** (**7e**, $n=2$: 1.95 g, 16.38 mmol; **7f**, $n=3$: 2.82g, 17.27 mmol; **7g**, $n=4$: 2.81g, 13.56 mmol) were dissolved in ethyl formate (20 mL) and refluxed for 12 hours. The volatiles were removed by rotary evaporation, (**e**, $n=2$: 0.91 g, 6.15 mmol; **f**, $n=3$: 2.30 g, 12.03 mmol; **g**, $n=4$: 1.53 g, 6.50 mmol), and the residue was dissolved in dry DCM (20 mL) and placed under a N_2 atmosphere. Diisopropylamine (**e**: 2.59 mL, 18.46 mmol; **f**: 5.06 mL, 36.08 mmol; **g**: 2.73 mL, 19.50 mmol) was added and the reaction mixture was cooled to 0 °C. Phosphorus oxychloride (**e**: 0.69 mL, 7.383 mmol; **f**: 1.35 mL, 14.43 mmol; **g**: 0.73 mL, 7.80 mmol) was added dropwise and brought to room temperature. The reaction mixture was stirred for additional 2 h before sodium carbonate (6.5 g in 35 mL of H_2O) was added. The resulting suspension was stirred for another 30 minutes and then diluted with water. The aqueous phase was extracted with DCM (3 x 40 mL), dried with Na_2SO_4 and the organic layers were removed by rotary evaporation. The compound was purified by silica column chromatography (95:5 DCM:MeOH).

8e: Yield: 0.6328 g, 80%. ^1H NMR (300 MHz, CDCl_3): δ (ppm) = 3.74 – 3.66 (m, 4H), 3.63 – 3.52 (m, 4H), 3.40 (s, 3H). ^{13}C NMR (75 MHz, CDCl_3): δ (ppm) = 157.51, 77.50, 77.08, 76.65, 71.84, 70.80, 68.68, 59.12, 41.82, 41.73, 41.63.

8f: Yield: 1.93 g, 93%. ^1H NMR (300 MHz, CDCl_3): δ (ppm) = 3.71 – 3.62 (m, 8H), 3.59 – 3.51 (m, 4H), 3.36 (s, 3H). ^{13}C NMR (75 MHz, CDCl_3): δ (ppm) = 77.57, 77.15, 76.72, 71.88, 70.81, 70.59, 70.57, 68.63, 59.02, 41.84, 41.74, 41.65.

8g: Yield: 1.19 g, 84%. ^1H NMR (300 MHz, CDCl_3): δ (ppm) = 3.69 – 3.56 (m, 12H), 3.54 – 3.45 (m, 4H), 3.31 (d, 3H). ^{13}C NMR (75 MHz, CDCl_3): δ (ppm) = 161.46, 77.62, 77.20, 76.77, 71.88, 71.82, 70.79, 70.59, 70.54, 70.46, 70.43, 70.38, 70.09, 69.53, 68.62, 58.97, 41.83, 41.73, 41.64, 37.73.

3.6.4 Scheme S.4 – Ugi reaction



Scheme S.4

Ugi reaction

Benzaldehyde (59 μ L, 0.58 mmol) and 2,4-dimethoxybenzylamine (87 μ L, 0.58 mmol) were stirred at 0 $^{\circ}$ C for 2 h in TFE (0.5 mL). Subsequently, **4** (50 mg, 0.12 mmol), *p*-toluenesulfonic acid (pTSA) (1 eq, 22 mg, 0.58 mmol), and the isocyanide (**8f**: *n*=0 (100 mg, 0.58 mmol); **9a**: *n*=1 (150 mg, 0.58 mmol); **9b**: *n*=2 (165.96 mg, 0.58 mmol); **9c**: *n*=3 (182 mg, 0.58 mmol; **9d**: *n*=4 (198 mg, 0.58 mmol)) in TFE (0.65 mL) were added and stirred at 55 $^{\circ}$ C for an additional 72h. The reaction mixture was stirred and monitored by LCMS until no further reaction was observed. The solvent was removed by rotary evaporation and the crude was purified by flash chromatography on a C18 silica column using a gradient of 10-90% H₂O/CH₃CN over 50 min.

10a: Yield: 49%. ¹H NMR (300 MHz, CDCl₃): δ (ppm) = 7.51 – 7.03 (m, 18H), 6.56 – 6.15 (m, 6H), 5.27 – 4.68 (m, 6H), 4.14 (m, 6H), 3.86 – 3.67 (m, 18H), 3.66 – 3.43 (m, 36H), 3.41 – 3.14 (m, 21H), 2.52 (s, 3H), 2.33 – 1.93 (m, 3H), 1.26 (s, 12H). ¹³C NMR (75 MHz, CDCl₃): δ (ppm) = 182.96, 179.20, 177.65, 169.47, 169.24, 168.49, 167.97, 160.55, 159.82, 157.04, 156.73, 156.64, 135.96, 134.81, 129.72, 128.94, 128.74, 128.38, 127.03, 118.04, 117.50, 104.79, 104.73, 98.50, 97.98, 71.73, 71.73, 70.21, 70.05, 69.29, 63.70, 58.49, 55.81, 55.62, 55.51, 54.51, 45.57, 40.80, 40.52, 40.24, 39.96, 39.68, 39.41, 39.13. MALDI: (*m/z*): 2003.88 [M+Na]⁺

10b: Yield: 41%. ¹H NMR (400 MHz, CDCl₃): δ (ppm) = 7.47 – 7.04 (m, 18H), 6.45 (m, 6H), 5.41 – 4.82 (m, 6H), 4.35 – 4.11 (m, 7H), 3.86 – 3.55 (m, 54H), 3.38 (d, 9H), 3.32 – 2.96 (m, 12H), 2.90 – 2.37 (m, 3H), 2.35 – 1.97 (m, 3H), 1.63 – 0.82 (m, 85H). ¹³C NMR (75 MHz, CDCl₃): δ (ppm) = 183.11, 169.57, 168.11, 161.17, 158.62, 156.66, 156.51, 130.85, 130.85, 129.69, 129.49, 129.36, 128.91, 128.73, 128.60, 128.36, 126.93, 117.01, 104.07, 98.52, 77.41, 77.09, 76.78, 71.92, 71.87, 70.52, 70.47, 70.44, 69.64, 63.77, 59.01, 55.36, 55.29, 45.15, 40.58, 40.44, 39.63, 39.43, 37.45, 37.11, 36.89, 31.95, 30.41, 29.73, 29.48, 29.39, 27.41, 27.33, 27.12, 24.49, 24.25, 22.72, 20.48, 19.98. MALDI: (*m/z*): 2086.64 [M+Na]⁺

10c: Yield: 59%, ¹H NMR (400 MHz, CDCl₃): δ (ppm) = 7.47 – 6.99 (m, 18H), 6.97 – 6.61 (m, 3H), 6.40 (m, 6H), 6.26 – 5.95 (m, 3H), 5.47 – 4.76 (m, 9H), 4.16 (dt, 6H), 3.85 – 3.60 (m, 48H), 3.54 (t, 6H), 3.36 (s, 9H), 3.24 – 3.02 (m, 12H), 2.79 – 2.37 (m, 3H), 1.52 – 1.12 (m, 30H). ¹³C NMR (100 MHz, CDCl₃): δ (ppm) = 183.22, 177.81, 172.83, 169.73, 169.40, 168.21, 161.12,

160.94, 160.40, 158.63, 158.22, 157.86, 156.56, 156.47, 156.44, 136.61, 135.00, 134.01, 130.84, 129.78, 129.05, 128.90, 128.71, 128.58, 128.39, 128.21, 128.09, 127.46, 126.85, 122.18, 121.76, 116.93, 116.80, 105.21, 105.02, 104.01, 98.89, 98.65, 98.36, 98.31, 95.42, 94.69, 77.49, 77.49, 77.17, 76.85, 71.90, 70.50, 69.61, 66.46, 65.81, 63.76, 59.00, 55.71, 55.57, 55.41, 55.38, 55.27, 55.17, 54.23, 47.00, 42.21, 41.49, 40.82, 40.69, 39.97, 39.70, 39.47, 31.91, 29.78, 29.68, 29.34, 29.03, 28.57, 28.34, 26.38, 26.26, 26.13, 22.68. MALDI: (m/z): 2172.27 [M+Na]⁺

10d: Yield: 46%. ¹H NMR (400 MHz, CDCl₃): δ (ppm) = 7.22 (d, 18H), 6.92 – 6.55 (m, 3H), 6.54 – 6.21 (m, 6H), 6.20 – 5.83 (m, 3H), 5.37 – 4.76 (m, 9H), 4.21 – 4.08 (m, 6H), 3.67 (d, 48H), 3.51 (t, 6H), 3.34 (s, 9H), 3.19 – 3.04 (m, 12H), 2.69 – 2.35 (m, 3H), 1.46 – 1.15 (m, 42H). ¹³C NMR (100 MHz, CDCl₃): δ (ppm) = 183.23, 177.84, 169.34, 168.13, 161.12, 160.92, 160.38, 158.71, 157.87, 156.46, 135.04, 133.96, 129.98, 129.05, 128.91, 128.71, 128.55, 128.37, 128.13, 127.90, 116.86, 116.74, 116.74, 104.96, 104.26, 98.84, 98.69, 98.01, 77.53, 77.22, 76.90, 71.88, 70.50, 70.46, 69.60, 64.17, 63.70, 58.98, 55.71, 55.52, 55.38, 55.32, 55.13, 54.13, 46.84, 42.09, 40.95, 40.18, 39.95, 39.77, 39.37, 31.88, 29.85, 29.64, 29.22, 29.11, 26.81, 26.62, 22.65. MALDI: (m/z): 2256.01 [M+Na]⁺.

10e: Yield: 36%. ¹H NMR (300 MHz, CDCl₃): δ (ppm) = 7.37 – 7.00 (m, 18H), 6.49 – 6.17 (m, 6H), 5.15 – 4.96 (m, 3H), 3.81 – 3.64 (m, 24H), 3.56 (m, 36H), 3.34 – 3.26 (m, 9H), 2.64 (t, 3H), 2.37 – 1.83 (m, 3H), 1.49 – 0.79 (m, 12H). ¹³C NMR (75 MHz, CDCl₃): δ (ppm) = 183.73, 183.25, 178.12, 169.44, 168.13, 161.10, 160.95, 160.37, 158.29, 157.91, 135.05, 134.91, 131.12, 130.65, 130.39, 129.86, 129.58, 129.45, 129.17, 128.93, 128.77, 128.62, 128.42, 128.22, 128.19, 127.88, 127.57, 126.81, 116.76, 116.61, 105.33, 105.24, 104.09, 103.99, 98.90, 98.76, 98.61, 98.15, 98.05, 77.50, 77.50, 77.07, 76.65, 71.85, 70.53, 70.44, 70.38, 70.22, 70.13, 69.73, 69.35, 65.67, 63.76, 58.91, 58.28, 55.81, 55.57, 55.40, 55.33, 55.24, 54.11, 47.07, 42.28, 41.37, 39.93, 39.70, 39.50, 29.68, 29.33, 28.30. MALDI: (m/z): 1742.103 [M+H+Na]⁺.

Synthesis of 1a-e

Deprotection of compounds **10a-e** (**10e**, n=0: 128.7 mg, 0.067 mmol; **10a**, n=1: 98.5 mg, 0.050 mmol; **10b**, n=2: 130.30 mg, 0.063 mmol; **10c**, n=3: 212.4 mg, 0.099 mmol; **10d**, n=4: 142.80 mg, 0.064 mmol) was performed

adding 15 mL DCM/TFA (1:1) at room temperature. The reaction mixture was stirred overnight and the solvent was evaporated by a gentle stream of air. The product was purified by flash chromatography on a C18 silica column using 10-90% H₂O/CH₃CN as gradient over 30 min.

1a: Yield: 51 mg, 66%. ¹H NMR (300 MHz, CDCl₃): δ (ppm) = 8.69 – 8.15 (m, 3H), 7.70 – 7.15 (m, 15H), 6.71 – 5.64 (m, 6H), 4.09 (s, 9H), 3.56 (d, 36H), 3.32 (s, 21H), 2.90 (d, 3H), 1.50 – 0.77 (m, 6H). ¹³C NMR (75 MHz, CDCl₃): δ (ppm) = 190.00, 170.78, 156.87, 148.70, 139.13, 128.96, 128.91, 127.23, 126.79, 77.49, 77.06, 76.64, 71.83, 71.81, 70.50, 70.37, 64.22, 63.87, 58.90, 54.62, 40.34, 39.85, 29.68. MALDI: (m/z): 1552.76 [M+Na]⁺.

1b: Yield: 59 mg, 58%. ¹H NMR (300 MHz, CDCl₃): δ (ppm) = 8.47 (s, 6H), 7.51 – 6.98 (m, 15H), 6.33 (m, 3H), 4.95 (s, 4H), 4.08 (s, 9H), 3.75 – 3.43 (m, 36H), 3.28 (s, 9H), 3.17 – 2.35 (m, 12H), 2.09 (d, 1.18 (s, 12H). ¹³C NMR (75 MHz, CDCl₃): δ (ppm) = 190.64, 169.32, 156.56, 144.58, 129.32, 129.31, 128.88, 128.29, 128.17, 126.92, 103.96, 98.41, 77.45, 77.02, 76.61, 71.88, 70.52, 70.44, 69.60, 66.52, 63.77, 58.97, 55.37, 53.66, 50.57, 41.92, 40.54, 39.27, 29.69, 26.19. LCMS: t=5.16 min (m/z) = 1614.19 m/z [M]⁺.

1c: Yield: 108 mg, 65%. ¹H NMR (300 MHz, CDCl₃): δ (ppm) = 8.50 (s, 3H), 7.68 – 7.02 (m, 15H), 6.16 (d, 3H), 5.45 – 5.06 (m, 3H), 4.17 (s, 9H), 3.84 – 3.48 (m, 36H), 3.35 (d, 9H), 3.05 (s, 12H), 2.68 (s, 3H), 1.88 – 0.83 (m, 30H). ¹³C NMR (75 MHz, CDCl₃): δ (ppm) = 188.70, 170.42, 156.52, 148.85, 139.40, 128.78, 128.56, 128.02, 127.75, 127.17, 77.51, 77.09, 76.66, 71.89, 70.53, 70.49, 70.45, 69.61, 69.61, 63.96, 63.77, 58.98, 55.11, 40.79, 39.81, 39.57, 29.70, 29.00, 26.27. MALDI: (m/z): 1721.23 [M+Na]⁺.

1d: Yield: 59 mg, 51%, ¹H NMR (300 MHz, CDCl₃): δ (ppm) = 8.48 (s, 3H), 7.77 – 7.16 (m, 15H), 6.54 – 5.95 (m, 3H), 5.25 – 4.77 (m, 3H), 4.66 – 4.01 (m, 9H), 3.99 – 3.41 (m, 36H), 3.37 (s, 9H), 3.28 – 2.82 (m, 12H), 2.67 (d, 3H), 1.48 – 0.85 (m, 42H). ¹³C NMR (75 MHz, CDCl₃): δ (ppm) = 187.65, 169.69, 156.51, 148.65, 138.11, 128.81, 126.61, 77.43, 77.11, 76.79, 71.93, 70.55, 69.67, 63.92, 63.82, 59.05, 53.49, 41.03, 39.86, 38.83, 29.93, 29.72, 29.17, 26.67. MALDI: (m/z): 1805.14 [M+H+Na]⁺

1e: Yield: 42.3mg, 58%. ¹H NMR (300 MHz, CDCl₃): δ (ppm) = 8.26 (dd, 6H), 7.39 (dt, 15H), 6.76 – 5.65 (m, 3H), 3.57 (d, 32H), 3.36 (d, 15H), 3.08 – 2.54 (m, 6H), 1.88 – 0.50 (m, 6H). ¹³C NMR (75 MHz, CDCl₃): δ (ppm) =

183.35, 182.94, 170.62, 168.59, 149.62, 139.23, 129.70, 128.93, 128.68, 128.50, 128.10, 127.89, 127.39, 127.06, 77.49, 77.17, 76.85, 71.92, 70.66, 70.42, 70.30, 69.49, 59.06, 55.11, 39.82, 29.80, 29.47, 22.80. MALDI: (m/z): 1292.88 [M+Na]⁺.

3.6.5 Self-assembly characterization

Sample preparation protocol

Water was added to **1a-e** to prepare stock solutions from 1 - 5 mM. Subsequently, aliquots from the stock were diluted to prepare solutions at the a given concentration for further study. All samples were equilibrated overnight before measurement.

UV-vis spectroscopy

Samples for UV-vis spectroscopy were prepared at a 15 μ M concentration in water as described according to the sample preparation protocol. The samples were placed in the spectrophotometer and a spectrum was recorded from 200-500 nm. The solutions were prepared in triplicate and for each solution a UV-vis spectrum was measured.

Atomic force microscopy

Compounds **1a** and **1e** were prepared according to the preparation protocol above at a concentration of 15 μ M and equilibrated overnight. An aliquot (25 μ L) from each of these solutions was pipetted on cleaved mica and dried overnight at RT before the measurement. The obtained AFM images were analyzed using the Nanoscope software.

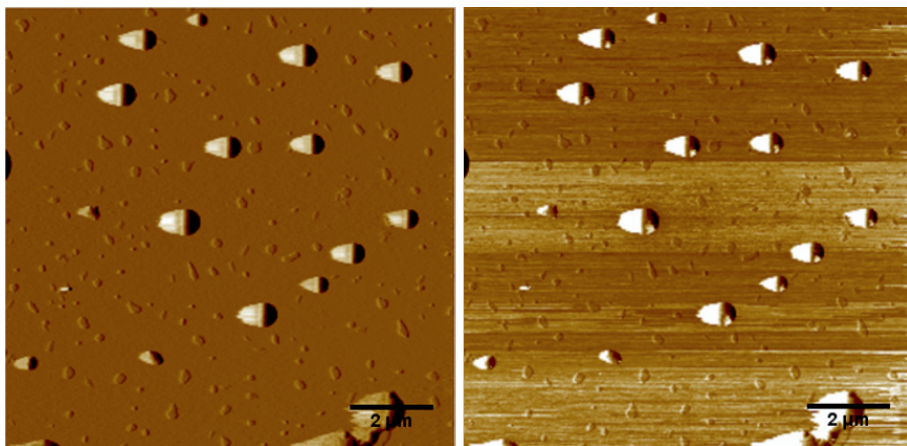


Figure S3.1 AFM micrographs of **1a** (amplitude and height, scale bar: 2 μm)

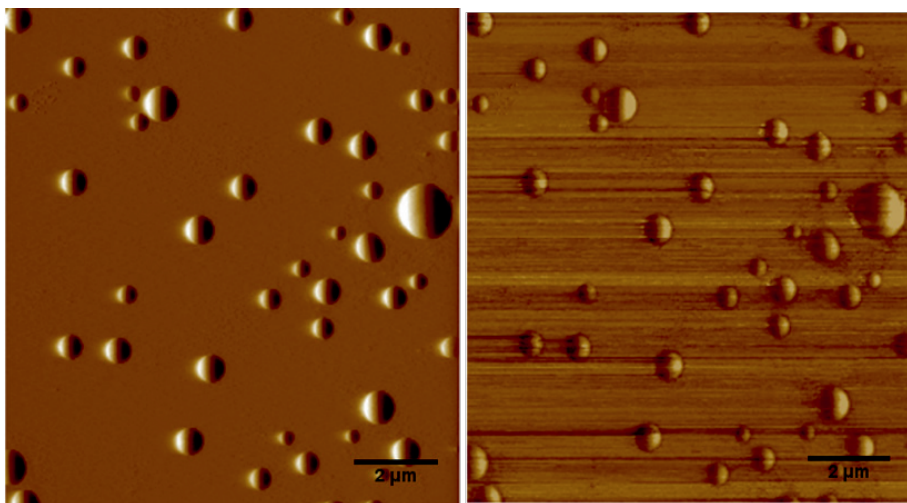


Figure S3.2 AFM micrographs of **1e** (amplitude and height image, scale bar: 2 μm)

3.6.5 LCMS Spectra

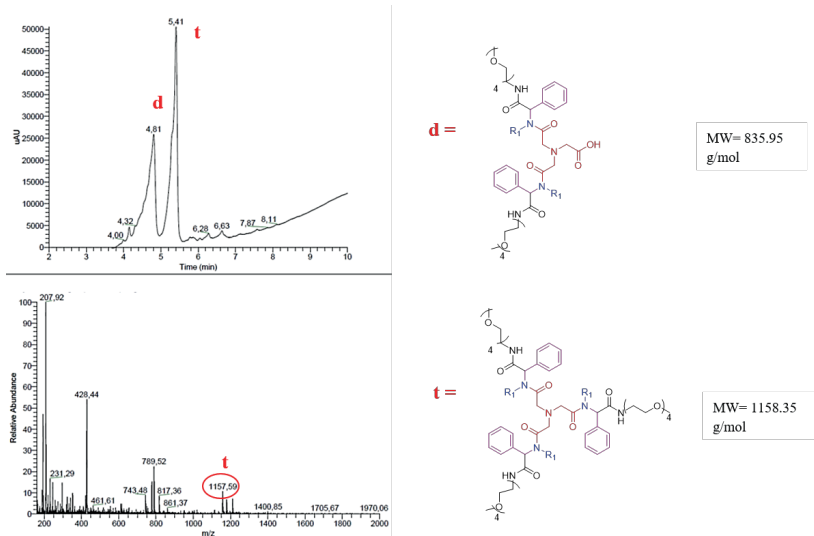


Figure S3.3 Chromatogram and corresponding mass spectrum for **entry 5** obtained by LC-MS. The relevant peaks are labelled and the chemical structure of the compounds are provided on the right side.

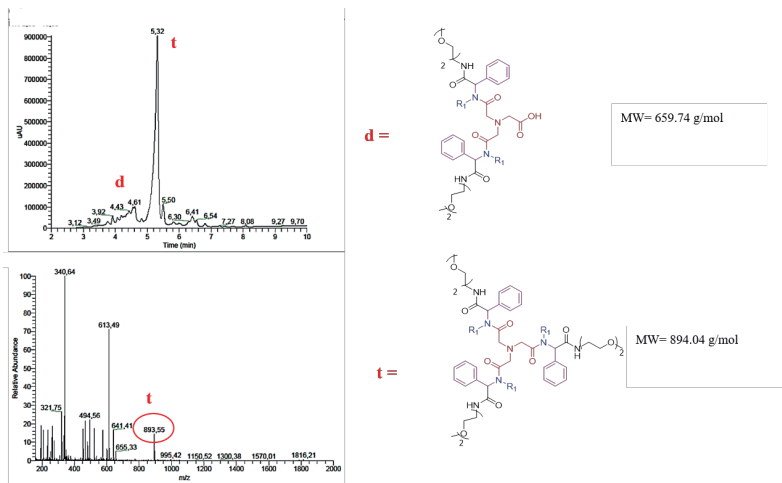


Figure S3.4 Chromatogram and corresponding mass spectrum for **entry 7** obtained by LC-MS. The relevant peaks are labelled and the chemical structure of the compounds are provided on the right side.

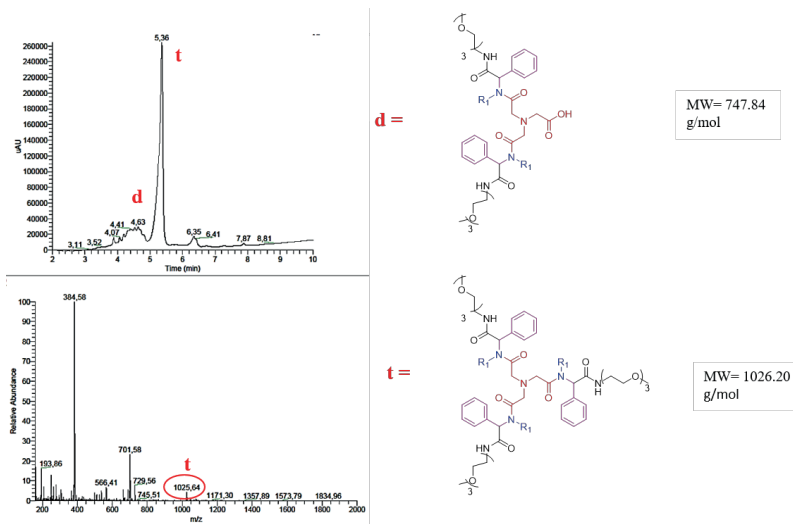


Figure S3.5 Chromatogram and corresponding mass spectrum for **entry 8** obtained by LC-MS. The relevant peaks are labelled and the chemical structure of the compounds are provided on the right side.

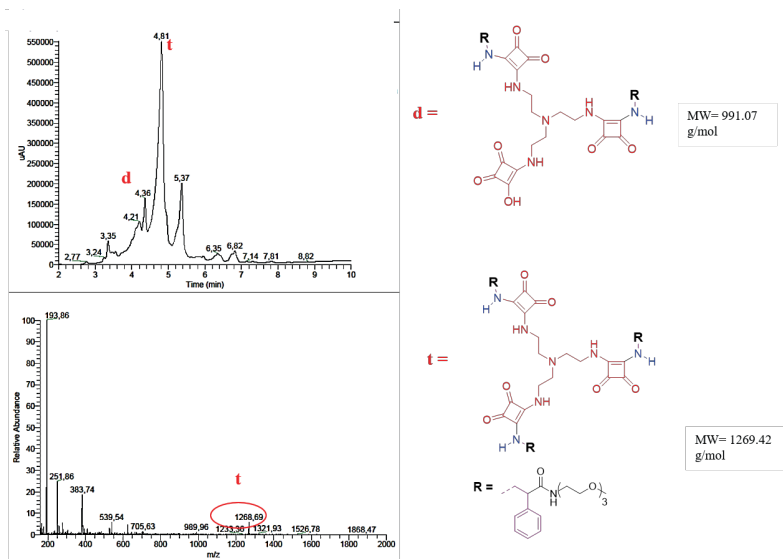


Figure S3.6 Chromatogram and corresponding mass spectrum for **entry 17** obtained by LC-MS. The relevant peaks are labelled and the chemical structure of the compounds are provided on the right side.

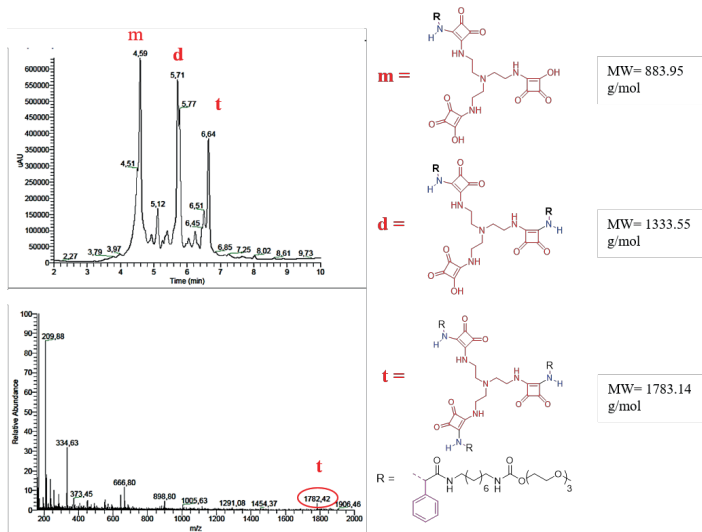


Figure S3.9 Chromatogram and corresponding mass spectrum for **entry 27** obtained by LC-MS. The relevant peaks are labelled and the chemical structure of the compounds are provided on the right side

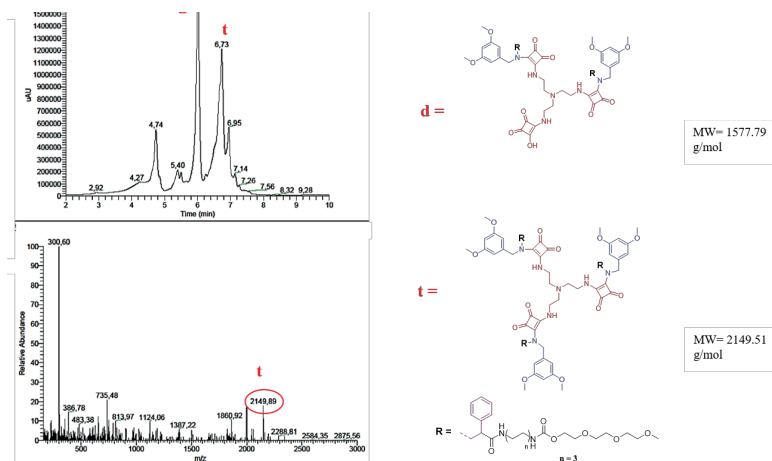
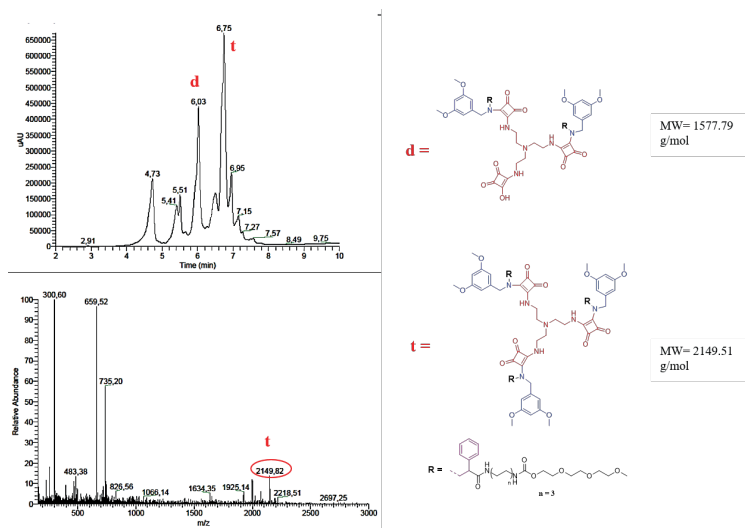
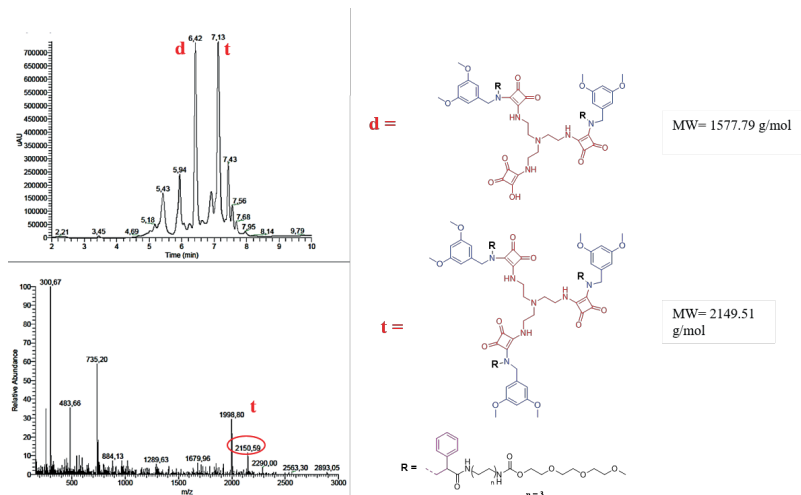
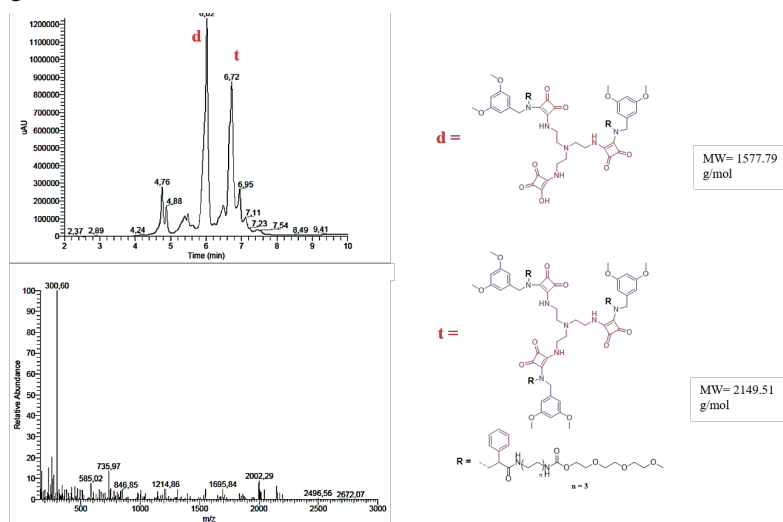
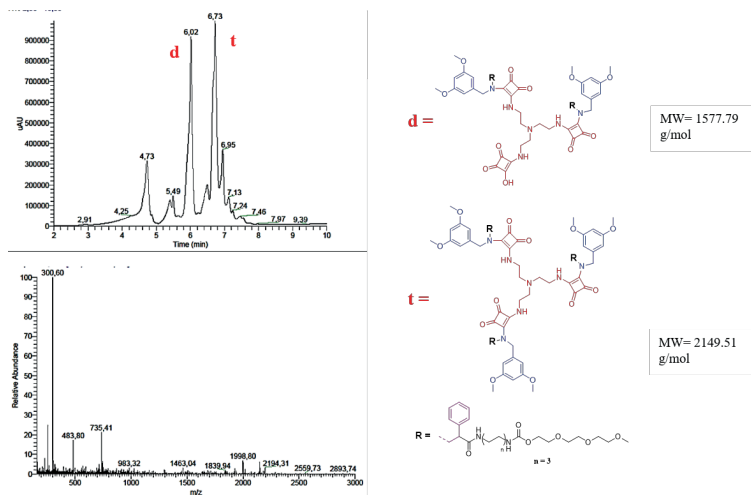


Figure S3.10 Chromatogram and corresponding mass spectrum for **entry 39** obtained by LC-MS. The relevant peaks are labelled and the chemical structure of the compounds are provided on the right side.





CHAPTER 4

Understanding the self-assembly of tripodal squaramide-based monomers through structural substitution

4.1 Abstract

The chemical structure of a supramolecular monomer and the environment it is placed in plays a critical role on its self-assembly and formation of supramolecular polymers. However, the structure and the properties of the formed polymers are difficult to predict starting from the monomers *a priori*. We earlier demonstrated that tripodal squaramide-based monomers self-assemble into long, flexible supramolecular polymers and gel-phase materials above a critical concentration in water. Modulation of the hydrophobic domains of the monomer, had a lesser impact on the formation of fibrillar aggregates, however gel-phase materials were only formed for monomers with a particular hydrophilic-hydrophobic ratio. In this chapter, I take a step further in designing a small library of squaramide-based monomers to delineate the structural modifications that are necessary to trigger the formation of fibrillar aggregates. Since self-assembly of the monomer in aqueous solution requires a synergy between hydrophobic and hydrogen bonding interactions, structural modifications to the monomer involving either or both of these interactions were examined. In particular, a family of squaramide monomers were designed to consider the effect of carbamate bond, ether linkage, decreasing the number of squaramide units from three to two and varying the number of tetraethylene glycol moieties. Substitution of carbamate linkage with an ether bond results in the formation of a 4-fold less stiff hydrogel relative to the native tripodal squaramide monomer. Reduction in the number of squaramide moieties resulted in the lack of monomer gelation at similar condition, but the formation of supramolecular polymers was still observed. Moreover, replacing one hydrophobic domain resulted in the solubilization of the monomer and the loss of the formed supramolecular polymers, further emphasizing the importance of the synergy of all monomer features on supramolecular polymerization and hydrogel formation.

4.2 Introduction

Supramolecular polymers have sparked much interest for a broad range of applications in healthcare due to their unique properties that arise from the inherent dynamic character of the interactions that hold them together.^{1,2} Accessible to this class of polymers are properties such as tunability, responsiveness, modularity, recyclability, and biomimicry.³ Consequently, they are being examined for several application areas such as tissue engineering,⁴ regenerative medicine,⁵ drug delivery⁶ and as mimics of extracellular matrix for 3D cell culture.^{7, 8} Two classes of materials are employed in this area, those consisting of polymers with modules that engage in molecular recognition and those that self-assemble through stacking of monomers under physiological conditions.³ In both of these classes, gel-phase materials can be formed when applied above a critical concentration depending on their molecular structure. Hence, gaining insight into the features of the monomers that drive supramolecular polymerization and their effect on the formation of water-based materials is critical to their application in the abovementioned areas.

In the design of a supramolecular monomer for polymerization, non-covalent interactions such as hydrogen bonding, π - π , electrostatic and hydrophobic interactions are strategically positioned taking into account the microenvironment of the selected interaction (e.g. with respect to the solvent) and combination of interactions. However, rational design of such monomers and prediction of the final self-assemblies remains challenging, especially in water that can have a potent effect on the self-assembly pathway of the aggregates. The hydrophobic effect⁹ drives the self-assembly of amphiphile molecules in combination with other directional interactions.¹⁰ Hydrogen bonding on supramolecular synthons such as 1,3,5-benzenetricarboxamide (BTAs),¹¹ peptides,^{12,13} and ureidopyrimidones¹⁴⁻¹⁶ have been employed in the monomer design to prepare supramolecular polymers and gel-phase materials in water.

Of the examined monomer geometries, tripodal and C_3 -symmetric cores, have been widely applied in the construction of supramolecular materials.¹⁷⁻¹⁹ BTAs represent one of the most studied scaffolds in supramolecular chemistry.¹¹ The self-assembly of BTAs into supramolecular polymers in organic solvent relies on a combination of π - π and hydrogen bonds interactions from the amide groups with a high degree of cooperativity.^{11,20,21} Reduction of the monomer to a C_2 -symmetry resulted in a ten-fold lower

cooperativity as compared to C_3 symmetry in methylcyclohexane (MCH). The consequence of reduced cooperativity results in a decreased size and morphological change of the resulting aggregates.²² When oligo(ethylene glycol) chains are added to the periphery of BTAs-based monomer, possibilities to use this synthon for self-assembly in water are unlocked.^{23,24} In this study, the minimum aliphatic chain length required for the self-assembly in water, but also the inclusion of stereogenic centers on chiral handedness of the final aggregates were disclosed.^{23,24} Besenius, Meijer and coworkers further examined the effect of installing periphery units that provide function on the BTA monomer such as Gd(III)–DTPA (diethylene triaminepentaacetic acid) introducing electrostatic effects into the self-assembly and potential for imaging.²⁵

Cyclohexane-based C_3 -symmetric 1,3,5-cyclohexane trisamide (CTA)-cores have also been examined to prepare materials in water, showing potent self-assembly and gelation properties.^{26–28} van Esch and coworkers prepared phenylalanine derivatives with a CTA core containing different stereogenic centers and demonstrated their effect on hydrogelation.²⁶ Moreover, Eelkema and coworkers investigated the potential to tune the morphology of the self-assembled CTAs by modulating the monomer structure.²⁹ In particular, the gelator was designed with two segments: a CTA core functionalized with three phenylalanines substituted with tetraethylene glycol chains and one with a hydrophobic aliphatic segment. When a chaperone was added, the self-assembly properties of each individual segments could be controlled resulting in a switch in morphology from twisted tapes to nanofibers and the loss of gel phase properties. On the other hand, addition of HFIP, a good solvent for the monomer and a hydrogen bond disrupting solvent resulted in the formation of micellar aggregates. While significant progress in understanding the effect of certain structural modifications on the self-assembly behaviour of C_3 -symmetric amphiphiles in organic solvents and water has been made in these studies, most examples have been limited to the use of amides as the ditopic hydrogen bonding unit.

Squaramides are ditopic hydrogen bonding synthons consisting of a cyclobutenedione ring that have applied in the areas of catalysis, bioconjugation, as ion receptors and in the design of supramolecular materials due to their ability to form strong hydrogen bonds.^{30–35} We recently reported a tripodal squaramide-based monomer that self-assembles into supramolecular polymers and gel-phase materials in water.³⁶ Specifically, the squaramide synthon was incorporated into the hydrophobic domain and surrounded with

tetraethylene glycol chains. Supramolecular monomers were designed with different aliphatic chain lengths ranging from 6-12 methylene units, but only those with 8 and 10 methylenes resulted in the formation of hydrogels highlighting the importance of the hydrophilic-hydrophobic balance on the self-assembly of the monomers. Inspired by these results, we were interested to further understand the self-assembly scope of this monomer, examining non-uniform changes to its geometry and hydrophobic content, as well as the number of squaramides and presence of the carbamate moiety. Herein a library of tripodal squaramide-based monomers was reported and the effect of these structural substitutions on their self-assembly into supramolecular polymers and hydrogels was examined.

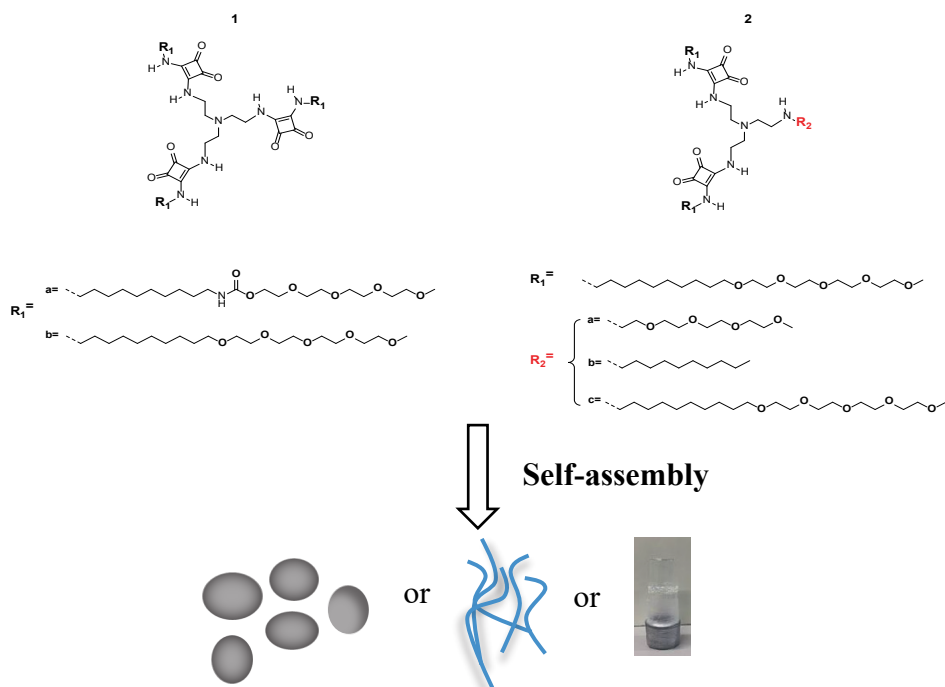


Figure 4.1 Squaramide-based tripodal supramolecular monomers used in this study and the examination of their self-assembly into supramolecular polymers and gel-phase materials.

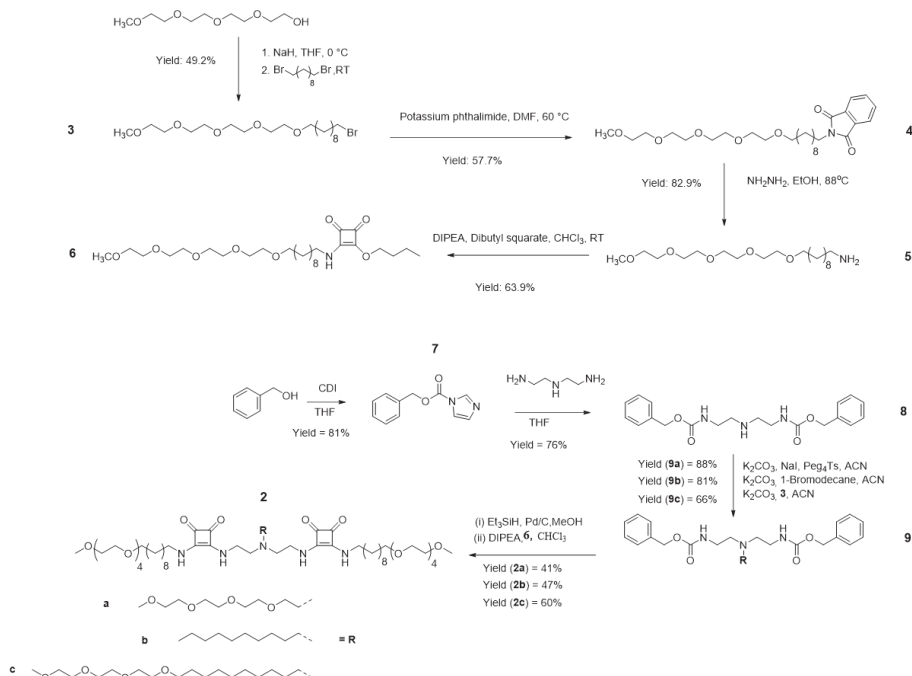
4.3 Results and discussions

In order to better understand the features of the tripodal squaramide-based monomer (**1a**) that enables it to form supramolecular hydrogel, a small library of monomers were prepared with various structural modifications. The molecular structure of the monomer contains three squaramide moieties, C10 aliphatic and tetraethylene glycol chains. The combination of these features drives their self-assembly into supramolecular polymers in water and thus, modifications that would impact this process were examined.³⁷ Hence, the effect of structural modifications involving either or both of these interactions simultaneously on the monomer were explored. In our earlier design, a carbamate moiety was used to connect the aliphatic spacers to the oligoethylene glycol chains because of its synthetic facility. However, to understand the effect of the carbamate bonds on supramolecular polymerization of the squaramide monomers, this linkage was exchanged for an ether in all molecules of the library (**1b** and **2a-c**).

Ether linkages were introduced into squaramide-based amphiphile (**6**) according to an earlier report by Meijer³⁸ and coworkers (**scheme 1**). Tetraethylene glycol monomethyl ether was coupled with the C10 aliphatic spacer in presence of NaH and 1,10-dibromodecane. The obtained amphiphile containing a halide (**3**) was converted in primary amine by the Gabriel synthesis in presence of potassium phthalimide and subsequent use of hydrazine monohydrate. The primary amine on the amphiphile (**5**) was subsequently coupled with 3,4-dibutoxy-3-cyclobutene-1,2-dione to obtain the squaramide-based amphiphile (**6**). The monomer **1b** was synthesized as reported previously by our group³⁶ with the coupling of tris(2-aminoethyl amine) (TREN) core in presence of an excess of squaramide amphiphile (**6**).

The effect of reducing the number of squaramide moieties and modifying the hydrophilic-hydrophobic ratio of the monomer were examined in a second group of monomers. Two of the tripodal arms were outfitted with the squaramide amphiphiles and third one was coupled with either an oligoethylene glycol **2a**, ($\omega_{\text{TEG}} = 0.55$), a chain short alkyl chain **2b**, ($\omega_{\text{TEG}} = 0.53$), or an alkyl and oligoethylene glycol **2c**, ($\omega_{\text{TEG}} = 0.46$) chain attached directly to the nitrogen of the monomer core. As reported in **scheme 1**, the syntheses of **2a-c** were performed starting from the squaramide-based amphiphile (**6**) that was coupled with N,N''-di-Z-diethylenetriamine functionalized with an oligoethylene glycol (**2a**), a short alkyl chain (**2b**) or an alkyl and oligoethylene glycol chain (**2c**) respectively. To prepare N,N''-

di-*Z*-diethylenetriamine, benzylic alcohol was first activated with 1,1-carbonyldiimidazole (CDI) and coupled to bis(2-aminoethyl)amine in excellent yields (**8**). The N,N''-di-*Z*-diethylenetriamine core was further reacted with oligoethylene glycol, a C10 alkyl chain or an alkyl and oligoethylene glycol chain as reported by Wadas³⁹ and coworkers. Subsequently, after hydrogenation *in situ* with Et₃SiH on Pd/C to remove the Cbz protecting group, the core was coupled with squaramide-based amphiphile (**6**) to obtain the monomers **2a-c**, in moderate yields.



Synthetic scheme 1: Synthesis of monomers 2a-c

Self-assembly of the tripodal squaramide-based monomers **1b** and **2a-c** were first examined at the molecular level in water using UV-vis spectroscopy (**Figure 4.2a**). In our previous publication³⁶ the self-assembly of **1a** in water resulted in two absorbance maxima at 255 and 329 nm from the HOMO-LUMO and HOMO-LUMO+1 transitions of the squaramide when self-assembled in a head-to-tail hydrogen bonding arrangement (**1a**). Here, the exchange of the carbamate moiety for ether bonds in the molecular structure of **1b**, resulted in a similar profile to **1a** with the transitions at 255 and 329 nm, respectively. The reduction to two squaramide moieties and one aliphatic spacer replaced with an oligoethylene glycol chain in **2a** resulted in the loss

of these transitions with only one band at 280 nm, consistent with the monomer species and suggestive of a distinct aggregation mode. The addition of an alkyl chain on the third position in **2b** to form a more hydrophobic monomer, gave rise to a UV-vis profile with two bands at 250 and 329 nm as in **1a**, **b**, but with decreased intensity likely due to its poor solubility. The addition of an amphiphile on the third position that lacks a hydrogen bonding group in **2c** results in two maxima at 260 and 329 nm, that are shifted to a lesser degree than either **1a** or **b**, is suggestive of the formation of shorter polymers. Overall, the differences in the shifts of the maxima and their absorbance intensity suggest a variable aggregation patterns of the various squaramide monomers in their respective assemblies.

To further probe the aggregate structures at the molecular level, a fluorescence spectroscopy experiment in the presence of Nile Red dye was performed (**Figure 4.2b**). The Nile Red dye is a hydrophobic probe that increases in fluorescence intensity with a blue-shifted maximum relative to its emission in water when in a hydrophobic environment. Consequently, this dye has been often used to understand the self-assembly of a range of amphiphiles in water.^{38,40} The fluorescence spectrum of the Nile Red dye in water displays a low intensity emission band at 640 nm. Monomer **1a** was previously demonstrated to show an intense blue-shifted emission band at 622 nm due to the size of the hydrophobic domains formed on self-assembly in water. The fluorescence spectrum of **1b** displays the same maximum at 622 nm suggesting formation of self-assembled aggregates on par with **1a** as suggested in UV-vis measurements. Because of the increased hydrophilic character of **2a**, the fluorescence emission is comparable to the band in water suggesting a lack of aggregation. Conversely, **2b** containing an aliphatic spacer shows a blue-shifted emission signal at 615 nm of decreased intensity compared to **1b**, whereas **2c** displays an increased fluorescent signal at 622 nm that is consistent with formation of supramolecular aggregates. Thus, the differences in the blue-shifting of the emission maxima and their intensity are consistent with the changes to the hydrophobic and hydrophilic domains of the monomers and their distinct mode of aggregation.

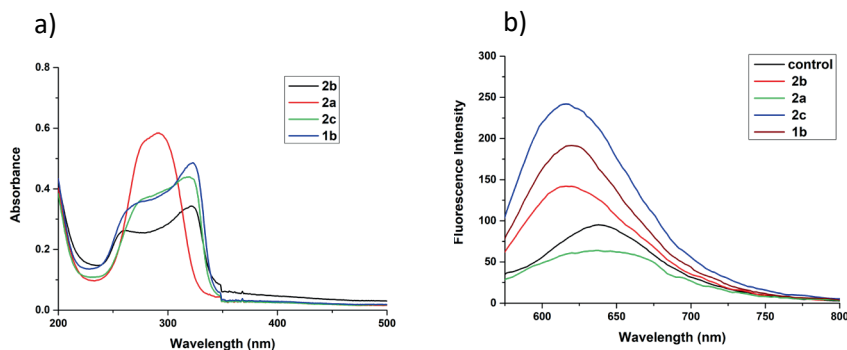


Figure 4.2 Spectroscopy of tripodal squaramide self-assemblies: (a) UV-vis absorption spectra of **1b**, **2a-c** ($c_{\text{sq}}=15\ \mu\text{M}$); (b) Fluorescence spectra ($c_{\text{sq}}=15\ \mu\text{M}$) of Nile Red dye embedded tripodal molecules (**1b**, **2a-c**): ($c_{\text{NileRed}}=0.005\ \text{mg/mL}$, $\lambda_{\text{exc}} = 550\ \text{nm}$, $\lambda_{\text{em}} = 570\text{-}800\ \text{nm}$), Nile red in MilliQ is used as a control.

Static light scattering (SLS) is a technique used to determine the critical aggregation concentration (CAC) of monomer or the concentration at which a supramolecular polymer is formed. This value is determined from the inflection point of the measured scattering intensity of monomer solutions as a function of concentration.⁴¹ In our previous publication, a concentration-based UV-vis experiment of **1a** displayed the retention of blue- and red shifted bands at even at low concentration ($3.75 \cdot 10^{-6}\ \text{M}$). Also, the distinct UV-vis profiles of **1b** and **2a** point to the importance of the hydrophobic/hydrophilic balance on monomer self-assembly. Therefore, the critical aggregation concentration was determined for these two monomers as shown in **Figure 4.3a** and **b**. The CAC of **1b** and **2a** was determined from samples prepared in a concentration range from $100\ \mu\text{M}$ to $10\ \text{nM}$. Despite their different UV-vis profiles and solubility in water, **1b** and **2a** displayed comparable CACs ($2.4 \cdot 10^{-5}\ \text{M}$ and $2.13 \cdot 10^{-5}\ \text{M}$).

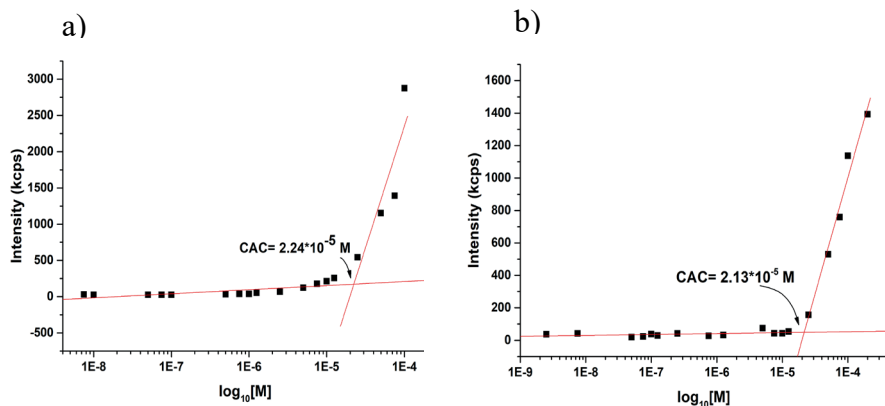


Figure 4.3 Variable concentration SLS measurement of a) **1b** and b) **2a** to determine the critical aggregation concentration.

To further probe the spectroscopic differences observed in UV-vis measurements that suggest a difference in the aggregation mode of the monomers, AFM imaging was performed to gain insight into the morphology of the aggregates (**Figure 4.4**). Self-assembly of **1b** in water results in the formation of nanofibers consistent with the observed UV-vis spectra (**Figure 4.3a**). Conversely, the increased hydrophilic character of **2a** resulted in the formation of amorphous structures (**Figure 4.3b**) that could be a drying effect and is consistent with a single absorption band at 280 nm and lack of fluorescent signal in the Nile Red experiment. In case of **2b** and **2c** (**Figure 4.3 c,d**) the formation of fibrillar aggregates is observed with lesser degree of polymerization compared to **1b**. These observed morphologies are in line with the results obtained from UV-vis spectroscopy and point to the importance of the hydrophilic-hydrophobic ratio in combination with the squaramide synthons inside the molecular structure to drive monomer self-assembly into fibrillar aggregates that entangle to form hydrogel materials. To gain further insight into the morphological differences between the aggregates of **1b**, **2b** and **2c**, measurements that are performed in the solution state such as small angle x-ray scattering and cryogenic electron microscopy are necessary.

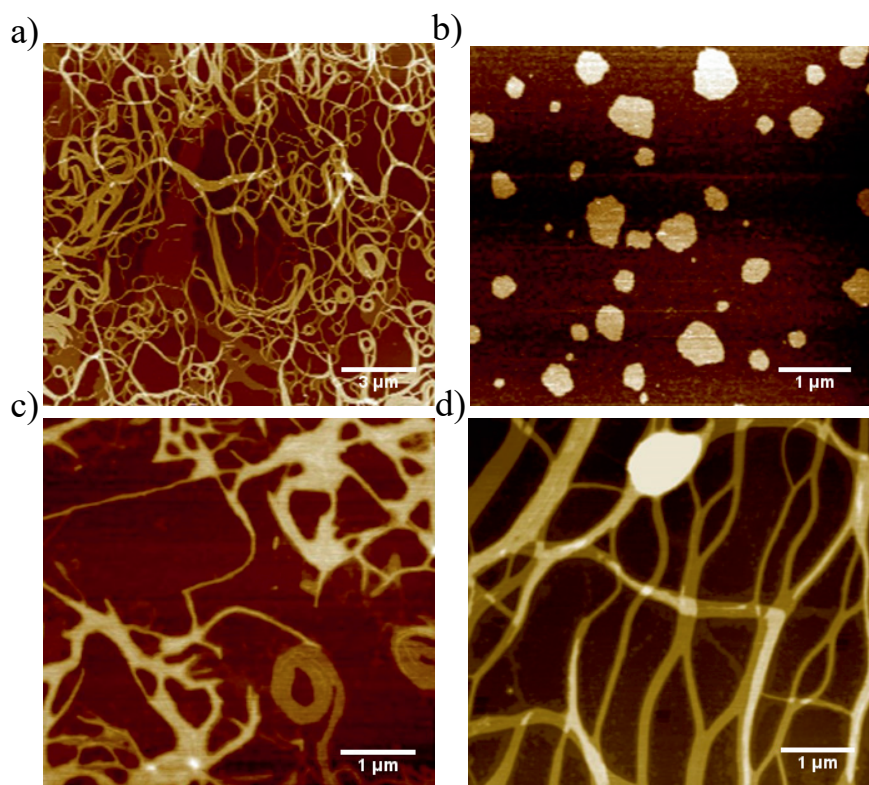


Figure 4.4 AFM micrographs of **1b** (a) (scale bar 3 μm), **2a** (b), **2b** (c) and **2c** (d), (scale bar: 1 μm).

The capacity of the monomers that form fibrillar aggregates to gelate water were probed by a gel inversion test and oscillatory rheology (**Figure 4.5**). Monomers **2b** and **2c** did not yield hydrogels, as they precipitated at a higher concentration of 1 mM likely due to their increased hydrophobic character in comparison to the other monomers. Alternatively, **1b** gelated water. In contrast to gelator **1a** that showed a cgc at 3.1 mM, **1b** exhibited higher cgc of 5 mM and viscous solutions at lower concentrations. The stiffness of the hydrogel composed of **1b** was further quantified by oscillatory rheology in a time sweep measurement. The storage modulus (G') at the end of the measurement was 16 Pa. This value is lower in comparison to the G' obtained for **1b** (67 Pa) in a similar concentration range.

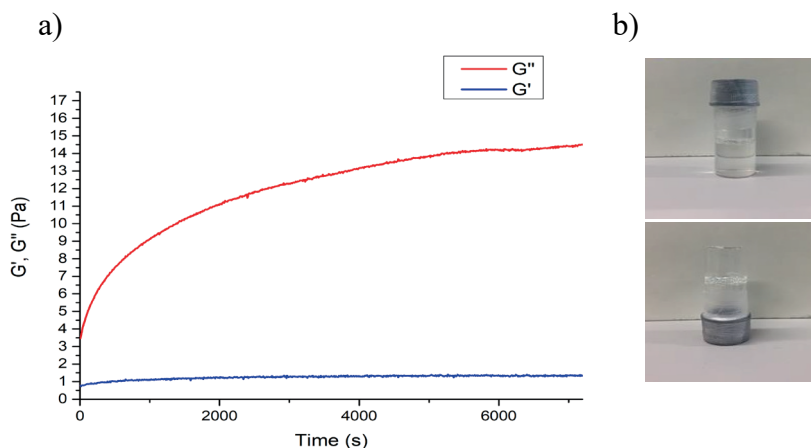


Figure 4.5 (a) Oscillatory rheology time sweep of **1b**, ($c_{\text{sq}}=5$ mM), Time sweep measurements were collected at a fixed frequency of 1.0 Hz and strain of 0.05% for up to 7200s. (b) Representative photograph of the gel inversion test for **1b** at 5 mM.

Overall, the structural modifications to monomers **1b** and **2a-c** and their self-assembly demonstrated the extent they could be altered while preserving supramolecular polymer assembly. Maintenance of a sufficient hydrophilic/hydrophobic ratio despite a reduction of one squaramide unit in **2b**, **2c** permitted the formation of supramolecular polymers, however gel phase materials are not obtained. More specifically, removal of the hydrophobic domain at the core in **2a** results in loss of nanofiber formation as evidenced by spectroscopic and AFM measurements. Retention of a hydrophobic domain at the core with and without oligoethylene glycol as in **2b** and **2c** provides nanofibers with increased flexibility and a lesser degree of polymerization compared to **1b**. Moreover, in these experiments the carbamate moiety in **1** was found to be relevant for increasing hydrogel stiffness. In the absence of the carbamate a four-fold lower storage modulus of the hydrogel was obtained.

4.4 Conclusions

In this study, the systematic modification of the chemical structure of tripodal squaramide monomer on their self-assembly properties was examined in water. Thus, a small library of monomers was synthesized in moderate yields and their self-assembly properties were investigated and compared with the corresponding parental tripodal squaramide-based hydrogelator. Exchange of the carbamates with the ether linkages resulted in a reduction in hydrogel stiffness, whereas reduction of the number of squaramide units resulted in inability to form gel phase materials. The observed effects on gelation likely result due to the reduced degrees of polymerization of the squaramide monomers with a reduction in the number of the squaramide synthons affecting their entanglement. Additionally, the hydrophobic shielding of the regions near squaramide are critical as an increase in hydrophilicity near the center of the monomer hinders the formation of fibrillar aggregates. These results point to the importance of the location of the hydrophilic moieties on the self-assembly of the aggregates, and the hydrophilic/hydrophobic ratio. Cumulatively, these demonstrate the necessary structural features to guide the gelation of tripodal squaramide-based monomers in solution, but also their hints at their tolerance to structural modifications for future works that involve their conversion into functional supramolecular biomaterials.

References

1. Aida, T.; Meijer, E. W.; Stupp, S. I., Functional Supramolecular Polymers. *Science* **2012**, *335*, 813-817
2. Yang, L.; Tan, X.; Wang, Z.; Zhang, X., Supramolecular polymers: historical development, preparation, characterization, and functions. *Chem. Rev.* **2015**, *115*, 7196-7239.
3. Webber, M. J.; Appel, E. A.; Meijer, E. W.; Langer, R., Supramolecular biomaterials. *Nat. Mater.* **2016**, *15*, 13-26.
4. El-Sherbiny, I. M.; Yacoub, M. H., Hydrogel scaffolds for tissue engineering: Progress and challenges. *Glob. Cardiol. Sci. Pract.* **2013**, *2013*, 316-42.
5. Guan, X.; Avci-Adali, M.; Alarcin, E.; Cheng, H.; Kashaf, S. S.; Li, Y.; Chawla, A.; Jang, H. L.; Khademhosseini, A., Development of hydrogels for regenerative engineering. *Biotechnol. J.* **2017**, *12*, 1-19.
6. Larraneta, E.; Stewart, S.; Ervine, M.; Al-Kasasbeh, R.; Donnelly, R. F., Hydrogels for Hydrophobic Drug Delivery. Classification, synthesis and Applications. *J. Funct. Biomater.* **2018**, *9*, 1-20.
7. Geckil, H.; Xu, F.; Zhang, X.; Moon, S.; Demirci, U., Engineering hydrogels as extracellular matrix mimics. *Nanomedicine (Lond)* **2010**, *5*, 469-484.
8. Rosales, A. M.; Anseth, K. S., The design of reversible hydrogels to capture extracellular matrix dynamics. *Nat. Rev. Mater.* **2016**, *1*, 1-15.
9. Eichstaedt, K.; Szpotkowski, K.; Grajda, M.; Gilski, M.; Wosicki, S.; Jaskólski, M.; Szumna, A., Self-Assembly and Ordering of peptide-based cavitands in water and DMSO: The power of hydrophobic effects combined with neutral hydrogen bonds. *Chem. Eur. J.* **2019**, *25*, 3091-3097.
10. Besenius, P.; Portale, G.; Bomans, P. H. H.; Janssen, H. M.; Palmans, A. R. A.; Meijer, E. W., Controlling the growth and shape of chiral supramolecular polymers in water. *Proc. Natl. Acad. Sci.* **2010**, *107*, 17888-17893.
11. Cantekin, S.; de Greef, T. F. A.; Palmans, A. R. A., Benzene-1,3,5-tricarboxamide: a versatile ordering moiety for supramolecular chemistry. *Chem. Soc. Rev.* **2012**, *41*, 6125-6137.
12. Cui, H.; Webber, M. J.; Stupp, S. I., Self-assembly of peptide amphiphiles: from molecules to nanostructures to biomaterials. *Biopolymers* **2010**, *94*, 1-18.
13. Hendricks, M. P.; Sato, K.; Palmer, L. C.; Stupp, S. I., Supramolecular assembly of peptide amphiphiles. *Acc. Chem. Res.* **2017**, *50*, 2440-2448.

14. Dankers, P. Y. W.; Hermans, T. M.; Baughman, T. W.; Kamikawa, Y.; Kieltyka, R. E.; Bastings, M. M. C.; Janssen, H. M.; Sommerdijk, N. A. J. M.; Larsen, A.; van Luyn, M. J. A.; Bosman, A. W.; Popa, E. R.; Fytas, G.; Meijer, E. W., Hierarchical formation of supramolecular transient networks in water: a modular injectable delivery system. *Adv. Mat.* **2012**, *24*, 2703-2709.
15. Ramaekers, M.; de Feijter, I.; Bomans, P. H. H.; Sommerdijk, N. A. J. M.; Dankers, P. Y. W.; Meijer, E. W., Self-Assembly of chiral supramolecular ureido-pyrimidinone-based poly(ethylene glycol) polymers via Multiple Pathways. *Macromolecules* **2014**, *47*, 3823-3828.
16. Nieuwenhuizen, M. M. L.; de Greef, T. F. A.; van der Bruggen, R. L. J.; Paulusse, J. M. J.; Appel, W. P. J.; Smulders, M. M. J.; Sijbesma, R. P.; Meijer, E. W., Self-Assembly of ureido-pyrimidinone dimers into one-dimensional stacks by lateral hydrogen bonding. *Chem. Eur. J.* **2010**, *16*, 1601-1612.
17. Long, K.; Liu, Y.; Li, Y.; Wang, W., Self-assembly of trigonal building blocks into nanostructures: molecular design and biomedical applications. *J. Mat. Chem. B* **2020**, *8*, 6739-6752.
18. Gibson, S. E.; Castaldi, M. P., C₃ symmetry: molecular design inspired by nature. *Angew. Chem. Int. Ed. Engl.* **2006**, *45*, 4718-4720.
19. Dorca, Y.; Matern, J.; Fernández, G.; Sánchez, L., C₃-Symmetrical π -scaffolds: useful building blocks to construct helical supramolecular polymers. *Isr. J. Chem.* **2019**, *59*, 869-880.
20. Smulders, M. M. J.; Schenning, A. P. H. J.; Meijer, E. W., Insight into the mechanisms of cooperative self-assembly: The “Sergeants-and-Soldiers” principle of chiral and achiral C₃-symmetrical discotic triamides. *J. Am. Chem. Soc.* **2008**, *130*, 606-611.
21. Stals, P. J. M.; Smulders, M. M. J.; Martín-Rapún, R.; Palmans, A. R. A.; Meijer, E. W., Asymmetrically substituted benzene-1,3,5-tricarboxamides: self-Assembly and odd–even effects in the solid state and in dilute solution. *Chem. Eur. J.* **2009**, *15*, 2071-2080.
22. Wang, F.; Gillissen, M. A. J.; Stals, P. J. M.; Palmans, A. R. A.; Meijer, E. W., Hydrogen bonding directed supramolecular polymerisation of oligo(Phenylene-Ethynylene)s: cooperative Mechanism, core symmetry effect and chiral amplification. *Chem. Eur. J.* **2012**, *18*, 11761-11770.
23. Leenders, C. M. A.; Albertazzi, L.; Mes, T.; Koenigs, M. M. E.; Palmans, A. R. A.; Meijer, E. W., Supramolecular polymerization in water harnessing both hydrophobic effects and hydrogen bond formation. *Chem. Comm.* **2013**, *49*, 1963-1965.

24. Leenders, C. M. A.; Baker, M. B.; Pijpers, I. A. B.; Lafleur, R. P. M.; Albertazzi, L.; Palmans, A. R. A.; Meijer, E. W., Supramolecular polymerisation in water; elucidating the role of hydrophobic and hydrogen-bond interactions. *Soft Matter* **2016**, *12*, 2887-2893.
25. Besenius, P.; van den Hout, K. P.; Albers, H. M. H. G.; de Greef, T. F. A.; Olijve, L. L. C.; Hermans, T. M.; de Waal, B. F. M.; Bomans, P. H. H.; Sommerdijk, N. A. J. M.; Portale, G.; Palmans, A. R. A.; van Genderen, M. H. P.; Vekemans, J. A. J. M.; Meijer, E. W., Controlled supramolecular oligomerization of C3-symmetrical molecules in water: the impact of hydrophobic shielding. *Chem. Eur. J.* **2011**, *17*, 5193-5203.
26. Friggeri, A.; van der Pol, C.; van Bommel, K. J. C.; Heeres, A.; Stuart, M. C. A.; Feringa, B. L.; van Esch, J., Cyclohexane-based low molecular weight hydrogelators: a chirality investigation. *Chem. Eur. J.* **2005**, *11*, 5353-5361.
27. van Bommel, K. J. C.; van der Pol, C.; Muizebelt, I.; Friggeri, A.; Heeres, A.; Meetsma, A.; Feringa, B. L.; van Esch, J., Responsive cyclohexane-based low-molecular-weight hydrogelators with modular architecture. *Angew. Chem. Int. Ed.* **2004**, *43*, 1663-1667.
28. Du, X.; Zhou, J.; Shi, J.; Xu, B., Supramolecular hydrogelators and hydrogels: from soft matter to molecular biomaterials. *Chem. Rev.* **2015**, *115*, 13165-13307.
29. Boekhoven, J.; Brizard, A. M.; van Rijn, P.; Stuart, M. C. A.; Eelkema, R.; van Esch, J. H., Programmed morphological transitions of multisegment assemblies by molecular chaperone analogues. *Angew. Chem. Int. Ed.* **2011**, *50*, 12285-12289.
30. Storer, R. I.; Aciro, C.; Jones, L. H., Squaramides: physical properties, synthesis and applications. *Chem. Soc. Rev.* **2011**, *40*, 2330-2246.
31. Wurm, F. R.; Klok, H. A., Be squared: expanding the horizon of squaric acid-mediated conjugations. *Chem. Soc. Rev.* **2013**, *42*, 8220-8236.
32. Marchetti, L. A.; Kumawat, L. K.; Mao, N.; Stephens, J. C.; Elmes, R. B. P., The versatility of squaramides: from supramolecular chemistry to chemical biology. *Chem.* **2019**, *5*, 1398-1485.
33. Saez Talens, V.; Englebienne, P.; Trinh, T. T.; Noteborn, W. E.; Voets, I. K.; Kieleyka, R. E., Aromatic gain in a supramolecular polymer. *Angew. Chem. Int. Ed.* **2015**, *54*, 10502-10506.
34. Zhao, B.-L.; Li, J.-H.; Du, D.-M., Squaramide-catalyzed asymmetric reactions. *Chem. Rec.* **2017**, *17*, 994-1018.

35. Jin, C.; Zhang, M.; Wu, L.; Guan, Y.; Pan, Y.; Jiang, J.; Lin, C.; Wang, L., Squaramide-based tripodal receptors for selective recognition of sulfate anion. *Chem. Commun. (Camb)* **2013**, *49*, 2025-2027.
36. Tong, C.; Liu, T.; Saez Talens, V.; Noteborn, W. E. M.; Sharp, T. H.; Hendrix, M.; Voets, I. K.; Mummery, C. L.; Orlova, V. V.; Kieltyka, R. E., Squaramide-based supramolecular materials for three-dimensional cell culture of human induced pluripotent stem cells and their derivatives. *Biomacromolecules* **2018**, *19*, 1091-1099.
37. Krieg, E.; Bastings, M. M.; Besenius, P.; Rybtchinski, B., Supramolecular Polymers in Aqueous Media. *Chem. Rev.* **2016**, *116*, 2414-2477.
38. Leenders, C. M.; Albertazzi, L.; Mes, T.; Koenigs, M. M.; Palmans, A. R.; Meijer, E. W., Supramolecular polymerization in water harnessing both hydrophobic effects and hydrogen bond formation. *Chem. Commun. (Camb)* **2013**, *49*, 1963-1965.
39. Pandya, D. N.; Pailloux, S.; Tatum, D.; Magda, D.; Wadas, T. J., Di-macrocyclic terephthalamide ligands as chelators for the PET radionuclide zirconium-89. *Chem. Comm.* **2015**, *51*, 2301-2303.
40. Stuart, M. C. A.; van de Pas, J. C.; Engberts, J. B. F. N., The use of Nile Red to monitor the aggregation behavior in ternary surfactant–water–organic solvent systems. *J. Phys. Org. Chem.* **2005**, *18*, 929-934.
41. Topel, Ö.; Çakır, B. A.; Budama, L.; Hoda, N., Determination of critical micelle concentration of polybutadiene-block-poly(ethyleneoxide) diblock copolymer by fluorescence spectroscopy and dynamic light scattering. *J. Mol. Liq.* **2013**, *177*, 40-43.
42. Chirkin, E.; Muthusamy, V.; Mann, P.; Roemer, T.; Nantermet, P. G.; Spiegel, D. A., Neutralization of Pathogenic Fungi with Small-Molecule Immunotherapeutics. *Angew. Chem. Int. Ed* **2017**, *56*, 13036-13040.

SUPPORTING INFORMATION

4.5 Material and methods

4.5.1 Materials

All reagents and chemicals were purchased from Sigma Aldrich, Acros Organics and Bioconnect and used without further purification. Deuterated chloroform was purchased from Euriso-top and Milli-Q water was employed for all experiments. Acetonitrile for the hydrogenation reaction was dried using molecular sieves 3 Å (20% w/v) and used after 24 h of equilibration. Tetraethylene glycol *p*-toluenesulfonate (Peg₄OTs) was synthesized as reported in literature.⁴²

4.5.2 Instrumentation

Compounds were either purified by normal-phase silica gel column chromatography or on a X1 flash chromatography system equipped with a C18 column from Grace Reveleris. ¹H-NMR and ¹³C spectra were obtained on a Bruker (300 MHz) or Bruker DMX-400 (400 MHz). LC-MS analyses were performed on a Finnigan Surveyor HPLC system equipped with a Gemini C18 50 x 4.60 mm column (UV detection at 254 and 214 nm) coupled to Finnigan LCQ Advantage Max mass spectrometer with ESI. For the mobile phase, a gradient of 10-90% of CH₃CN/ H₂O with 0.1% trifluoroacetic acid over 13.5 minutes was used. MALDI-TOF-MS spectra were obtained on a Bruker Microflex LRF mass spectrometer in reflection positive mode using α -cyano-4-hydroxycinnamic acid as a matrix with a laser power of 30%. UV-vis measurements were performed on a Cary 300 UV-vis spectrophotometer using a quartz cuvette of a 1 cm path length. DLS measurements were carried out using a Malvern Zetasizer Nano ZS ZEN3500 equipped with a laser of 633 nm and with a scattering angle of 173°. Fluorescence experiments were recorded on an Infinite M1000 Pro Tecan plate reader using a 96-well plate with a black background. Atomic force microscopy (AFM) images were recorded in tapping mode on a Veeco-Bruker Multimode AFM with a Nanoscope IIIa controller at room temperature. The AFM tips used were Oltespa Opus probes with a reflex aluminium coating with a nominal spring constant of 2 N/m, a nominal resonance frequency of 70 kHz and a tip radius of 7 nm. The images were processed using Nanoscope software. The mechanical properties of the squaramide-based hydrogels were measured on a Discovery HR-2 hybrid rheometer using cone-plate geometry (40 mm,

1.995°) at 25 ± 0.2 °C with a Peltier-based temperature controller and a solvent trap.

4.6.1 Synthetic procedure 1: Squaramide amphiphile synthesis

COCCOCCOCCOCCO
 Yield: 49.2%
 1. NaH, THF, 0 °C
 2. Br(CH₂)₈Br, RT
3 COCCOCCOCCOCCOCCCCCCCCCBr
 Yield: 57.7%
 Potassium phthalimide, DMF, 60 °C
4 COCCOCCOCCOCCOCCCCCCCCCN1C(=O)c2ccccc2C1=O
 Yield: 82.9%
 NH₂NH₂, EtOH, 80 °C
5 COCCOCCOCCOCCOCCCCCCCCCN
 DIPEA, CHCl₃, RT
 Yield: 63.9%
CCCCOC1=C(C(=O)OCC)C(=O)C1=O
6 COCCOCCOCCOCCOCCCCCCCCCN1C(=O)c2ccccc2C1=O

Synthesis of 3

Tetraethylene glycol monomethyl ether (3.8 mL, 19.21 mmol) was dissolved in dry THF (20 mL) at 0 °C. NaH (0.768 g, 19.21 mmol) was added in portions resulting in a foaming solution. When the foaming ceased, the ice bath was removed. Subsequently, 1,10-dibromodecane (12.94 mL, 57.62 mmol) was added and the reaction mixture was stirred overnight at room temperature. The reaction was quenched with H₂O (20 mL) and extracted with diethyl ether (3 x 40 mL). The combined organic fractions were collected, dried with MgSO₄, filtered, and concentrated. The product was purified by silica column chromatography (eluent: petroleum ether/EtOAc 8/2-5/5 v/v) and was isolated as a colorless oil.

Yield = 4.04 g, 49.2%. ¹H NMR (300 MHz, CDCl₃): δ (ppm) = 3.58-3.46 (m, 16H), 3.39-3.30 (m, 5H), 1.79-1.72 (t, 2H), 1.52-1.47 (t, 2H), 1.35-1.22 (d, 14H). ¹³C NMR (75 MHz, CDCl₃): δ (ppm) = 71.87, 71.38, 70.53, 70.45, 70.01, 58.94, 33.87, 33.74, 32.72, 29.56, 29.38, 29.35, 29.29, 28.99, 28.83, 28.66, 28.08, 26.00. TLC-MS (m/z): 450.1 [M+Na]⁺.

Synthesis of 4

3 (4.04 g, 9.45 mmol) and potassium phthalimide (2.45 g, 13.23 mmol) were dissolved in DMF (15 mL) and the mixture was refluxed for 2 hours. After the removal of the solvent by rotary evaporation, the residue was re-dissolved in DCM (50 mL), extracted with 2 M HCl (2 x 30 mL), dried with MgSO₄, filtered, and concentrated. The compound was purified by silica column chromatography (petroleum ether/EtOAc, 1/1) and obtained as colorless oil.

Yield = 2.69 g, 57.7%. ¹H NMR (300 MHz, CDCl₃): δ (ppm) = 7.75 (d, 4H), 3.4 (m, 18H), 3.35 (s, 3H), 1.6 (d, 4H), 1.24 (s, 14H). ¹³C NMR (75 MHz, CDCl₃): δ (ppm) = 168.40, 133.81, 132.14, 123.10, 71.91, 71.48, 70.57, 70.49, 70.02, 59.00, 38.02, 29.59, 29.46, 29.39, 29.13, 28.56, 26.81, 26.03. TLC-MS (m/z): 516.5 [M+Na]⁺, 532.5 [M+K]⁺.

Synthesis of 5

Hydrazine monohydrate (3.8 mL, 78.34 mmol) was added to a stirred solution of **4** (2.69 g, 5.45 mmol) in EtOH (50 mL) and the mixture was refluxed overnight. The solvent was removed by rotary evaporation and the mixture was dissolved in chloroform (100 mL), extracted with NaOH (3 x 100 mL, 1 M) and the organic layers were dried with MgSO₄, filtered, and concentrated. The compound was isolated as white solid and used for the next step without any further purification.

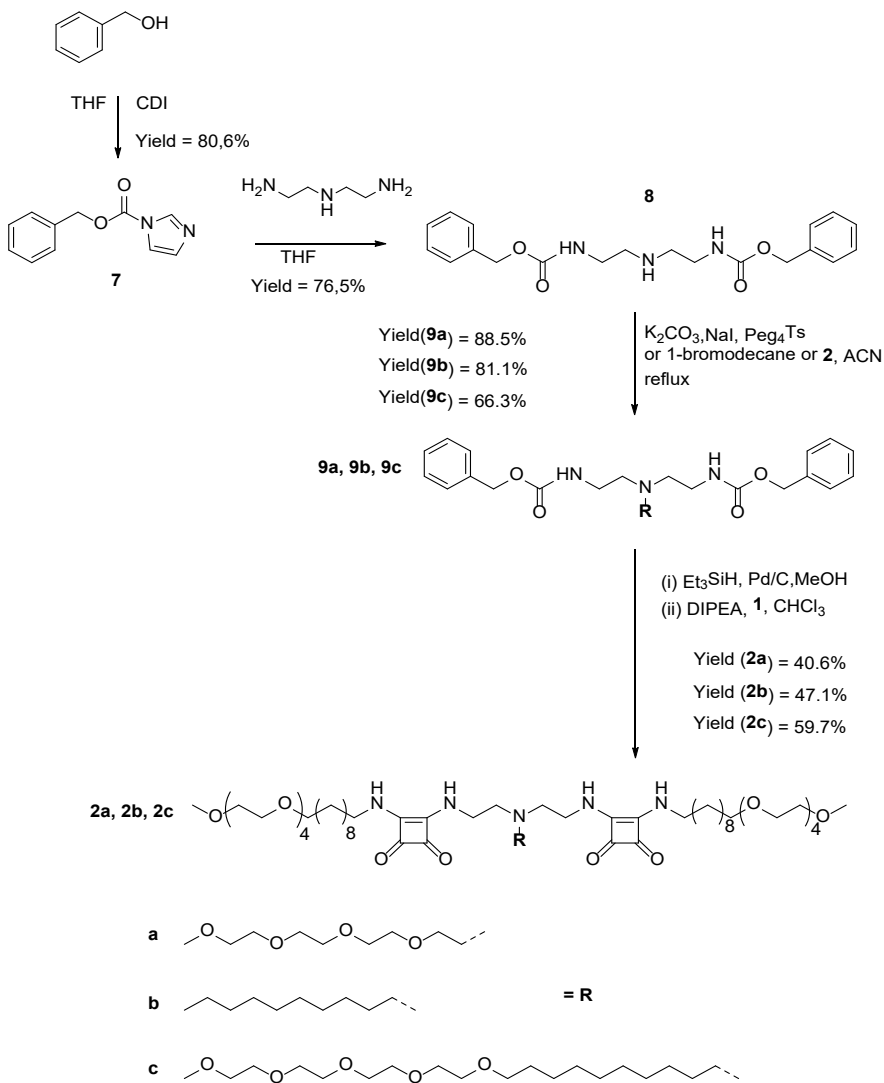
Yield = 1.64 g, 82.9%. ¹H NMR (300 MHz, CDCl₃): δ (ppm) = 3.40 (m, 16H), 3.26 (t, 2H), 3.20 (s, 3H), 2.50 (t, 2H), 1.80 (s, 3H), 1.30 (m, 4H), 1.11 (s, 12H). ¹³C NMR (75 MHz, CDCl₃): δ (ppm) = 71.77, 71.28, 70.43, 70.33, 69.90, 58.81, 41.90, 33.31, 29.47, 29.39, 29.37, 29.30, 26.72, 25.92. TLC-MS (m/z): = 364.5 [M+H]⁺, 386.5 [M+Na]⁺.

Synthesis of 6

5 (1.18 g, 3.26 mmol), 3,4-dibutoxy-3-cyclobutene-1,2-dione (0.9 mL, 3.91 mmol), and DIPEA (0.9 mL, 4.89 mmol) were dissolved in CHCl₃ (50 mL) and were stirred at room temperature for 2 h. The mixture was purified by silica column chromatography (DCM/MeOH, 98/2). The product was isolated as light brown oil.

Yield = 1.07 g, 63.9%. ¹H NMR (300 MHz, CDCl₃): δ (ppm) = 4.73 (t, 2H), 3.66 (m, 16H), 3.43 (t, 4H), 1.77 (q, 2H), 1.56 (m, 4H), 1.44 (m, 2H), 1.27 (s, 12H), 0.96 (t, 3H). ¹³C NMR (75 MHz, CDCl₃): δ (ppm) = 177.48, 73.38, 71.89, 71.47, 70.58, 70.54, 70.47, 70.02, 59.00, 44.88, 31.99, 30.65, 29.59, 29.44, 29.39, 29.10, 26.34, 26.03, 18.63, 13.65. LC-MS: t = 7.65 min, (m/z): 515.69.[M]⁺

4.6.2 Synthetic procedure 2: Synthesis of 2a, 2b and 2c



Synthesis of 7

Benzyl alcohol (1.6 mL, 15.42 mmol), and CDI (5.00 g, 30.83 mmol) were dissolved in THF (20 mL) and were stirred at RT for 30 minutes under N₂ atmosphere. After quenching the reaction with distilled H₂O (70 mL) and extraction with EtOAc (3 x 100 mL), the combined organic fractions were dried with MgSO₄, filtered, and concentrated. The solution was purified by silica column chromatography (EtOAc/hexane, 1/2) and the product was isolated as a colorless oil.

Yield = 2.51 g, 80.6%. ¹H NMR (300 MHz, CDCl₃): δ (ppm) = 8.07 (s, 1H), 7.34 (m, 6H), 6.98 (m, 1H), 5.32 (s, 2H). ¹³C NMR (75 MHz, CDCl₃): δ (ppm) = 148.51, 137.09, 134.02, 130.58, 128.95, 128.78, 128.64, 117.10, 69.73. TLC-MS (m/z): 203.2 [M+H]⁺, 228.2 [M+Na]⁺.

Synthesis of 8

7 (2.51 g, 12.41 mmol) was dissolved in THF (50 mL) and diethylenetriamine (0.6 mL, 5.77 mmol) was added dropwise to the reaction mixture and stirred for 2 h at RT. The solution was purified by flash chromatography on a C18 silica column using a gradient of H₂O/CH₃CN 10-90 % over 35 minutes. The product was concentrated and lyophilized.

Yield = 1.64 g, 76.5%. ¹H NMR (300 MHz, CDCl₃): δ (ppm) = 7.33 (s, 10H), 5.65 (t, 2H), 5.08 (s, 4H), 3.25-3.21 (t, 4H), 2.68 (t, 4H), 1.33 (s, 1H). ¹³C NMR (300 MHz, CDCl₃): δ (ppm) = 156.77, 136.60, 128.50, 128.09, 66.64, 48.59, 40.70. TLC-MS (m/z): 394.3 [M + Na]⁺.

Synthesis of 9a

Tetraethylene glycol *p*-toluenesulfonate (0.42 g, 1.15 mmol), **8** (0.23 g, 0.62 mmol), K₂CO₃ (0.12 g, 0.88 mmol), and NaI (0.096 g, 0.64 mmol) were dissolved in anhydrous acetonitrile (15 mL) and were refluxed for 36 hours. The solution was concentrated and the residue was redissolved in DCM (25 mL). After washing with 1 M NaOH (15 mL) and back extraction of the aqueous layers with DCM (3 x 10 mL), the combined organic fractions were dried with MgSO₄, filtered, and concentrated. The residue was purified by flash column chromatography on C18 silica column using a gradient of H₂O/CH₃CN: 10-90% over 40 minutes.

Yield = 0.31 g, 88.5%. ^1H NMR (300 MHz, CDCl_3): δ (ppm) = 7.29 (s, 10H), 5.91 (t, 2H), 5.05 (s, 4H), 3.50 (s, 12H), 3.41 (t, 2H), 3.33 (s, 3H), 3.219 (q, 4H), 2.61 (t, 6H). ^{13}C NMR (75 MHz, CDCl_3): δ (ppm) = 156.80, 136.86, 128.38, 128.05, 127.90, 71.84, 70.49, 70.46, 70.35, 70.32, 70.16, 69.99, 66.39, 58.96, 54.23, 53.19, 39.17.

Synthesis of 2a

9a (0.149 g, 0.265 mmol) and Pd/C (0.021 g, 0.197 mmol) were dissolved in dry MeOH (10 mL) and placed under a N_2 atmosphere. Et_3SiH (4.5 mL, 26.5 mmol) was added dropwise to the reaction mixture and stirred at RT overnight. The solution was filtered over celite and the solvent was removed by a stream of N_2 gas. Subsequently, the residue was dissolved in CHCl_3 (50 mL) and **6** (0.30 g, 0.59 mmol) and DIPEA (0.14 mL, 0.80 mmol) were added and refluxed overnight. After the removal of the solvent by rotary evaporation, the residue was redissolved in DCM (20 mL), washed with H_2O (3 x 10 mL) and dried with MgSO_4 , filtered, and concentrated. The final compound was purified by silica column (DCM/MeOH, 9/1), lyophilized and obtained as white solid.

Yield = 0.122 g, 40.6%. ^1H NMR (300 MHz, CDCl_3): δ (ppm) = δ 3.59 (m, 50H), 3.42 (t, 8H), 3.35 (s, 6H), 3.31 (s, 3H), 2.68 (m, 6H), 1.58 (m, 12H), 1.24 (s, 20H). ^{13}C NMR (75 MHz, CDCl_3): δ (ppm) = 183.25, 181.50, 168.98, 168.81, 72.26, 71.82, 71.67, 71.49, 70.87, 70.53, 70.49, 70.44, 70.36, 69.92, 58.98, 57.15, 53.89, 44.61, 43.52, 31.14, 29.55, 29.51, 29.44, 29.25, 26.50, 26.03. LC-MS: t_r = 6.20 min, (m/z): 1175.42 $[\text{M}]^+$, MALDI (m/z): 1177.95, $[\text{M}+\text{H}]^+$

Synthesis of 9b

8 (0.21 g, 0.58 mmol), 1-bromodecane (0.14 mL, 0.67 mmol) and K_2CO_3 (0.37 g, 2.69 mmol) were dissolved in dry acetonitrile (30 mL) and refluxed overnight. The compound was purified by silica column chromatography (DCM/MeOH: 95/5).

Yield = 0.24 g, 81.1 %. ^1H NMR (300 MHz, CDCl_3): δ (ppm) = 7.32 (s, 10H), 5.08 (s, 2H), 3.23 (t, 4H), 2.48 (m, 6H), 1.27 (d, 16H), 0.91 (t, 3H). ^{13}C NMR (75 MHz, CDCl_3): δ (ppm) = 156.68, 136.72, 128.44, 128.01, 127.98, 66.56, 54.03, 53.51, 38.86, 34.01, 31.93, 31.90, 29.71, 29.62, 29.53, 29.36, 29.30, 27.39, 26.89, 22.71, 14.16. TLC-MS (m/z): 512.7 $[\text{M} + \text{H}]^+$, 534.7 $[\text{M} + \text{Na}]^+$.

Synthesis of 2b

9b (0.71 g, 1.39 mmol) and Pd/C (0.08 g, 0.72 mmol) were dissolved in dry MeOH (30 mL) and flushed with argon for 10 minutes. Et_3SiH (11.0 mL, 68.9 mmol) was added dropwise to the reaction mixture and stirred overnight at RT. The solution was filtered over celite and the solvent was removed by a stream of N_2 gas. Subsequently, the residue was redissolved in CHCl_3 (50 mL) and **6** (0.32 g, 0.61 mmol) and DIPEA (0.17 mL, 0.99 mmol) were added and refluxed overnight. After the removal of the solvent by rotary evaporation, the mixture was dissolved in DCM (20 mL) and washed with H_2O (3 x 10 mL) and dried with MgSO_4 . The product was purified silica column chromatography using DCM/MeOH (9:1) and successively lyophilized to obtain the final compound as a white powder.

Yield = 0.17 g, 47.1%. ^1H NMR (300 MHz, CDCl_3): δ (ppm) = δ 3.65 (m, 35H), 3.44 (t, 4H), 3.38 (s, 5H), 2.73 (t, 6H), 1.59 (m, 12H), 1.25 (d, 36H), 0.88 (m, 3H). ^{13}C NMR (75 MHz, CDCl_3): δ (ppm) = 181.81, 168.79, 167.18, 71.85, 71.53, 70.57, 70.53, 70.46, 70.38, 70.01, 69.94, 59.01, 57.41, 54.76, 44.68, 31.91, 31.07, 29.63, 29.59, 29.54, 29.50, 29.35, 29.29, 26.57, 26.07, 22.68, 14.13. LC-MS: t_r = 8.06 min, (m/z): 1125.62 $[\text{M}]^+$, MALDI (m/z): 1127.23 $[\text{M} + \text{H}]^+$.

Synthesis of 9c

8 (0.20 g, 0.54 mmol) and **3** (0.29 g, 0.67 mmol) and K_2CO_3 (0.37 g) were dissolved in dry acetonitrile (30 mL) and refluxed overnight. The purification was performed by flash chromatography on a C18 silica column using a gradient of $\text{H}_2\text{O}/\text{CH}_3\text{CN}$ (10-90%) over 40 min.

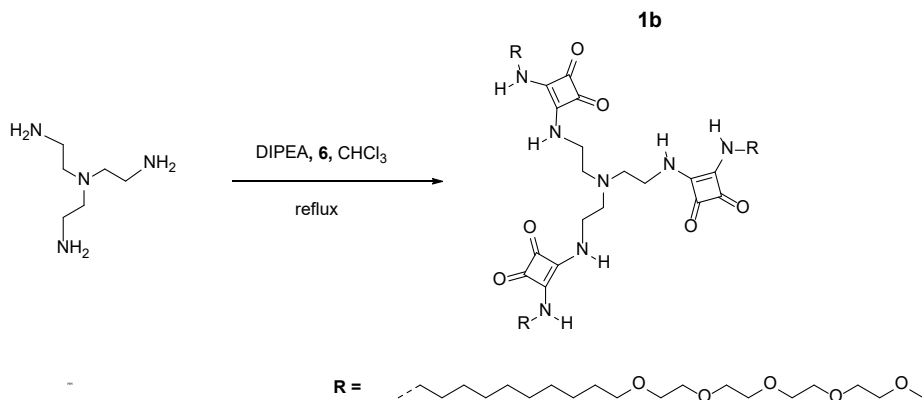
Yield = 0.26 g, 66.3 %. ^1H NMR (300 MHz, CDCl_3): δ (ppm) = 7.33 (d, 10H), 5.08 (s, 4H), 3.66 (m, 17H), 3.57 (m, 4H), 3.45 (m, 3H), 3.39 (d, 3H), 3.26 (s, 2H), 2.52 (d, 4H), 1.58 (t, 3H), 1.27 (d, 16H). ^{13}C NMR (75 MHz, CDCl_3): δ (ppm) = 136.61, 128.45, 128.02, 71.93, 71.52, 70.61, 70.59, 70.51, 70.05, 66.63, 54.06, 53.55, 29.63, 29.55, 29.46, 27.30, 26.08.

Synthesis 2c

7c (0.18 g, 0.25 mmol), and Pd/C (13 mg, 0.13 mmol) were dissolved in MeOH (30 mL) and flushed with N_2 gas for 10 minutes. Et_3SiH (4.0 mL, 25.21 mmol) was added dropwise and the reaction mixture stirred overnight at RT. The solution was filtered over celite and concentrated using a gentle stream of N_2 gas. Subsequently, the residue, **6** (0.44 g, 0.85 mmol) and DIPEA (0.19 mL, 1.10 mmol) were dissolved in chloroform and refluxed overnight. After the removal of the solvent, the residue was dissolved in DCM (20 mL), washed (3 x 10 mL) with H_2O and dried with MgSO_4 . The compound was purified by silica column chromatography using EtOAc and then DCM/MeOH (9/1). Successively, the final compound was lyophilized and isolated as a white powder.

Yield = 0.11 g, 21.5%. ^1H NMR (300 MHz, CDCl_3): δ (ppm) = 3.58 (m, 54H), 3.45 (m, 8H), 3.37 (s, 9H), 2.56 (d, 6H), 1.40 (m, 46H). ^{13}C NMR (75 MHz, CDCl_3): δ (ppm) = 185.16, 168.71, 167.27, 71.89, 71.85, 71.53, 70.56, 70.52, 70.44, 70.37, 70.02, 69.92, 69.56, 59.01, 44.59, 37.71, 31.08, 26.54, 26.06. LC-MS: t_r = 7.14 min, (m/z): 1331.65 $[\text{M}]^+$, MALDI (m/z): 1355.31 $[\text{M}+\text{Na}+\text{H}]^+$.

4.6.3 Synthetic procedure 3: Synthesis of 1b



Synthesis of 1b

Tris(2-aminoethyl)amine (0.015 mL, 0.10 mmol), **6** (0.17 g, 0.34 mmol) and DIPEA (0.071 mL, 0.05 mmol) were dissolved in chloroform (50 mL) and refluxed overnight. The solvent was removed by rotary evaporation and the residue was dissolved in DCM (15 mL), washed with H_2O (3 x 10 mL) and dried with MgSO_4 . The compound was purified by silica column chromatography using EtOAc and then DCM/MeOH (9/1) to isolate the product was isolated as a colourless oil.

Yield = 0.131 g, 86.9%. ^1H NMR (300 MHz, CDCl_3): δ (ppm) = 7.65 (s, 4H), 3.60 (m, 60H), 3.45 (t, 6H), 3.38 (d, 9H), 2.62 (s, 4H), 1.57 (m, 12H), 1.35 (d, 6H), 1.25 (s, 30H). ^{13}C NMR (75 MHz, CDCl_3): δ (ppm) = 182.66, 168.50, 167.17, 71.66, 71.52, 70.31, 70.19, 70.16, 70.11, 70.04, 69.71, 59.01, 56.69, 55.65, 44.50, 31.08, 29.51, 29.44, 29.24, 26.46, 25.96. LC-MS: t_r = 6.99 min, (m/z): 1469.83 $[\text{M}]^+$, MALDI (m/z): 1470.87 $[\text{M}+\text{H}]^+$.

4.7 Characterization

Sample preparation protocol

Water was added to **1b** and **2a-c** to prepare solutions at a concentration of 1 mM - 5 mM and sonicated for 20 min using a Branson 2510 Ultrasonic cleaner bath. Subsequently, aliquots from the stock solution were taken to prepare solutions at the desired concentration for solution phase measurements and used for gelation experiments. All samples were left to stand overnight before measurement.

UV-vis spectroscopy

Samples for UV-vis spectroscopy were prepared at a 15 μ M concentration in water as described according to the sample preparation protocol above. The samples were placed in the UV-vis and a spectrum was recorded from 200-500 nm. The solutions were prepared in triplicate and for each solution the UV-vis spectra was measured.

Fluorescence spectroscopy

A stock solution of Nile Red dye (0.005 mg/mL) was prepared in MeOH. The stock solution was pipetted into 4 individual wells of a 96-well plate (12 μ L) and the solvent was removed using a vacuum oven for 2 h. Subsequently **2a**, **2b**, **2c** and **1a** were prepared at a 15 μ M concentration as described according to the self-assembly protocol. Aliquots of **1a** and **2a-c** (200 μ L) were pipetted into a 96-well plate and equilibrated overnight before the measurement. Water (200 μ L) was measured as a negative control. The experiment was performed using Infinite M1000 Pro Tecan plate reader, with an excitation wavelength of 550 nm and measuring fluorescence emission from 570 to 800 nm. The solutions were prepared in triplicate and for each solution the emission spectra was measured.

Critical aggregation concentration determination

The critical aggregation concentration (CAC) of **1b** and **2a** was determined by first preparing a stock solution at 1 mM concentration that was equilibrated overnight. The stock solution was diluted to several concentrations between 100 μ M to 10 nM and equilibrated for at least 3h prior to measurement of

scattering intensity. Each measurement was carried out using a disposable DLS cuvette. The data was plotted using the scattering intensity as a function of $\log [C]$. The critical aggregation concentration was then determined from the intersection of the two lines drawn through the points collected for the scattering intensities collected at the various concentrations.

Atomic force microscopy (AFM)

1b and **2a-c** were prepared according to the preparation protocol above at a concentration of 15 μM and equilibrated overnight. An aliquot (25 μL) from each of these solutions was pipetted on cleaved mica and dried overnight at RT before the measurements. The analysis of AFM images was performed using the Nanoscope software.

Critical gelation concentration (CGC)

The CGC of compounds **1b** and **2a-c** was determined by the gel inversion method. Compounds **1b** and **2a-c** were weighed in the appropriate quantities in 500 μL of water to prepare gels with final gelator concentrations from 1-5 mM according to the sample preparation protocol above.

Oscillatory rheology

Because compound **1a** resulted in a viscous solution at a concentration of 5 mM in water after sonication, an oscillatory rheology measurement was performed to gain insight into the gel properties. The pre-made hydrogel (600 μL) was gently pipetted onto the lower plate and a gap distance was set at 54 μm . Time sweep measurements were collected at a fixed frequency of 1.0 Hz and strain of 0.05% for up to 7200s.



Figure S1 Representative photograph of gel inversion test for **1b** at 5 mM.

Table S1

TEG weight fraction (ω_{TEG}) of the monomers

Monomers	ω_{TEG}
1a	0.42
2a	0.55
2b	0.53
2c	0.46

References

1. Chirkin, E.; Muthusamy, V.; Mann, P.; Roemer, T.; Nantermet, P. G.; Spiegel, D. A., Neutralization of Pathogenic Fungi with Small-Molecule Immunotherapeutics. *Angew. Chem. Int. Ed.* **2017**, *56*, 13036-13040.

CHAPTER 5

**Visible light crosslinking of squaramide-based
supramolecular polymers through tyrosine cross-
linking**

5.1 Abstract

Supramolecular materials that are held together by non-covalent interactions are gaining remarkable attention in the biomedical field for their capacity to mimic structural and functional attributes of ECM proteins. However, in comparison to the covalent polymers that are held together with largely irreversible bonds, supramolecular materials display weak mechanical properties that limit their applications. A powerful strategy to tune the mechanical properties of the resultant self-assembled materials is through the application of covalent crosslinks. When photoreactive groups are used, spatiotemporal control over materials properties can be achieved using light as an external stimulus. We herein examine the inclusion of tyrosine moieties into a squaramide-based supramolecular monomer to enable its visible light crosslinking. More specifically, a tyrosine dipeptide-functionalized squaramide-based monomer was synthesized to obtain supramolecular polymers and its visible light cross-linking with the use of FMN and $\text{Ru}(\text{bpy})_3^{2+}$ photoinitiators to prepare gel materials is disclosed.

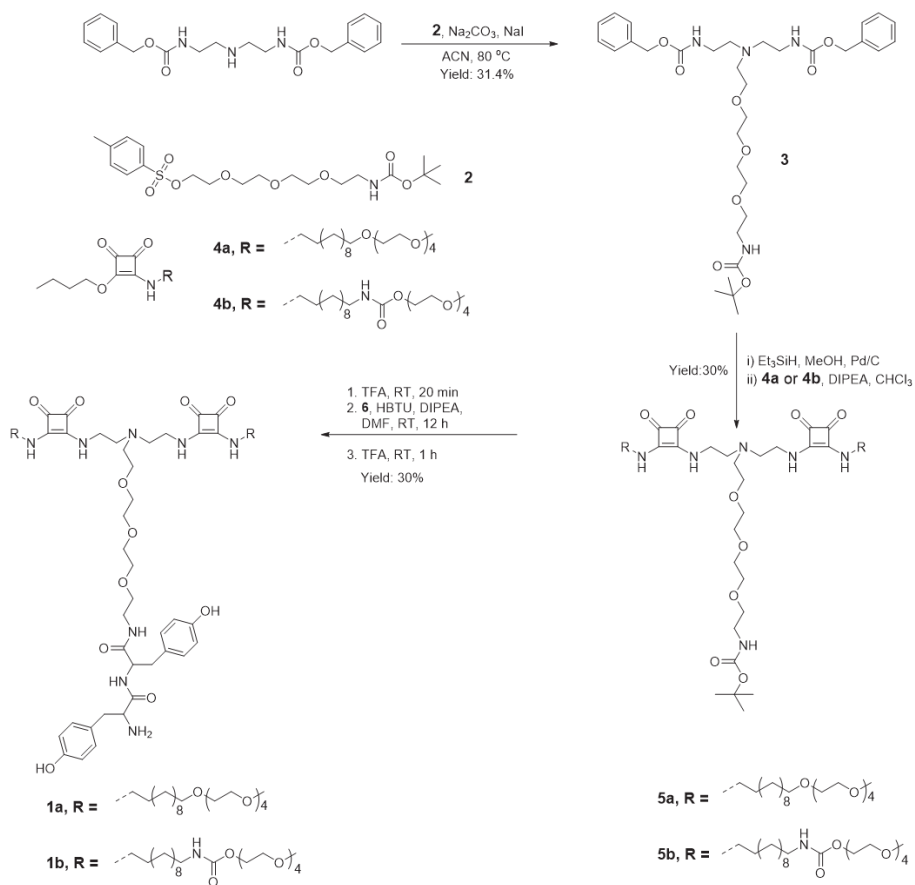
5.2 Introduction

Functional supramolecular hydrogels based on peptides are considered as promising candidates for tissue engineering and regenerative medicine because of their biocompatible and biodegradable nature.¹⁻⁵ Moreover, their self-assembly starting from small molecules provide numerous opportunities to modulate the properties of the formed materials based on the features of the designed monomer, namely its sequence.^{6,7} The amino acid sequence with the relative positioning of the units dictates the non-covalent interactions (e.g. π - π stacking, hydrogen bonding and hydrophobic interactions) that will work together to form the polymers.^{8,9} Short peptide sequences involving two, three or four amino acids have shown the ability to form a diverse array of filamentous nanostructures and hydrogel materials.^{6,10,11} Often their design is based on sequences containing aromatic units (e.g. Phe, Tyr) and can include larger non-amino acid units (e.g. Fmoc).¹²⁻¹⁴ However, a major challenge for these materials once assembled is their weak mechanical properties that limit their application in the biomedical area, thus further tuning of their properties on self-assembly is necessary. One strategy to improve the properties of these materials is to introduce units that would enable their covalent crosslinking under cell culture conditions. Such crosslinking has been achieved using various conjugation chemistries such as Schiff-base, hydrazone, acylhydrazone, Diels-Alder, and disulfide, and thiol-ene reactions.^{12,15-18} However, the use of light activatable chemistries is highly attractive as it provides opportunities for spatiotemporal control of mechanics and bioactivity of these materials.

UV or visible light have been used to stimulate photocrosslinking in covalent polymer hydrogels with the aid of a photoinitiator.^{19,20} Photoinitiators such as lithium phenyl-2,4,6-trimethylbenzoylphosphinate (LAP), flavin mononucleotide (FMN), Eosin-Y and tris(bipyridine)ruthenium(II) $[\text{Ru}(\text{bpy})_3]^{2+}$ have been used to provide a radical source to trigger crosslinking. More recently, visible light photoinitiators (e.g. FMN, $\text{Ru}(\text{bpy})_3^{2+}$) have been examined to crosslink of phenol-based molecules (e.g. tyrosine) in peptide and polymer materials for a range of 3D cell culture applications, including bioprinting. Tyrosine dimerization can be easily followed with the characteristic absorption and emission of dityrosine ($\lambda_{\text{abs}} = 320 \text{ nm}$; $\lambda_{\text{em}} = 420 \text{ nm}$) as compared to the unreacted amino acid ($\lambda_{\text{abs}} = 280 \text{ nm}$; $\lambda_{\text{em}} = 305 \text{ nm}$).^{21,22} In a PEG-peptide hydrogel containing tyrosine (e.g., CYGGGYC), the mechanical properties were modulated by the time of light exposure, FMN concentration and number tyrosine residues.²² Importantly, tyrosine

5.3 Results and discussion

In chapter 4, we found that removing one squaramide arm from a tripodal squaramide derivative and the addition of a tetraethylene glycol chain results in a lack of aggregation on self-assembly as consequence of its increased hydrophilic character. We selected this monomer because of the hydrophobic nature of the dityrosine that is expected to increase on self-assembly and after light-mediated crosslinking.



Scheme 2. Synthetic route to tyrosine dipeptide-coupled squaramide-based monomer **1a** and **1b**.

Moreover, the tyrosine dipeptide has also been reported to self-assemble on its own into nanofibers²³ (Scheme 1). Though a single tyrosine moiety is sufficient cross-linking, we applied the tyrosine dipeptide to additionally benefit from the potential synergistic effect of the self-assembly of the dipeptide that could influence the squaramide supramolecular polymer structure prior to crosslinking. We examine the effect of its conjugation to squaramide monomers (**1a** and **1b**) on modulating the self-assembly before and after visible light irradiation.

The tyrosine dipeptide-coupled squaramide-based monomers, **1a** and **1b**, were synthesized through a multistep reaction sequence as shown in Scheme 2. Initially, compound **6** was synthesized by reacting Ac-O-(*tert*-butyl)-L-tyrosine with O-(*tert*-butyl)-L-tyrosine via DCC/NHS coupling in DMF with 75% yield. The heterobifunctional tetraethyleneglycol (**2**), squaramide amphiphile with a decyl spacer and a carbamate (**4a**) and without carbamate group (**4b**) were separately synthesized using literature reported procedures.³² The synthesis of tripodal amphiphiles commenced with the reaction of *N,N'*-di-*Z*-diethylenetriamine with **2** in the presence of sodium carbonate to provide **3** in 31% yield. The Cbz group was subsequently deprotected by *in situ* hydrogenation with triethylsilane on activated palladium and substituted with squaramide units to yield **5a** (30%) and **5b** (28%). The product was further treated with 50% trifluoroacetic acid in chloroform for boc-deprotection and then coupled with tyrosine dipeptide using HBTU in DMF. The final product was isolated after deprotection of the *tert*-butyl group using TFA at RT to yield **1a** (57%) and **1b** (30%).

To understand the changes in the assembly of the supramolecular induced by the conjugation of the tyrosine dipeptide, AFM experiments were performed. When the tyrosine peptide is conjugated to the tripodal squaramide-based supramolecular monomer, **1a**, spherical aggregates are observed on dilution from a 1 mM stock solution on mica (15 μ M) (**Figure 2a**). The lack of aggregates with a fibrillar morphology could be due to the position of the hydrophilic domain in the monomer structure, as it is conjugated to the central nitrogen in the monomer core and can hinder the formation of the other non-covalent interactions between monomers.

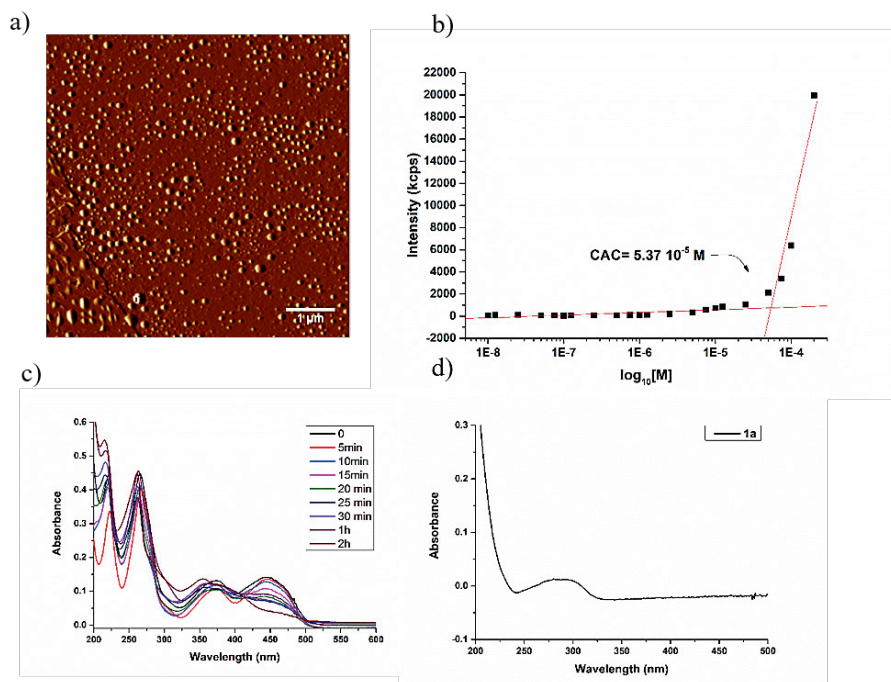


Figure 2 (a) AFM micrographs of **1a**, stock solution 1 mM diluted to 15 μ M (scale bar = 1 μ m) (b) Critical aggregation concentration of **1a** by static light scattering (SLS) ; (c) UV-vis spectra of **1a** (1 mM diluted to 15 μ M); in presence of FMN (15 μ M) at different irradiation times at 450 nm; d) UV-vis spectrum of **1a** (15 μ M).

The self-assembly of **1a** at the molecular level was further evaluated by UV-vis spectroscopy. A broad absorption band between 250-320 nm lacking the characteristic red- and blue-shifting of the HOMO-LUMO and HOMO-LUMO+1 transitions of squaramide synthon on self-assembly was observed (**Figure 2d**). Combined with the observations in AFM imaging, namely the formation of spherical aggregates, these results point to monomer **1a** being unable to form fibrillar aggregates at the tested concentration. Despite earlier reports that show the formation of supramolecular polymers from tyrosine dipeptides,²³ this result suggests that the aliphatic spacer between TREN core and peptide is likely necessary for the retention of one-dimensional nanostructures at monomer concentrations in the low micromolar range, as observed for other tripodal monomers reported in Chapter 4. Moreover, the self-assembly of **1a** was further investigated by SLS (static light scattering) to determine the critical aggregation concentration (CAC) or the concentration above which the supramolecular polymers are formed (**Figure 2b**). The CAC

of **1a**, was determined from the inflection point of the scattered intensities of monomer solutions between 100 μ M and 10 nM and was comparable to that one previously calculated for the compound **2a** (chapter 4, 2.13×10^{-5} M), further confirming the approach of self-assembly at a higher monomer concentration and its subsequent dilution for analysis.

Once aggregation behavior of the monomer was assessed, the potential of the tyrosine dipeptide unit to undergo cross-linking with visible light irradiation ($\lambda = 440$ nm) was examined. Using conditions reported by Liu *et al.*,³³ compound **1a** (1 mM) above the CAC was irradiated with visible light at 440 nm in the presence of the FMN photoinitiator at a 1 mM concentration with different irradiation times (0, 5, 10, 15, 20, 25, 30, 60 and 120 min). It was previously reported that the formation of tyrosine dimers could be identified by the growth of a new UV-vis band at 330 nm and a fluorescent signal at 420 nm.²¹ Therefore, we collected UV-vis and fluorescence spectra of **1a** in the presence of FMN (1 mM) before and after being irradiated with visible light for different irradiation times until when no further spectral changes were observed (**Figure 2d**). The UV-vis profile before irradiation ($t = 0$ min) displayed bands at 255, 370 and 450 nm, which are consistent with the characteristic absorption of the FMN photoinitiator.³⁴ A control sample where visible light irradiation was applied to the FMN photoinitiator in water was performed (**Figure S5.2**). With increasing the irradiation time in the experiment, a decrease in the absorption spectrum at 450 nm was observed due to the degradation of the photoinitiator.³⁵

To further confirm tyrosine crosslinking between squaramide monomers, emission spectra of **1a** were recorded after irradiation with visible light for various durations (**Figure 3**). In absence of visible light irradiation, the emission profile is typical of the photoinitiator (**Figure S5.3**). On the application of visible light, the initial transitions at 525 and 550 nm disappeared and a new band at 470 nm was observed. These trends matched those observed in UV-vis experiments and are consistent with the photodegradation of FMN in water as outlined by Edwards.^{35–37} Both the lack of the UV-vis band at 330 nm and the fluorescent signal at 420 nm point to the inability of the tyrosine dipeptide to crosslink within this supramolecular system. We postulate that this result could arise for two reasons; either the lack of ‘exposure’ of phenolic hydroxyl group of tyrosine to the excited photoinitiator to trigger the radical reaction or too large of a distance between tyrosines to enable crosslinking. However, we also do not rule out the monomer concentration or choice of the photoinitiator to give rise to the

observed result, as faster initiation, on the order of seconds, can be achieved with $\text{Ru}(\text{bpy})_3^{3+}$.

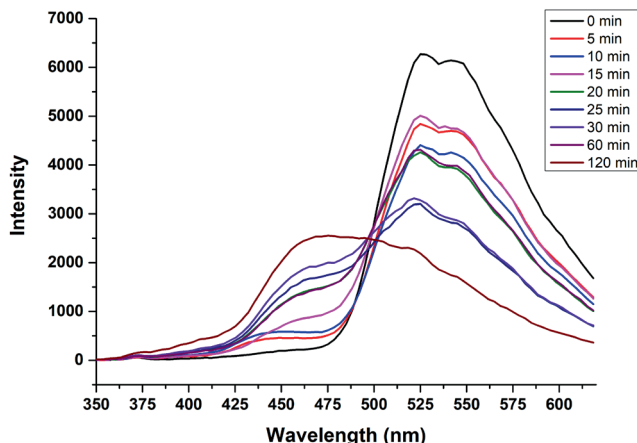


Figure 3 Emission spectra of diluted samples of **1a** (15 μM) after different visible light irradiation times (330 nm) using FMN (15 μM) as a photoinitiator. Fluorescence spectra were taken by excitation at 330 nm and collection from 350 to 620 nm.

In order to further modulate the self-assembly behaviour and photo-crosslinking of the monomer, we designed compound **1b** with a carbamate linkage at the interface of the hydrophilic and hydrophobic domains. In Chapter 4, it was demonstrated that the absence of a carbamate moiety in the tripodal squaramide monomer results in a decrease in the storage modulus (G') of the hydrogel. Therefore, the impact of using a carbamate linker on self-assembly of the tyrosine dipeptide containing monomer was examined. The UV-vis spectra on dilution of **1b** (15 μM) after self-assembly in water and CH_3CN shows a spectral profile consistent with a lack of head-to-tail aggregation of the squaramide synthons (**Figure 4a**). The slight increase in the absorption intensity in acetonitrile may be due to the increased solubility of **1b** in acetonitrile in comparison to water. Based on earlier critical aggregation concentration measurements for the ether derivative, **1a**, UV-vis spectra were taken for **1b** up to 1 mM. Upon increasing the concentration of **1b**, new absorption bands at 247 nm and 325 nm were observed (**Figure 4b**). These shifting of the HOMO-LUMO and HOMO-LUMO+1 transitions are consistent with the self-assembly of the squaramide synthon in a head-tail hydrogen bonding arrangement. The dilution of a concentrated solution of **1b**

to 0.021 mM resulted the disappearance of these bands; this concentration-dependent aggregation behaviour that can further be fit with models to gain insight into the supramolecular polymerization mechanism. DLS measurements of **1b** exhibited an increased size in water relative to acetonitrile further consistent with the formation of supramolecular polymers of **1b** in water (**Figure 4c**).

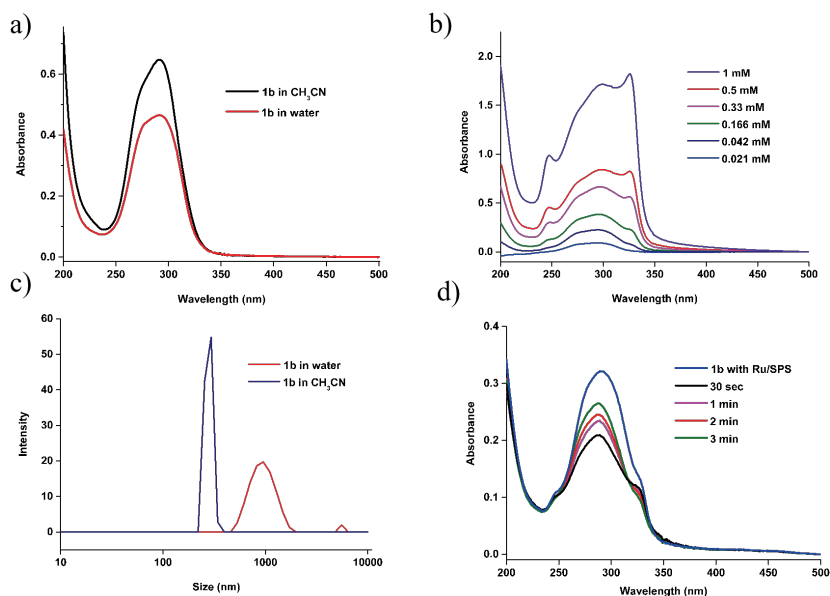


Figure 4 a) UV-vis spectra of **1b** (15 μM) in water and CH_3CN ; b) Concentration-dependent absorption of **1b** in water; c) Size distribution data measured by DLS (0.166 mM) in water and CH_3CN ; d) Photoirradiation of **1b** (0.166 mM) in the presence of $\text{Ru}(\text{bpy})_3^{2+}$ (16.7 μM) and SPS (0.183 μM) using 450 nm visible light as a function of time.

Tyrosine crosslinking in supramolecular polymer **1b** was subsequently studied in the presence of $\text{Ru}(\text{bpy})_3^{2+}$ and sodium persulfate (SPS) photoinitiators because of their capacity to enable rapid crosslinking, on the order of seconds, in the visible range at 450 nm. The concentration of **1b** was chosen at which it is in self-assembled state (0.166 mM). The photoinitiators $\text{Ru}(\text{bpy})_3^{2+}$ (16.7 μM) and SPS (0.183 μM) were added to the solution prior to photoirradiation using 450 nm visible light. Upon photoirradiation of **1b** for 30 sec, a slight decrease in the UV absorption intensity was observed (**Figure 4d**). Extending the time of irradiation for up to 3 min resulted in an increase of the absorption band at 297 nm consistent with the monomer species and a

decrease of aggregation band at 325 nm belonging to the aggregated species. The overall decrease of the UV-vis spectra after visible light irradiation can be attributed to an increase in hydrophobicity of the cross-linked tyrosines in the supramolecular polymers. Photoirradiation of **1b** under the similar experimental conditions at low (30 μM) and high (0.5 mM) concentrations did not show any noticeable changes in the UV-vis spectra (**Figure 5a** and **5b**). As a control, a solution containing the same concentration of $\text{Ru}(\text{bpy})_3^{2+}$ and SPS was prepared to confirm spectral changes were due to the reacted self-assembling molecules. Though it is anticipated that cross-linking of tyrosine would be highly efficient in the self-assembled state due to the close proximity of the tyrosine dipeptides on self-assembly, further investigation into the effect of self-assembly on crosslinking by varying the concentration of photoinitiator, nature of supramolecular polymers and visible light exposure time are highly necessary. While these results demonstrate that the tyrosine unit is a valid platform to modulate the self-assembly properties of supramolecular monomers, their position in the monomer structure, more specifically in their relation to their hydrophobic domains is critical for the control of supramolecular aggregates.

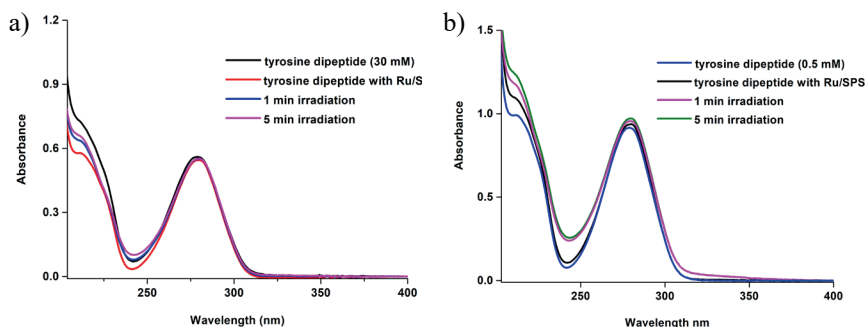


Figure 5: UV-visible spectra after photo-irradiation of tyrosine dipeptide a) at low concentration (30 μM) in the presence of $\text{Ru}(\text{bpy})_3^{2+}$ (1.67 μM) and SPS (0.183 μM) and b) at high concentration (0.5 mM) in the presence of $\text{Ru}(\text{bpy})_3^{2+}$ (16.7 μM) and SPS (183 μM) using 450 nm visible light as a function of time.

5.4 Conclusions

In this chapter, the effect of introducing tyrosine dipeptides on modulating the self-assembly properties of a tripodal squaramide-based supramolecular monomer was examined. Since tyrosine has been previously shown to self-assemble in nanofibers, we investigated if this self-assembling unit can influence the formation of supramolecular polymers. Head-to-tail hydrogen bonding of the squaramide synthons was achieved when a carbamate moiety was included to link together hydrophilic and hydrophobic domains, unlike when an ether linkage was used. Neither FMN or $\text{Ru}(\text{Bpy})^{3+}$ photoinitiators resulted in the formation of tyrosine crosslinks after visible light irradiation at various monomer concentrations. These results suggest that the tyrosine moiety may be inaccessible to the photoinitiator for crosslinking, and thus further optimization with respect to the monomer or photocrosslinking conditions is required to enable dityrosine formation to drive changes in the formed supramolecular polymers and materials.

References

1. Li, J.; Xing, R.; Bai, S.; Yan, X., Recent advances of self-assembling peptide-based hydrogels for biomedical applications. *Soft Matter* **2019**, *15*, 1704–1715.
2. Dasgupta, A.; Mondal, J. H.; Das, D., Peptide hydrogels. *RSC Adv.* **2013**, *3*, 9117–9149.
3. Webber, M. J.; Appel, E. A.; Meijer, E. W.; Langer, R., Supramolecular biomaterials. *Nat. Mater.* **2016**, *15*, 13–26.
4. Mondal, S.; Das, S.; Nandi, A. K., A review on recent advances in polymer and peptide hydrogels. *Soft Matter* **2020**, *16*, 1404–1454.
5. Diaferia, C.; Netti, F.; Ghosh, M.; Sibillano, T.; Giannini, C.; Morelli, G.; Adler-Abramovich, L.; Accardo, A., Bi-functional peptide-based 3D hydrogel-scaffolds. *Soft Matter* **2020**, *16*, 7006–7017.
6. Sun, B.; Ariawan, A. D.; Warren, H.; Goodchild, S. C.; In Het Panhuis, M.; Ittner, L. M.; Martin, A. D., Programmable enzymatic oxidation of tyrosine-lysine tetrapeptides. *J. Mater. Chem. B* **2020**, *8*, 3104–3112.
7. Lampel, A.; McPhee, S. A.; Park, H. A.; Scott, G. G.; Humagain, S.; Hekstra, D. R.; Yoo, B.; Frederix, P. W. J. M.; Li, T. De; Abzalimov, R. R.; Greenbaum, S. G.; Tuttle, T.; Hu, C.; Bettinger, C. J.; Ulijn, R. V., Polymeric peptide pigments with sequence-encoded properties. *Science*, **2017**, *356*, 1064–1068.
8. Handelman, A.; Beker, P.; Amdursky, N.; Rosenman, G., Physics and engineering of peptide supramolecular nanostructures. *Phys. Chem. Chem. Phys.* **2012**, *14*, 6391–6408.
9. Lou, S.; Wang, X.; Yu, Z.; Shi, L., Peptide Tectonics: Encoded structural complementarity dictates programmable self-assembly. *Adv. Sci.* **2019**, *6*, 1802043, 1–24.
10. Adams, D. J., Dipeptide and tripeptide conjugates as low-molecular-weight hydrogelators. *Macromol. Biosci.* **2011**, *11*, 160–173.
11. Levin, A.; Hakala, T. A.; Schnaider, L.; Bernardes, G. J. L.; Gazit, E.; Knowles, T. P. J., Biomimetic peptide self-assembly for functional materials. *Nat. Rev. Chem.* **2020**, *4*, 615–634.
12. Draper, E. R.; Morris, K. L.; Little, M. A.; Raeburn, J.; Colquhoun, C.; Cross, E. R.; McDonald, T. O.; Serpell, L. C.; Adams, D. J., Hydrogels formed from Fmoc amino acids. *CrystEngComm* **2015**, *17*, 8047–8057.
13. Arakawa, H.; Takeda, K.; Higashi, S. L.; Shibata, A.; Kitamura, Y.;

- Ikeda, M., Self-assembly and hydrogel formation ability of Fmoc-dipeptides comprising α -methyl-L-phenylalanine. *Polym. J.* **2020**, *52*, 923–930.
14. Liebmann, T.; Rydholm, S.; Akpe, V.; Brismar, H., Self-assembling Fmoc dipeptide hydrogel for in situ 3D cell culturing. *BMC Biotechnol.* **2007**, *7*, 1–11.
 15. Arkenberg, M. R.; Nguyen, H. D.; Lin, C. C., Recent advances in bio-orthogonal and dynamic crosslinking of biomimetic Hydrogels, *J. Mater. Chem. B*, **2020**, *8*, 7835-7855
 16. Echali r, C.; Valot, L.; Martinez, J.; Mehdi, A.; Subra, G., Chemical cross-linking methods for cell encapsulation in hydrogels. *Mater. Today Commun.* **2019**, *20*, 100536, 1-44
 17. Huang, S.; Kong, X.; Xiong, Y.; Zhang, X.; Chen, H.; Jiang, W.; Niu, Y.; Xu, W.; Ren, C., An overview of dynamic covalent bonds in polymer material and their applications. *Eur. Polym. J.* **2020**, *141*, 110094, 1-18
 18. GhavamiNejad, A.; Ashammakhi, N.; Wu, X. Y.; Khademhosseini, A., Crosslinking strategies for 3D bioprinting of polymeric hydrogels. *Small* **2020**, *16* (35), 2002931, 1-30
 19. Li, L.; Scheiger, J. M.; Levkin, P. A., Design and applications of photoresponsive hydrogels. *Adv. Mater.* **2019**, *31*, 1807333, 1-17
 20. Hu, W.; Wang, Z.; Xiao, Y.; Zhang, S.; Wang, J., Advances in crosslinking strategies of biomedical hydrogels. *Biomater. Sci.* **2019**, *7*, 843–855.
 21. Lee, J.; Ju, M.; Cho, O. H.; Kim, Y.; Nam, K. T., Tyrosine-rich peptides as a platform for assembly and material synthesis. *Adv. Sci.* **2019**, *6*, 1-15
 22. Liu, H.-Y.; Nguyen, H. D.; Lin, C.-C., Dynamic PEG–peptide hydrogels via visible light and FMN-induced tyrosine dimerization. *Adv. Healthc. Mater.* **2018**, *7*, 1800954, 1-10.
 23. Jang, H. S.; Lee, J. H.; Park, Y. S.; Kim, Y. O.; Park, J.; Yang, T. Y.; Jin, K.; Lee, J.; Park, S.; You, J. M.; Jeong, K. W.; Shin, A.; Oh, I. S.; Kwon, M. K.; Kim, Y. Il; Cho, H. H.; Han, H. N.; Kim, Y.; Chang, Y. H.; Paik, S. R.; Nam, K. T.; Lee, Y. S., Tyrosine-mediated two-dimensional peptide assembly and its role as a bio-inspired catalytic scaffold. *Nat. Commun.* **2014**, *5*, 1–11.
 24. Min, K. I.; Yun, G.; Jang, Y.; Kim, K. R.; Ko, Y. H.; Jang, H. S.; Lee, Y. S.; Kim, K.; Kim, D. P., Covalent self-assembly and one-step photocrosslinking of tyrosine-rich oligopeptides to form diverse

- nanostructures. *Angew. Chemie - Int. Ed.* **2016**, *55*, 6925–6928.
25. Partlow, B. P.; Bagheri, M.; Harden, J. L.; Kaplan, D. L., Tyrosine templating in the self-assembly and crystallization of silk fibroin. *Biomacromolecules* **2016**, *17*, 3570–3579.
 26. Zhang, X.; Zhang, Y.; Chen, W.; Xu, L.; Wei, S.; Zheng, Y.; Zhai, M., Biological behavior of fibroblast on contractile collagen hydrogel crosslinked by γ -irradiation. *J. Biomed. Mater. Res. Part A* **2014**, *102*, 2669–2679.
 27. Al, E.; Güçlü, G.; İyim, T. B.; Emik, S.; Özgümüş, S., Synthesis and properties of starch-graft-acrylic acid/Na-montmorillonite superabsorbent nanocomposite hydrogels. *J. Appl. Polym. Sci.* **2008**, *109*, 16–22.
 28. Rosales, A. M.; Anseth, K. S., The design of reversible hydrogels to capture extracellular matrix dynamics. *Nat. Rev. Mater.* **2016**, *1*, 15012, 1-15.
 29. Tong, C.; Wondergem, J. A. J.; Heinrich, D.; Kieltyka, R. E., Photopatternable, branched polymer hydrogels based on linear macromonomers for 3D cell culture applications. *ACS Macro Lett.* **2020**, *9*, 882–888.
 30. Tong, C.; Liu, T.; Saez Talens, V.; Noteborn, W. E. M.; Sharp, T. H.; Hendrix, M. M. R. M.; Voets, I. K.; Mummery, C. L.; Orlova, V. V.; Kieltyka, R. E., Squaramide-based supramolecular materials for three-dimensional cell culture of human induced pluripotent stem cells and their derivatives. *Biomacromolecules* **2018**, *19*, 1091–1099.
 31. Liu, T.; van den Berk, L.; Wondergem, J. A. J.; Tong, C.; Kwakernaak, M. C.; Braak, B. ter; Heinrich, D.; van de Water, B.; Kieltyka, R. E., Squaramide-based supramolecular materials drive HepG2 spheroid differentiation. *Adv. Healthc. Mater.* **2021**, *10*, 2001903, 1-10.
 32. Pandya, D. N.; Pailloux, S.; Tatum, D.; Magda, D.; Wadas, T. J., Di-macrocylic terephthalamide ligands as chelators for the PET radionuclide zirconium-89. *Chem. Commun.* **2015**, *51*, 2301–2303.
 33. Liu, H. Y.; Nguyen, H. D.; Lin, C. C., Dynamic PEG–peptide hydrogels via visible light and FMN-induced tyrosine dimerization. *Adv. Healthc. Mater.* **2018**, *7*, 1–10.
 34. Edwards, A. M., Structure and general properties of flavins. In *Flavins and Flavoproteins: Methods and Protocols*; Weber, S., Schleicher, E., Eds.; Springer New York: New York, NY, 2014; 3–13.
 35. Holzer, W.; Shirdel, J.; Zirak, P.; Penzkofer, A.; Hegemann, P.; Deutzmann, R.; Hochmuth, E., Photo-induced degradation of some

- flavins in aqueous solution. *Chem. Phys.* **2005**, *308*, 69–78.
36. Edwards, A. M.; Bueno, C.; Saldaño, A.; Silva, E.; Kassab, K.; Polo, L.; Jori, G., Photochemical and pharmacokinetic properties of selected flavins. *J. Photochem. Photobiol. B Biol.* **1999**, *48*, 36–41.
37. Görner, H., Oxygen uptake after electron transfer from amines, amino acids and ascorbic acid to triplet flavins in air-saturated aqueous solution. *J. Photochem. Photobiol. B Biol.* **2007**, *87*, 73–80.
38. Zhang, X.; Wu, X.; Jiang, S.; Gao, J.; Yao, Z.; Deng, J.; Zhang, L.; Yu, Z., Photo-accelerated “click” reaction between diarylsydnone and ring-strained alkynes for bioorthogonal ligation. *Chem. Commun.* **2019**, *55*, 7187–7190.

SUPPORTING INFORMATION

5.5 Materials and methods

5.5.1 Materials

All reagents and chemicals were purchased from Sigma Aldrich, Acros Organics and Bioconnect, and used without further purification. Deuterated chloroform was purchased from Euriso-top and Milli-Q water was employed for all experiments. Acetonitrile for the hydrogenation reaction was dried by molecular sieves 3Å (20 % w/v) and used after 24h. Compound **5a** was synthesized as previously reported.³⁸

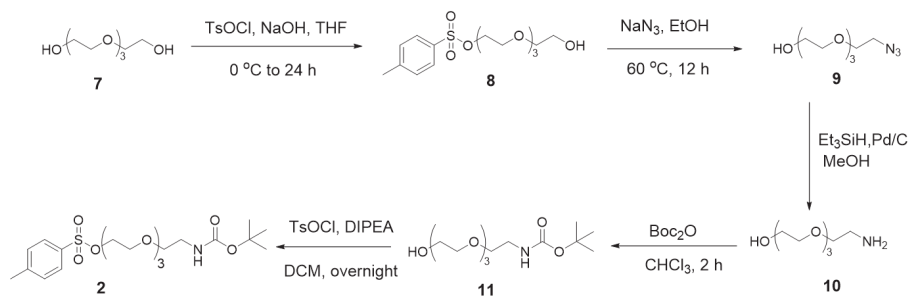
5.5.2 Methods

Compounds were either purified by silica gel column chromatography or on X1 flash chromatography system equipped with a C18 column from Grace Reveleris using a gradient of H₂O/CH₃CN. ¹H-NMR and ¹³C spectra were obtained on a Bruker (300 MHz) or Bruker DMX-400 (400 MHz). LC-MS analysis was performed on a Finnigan Surveyor HPLC system equipped with a Gemini C18 50 x 4.60 mm column (UV detection at 254 and 214 nm) coupled to Finnigan LCQ Advantage Max mass spectrometer with ESI. For the mobile phase, a gradient of 10-90% of CH₃CN/H₂O with 0.1% trifluoroacetic acid over 13.5 minutes was used. MALDI-TOF-MS spectra were obtained on a Bruker Microflex LRF mass spectrometer in reflection positive mode using α-cyano-4-hydroxycinnamic acid with a laser power of 30%. UV-vis measurements were performed on a Cary 300 UV-vis spectrophotometer using a quartz cuvette of 1 cm path length. The High resolution mass spectra (HR-MS) were collected on a Thermo Fisher LTQ Orbitrap mass spectrometer equipped with an electrospray ion source in positive mode (resolution R = 60000). The spectra were obtained by direct injection (2 μL) of samples (1 μM in H₂O-CH₃CN 50/50 v/v) via Ultimate 3000 nano UPLC (Dionex) system with an external calibration (Thermo Scientific) and recorded with a mass range of 150-2000. DLS measurements were carried out using a Malvern Zetasizer Nano ZS ZEN3500 equipped with a laser of 633 nm at a scattering angle of 173°. Atomic force microscopy (AFM) images were recorded in a tapping mode on a Veeco Multimode AFM with a Nanoscope IIIa controller device at room temperature and processed

using the Nanoscope software. Atomic force microscopy (AFM) images were recorded in tapping mode on a Veeco-Bruker Multimode AFM with a Nanoscope IIIa controller at room temperature. The AFM tips used were Oltespa Opus probes with a reflex aluminium coating, with a nominal spring constant of 2 N/m, a nominal resonance frequency of 70 kHz and a tip radius of 7 nm. The images were processed using Nanoscope software. Fluorescence experiments were recorded on an Aqualog Horiba Scientific fluorimeter with a quartz cuvette of 10 mm. The mechanical properties of the squaramide-based hydrogels were measured on a Discovery HR-2 hybrid rheometer with a Peltier-based temperature controller and a solvent trap. The cone-plate geometry (40 mm, 1.995°) was used and the pre-made hydrogel (600 μ L) were gently pipetted into the lower plate. The gap was set at 54 μ m. The sample was covered with the oil to avoid the drying during the measurement. The temperature ramp experiment was performed starting from 25 °C and ending at 85 °C with the constant ramp rate at 1 °C/min. The measurement was performed at a fixed frequency (1 Hz) and strain (0.05%).

5.7 Synthetic routes

5.7.1 Synthesis of 2



Scheme S1: Synthetic route for molecule 2.

Synthesis of 8

Tetraethylene glycol (20.0 g, 0.1 mol), was dissolved in DCM (300 mL) and Et_3N (2.09 mL, 0.015 mol) was added. The reaction mixture was cooled down at $0\text{ }^{\circ}\text{C}$ and a solution of tosyl chloride (1.96 g, 0.010 mol) was added dropwise in 2h and stirred overnight at RT. The reaction mixture was concentrated by rotary evaporation and was redissolved in DCM (200 mL). The organic layers were washed with water (3x 200 mL), dried with MgSO_4 and concentrated by rotary evaporation yielding as a colorless oil.

Yield: 25 g, 71.7%. ^1H NMR (300 MHz, CDCl_3) δ 6.75 – 6.66 (m, 2H), 6.32 – 6.23 (m, 2H), 4.25 (s, 3H), 3.12 – 3.02 (m, 2H), 2.68 – 2.52 (m, 9H), 2.49 (m, 7H), 2.19 – 2.07 (m, 1H), 1.36 (s, 3H). ^{13}C NMR (75 MHz, CDCl_3) δ 143.83, 131.75, 129.88, 126.38, 76.76, 76.33, 75.90, 71.70, 71.44, 69.51, 69.46, 69.35, 69.28, 69.15, 68.86, 68.30, 67.49, 60.40, 52.61, 44.95, 20.49.

Synthesis of 9

8 (3.12g, 8.97 mmol) was dissolved in DMF (20 mL) and NaN_3 was added. The reaction mixture was refluxed overnight at $60\text{ }^{\circ}\text{C}$. The solvent was removed by rotary evaporation and the residue was redissolved in water (20 mL) and extracted with EtOAc (3 x 20 mL). The organic layers were dried with MgSO_4 and concentrated by rotary evaporation. The compound was

purified by chromatographic silica column (EtOAc 100%, EtOAc/PE 9/1) and isolated as a yellowish oil.

Yield: 0.770g, 40%. ^1H NMR (300 MHz, CDCl_3) δ (ppm): 3.63 – 3.50 (m, 11H), 3.47 (m, 2H), 3.27 (t, 2H). ^{13}C NMR (75 MHz, CDCl_3) δ (ppm): 162.55, 77.75, 77.33, 76.90, 72.46, 70.52, 70.47, 70.41, 70.17, 69.89, 61.42, 50.50.

Synthesis of 10

9 (0.770 g, 3.5 mmol) was dissolved in dry MeOH (10 mL) and Pd/C (0.186 g, 1.75 mmol) was added under N_2 atmosphere. Et_3SiH (17 mL, 105 mmol) was added dropwise and the mixture was stirred overnight. After the filtration on celite, the residue was isolated removing the solvent under a gentle stream of N_2 gas. The reaction was quantitative and the compound was isolated as a yellowish oil.

^1H NMR (400 MHz, CDCl_3) δ (ppm): 3.77 – 3.46 (m, 20H), 2.90 – 2.74 (m, 2H). ^{13}C NMR (75 MHz, CDCl_3) δ 163.42, 77.88, 77.45, 77.02, 72.60, 72.36, 71.34, 71.04, 70.88, 70.38, 70.25, 70.20, 70.12, 69.97, 69.91, 69.87, 69.83, 69.76, 69.42, 62.02, 60.87, 60.77, 48.60, 42.55, 41.18, 40.59.

Synthesis of 11

10 (0.841g, 4.35 mmol) was dissolved in EtOH (20 mL) and Boc_2O (1.04g, 94.78 mmol) was added to the reaction mixture and stirred at RT for 2h. After the removal of the solvent by rotary evaporation, the crude was redissolved in DCM, washed with water (2 x 20 mL), and dried with MgSO_4 . The organic layers were concentrated and the compound, isolated as a white powder, was used for next step without further purification.

^1H NMR (300 MHz, CDCl_3) δ (ppm): 3.74 (m, 2H), 3.58 – 3.42 (m, 12H), 3.22 (m, 2H), 1.42 (s, 9H). ^{13}C NMR (75 MHz, CDCl_3) δ (ppm): 156.14, 77.57, 77.14, 76.72, 72.60, 72.53, 70.63, 70.56, 70.54, 70.48, 70.37, 70.32, 70.27, 70.18, 70.14, 70.02, 69.53, 62.20, 61.51, 40.30, 28.47, 4.30.

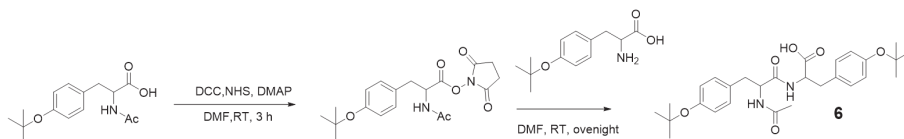
Synthesis of 2

11 (1.17g, 3.98 mmol) was dissolved in DCM (20 mL) and tosyl chloride (0.91 g, 4.78 mmol), trimethylamine (0.832 mL, 5.97 mmol) and a catalytic amount of 4-(dimethylamino)-piperidine (0.024 g, 0.199 mmol) were added.

The reaction mixture that was stirred overnight at RT. Subsequently, water (20 mL) was added to the reaction mixture and the aqueous layers were extracted with DCM (3 x 20 mL). The organic layers were combined and dried with MgSO₄ and concentrated by rotary evaporation. The crude was purified by chromatographic silica column (DCM/MeOH 95/5) and the product was obtained as a colorless oil. LCMS (t= 7.12 min, (m/z): 469.44 [M+Na]⁺

Yield: 1.5g, 84.2%. ¹H NMR (400 MHz, CDCl₃) δ (ppm): 7.83 (d, 2H), 7.37 (d, 2H), 4.18 (m, 2H), 3.83 – 3.42 (m, 21H), 3.37 – 3.29 (m, 2H), 2.48 (s, 3H), 1.47 (s, 9H). ¹³C NMR (101 MHz, CDCl₃) δ (ppm) = 145.08, 129.84, 127.27, 77.39, 77.07, 76.76, 72.69, 70.78, 70.57, 70.53, 70.23, 69.25, 68.71, 62.28, 40.35, 28.43, 20.70, 4.37.

5.7.2 Synthesis of 6



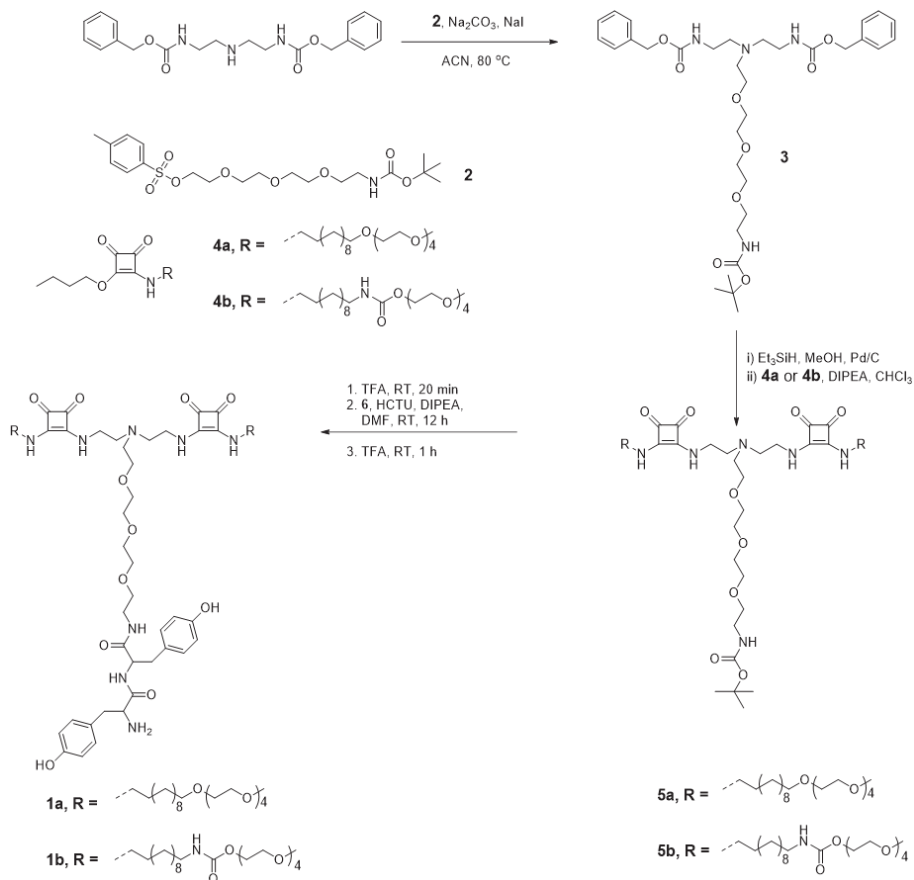
Scheme S2: Synthetic route for protected dityrosine **6**.

Acetyl-O-(tert-butyl)-L-tyrosine (0.600 g, 2.14 mmol) was dissolved in dry DMF (10 mL) and N,N-dicyclohexylcarbodiimide (0.529 g, 2.57 mmol) and 4-dimethylaminopyridine (DMAP) (0.026 g, 0.214 mmol) were stirred for 20 min at RT. N-hydroxysuccinimide (0.320 g, 2.57 mmol) was added and the mixture was stirred for an additional 3 h. Subsequently O-tert-butyl-L-tyrosine was added and the reaction mixture was stirred overnight. The crude was filtered and the solvent was removed under vacuum. EtOAc was added to the residue and filtered a second time to remove DCU. The organic layer was washed with water (3x) and dried with MgSO₄. The compound was purified by flash chromatography using H₂O/CH₃CN (10-90 %) over 40 min and was obtained as a colorless oil.

Yield: 0.8 g, 75%. ¹H NMR (300 MHz, CDCl₃): δ (ppm) = 7.08 – 6.95 (m, 2H), 6.81 (m, 3H), 3.55 (m, 1H), 3.21 – 2.75 (m, 4H), 1.89 (d, 3H), 1.34 – 1.19 (m, 18H). ¹³C NMR (75 MHz, CDCl₃): δ (ppm) = 175.00, 174.54, 170.20, 169.89, 169.77, 169.72, 153.99, 153.94, 153.67, 153.56, 132.99, 132.93, 131.88, 131.64, 130.22, 130.16, 129.48, 123.05, 121.23, 78.22, 78.06, 77.51, 77.09,

76.67, 55.95, 54.39, 41.08, 37.99, 37.72, 37.40, 37.09, 28.80, 21.84. LC-MS:
 $t = 6.71$ min, $(m/z): 499.50 [M]^+$, HRMS $(m/z): 499.00 [M]^+$.

5.7.3 Synthesis of 1a and 1b



Scheme S3: Synthetic route for molecule **1a** and **1b**.

Synthesis of 3

N,N -Di- Z -diethylenetriamine (0.230 g, 0.62 mmol) was dissolved in anhydrous CH_3CN , and successively, K_2CO_3 (0.128 g, 0.93 mmol), **5** (0.513 g, 1.15 mmol) and NaI (0.096 g, 0.64 mmol) were added and refluxed for 36 h. Subsequently, the solvent was removed under vacuum and the crude was

redissolved in DCM. The organic layers were washed 3x times with NaOH 1 M and were dried with Na₂SO₄. The compound was purified by flash chromatography using a gradient of H₂O/CH₃CN 10-90% over 40 min and was obtained as a white powder.

Yield: 0.126g, 31.4 % ¹H NMR (400 MHz, CDCl₃): δ (ppm) = 7.33 (m, 10H), 5.98 (s, 2H), 5.08 (s, 4H), 3.75 – 3.39 (m, 13H), 3.25 (m, 6H), 2.65 (m, 6H), 1.46 (s, 9H). ¹³C NMR (100 MHz, CDCl₃): δ (ppm) = δ 156.81, 156.02, 136.86, 128.34, 128.06, 79.15, 77.46, 77.14, 76.83, 71.99, 70.44, 70.24, 70.14, 69.87, 66.48, 54.29, 53.29, 40.31, 39.17. LC-MS: t= 6.45 min, (m/z): 646.50 [M]⁺, MALDI (m/z): 646.50 [M+H]⁺.

Synthesis of 5a

3 (0.287 g, 0.430 mmol) was dissolved in dry MeOH (6 mL) and Pd/C (0.5 eq, 0.215 mmol, 0.023 g) was added. The reaction mixture was placed under a nitrogen atmosphere and Et₃SiH (20 eq, 5.74 mmol, 0.916 mL) was added dropwise prior to stirring the reaction overnight. The deprotection was verified by LCMS (t= 3.55 min, m/z: 378.14 [M]⁺). Subsequently, the reaction mixture was filtered over celite and the solvent was removed by a gentle stream of N₂. The residue (0.189 g, 0.5 mmol) was redissolved in CHCl₃, and **4a**, (0.592 g, 1.15 mmol) or **4b** (0.62 g, 1.1 mmol) and DIPEA (3 eq, 1.5 mmol, 0.262 mL) were added and refluxed overnight. The crude was extracted with water (3x 20 mL) and dried by Na₂SO₄. The compound was purified on a silica column chromatography (EtOAc 100%, DCM/ MeOH (95:5) to obtain the compound **5a** as a white solid.

5a: Yield: 0.18g. 30 %, ¹H NMR (300 MHz, CDCl₃): δ (ppm) = 3.68 – 3.61 (m, 38H), 3.61 – 3.50 (m, 13H), 3.44 (m, 5H), 3.38 (s, 6H), 3.29-3.23 (m, 2H), 2.07 (s, 5H), 1.64 (m, 4H), 1.57 (m, 4H), 1.44 (s, 9H), 1.39 – 1.22 (m, 26H). ¹³C NMR (75 MHz, CDCl₃): δ (ppm) = 182.67, 181.92, 168.72, 167.24, 156.00, 77.52, 77.09, 76.67, 71.85, 71.51, 70.52, 70.47, 70.40, 70.25, 69.99, 69.95, 58.99, 44.59, 42.49, 40.23, 31.12, 29.58, 29.47, 29.27, 28.41, 26.55, 26.05. MALDI (m/z): 1283.03 [M+H]⁺.

Synthesis of 5b

3 (200 mg, 0.3 mmol) was dissolved in dry MeOH (5 mL) and Pd/C (64 mg, 0.215 mmol) was added. The reaction mixture was placed under a nitrogen atmosphere and triethylsilane (500 μL, 3.09 mmol) was added dropwise for

30 min and stirred for 2 hrs. The deprotection was verified by LC-MS (t_r = 3.19 min, m/z : 379.33 $[M]^+$). Subsequently, the reaction mixture was filtered over celite and washed with methanol. The solvent was removed through rotavapor. The residue was redissolved in $CHCl_3$, and **4b** (168 mg, 0.6 mmol) and DIPEA (46 μ L, 0.264 mmol) were added and refluxed overnight. The crude was purified through silica column chromatography (MeOH/DCM = 2:8) and removed the solvent to obtain the compound **5b** as a white solid.

5b: Yield: 0.18g, 30 %, 1H NMR (300 MHz, $CDCl_3$): δ (ppm) = 3.68 – 3.61 (m, 38H), 3.61 – 3.50 (m, 13H), 3.44 (m, 5H), 3.38 (s, 6H), 3.29-3.23 (m, 2H), 2.07 (s, 5H), 1.64 (m, 4H), 1.57 (m, 4H), 1.44 (s, 9H), 1.39 – 1.22 (m, 26H). ^{13}C NMR (75 MHz, $CDCl_3$): δ (ppm) = 182.67, 181.92, 168.72, 167.24, 156.00, 77.52, 77.09, 76.67, 71.85, 71.51, 70.52, 70.47, 70.40, 70.25, 69.99, 69.95, 58.99, 44.59, 42.49, 40.23, 31.12, 29.58, 29.47, 29.27, 28.41, 26.55, 26.05. LCMS: t_r = 6.19 min, m/z : 1369.15 $[M+Na]^+$.

Synthesis of **1a**

5a (0.144 mmol, 0.167 g) was dissolved in TFA and stirred at RT for 20 min to remove the boc protecting group. Afterwards, the TFA was removed by a gentle stream of N_2 and the reaction was dissolved in 10 mL of DMF and HCTU (0.268 g, 0.648 mmol), **6** (0.358 g, 0.719 mmol) and DIPEA (0.250 mL, 1.44 mmol) were added and stirred overnight. The solvent was removed under vacuum and purified by flash chromatography using a gradient of H_2O/CH_3CN from 10-90 % over 40 min. The tert-butyl group of dityrosine was then removed using TFA (3 mL) in 1 h at RT and the compound **1a** was purified by flash chromatography on a C18 silica column using a gradient of H_2O/CH_3CN 10-90 % over 35 minutes. The final compound was obtained as a colorless sticky oil.

1a: Yield: 0.100 g, 57 % 1H NMR (400 MHz, $CDCl_3$): δ (ppm) = 8.50 (s, 2H), 6.95-6.6 (m, 9H), 3.67 – 3.59 (m, 31H), 3.59 – 3.51 (m, 13H), 3.50 – 3.39 (m, 13H), 3.36 (s, 6H), 2.84 (s, 4H), 2.40 (s, 4H), 1.87 (s, 2H), 1.67-1.50 (m, 9H), 1.37 – 1.19 (m, 27H). ^{13}C NMR (100 MHz, $CDCl_3$): δ (ppm) = 181.97, 146.91, 128.81, 128.71, 127.99, 127.32, 77.40, 77.08, 76.76, 71.85, 71.59, 70.48, 70.43, 70.39, 70.34, 69.92, 59.01, 30.94, 29.57, 29.49, 29.27, 26.48, 26.05. LC-MS: t_r = 6.04 min, (m/z): 1529.4 $[M+H]^+$, MALDI (m/z): 1567 $[M+K]^+$.

Synthesis of **1b**

5b (10 mg, 7.4 mmol) was dissolved in 50% DCM/TFA and stirred at room temperature for 2 hr. The deprotection was verified by LCMS (t_r 5.31 min, m/z : 1269.18 $[M+Na]^+$). Afterwards, the TFA was removed by a gentle stream of N_2 and the reaction was dissolved in 10 mL of chloroform and NHS activated dityrosine (**6**) (9 mg, 14.8 mmol) and DIPEA (13 μ L, 74.2 mmol) were added and stirred overnight. The solvent was removed under vacuum. The formation of product was characterized by LC-MS (t_r 6.12 min, m/z : 1728.08 $[M+H]^+$). The tert-butyl group in the dityrosine part was then removed using 50% DCM/TFA (10 mL) in 2 h at RT and the compound **1b** was purified by reverse phase HPLC on a C18 silica column using a gradient of H_2O/CH_3CN 10-90 % over 20 minutes.

1b: Yield: 0.100 g, 30 %. 1H NMR (300 MHz, $CDCl_3$): δ (ppm) = 8.9 (s, 2H), 6.92 (m, 4H), 6.83 (m, 4H), 4.92 (t, 2H), 4.2 (m, 4H), 3.69 – 3.52 (m, 36H), 3.41 (s, 6H), 3.35 (m, 16H) 3.18 (m, 6H), 2.51 (m, 6H), 1.84 (s, 3H), 1.5 – 1.28 (m, 32H). LC-MS: t_r 5.92 min, (m/z): 1614.12 $[M]^+$.

5.7.1 Characterization

Sample preparation

A stock solution of compound **1a** in DMSO at concentration of 1 mM was prepared and the solvent was removed by a stream of N₂. The solution was rehydrated with water at a concentration of 1 mM. Subsequently, aliquots from the stock solution were taken to prepare solutions at the desired concentration for solution phase measurements and used as is for gel phase experiments. All samples were left to stand overnight before measurement.

For samples using the photoinitiator riboflavin 5'-mononucleotide (FMN), a stock solution of FMN was prepared at 10 mM. An aliquot of the photoinitiator solution was diluted in presence of **1a** (1 mM) to provide a final concentration of 1 mM. After irradiation at 440 nm, aliquots from the stock solution were taken to prepare solutions at the desired concentration for solution phase measurements.

Photo-crosslinking of **1b** was performed using a stock solution of **1b** (1 mM), [Ru(bpy)₃]²⁺ (2.2 mM) and SPS (22 mM). The sample containing **1b** in self-assembled state (0.166 mM) in the presence of [Ru(bpy)₃]²⁺ and SPS was photoirradiated using visible light ($\lambda = 450$ nm).

UV-vis spectroscopy

Solutions of **1a** at 15 μ M concentration in water were prepared as described according to the sample preparation protocol above. The samples were placed in the UV-vis and a spectrum was recorded from 200-500 nm. The solutions were prepared in triplicate and for each solution the UV-vis spectra was measured.

The solutions containing the photoinitiator, as described in the protocol above, were irradiated at 440 nm at different times (5, 10, 15, 20 25, 60 and 120 min). Subsequently, aliquots from the stock were taken to prepare solutions at 15 μ M and were equilibrated overnight prior the measurements. The samples were placed in the UV-vis and a spectrum was recorded from 200-500 nm. The solutions were prepared in triplicate and for each solution the UV-vis spectra was measured.

In the case of **1b**, absorption changes were measured after photoirradiation at 450 nm in the presence of photoinitiator ($[\text{Ru}(\text{bpy})_3]^{2+}$ and SPS). The photoirradiation and absorption changes at high concentrations were performed using 1 mm cuvette. The baseline correction was carried out using blank containing photoinitiator at the similar concentrations.

Fluorescence measurements

Solutions of **1a** (1 mM) in presence of FMN (1 mM) were prepared in different vials and irradiated at different times (5, 10, 15, 20 25, 60 and 120 min) with visible light at 330 nm. Subsequently, aliquots from the stock solutions were taken to prepare solutions a at 15 μM concentration for measurement. Fluorescence spectra were recorded using an excitation wavelength at 330 nm and the emission spectra were recorded from 350 to 620 nm at RT.

Critical aggregation concentration determination

A stock solution of **1a** at 1 mM concentration was prepared and equilibrated overnight. The stock solution was diluted to several concentrations between 100 μM to 10 nM and equilibrated for at least 3h prior to measurement of scattering intensity. Each measurement was carried out using a disposable DLS cuvette and performed in triplicate. The data was plotted using the scattering intensity as a function of $\log [C]$. The critical aggregation concentration was then determined from the intersection of the two lines drawn through the points collected for the scattering intensities collected at the various concentrations.

Atomic force microscopy (AFM)

A solution of **1a** was prepared according to the preparation protocol above at a concentration of 15 μM and equilibrated overnight. An aliquot (25 μL) of this solution was pipetted on cleaved mica and dried overnight at RT before the measurement. The analysis of AFM images was performed using the Nanoscope software.

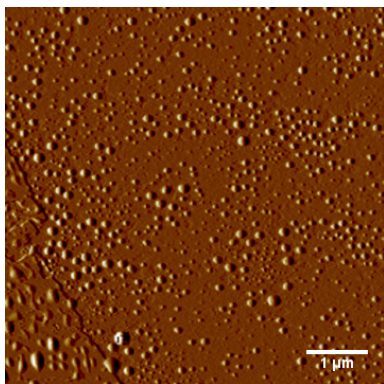


Figure S5.1 AFM micrograph of **1a** (amplitude) (scale bar: 1 μm).

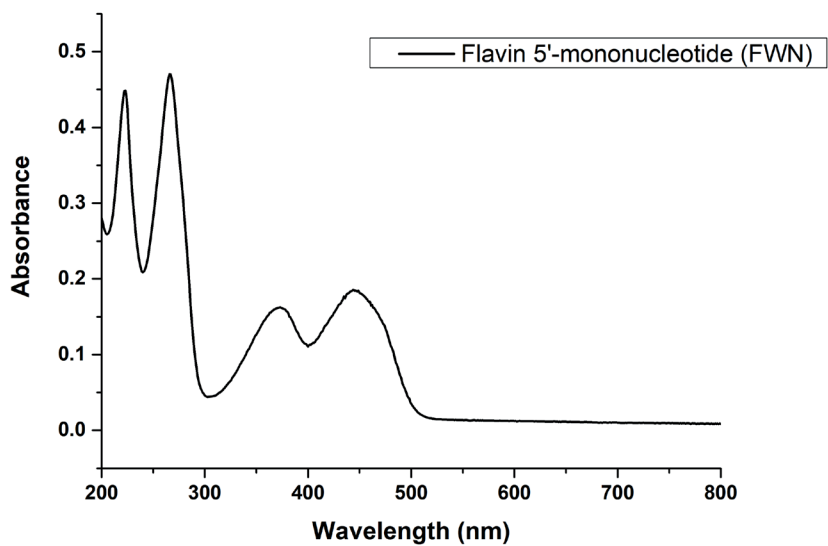


Figure S5.2 UV-vis spectra of FMN at 15 μM

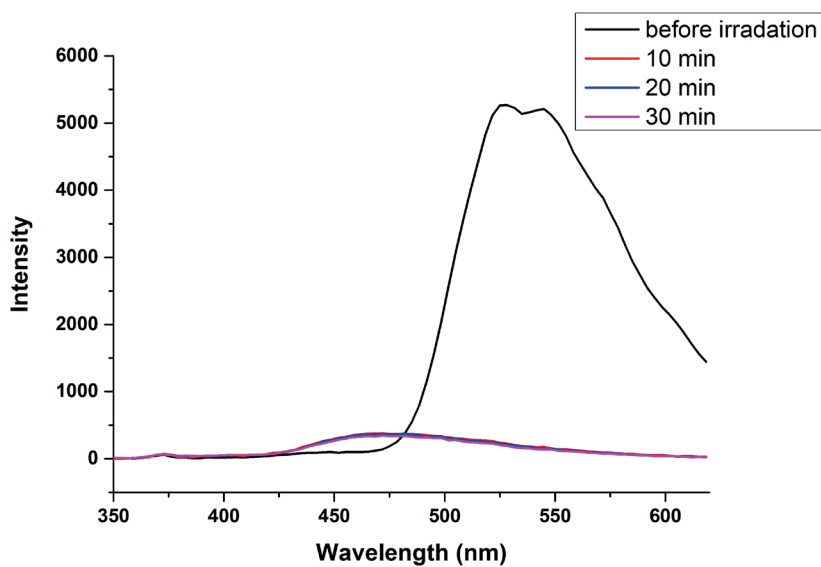


Figure S5.3 Emission spectra of FMN at 15 μM after different visible light irradiation times (10, 20 and 30 min).

CHAPTER 6

SUMMARY AND PERSPECTIVES

Supramolecular polymers are class of materials that are held together by non-covalent interactions such as hydrogen bonding, π - π interactions, electrostatic interactions and the hydrophobic effect. In the last decade, while most studies probed their assembly behaviour in organic solvents, the development of monomers that self-assemble in water is a rapidly growing area that provides opportunities to better understand the effects of this unique solvent on their formation and application. An often-used strategy for the formation of stable and well-defined aggregates in water, involves the coupling of the hydrophobic effect with hydrogen bonding interactions in the monomer design. The strength of the hydrogen bonds can be retained by their embedding within the hydrophobic domain of the monomer removing competition with water and further tuned by their number and arrangement of hydrogen bond donors and acceptors. In the case of squaramides, it was recently demonstrated they can be further affected by the aromatic character of the molecules strengthening the hydrogen bonds through an increased π delocalization on self-assembly. This effect in squaramides as demonstrated by the aromatic stabilization energy shows its significant contribution to the total interaction energy; in the range of 30%. Taking advantage of this minimalistic ditopic hydrogen bonding unit, the Kieltyka group has shown this unit play an active role in the formation of supramolecular materials taking them outside of the range of anion recognition and medicinal chemistry, and extending their application in the biomedical field. In their first publication, the capacity of the squaramide-based bolaamphiphiles to self-assemble into supramolecular polymers in water was investigated examining this process at several length scales. The synergy of very strong hydrogen bonding and aromatic gain was demonstrated to be the driving force for the formation of nanofibers. In a subsequent work, this effect was compared against its thiosquaramide counterpart, that displayed a distinct self-assembly mode that involves stacking rather than head-to-tail hydrogen bonding that also results in aromatic gain within the monomer unit showing the importance of this effect for this synthon. Additionally, it was demonstrated that by changing the monomer geometry from linear to tripodal, lateral aggregation is suppressed changing the morphology of the fibrillar aggregates from being rigid with a high persistence length and dimensions on the nanoscale to flexible with a low persistence length and on the micron scale. In this thesis, I examined the potential to use this panel of monomers to study the accessible range of formed polymers through modulating the monomer chemical structure, co-assembly and introduction of chemistries that are responsive to light to provide insight on how to design new materials at several length scales.

In **chapter 2**, the potential to control the microstructure of a squaramide supramolecular polymer was explored through copolymerization of oxo and thiosquaramide-based bolaamphiphiles in water. In this chapter, the distinct modes of self-assembly of the two bolaamphiphiles were exploited; oxosquaramide bolaamphiphiles adopt a head-to-tail hydrogen-bonding configuration on aggregation, whereas thiosquaramide prefer a stacked configuration. This difference originates due to the less directional and weaker character of hydrogen bonds formed by sulfur, in comparison to oxosquaramide. In this chapter, the effect of O→S substitution in the squaramide bolaamphiphile on its supramolecular polymerization mechanism and its associated thermodynamics was first examined. NMR and DLS studies confirmed that HFIP (hexafluoroisopropanol) is a good solvent for oxosquaramide, and THF is a good solvent for thiosquaramide. This study was performed taking advantage of their solvent-induced depolymerization, where the self-assembled monomers were titrated with a good solvent to depolymerize the monomers and the solvent denaturation model was further applied to the data. Despite their different self-assembly modes, both of the monomers self-assemble according to a cooperative mechanism. To gain insight into the microstructure of the formed polymers and their dynamics fluorescently-labeled monomers with cyanine dyes (5/3) were prepared and their co-assembly experiment was examined through fluorescence studies. On co-assembly shorter fibers with a decreased persistence length were observed as compared to pure oxo-squaramide by cryoEM.

Since these results suggest co-assembly of the monomers, further insight in the microstructure of the final copolymers (alternating, random, block) should be investigated. Therefore, microscopy experiments such as SIM, STORM need to be performed. Moreover, since the individual monomers show different self-assembly modes, computational calculations can be a future route to better understand their interaction on co-assembly in the polymers. Additionally, since the co-assembly of oxo- and thiosquaramide was investigated only at 1:1 molar ratio, the effect of excess of one of the components could be investigated.

In **chapter 3**, a novel method for the synthesis of tripodal monomers for supramolecular polymerization by the Ugi reaction was developed. The Ugi reaction is a multicomponent reaction involving an isocyanide, amine, carboxylic acid and aldehyde or ketone that generates compounds with a

peptide-like bonds that are widely used in the chemical structures of supramolecular biomaterials. Trisquaric and nitriloacetic acid were used as the acidic component of this four component reaction along with modified amine, isocyanide and an aldehyde or ketone to construct tripodal scaffolds. As the synthesis of supramolecular monomers can be laborious, the multicomponent approach can be considered as a valid approach to find gelators in an efficient way with minimal synthetic effort. The success of the Ugi reaction is determined by parameters such as temperature, concentration and the choice of acidic component, thus these variables were examined to guide the distribution of mono- and disubstituted compounds to the trisubstituted product. To obtain a peptide-functionalized monomer, nitrilotriacetic acid was also examined as a core with benzaldehyde, oligoethylene glycol-isocyanide and ammonium carbonate. The low yield of the reaction was overcome using nitrilotrisquaric acid and replacing the ammonium carbonate with 2,4-dimethoxybenzylamine to overcome the unstable imine, and subsequently was deprotected under acidic conditions. Using this optimized protocol, a small family of compounds with different aliphatic spacers was synthesized. These compounds were found to form spherical aggregates likely due to the presence of three stereocenters that preclude their stacking in to fibrous aggregates.

Despite the lack of self-assembly, this optimized Ugi reaction could be exploited as source of inspiration for the synthesis of tripodal compounds using squaric acid. Moreover, to surmount the inability of the monomer to self-assemble, the Ugi reaction could be pursued using symmetrical ketones such as acetone, diethyl ketone or a chiral acid catalyst to prevent the formation of diastereomers. Provided that the Ugi reaction can be harnessed to prepare tripodal compounds based on squaramides, new opportunities will arise to prepare modules for supramolecular assembly that can result in discrete structures or materials.

In **chapter 4**, the self-assembly of small family of tripodal squaramide-based supramolecular polymers with respect to various structural substitutions including modulation of the hydrophilic and hydrophobic domains, the number of squaramide units and covalent linkages (e.g. carbamate, ether) for connection to the core of the monomer was examined. The self-assembly of the monomers was characterized at the molecular level through spectroscopic techniques such as UV-vis and fluorescence spectroscopy, at the nanoscale through AFM and at the macroscale using oscillatory rheology. The monomer

containing three squaramide moieties has the ability to self-assemble in nanometer fibers and to hydrogelate at a concentration of 5 mM. When the number of squaramides is reduced, the monomers with three aliphatic spacers still have the ability to self-assemble in fibers but no hydrogelation was observed. Conversely, the most hydrophilic monomer results in the formation of spherical aggregates. These studies supported the strong relationship between the monomer chemical structure and their self-assembly into supramolecular polymers. More specifically, the difference in the observed morphologies and ability for the monomers to self-assemble point to the importance of a certain ratio between the hydrophilic and hydrophobic domains, as a reduction of squaramides still results in self-assembly.

Further insight into the polymerization of the monomers can be gained by examining the supramolecular polymerization mechanism to understand how structural modifications affects their self-assembly behaviour and if any changes in mechanism is observed. Thoroughly investigating the self-assembly behaviour of this library of squaramide monomers, especially the extent to which various structural modifications influence their properties, will provide a framework for the design of new squaramide monomers that can be used in the biomedical area.

In **chapter 5**, a visible light-mediated strategy to modulate the self-assembly a tyrosine-dipeptide outfitted supramolecular monomer in water was examined. Since the tyrosine dipeptide has been shown to self-assemble into nanofibers and tyrosines have been used to cross-link polymer materials, the tyrosine dipeptide was conjugated to the tripodal core with two squaramide arms appended to a hydrophobic decyl spacer and hydrophilic tetraethylene glycol chain with either a carbamate or ether linkages between the segments. Self-assembly of the squaramide in a head-to-tail hydrogen bonding arrangement was observed in the case of the carbamate derivative in a concentration-dependent manner, but not in the case of the ether molecule. Further irradiation of the monomer with visible light at 440 nm in the presence of either FMN or Ru(bpy)³⁺/SPS photoinitiators, did not yield formation of the tyrosine dimer as expected. These results suggest either a lack of exposure of the tyrosine moieties to the photoinitiator or a distance too large between them in the assembly for crosslinking.

In the future design of this type of monomers, the reduction of the chain length of the oligoethylene glycol or its exchange for a hydrophobic linker should be

considered. Moreover, the type of photoinitiator and photocrosslinking conditions should be probed further to understand their effect on self-assembly. Achieving this rapid, visible light mediated polymerization on supramolecular polymers will provide new opportunities for controlling supramolecular polymerization in the presence of cells either as nanoparticles or material

Samenvatting

Supramoleculaire polymeren zijn een klasse van materialen die bij elkaar gehouden worden door non-covalente interacties, zoals waterstofbruggen, π - π -interacties, electrostatische interacties en het hydrofobe effect. De formatie van stabiele, goed gedefinieerde aggregaten wordt bepaald door de structuur van het monomeer en het oplosmiddel waar deze zich in bevindt. In water valt of staat het ontwerp en de formatie van stabiele supramoleculaire polymeren met het hydrofobe effect en de directionaliiteit van de waterstofbruggen. Squaramides, cyclobutenen bestaande uit twee waterbrugdonoren tegenover twee waterbrugacceptoren, staan bekend om hun toepassing in de medicinale chemie en in anion receptoren, maar worden nog nauwelijks gebruikt in supramoleculaire chemie. Recentelijk heeft de Kieltyka onderzoeksgroep laten zien dat zogeheten oxosquaramides, in de vorm van bolaamfifielen, assembleren in een kop–staart orientatie waarbij supramoleculaire polymeren gevormd worden in water. In dit proefschrift onderzoek ik nieuwe methoden om squaramide monomeren te maken, en onderzoek de zelf-assemblage in water om zo polymeren en gel-fase materialen te vormen, en het gebruik van dit synthon in het veld van supramoleculaire materialen uit te breiden.

In hoofdstuk 2 wordt de mogelijkheid onderzocht om de microstructuur van squaramide supramoleculaire polymeren te controleren middels de co-polymerisatie van oxo- en thiosquaramide gebaseerde bolaamfifielen in water. Terwijl oxosquaramide bolaamfifielen een kop-staart waterstofbrugconfiguratie aannemen tijdens de aggregatie, vormen thiosquaramides een gelaagde zelf-assemblage structuur. Dit verschil komt voort uit de minder sterke directionaliiteit en het zwakkere waterstofbrugvormende karakter van zwavel in vergelijking tot zuurstof. Allereerst werd het zelf-assemblage mechanisme van individuele monomeren onderzocht middels oplosmiddel-geïnduceerde depolymerisatie. Ondanks de verschillen in assemblage assembleren beide monomeren middels een coöperatief mechanisme. Om inzicht te verkrijgen in de microstructuur van de gevormde polymeren en hun dynamiek werden squaramide monomeren gelabeld met fluorescente cyanine kleurstoffen gesynthetiseerd en co-assemblage werd bestudeerd middels fluorescentie en electronenmicroscopie (cryoEM). Bij co-assemblage van thio-squaramide monomeren werden kortere vezels met verminderde persistentie-lengte geobserveerd in vergelijking met vezels bestaande uit louter oxo-squaramide monomeren.

In hoofdstuk 3 wordt een nieuwe methode beschreven voor de synthese van tripodale squaramide-gebaseerde monomeren voor gebruik in supramoleculaire polymerisatie, gebruikmakende van de Ugi reactie. De Ugi reactie is een multicomponentreactie waarbij een isocyanide, amine, carbonzuur en aldehyde of keton worden gemengd resulterend in de vorming van nieuwe monomeren met hoge opbrengst. De synthese van supramoleculaire monomeren kan een tijdrovende aangelegenheid zijn en de multicomponent-methode is potentieel een efficiënte manier om met minimale synthetische inspanning nieuwe gelatoren te synthetiseren. In dit hoofdstuk werden trisquarisch en nitrilo-azijnzuur gebruikt als de zuur-component in deze reactie in combinatie met een amine, isocyanide en een aldehyde om tot de vorming van tripodale monomeren te komen. Het succes van de Ugi reactie wordt bepaald door parameters zoals temperatuur, concentratie en de keuze van het zuur-component, daarom werd de invloed van deze parameters onderzocht om de formatie van het drievoudig-gesubstitueerde product te optimaliseren. Een peptide-band houdende monomeer werd geprepareerd vanuit nitriloazijnzuur in combinatie met benzaldehyde, oligoethyleen glycol-isocyanide en ammonium carbonaat. De initiële lage opbrengst van het product werd verbeterd door nitrilotrisquarisch zuur te gebruiken als de kern en ammonium carbonaat te vervangen door 2,4-dimethoxybenzylamine, resulterend in de vorming van een meer stabiel imine tijdens de reactie. Een kleine familie van verbindingen met een squaramide kern en verschillende alifatische *spacers* werd gesynthetiseerd en zelf-assemblage resulteerde in de vorming van sferische aggregaten.

In hoofdstuk 4 wordt de zelf-assemblage van een kleine familie tripodale squaramide-gebaseerde supramoleculaire monomeren in water beschreven. Verscheidene structurele varianten van het squaramide monomeer werden bestudeerd door de hydrofiele en hydrofobe domeinen te variëren, het aantal squaramide-eenheden, en met variatie in het type covalente binding (carbamaat *versus* ether). De zelf-assemblage van de monomeren werd gekarakteriseerd op een moleculair niveau middels spectroscopische technieken zoals UV-vis en fluorescentie spectroscopie, op de nanoschaal middels AFM, en op de macroschaal middels oscillatoire rheologie. Monomeren bestaande uit drie squaramide eenheden assembleerde tot nanometer lange vezels en de vorming van een hydrogel werd waargenomen bij een concentratie >5 mM. Wanneer het aantal squaramide eenheden wordt gereduceerd, vormen de monomeren met drie alifatische *spacers* nog wel vezels, maar werd er geen hydrogel meer gevormd, terwijl het meest

hydrofiele monomeer sferisch aggregaten vormde. Deze studie onderstreept de sterke relatie tussen de chemische structuur van het monomeer en het resulterende supramolecular polymer.

In hoofdstuk 5 werd een zichtbaar licht-gemedieerde strategie onderzocht om de zelf-assemblage van tyrosine-dipeptide gedecoreerde supramoleculaire monomeer in water te moduleren. Tyrosine-dipeptide assembleren tot nanovezels, en de tyrosines kunnen gebruikt worden om de assemblages stabiel te maken door middel van dimerisatie van dit aminozuur (*i.e.* crosslinking). Daarom werd een tyrosine dipeptide geconjugeerd aan een tripodale kern. Zelf-assemblage van dit molecuul in een kop-staart waterstofbrugconfiguratie werd waargenomen met behulp van UV-vis spectroscopie in een concentratie-afhankelijke wijze voor de carbamaat analoog, maar niet voor de ether analoog. Bestraling van het monomeer met zichtbaar licht met een golflengte van 440 nm in de aanwezigheid van de fotoinitiatoren FMB of $\text{Ru}(\text{bpy})_3^{3+}/\text{SPS}$, resulteerde niet in crosslinking. Dit kan verklaard worden door de geringe blootstelling van de tyrosine-eenheden aan de fotoinitiator, of door de te grote afstand tussen tyrosines welke dimerisatie minder efficiënt maakt. De beschreven resultaten kunnen dienen als basis voor de toekomstige ontwikkeling van nieuwe squaramide monomeren met tyrosine-eenheden voor licht gecontroleerde assemblage en stabilisatie van functionele biomaterialen.

Curriculum vitae

Francesca Lauria was born on the 11th of December 1990 in Naples, Italy. From 2004 until 2009 she attended the scientific high school in Caserta graduating with the maximum score. Afterwards, she pursued her scientific interest attending the Bachelor degree in Chemistry at the University of Naples “Federico II” (2009-2012). She obtained her BSc with honours (110/110 summa cum laude) and the topic of her Bachelor thesis was the physico-chemical investigation of the interaction of a telomeric G-quadruplex with porphyrin-peptide conjugates as potential anticancer applications.



Francesca decided to continue her scientific education and obtained a Master degree in “Chemical Sciences” at University of Naples again with honors (110/110 summa cum laude) in 2014. During her master thesis she continued working with nucleic acids performing physico-chemical characterization of telomeric G-quadruplexes containing a modified thymine.

Before to start the PhD, she worked as research assistant at IIT (Istituto Italiano di Tecnologia) in Naples focusing on the preparation of nanoemulsions using layer-by-layer deposition technique for diagnostic and therapeutic applications (2014-2015). In May 2015 Francesca started her PhD at Supramolecular & Biomaterials Chemistry department of the Faculty of Science - University of Leiden under the supervision of Dr. Roxanne Kieltyka in the group of Prof. Dr. Alexander Kros. During her PhD, she expanded her knowledge in the supramolecular polymers field. In particular, her work was focused on the design, synthesis and characterization of squaramide-based supramolecular polymers in aqueous solution.

After 6 months of Internship at Rebel Nature Cosmetics Laboratory (November 2020-April 2021), from June 2021 until the end of the year, she worked as a Quality Control Analyst at Wacker Biotech in Amsterdam where she validated analytical methods by HPLC/UPLC according to the ICH guidelines. From January 2022, she works at Quality Control Department (Method, Implementation and Transfer) of Teva Pharmaceuticals in Haarlem.

List of publications

1. Victorio Saez Talens, Joyal Davis, Chia-Hua Wu, Zhili Wen, **Francesca Lauria**, Karthick Babu Sai Sankar Gupta, Raisa Rudge, Mahsa Boraghi, Alexander Hagemeijer, Thuat T. Trinh, Pablo Englebienne, Ilja K. Voets, Judy I. Wu, and Roxanne E. Kieltyka. Thiosquaramide-Based Supramolecular Polymers: Aromaticity Gain in a Switched Mode of Self-Assembly. *J. Am. Chem. Soc.* 2020, 142, 19907–19916.